SAPIENZA
UNIVERSITÀ DI ROMA

Lattice Models for Granular and Active Matter Fluctuating Hydrodynamics

Scuola di Dottorato *Vito Volterra*

Dottorato di Ricerca in Physics – XXIX Ciclo

Candidate

Alessandro Manacorda

ID number 1186021

Thesis Advisor

Dr. Andrea Puglisi

A thesis submitted in partial fulfillment of the requirements
for the degree of Doctor of Philosophy in Physics

July 2017

Thesis defended on 20 september 2017
in front of a Board of Examiners composed by:

Prof. Mauro Carfora (chairman)
Dr. Antonello Scardicchio
Prof. Sergio Caracciolo

Lattice Models for Granular and Active Matter Fluctuating Hydrodynamics
Ph.D. thesis. Sapienza – University of Rome

This thesis has been typeset by LaTeX and the Sapthesis class.

Author's email: alessandro.manacorda@roma1.infn.it

A Valeria, Silvia, Giuliano e Carlo

Contents

Introduction

Granular and active matter are among the most studied systems in out of equilibrium statistical physics.

The study of out of equilibrium systems is still under development and represents one of the most important progresses of statistical physics in the last century. At the end of the 19^{th} century, equilibrium statistical physics has developed the main tools to investigate the physical properties of macroscopic systems as a statistical consequence of their macroscopic behavior. The development of the *kinetic theory* has related the time evolution and the equilibrium values of thermodynamic observables such as temperature and pressure to the microscopic dynamics of the enormous number of particles constituting the material of observation. The existence of conservation laws such as the energy conservation principle is the basis to define the tendency to *equilibrium* normally observed in gases and liquids: no matter the initial configuration of the system, the microscopic dynamics of the system leads it to a macroscopic equilibrium state with a given probability distribution of its dynamical coordinates, namely positions and velocities of the particles of a gas, determined by the Boltzmann formula $e^{-\beta H}$ for Hamiltonian systems. The existence of an equilibrium state allows to define the Gibbs ensembles description and define thermodynamical functions such as the Helmoltz free energy, the entropy and so on.

However, out of equilibrium systems are ubiquitous. First, every system at equilibrium can be driven out of it from a perturbation, inducing a heat or mass current into the system, developing spatial gradients coupled with a temporal evolution of thermodynamical quantities. This is what ceaselessly happens in *transport processes*, e.g. when a fluid is flowing under a pressure gradient or an electric current arises because of the application of a voltage. Nonequilibrium phenomena are involved in a large amount of research fields, such as climate dynamics, chemical reactions, biological physics and applications of physics to economics and social science. The basis of nonequilibrium statistical physics rely on *probability* and *stochastic processes* theory: while on one hand the huge number of microscopic components forbid any possibility of analytical computation of their motion one by one, on the other hand it allows to use limit theorems such as the Law of Large Numbers or the Central Limit Theorems, getting more precise predictions as the number of microscopic particles increase. The most ambitious goal of statistical physics is to derive the probability distribution of the microscopic variables of the considered system: if this is achieved, the computation of macroscopic observables is generally almost straightforward.

Granular and active matter are two kinds of out of equilibrium statistical systems. *Granular matter* is everything that is made of *grains*, like powders, sand, cereals, pills etc. A grain is a solid particle following the laws of classical mechanics and interacting among each other through *dissipative* collisions. The last feature is what actually makes granular matter out of equilibrium, differentiating it from colloidal particles which follow classical mechanics but undergo elastic collisions. A system can be at equilibrium if a phase-space trajectory and its time-reversed one have the same probability to occur *a priori*. It will be shown that dissipation makes it impossible for granular materials. Therefore, being out of equilibrium in granular matter is not the consequence of a perturbation but rather an *intrinsic* property of the physical system. This is possible because the granular description introduces a coarse-graining of the system at a mesoscopic scale, disregarding the microscopic degrees of freedom involved in collisions and absorbing the dissipated kinetic energy, restoring the energy conservation principle at a more fundamental level. Nevertheless, the description introduced has revealed to be of practical use to describe the main properties of granular materials. Research on granulars started from the observation of many unknown features in industrial devices: the observation that pressure and stress propagation followed a rather different behavior from elastic materials inaugurated a new research area, with many possible interactions with engineering problems such as the transport of grains, the mixing or separation of different kind of powders, the prevention of avalanches and the diffusion of fluids into a granular material.

Active matter is every system composed by many *self-propelled* units. The most natural examples are animals: their biological structure provide them the *motility*, i.e. the capability to sustain a state of motion by converting the chemical energy stored into kinetic energy. As it will be shown, the research has identified a plethora of active systems, including humans which obviously move across the space. Active matter exhibits a spectacular behavior when the units coordinate themselves and give rise to *collective motion*: this is what we observe when fishes move together in huge schools, travelling across the sea and defending from predators, or when birds coordinate their motion forming amazing flocks. Thus, active matter phenomena are the combination of the individual self-propulsion of the units with the reciprocal interactions established among them. Living units are very complex systems, and the derivation of interaction rules from their biological properties is currently out of reach. Therefore, research on active matter in the last two decades focused on the proposal of minimal models capable to reproduce the main features of collective motion observed in experiments.

Granular and active matter share two main properties:

- they are both intrinsically out of equilibrium: indeed, active matter continuously converts internal energy - absorbed somehow from the environment - in kinetic energy to sustain its state of motion; furthermore, when moving in a viscous fluid or substrate, kinetic energy is dissipated all along the motion. This implies the presence of continuous balance of energy injec-

tion/dissipation during the motion of the particle. The same balance occurs in a driven granular gas: to avoid the global "cooling" of granular motion caused by collisions, one can inject energy in a granular media through some mechanical process, like shearing or shaking the granular. Therefore, granular and active matter seem to have a *specular behavior*: while the former loses kinetic energy in its free motion and needs to absorb it from the environment, the latter vice versa "creates" kinetic energy from stored internal energy and dissipates it interacting with the environment.

- grains and active units are generally *small systems*: even if in some physical situations they can be made of $N \sim 10^5$ particles, this number is quite far from Avogadro's number $N_A \sim 10^{23}$. Therefore, the validity of limit theorems is more delicate, *fluctuations* become relevant and can usually be compared with the magnitude of macroscopic quantities of the system. A probabilistic approach must not disregard them but rather include them in a more accurate description.

The specularity between granular and active particles is not an invention of this thesis: many studies have connected the two, and several experiments on shaken nematic or polar rods have shown their "active behavior". Actually, it is established that driven *asymmetrical* granular particles can behave as active units, because nematic or polar interactions can produce an alignment and increase of velocity correlations leading to some collective motion. Nevertheless, what has been observed numerically - and confirmed analytically in this thesis - is that dissipative granular collisions are sufficient to create velocity correlations leading a granular system to an ordered motion, even for apolar and isotropic particles.

There are several possible descriptions when looking at granular and active matter: we are interested in their *hydrodynamic description*. Namely, a granular material or an active system can be treated as a *fluid*, where each unit is analogous to a molecule of the fluid and the dynamical observables are the macroscopic fields of density, velocity and temperature, defined from classical hydrodynamic description of real fluids. This representation allows to recognize many collective phenomena of granular and active motion such as vortex formation, clustering, swarming and so on. Hydrodynamics is deeply related to kinetic theory, providing a statistical derivation of macroscopic observables without the need of equilibrium assumptions. Furthermore, in the last decades the theory of *fluctuating hydrodynamics* has begun to develop, aiming at reintroducing in hydrodynamic theory all the fluctuations which are typically neglected when considering systems with a huge number of particles. However, fluctuating hydrodynamics of nonequilibrium systems often relies on equilibrium assumptions; otherwise, some successful attempts of rigorous derivation for nonequilibrium systems have been done, but represent a very hard technical challenge and therefore are limited to some specific cases.

The goal of this thesis is to derive a fluctuating hydrodynamic description of granular and active matter by means of controlled and transparent mathematical assumptions. The main hypothesis that we want to prove is not only that such a

description is possible, but that the specularity between granular and active matter generates a powerful symmetry in their description, and that the theoretical and phenomenological description of one of them can be used to describe the other.

To achieve this result, we have made use of *lattice models*. These are a powerful tool in statistical physics, and since their introduction in the description of equilibrium phenomena such as phase transition in ferromagnetism (Ising or Heisenberg model) or diffusive behavior (Kipnis-Marchioro-Presutti model or exclusion processes) they lead to a large number of analytical results. While some realism is necessarily sacrificed when constraining continuous observables such as space and time on a lattice, one can recover *exactly* an off-lattice behavior in the continuum limit of large system size or number of particles. Thus, we look for a lattice model which is able to reproduce the average hydrodynamical features and at the same time produce new predictions on fluctuating hydrodynamics.

To do this, this thesis is organized as follows:

- The **First Chapter** is devoted to introduce granular matter, giving a precise definition of what is granular and a review of its principal phenomenological properties. The formulation of kinetic theory for conservative interactions is given, and later applied to the granular case where it is shown to be consistent and predictive. Some of the most important granular states will be introduced, before discussing their hydrodynamic behavior in the third Chapter.

- The **Second Chapter** introduces the reader to active matter: again, in the first section a review of active systems, phenomenology and principal experiments are given. The second section focuses on the modelization of active matter, introducing the most important models formulated in the last years to reproduce self-propulsion and active interactions. The last section is dedicated to the analysis of some key experiments showing a possible active behavior for driven granular systems.

- The **Third Chapter** is dedicated to hydrodynamics. The classic formulation of hydrodynamics through the Chapman-Enskog approach is sketched, and later applied to the granular case and the study of its hydrodynamical instabilities. An overview of hydrodynamics of active matter is given and compared with previous cases. Finally, some of the most important lattice models are introduced both for conservative and dissipative systems: the latter have been the main source of inspiration to develop the content of this thesis.

- The **Fourth Chapter** introduces a granular lattice model to investigate fluctuating hydrodynamics of shear modes: the hydrodynamic equations are derived from microscopic dynamics through a continuum limit. Depending on boundary conditions, the model is able to reproduce several granular states such as the Homogeneous Cooling State, the Uniform Shear Flow state and the Couette Flow state. The former is known to be unstable for high dissipation or system size: threshold values are found from analytical calculations,

confirming the correspondence between the lattice model and off lattice behavior. Furthermore, we move to fluctuating hydrodynamics description, and the noise properties of hydrodynamic currents are derived without the need of equilibrium approximations. The numerical study of these analysis is presented, observing an excellent agreement between theoretical results and simulated behavior

- The **Fifth Chapter** contains the properties of the granular model introduced when Molecular Chaos assumption is abandoned, i.e. next-neighbor correlations are reintroduced in the dynamics. Interestingly, for the defined model it is possible to compute the velocity correlations, showing how they affect temperature evolution in the Homogeneous Cooling State. Indeed, it is possible to derive a closed set of equations for temperature and velocity which can be solved in the continuum limit. The analytical results explain some numerical discrepancies observed in the temperature decay. Furthermore, the total energy fluctuations are computed: with a similar procedure, their divergence from the Local Equilibrium value is explained for a wide range of dissipation magnitudes.

- The **Sixth Chapter** introduces a lattice model of active matter. Through the procedure applied in the two previous chapters, it is possible to define a lattice model of self-propelling particles and derive its hydrodynamic equations, showing the presence of experimentally observed collective behavior such as swarming and clustering depending on microscopic parameters such as dissipation rate and self-propulsion noise. The model generalizes the previous model to hopping particles in $d > 1$. The noise of density, momentum and energy current can be derived as before. Simulations have confirmed the linear stability analysis of the disordered state and the transition to ordered motion, as well as theoretical predictions on fluctuating hydrodynamic currents

- The **Appendices** contain the derivation of analytical results for the granular model presented in Chapter 4 and 5 (Appendix A) and for the active model of Chapter 6 (Appendix B). The Appendix C contains a list of link to videos, aimed at a novel reader to illustrate the phenomenology introduced in the first part.

Part I

Granular and Active Matter

Like lesser birds on the four winds
Like silver scrapes in May
Now the sands become a crust
And most of you have gone away

1 Granular Matter

1.1 What is granular matter

Every physical system made by a large amount of macroscopic or mesoscopic particles, called *grains*, is a granular material: typical examples are sand, dust, pills, seeds, as well as iceberg groups and Saturn rings [98, 159]. Granular matter is ubiquitous in everyday life: when we transport food, build houses, stock products, project industrial processes and so on. Understanding its qualities has a great importance to predict and reproduce the behavior of such materials.

Granular materials share the following properties:

- grains are *macroscopic*: they follow the laws of classical mechanics and have a large number of internal degrees of freedom, which one does not directly observe during experiments;
- grains are *solid*: they occupy a volume which is excluded to other grains during their motion;
- grains interact by means of *dissipative interactions*: because of the presence of internal degrees of freedom, after a collision the total energy of two particles is partially dissipated, mainly because of grains deformation, as heat. Therefore friction occurs at the first level of description for a granular fluid;
- temperature doesn't affect granular dynamics, i.e. grains can always be considered at $T = 0$. Indeed, since grains are macroscopic their mechanical energy is typically many order of magnitude larger than their internal energy, namely $mv^2 \gg k_B T$ for a particle moving with velocity v. In kinetic theory a *granular temperature* can be introduced from statistical properties of granular motion, but it has nothing to do with room temperature.

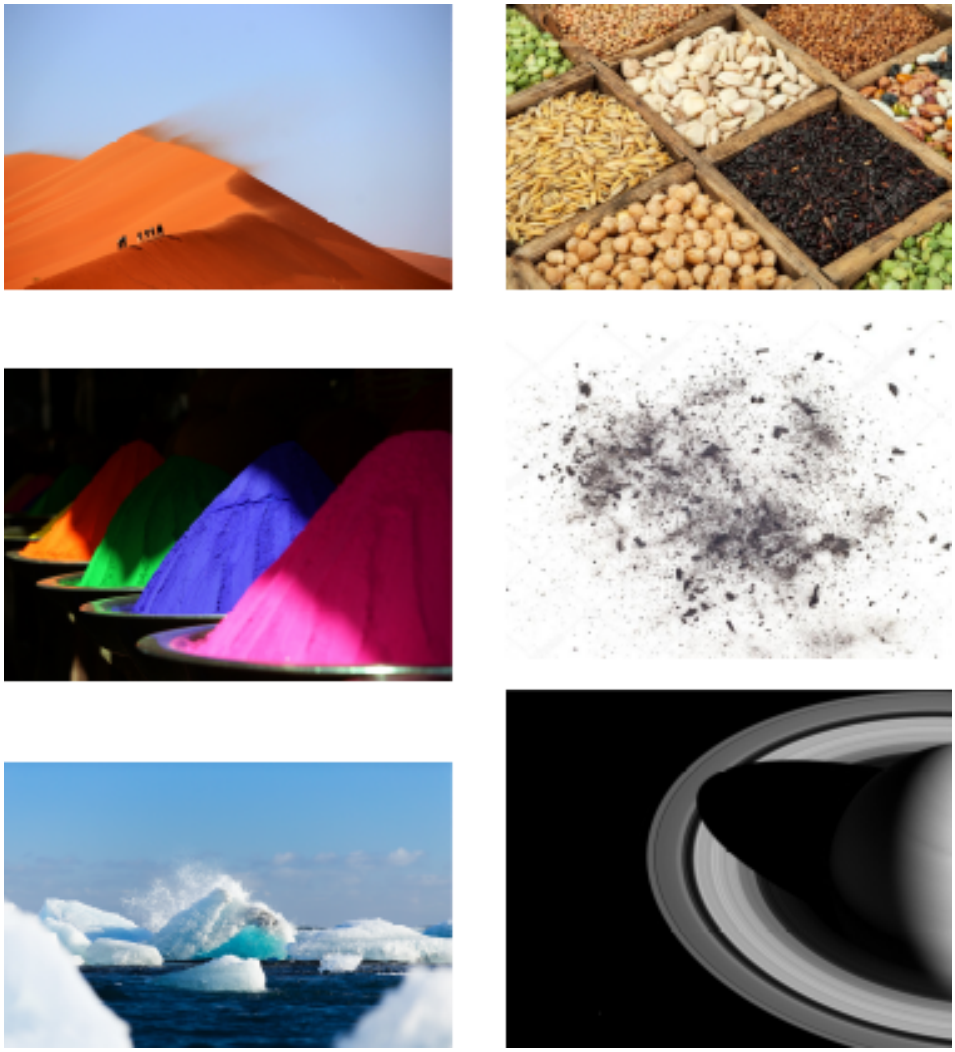

Figure 1.1. Several examples of granular materials. From top to bottom: sand dunes, color powders and iceberg group (left column), cereals and legumes, carbon dust, Saturn rings (right column).

Let us try to explain their physical meaning: since a granular material is made by many particles, statistical mechanics is the principal theoretic tool to understand its behavior. However, even if all the above-stated properties are quite general, one can see that a granular material is intrinsically different from an elastic fluid or a solid: the classic nature of grains makes the law of quantum mechanics unnecessary, and therefore the correct statistical representation must consider classic observables and interactions. Of course, each grain is made by atoms following the laws of quantum mechanics, but at this stage the grains are the "elementary particles" of our system.

Another key feature to understand granular dynamics is the role of *inelasticity*: it is known that elastic collisions are not an ideal case in physics but they ceaselessly occurs between atoms and molecules because of energy conservation. Since grains have many internal degrees of freedom, after a collision they can distort and

even break into more parts; these processes need energy which comes from the kinetic energy of grains, which therefore decreases after a collision. Typically, the inelasticity is measured by the *restitution coefficient* α (see Sec. 1.4), which ranges from 1 in the elastic case to 0 when collisions are totally inelastic.

The dissipative nature of interactions has lots of consequences in granular physics; one of the most important, which will be persistently remarked all along this thesis, is that granular matter is intrinsically *out of equilibrium*: the lack of energy conservation at this level of description imply that phase-space trajectories are not symmetric under time reversal. This is evident in the case of granular cooling, when energy dissipation leads the system to a metastable state where all the grains stop with zero kinetic energy.

The only way to avoid the inevitable cooling of a freely evolving granular gas is to *drive* the system by supplying power from outside: this is done both theoretically and experimentally by means of some shaking or shearing mechanism. These provide continuous injection/dissipation of energy in the system leading to a *non equilibrium steady state* (NESS).

The reader must then move away from classical concepts elaborated in statistical mechanics, and forget about temperature as a physical parameter of the reservoir surrounding the system. From now on, only granular temperature is considered, which depends on kinetic energy of grains and generally coincides with the variance of their velocity (if $m = k_B = 1$). Driving devices act as a thermostat, forcing granular velocity distribution toward a given temperature. Typically, when considering shaken granular gases subject to the force of gravity, the shaking acceleration needs to be larger than the gravity acceleration g, so that a grain colliding with a wall in the bottom gets the kinetic energy to reach the maximum height of the physical system. The energies involved in this process are then kinetic energy and gravitational potential energy. Furthermore, from now on materials with elastic interactions will be indicated as elastic materials, as distinct from granular materials which are always inelastic.

All the properties above-stated define a granular material: evidently they are not independent one from another but deeply related – the dissipation is the consequence of the mesoscopic space scale chosen, which is possible only in classical mechanics. There is another feature which is not required to be granular but that occurs in almost all granular systems: the *number of particles* in a granular material is large, typically ranging from 10^2 to 10^5 in most experiments and physical systems studied, therefore statistical mechanics description is adopted because following the individual motion of each particle is impossible at a theoretical level. However, if compared with molecular materials, containing an Avogadro's number of particles $N_A \sim 10^{23}$, the number of grains is very small. This is a crucial property: indeed statistical mechanics makes plentiful use of thermodynamic limit, to exploit limit theorems such as Law of large numbers and Central limit theorem. This can be done in granular matter as well, but fluctuations become very relevant when compared with molecular systems. Therefore, their theoretical and experimental description is a key point to understand granular dynamics: this is typically carried on by means of mathematical tools such as stochastic equations and large deviations theory. The goal of this thesis is to formulate a hydrodynamic description of granular and active matter capable to accounting for large fluctua-

tions: this kind of theory is called *fluctuating hydrodynamics*, and will be described in Sec. 3.2.

1.2 Granular states

Here some particular properties of granular materials at rest are reviewed: the reader may find a more detailed and complete overview in [59, 98], with a comparison between granular phases (solid, liquid, gases). The aim of the present section is to introduce some characteristic granular properties underlining their differences with molecular materials and show their connections with equilibrium statistical physics, when they can be done.

1.2.1 Granular pressure, internal stresses, jamming

When a silo is filled with a granular, the pressure at the bottom grows with the height of the filling in a rather different form from a classic fluid: indeed, a Newtonian fluid follows Stevin law [119]

$$p_v(h) = \rho g h \tag{1.1}$$

with p_v the vertical pressure, ρ the density of the fluid, g the gravity acceleration and h the height of the fluid column above the position of measurement. The pressure in a granular material follows a different law, discovered by H. A. Janssen in 1895 [100], i.e.

$$p_v(h) = \Lambda\rho g - (\Lambda\rho g - p_v(0))e^{-h/\Lambda} \tag{1.2}$$

where Λ is a characteristic length of the order of the cylinder radius R. Janssen law accounts for saturation in granular cylinders, which guarantees a constant flow rate in a hourglass. Janssen himself gave a first derivation, with the following assumptions:

1. the vertical pressure p_v is constant in the horizontal plane;
2. the horizontal pressure p_h is proportional to the vertical pressure, i.e. $K = p_h/p_v$ constant in space;
3. the wall friction $f = \mu p_h$ sustains the vertical load at contact with the wall;
4. the granular material has constant density ρ at all heights.

The mechanical equilibrium of a granular disk of radius R and height dh therefore reads

$$\pi R^2 \frac{dp_v}{dh} dh + 2\pi R\mu K p_v dh = \pi R^2 \rho g dh \tag{1.3}$$

leading to

$$\frac{dp_v}{dh} + \frac{p_v}{\Lambda} = \rho g \tag{1.4}$$

where $\Lambda = R/(2\mu K)$. Janssen law in eq. (1.2) is the corresponding solution with boundary condition $p_v(0)$.

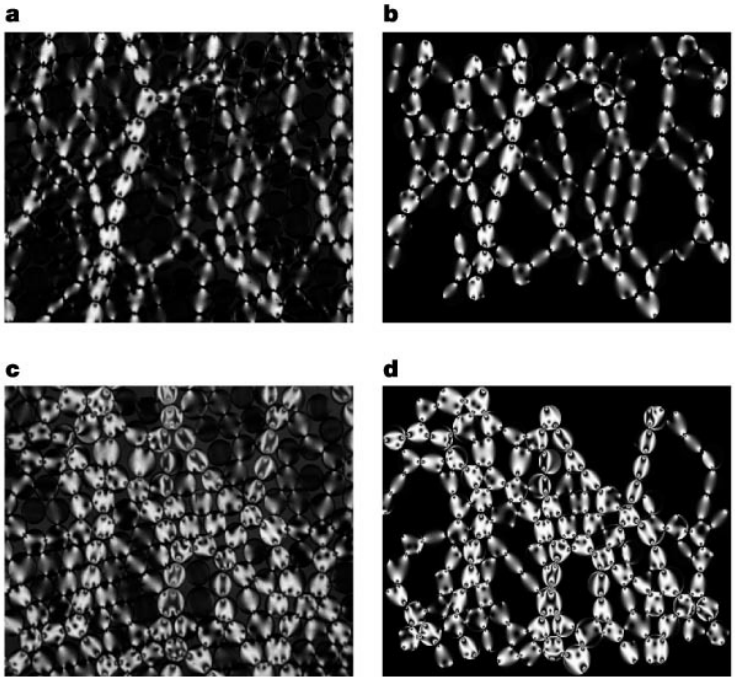

Figure 1.2. Force chains in a granular material, experimental observations (a,c) and numerical simulations (b,d). Grains are photoelastic birefringent disks subjected to pure shear (top pair) or isotropic compression (bottom pair) [131].

Previous assumptions are not obvious: the first one is generally false because the pressure depends also on the radial distance from the cylinder axis, while the second assumption should be justified from constitutive relations, relying on microscopical features of the model. Nevertheless, Janssen law is a good first step to go beyond elastic fluids laws. Vertical and horizontal pressure are connected with *stresses*: in an elastic fluid at equilibrium, it is known that stress tensor is uniform, isotropic and diagonal. This is not what actually happens in granular materials: every grain discharges its load to underlying grains, creating long force chains and propagating the stress in random directions depending on the specific configuration at rest. An experimental and numerical observation of force chains is shown in Fig. 1.2.

Another remarkable phenomenon revealed by experiments on granular statics are *pressure fluctuations*: when a container is poured several times with a granular material, pressure at its bottom can change of more than 20% between two distinct realizations [36]. Furthermore when considering a single pouring, the distribution of stresses in the bulk or at the bottom of the silo shows an exponential tail [148].

Internal pressure behavior is directly related with *sound propagation* in granular mediums: it has been experimentally shown by Liu and Nagel [126] that when the bulk is perturbed by a harmonic force (4 Hz) fluctuations can be very large, with a power-law spectrum $f^{-\alpha}$ where $\alpha = 2.2 \pm 0.05$. Also, the same authors observed that the sound group velocity can reach 5 times the phase velocity and that changing the amplitude of vibration gives rise to an hysteretic behavior [127].

As it has been shown, pressure act on granular particles in a quite different

way from an elastic medium, because of formation of long-ranged threadlike force chains and presence of strong fluctuations, signature of the strong disorder in the bulk of the medium. A consequence of these features is the phenomenon of *arch formation*: when a granular is flowing through a hopper, the flow can suddenly stop because of the formation of a stable arch over the opening, able to sustain the entire load of the grains overhead (see Fig. 1.3). This phenomenon is a very well known experience in everyday life: many times, when pouring a granular substance from one container to another, if the outlet is too small the grains spontaneously stop pouring and one typically needs to shake the medium to start again. Generally speaking, the transition occurring when vibrated or flowing granular particles get stuck together in a single compact aggregate is called *jamming transition*.

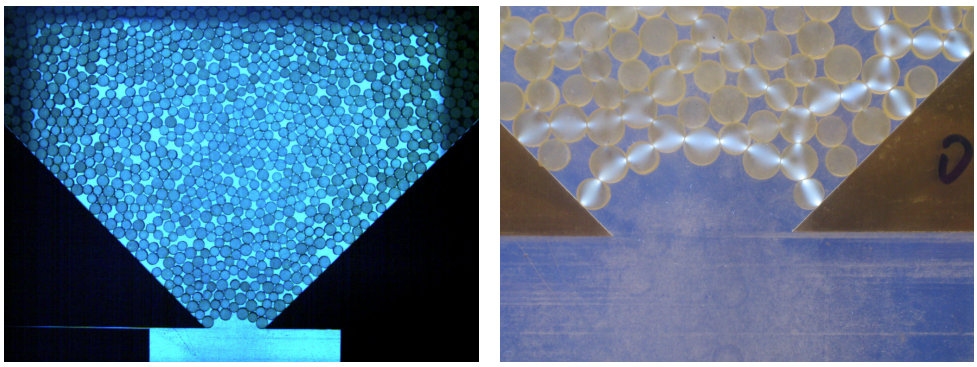

Figure 1.3. Arch formation and granular jamming. Left panel shows how a concave arch supports the whole granular above it. Right panel show arch forces near the outlet.

In 1961, Beverloo *et al.* experimentally found the existence of a critical opening size below which jamming occurs [22]; more recently [183], experiments have shown the quantitative behavior of the jamming probability in function of the opening parameter $d = R/D > 1$ and the hopper angle φ, where R is the diameter of the outlet and D is the radius of monodisperse spherical grains (see Fig. 1.4a). This effect has recently been studied in experiments by Tang and Behringer [180, 179]:

Jamming transition is a typical example of a granular *phase transition*, although being out of equilibrium this has not the same meaning of equilibrium transitions, where a free energy can be defined and the transition shifts the system from an equilibrium state to another. Jamming transition has been investigated theoretically [39, 125, 173, 110] and experimentally [58, 132], leading to a strong comparison with liquid-glass transition in glassy systems. Specifically, a phase diagram can be written in terms of granular temperature, packing fraction and external stress [125]. When considering the behavior of dense packing of granular particles flowing down a rough, inclined plane, it has been shown that the tilt angle θ plays the role of control parameter in analogy with the temperature T in glass transition [173]. Furthermore, experiments in a $2d$ granular system of photoelastic bidisperse disks with moving walls have shown a power-law behavior of the mean contact number Z and the granular pressure P above the critical value of packing fraction $\phi_c = 0.8422$, namely $Z \sim P \sim (\phi - \phi_c)^\beta$, with $0.5 < \beta < 0.6$ [132]. All the

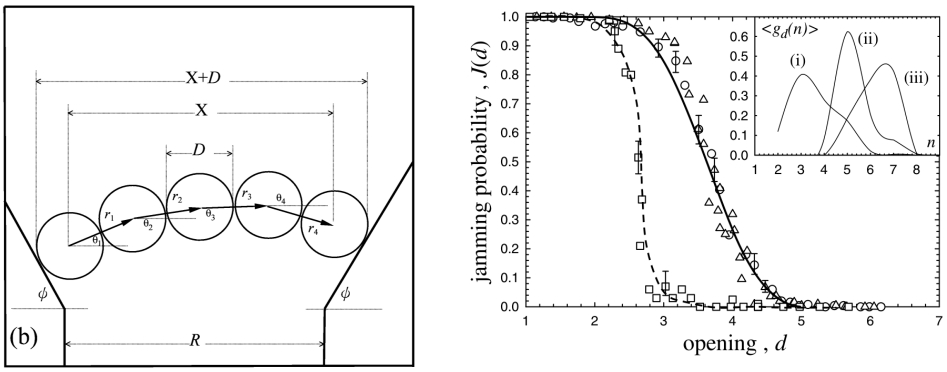

(a) (b)

Figure 1.4. Granular jamming probability flowing through a hopper [183], experimental setup (left) and jamming transition (right). The jamming probability $j(d)$ is plotted versus the opening parameter d, for three hopper angles φ= 34° (circles), 60° (triangles) and 75° (squares). The solid line is a theoretical prediction provided by the authors, the dashed line is a guide to the eye for the φ=75° case.

cited studies converged in stating that in granular jamming a critical behavior is actually observed, even though granular materials are far from equilibrium.

1.3 Granular flows

When a granular material is flowing, two kinds of regime can occur: *slow* or *rapid* flow. While in the former grains are always in contact with their neighbors and interact frictionally for macroscopic times, in the latter they typically move ballistically between two inelastic collisions, which are instantaneous events. The rapid or slow behavior is generally governed by the granular density, its typical acceleration and boundary conditions. In rapid granular flows the analogy with kinetic representation describing elastic gases is strong: in the next sections it will be shown how a kinetic theory can be built from microscopic interactions, leading to a macroscopic picture of granular flow and to hydrodynamics. In this section some characteristic features of rapid granular flows are introduced.

1.3.1 Rapid granular flows

Many experiments have been made to investigate the behavior of *sheared* and *shaken* granular fluids [164]. Two kinds of experimental setups can be distinguished:

- *Couette rheology*, consisting of a granular medium placed between two cylindrical walls with the same axis, and rotating one or both of them to induce shear formation in the granular. Physical parameters are the distance between the cylinders, rotational speed and packing fraction of the granular.

- *Shakers*, consisting of a granular medium in a container whose one or more walls are vibrated. Typical parameters of these systems are vibrations amplitude A and frequency ω, which can be compared with gravity acceleration

g through the vibration parameter $\Gamma = A\omega^2/g$: when $\Gamma > 1$, the vibration is strong enough to produce many phenomena that will be described below. The transition from slow to rapid granular flow induced by vibration is often called *vibrofluidization*.

In both cases the shear or the shaking can be sufficient to lead the system to a stationary state, i.e. to avoid the inelastic cooling. However, tuning the above-stated parameters the granular medium can change qualitatively its features, moving from a slow granular motion to a fluidized state of rapid flow. Here some characteristic phenomena of granular fluids are reviewed:

- **Stress fluctuations**: it has already been mentioned that in granular statics stresses are not homogeneous and exhibit strong fluctuations; when a $2d$ bidisperse granular is sheared in a Couette geometry, a strengthening/softening transition has been observed [93]. Below a threshold value of the packing fraction $\phi_c \simeq 0.776$, stress fluctuations are small, the granular is compressible and stress chains are long and radial; above this value strong fluctuations occurs, compressibility becomes large and the network of stress chains becomes tangled and dense.

- **Slow convection and size segregation**: when a granular is shaken or sheared, convection takes place. If the granular is heterogeneous, size segregation occurs as well. These features are known for a long time and have been recently investigated in experiments with Couette cylinders [106] and vertically vibrated granulars [95]: larger particles use to rise to the top of the granular medium during its motion, carried by convective cells formation. This effect is also known as the *Brazil-nut effect*, because when opening a box of cereals it is common to find the larger ones (Brazil-nuts) at the top [146]. Further experiments have shown that size segregation depends both on relative diameter, density and on shaking frequency: indeed, at low frequencies segregation is governed by inertia and convection, and denser particles rise faster. On the other hand, at high frequencies the granular is fluidized and there is no convection, so an intruder sinks if it is denser than the surrounding grains, and buoys up otherwise [95].

- **Pattern formation**: experiments have shown the formation of surface waves patterns in vertically vibrated granular layers [144, 145, 107, 3], which exhibit various and fascinating textures (see Fig. 1.5a) depending on the set of parameters of the granular system: vibration frequency, vibration parameter Γ, size of the system, size and shape of the grains, and so on. This behavior has been associated also to the presence of *oscillons*, namely spatially localized excitations with the propensity to assemble into molecular or crystalline structures, see Fig. 1.5b [187].

- **Clustering**: cluster formation in granular fluids has been analyzed numerically and theoretically in granular cooling [83] and later observed experimentally in shaken systems [115, 113, 73, 72]. Clustering is not observed in elastic fluids, and is carried on by inelastic collisions: actually in a dense region granular temperature decreases faster than in a dilute one because col-

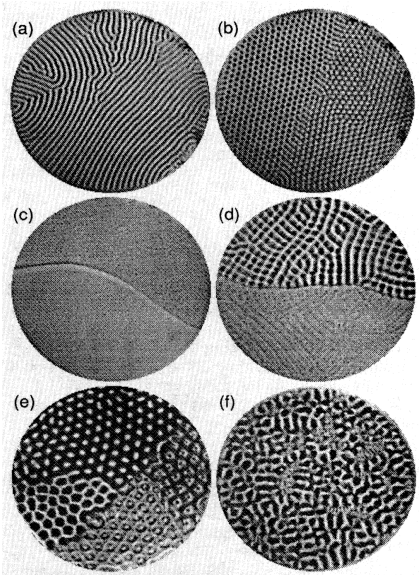

(a) Patterns in a vertically vibrated granular layer: stripes (a), hexagons (b,e), flat with kink (c), competing squares and stripes (d), and disorder (f) [145].

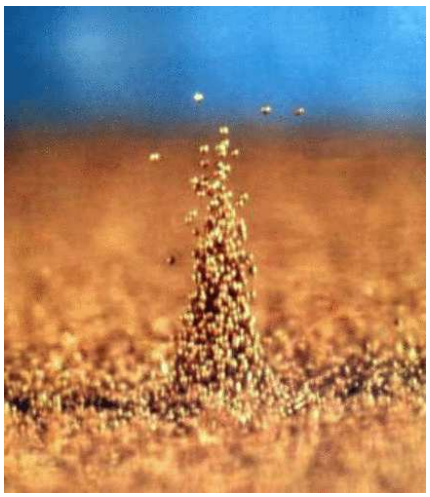

(b) An oscillon, a solitary standing wave on the surface of a vibrated granular layer [3].

Figure 1.5. Patterns (left) and oscillons (right).

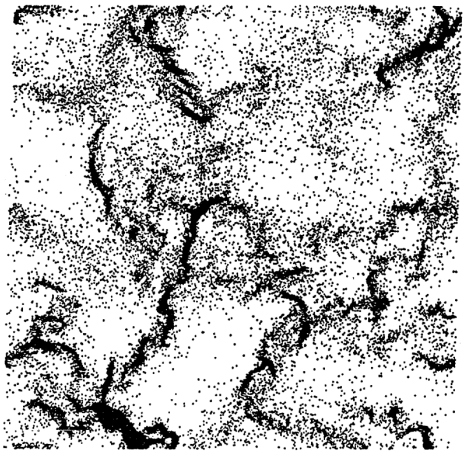

(a) Snapshot of a clustered granular system [83].

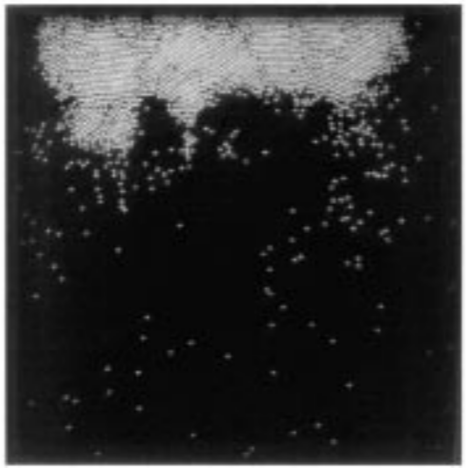

(b) Cluster formation in a granular fluid shaken by the horizontal wall at the bottom [73].

Figure 1.6. Clustering: numerical simulations (left) and experiments (right)

lisions are dissipative, yielding a decrease of the granular pressure: the pressure gradient created leads then to a migration towards the dense region. Therefore, once a density fluctuation appears, the dense region will attract

other particles and grow, unless some hydrodynamic mechanism intervene to scatter particles faster than the clustering process [83]. A numerical sketch of a granular cluster is shown in Fig. 1.6a. Clustering appears as a *hydrodynamic instability* of the homogeneous cooling state of a granular medium, connected as well with shear instability: the study and analysis of instabilities will play a crucial role in Part II of this thesis. Finally, in above-cited experiments [73, 72] a transition has been observed when the number of particles is increased, moving from a gas-like behavior to a collective solid-like behavior: the latter is shown in Fig. 1.6b.

- **Non-Gaussian velocities**: velocity distributions in granular fluids are often non-Gaussian: this feature has been observed in numerical simulations and confirmed by experiments [150, 151, 113], which have proved a strong connection between clustering and velocity distributions [166]. Indeed, when particles cluster, *inelastic collapse* can occur [141, 142], namely particles stuck together because of inelastic collisions and start moving at the same parallel velocity. Clustering and inelastic collapse create regions with high density and low velocities, resulting in nearly exponential tails in velocity distribution, see Fig. 1.7. In a different experiment [128], velocity distributions revealed exponential tails in a cooling state and $\exp(-v^{3/2})$ tails in a driven state, verifying theoretical predictions in [188]. Nevertheless, non-Gaussianity can be observed in absence of clustering as well: a successive experiment measured the horizontal velocity distribution of a vertically vibrated vertical monolayer, obtaining again a $\exp(-v^{3/2})$ velocity distribution also without clustering.

- **Velocity correlations**: strong long-range velocity correlations between granular particles have been revealed in experiments with dense granular gases [26], similar to the setup of [113] used to investigate non-Gaussian distributions. Furthermore, recent experiments studied velocity structure factors in a quasi-$2d$ vertically vibrated horizontal granular monolayer by means of fluctuating hydrodynamics (see Sec. 3.2), confirming the validity of the theory [85, 165]. Experiments also displayed a correlation length which increases with the packing fraction.

- **Thermal convection**: very recently, an experiment on a vibrofluidized granular gas has shown the existence of a convection mechanism driven by the inelastic interactions with the walls of the container where the granular is shaken [157]. We already discussed the case of slow convection, which is generally a phenomenon driven by bulk buoyancy for slow flows. Experiments and simulations considered the case of a vibrated granular gas on a $2d$ inclined plane: the bottom wall is shaking the gas with accelerations much greater than the effective gravity. The presence of inelastic vertical walls is the key point of the establishment of thermal convection: since energy is dissipated at the boundaries, an *horizontal* temperature gradient is induced: thus, in the system described any steady state must have flow and, since the system is closed in the horizontal, the flow will be convective.

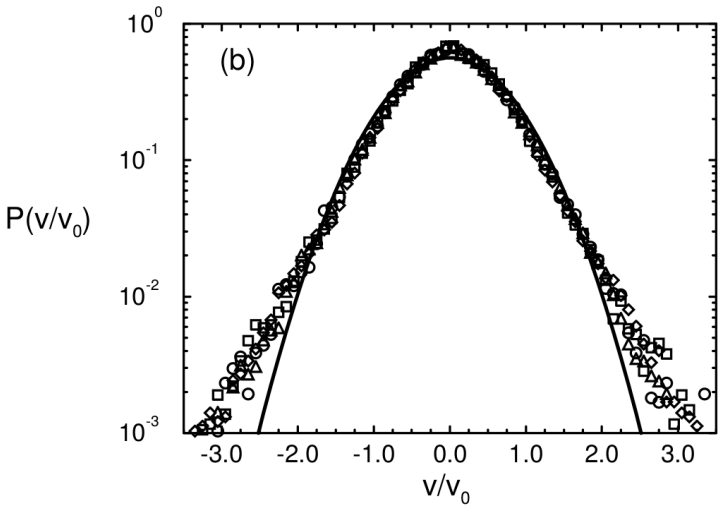

Figure 1.7. Horizontal velocity distributions in a vertically vibrated granular monolayer, rescaled by the second moment, for different vibration amplitudes Γ [150].

The granular features above-described have been chosen among the main studied and will be recalled in the following of this thesis; nevertheless, several outstanding features and applications of granular flows have been investigated in the last years, such as *granular jets* [182], *stick-slip frictional properties* [4, 111], a granular *Leidenfrost effect* [71], Kovacs-like memory effects [102, 31, 163] and *granular ratchets* [50, 53, 70] - see also Sec. 2.3. In Appendix C one can found several links to videos showing many of these granular effects.

Many of these studies converged in giving an experimental validation of kinetic theory [129, 194, 196]: the latter is actually the starting point of the present theoretical investigation.

1.4 Kinetic Theory of Rapid Granular Flows

A powerful approach to the study of rapid granular flows is given by *kinetic theory*: established for the study of elastic gases, its aim is to describe a gas in term of mechanical coordinates of all its particles to derive its macroscopic properties such as pressure, energy and entropy through the statistical properties of the microscopic variables. This method, which was derived for elastic gases, can apply also for granular materials.

In the present section classical kinetic theory will be introduced, showing how one can derive Boltzmann Equation from Liouville equation for *elastic* smooth hard spheres, moving later to inelastic hard spheres. Kinetic theory will be used to describe the simplest granular regime, the *homogeneous cooling state*, and its instabilities. The last part of this section is an introduction of granular *steady states* and the so-called *steady state representation*. This section is based on the analysis described in [45, 94] for elastic models, while granular kinetic theory has been deeply studied in [158, 34]. The following section follows the formulation presented in [164].

1.4.1 From Liouville to Boltzmann Equation

A system of N classical particles in a container of volume V is fully determined once the particles' positions and momenta configuration $\mathbf{z}(t)$ at a given time t and their interaction are known, where

$$\mathbf{z}(t) = \{\mathbf{r}_1(t), \mathbf{v}_1(t), \mathbf{r}_2(t), \mathbf{v}_2(t), \ldots, \mathbf{r}_N(t), \mathbf{v}_N(t)\} \in V^N \times \mathbb{R}^{3N} = \Gamma \tag{1.5}$$

introducing Γ as the full phase-space of the system. For an Hamiltonian system, the configuration is given by generalized coordinates and momenta, for which kinetic theory is usually developed. However this is not our case, because granular matter is not Hamiltonian. Since it is impossible to follow the equations of motion of $N \gg 1$ particles, kinetic theory looks at the time-dependent probability density function $\mathcal{P}(\mathbf{z}, t)$, representing the probability of finding the system in a configuration $\mathbf{z}$ at time t. This implies that the value of a dynamical observable $A(\mathbf{z})$ is equivalent to

$$\int_\Gamma \mathrm{d}\mathbf{z}\mathcal{P}(\mathbf{z}, 0)A(\mathbf{z}(t)) = \int_\Gamma \mathrm{d}\mathbf{z}\mathcal{P}(\mathbf{z}, t)A(\mathbf{z}), \tag{1.6}$$

which respectively correspond to the Lagrangian and Eulerian averages. The evolution of A is given by the equations of motions of the configuration $\mathbf{z}$, but can be resumed into the *streaming operator* S_t, defined by $A(\mathbf{z}(t) \equiv S_t(\mathbf{z})A(\mathbf{z})$ [164]. Therefore, the equivalence in (1.6) means that

$$\mathcal{P}(\mathbf{z}, t) = S_t^\dagger \mathcal{P}(\mathbf{z}, 0). \tag{1.7}$$

where S^dagger_t is the adjoint operator of S_t. In a general system where particles are subjected to conservative and additive interactions and no external field is present, the streaming operator reads

$$S_t(\mathbf{z}) = \exp[tL(\mathbf{z})] = \exp\left[t\left(\sum_i L_i^0 - \sum_{i<j}\Theta_{ij}\right)\right], \tag{1.8}$$

where the *Liouville operator* $L(\mathbf{z})\cdot \equiv \{H(\mathbf{z}), \cdot\}$ is the Poisson bracket with the Hamiltonian function, so that

$$L_i^0 = \mathbf{v}_i \cdot \frac{\partial}{\partial \mathbf{r}_i}, \tag{1.9a}$$

$$\Theta_{ij} = \frac{1}{m}\frac{\partial U(r_{ij})}{\partial \mathbf{r}_{ij}} \cdot \left(\frac{\partial}{\partial \mathbf{v}_i} - \frac{\partial}{\partial \mathbf{v}_j}\right), \tag{1.9b}$$

represent respectively the free streaming operator L_i^0 and the interaction term Θ_{ij} depending from the form of the binary interaction among the particles, $U(r_{ij})$. S_t is a unitary operator, with $S_t^\dagger = S_{-t}$ and $L^\dagger = -L$. Rewriting Eq. (1.7) in terms of Eq. (1.8) the *Liouville equation* is obtained

$$\frac{\partial}{\partial t}\mathcal{P}(\mathbf{z}, t) = \left(-\sum_i L_i^0 + \sum_{i<j}\Theta_{ij}\right)\mathcal{P}(\mathbf{z}, t) \tag{1.10}$$

which expresses the incompressibility of the flow in phase space. Textbooks use to refer to this equation when introducing Liouville's Theorem [94], stating that the distribution function of an Hamiltonian system is constant along any trajectory in the phase space, namely

$$\frac{\mathrm{d}}{\mathrm{d}t}\mathcal{P}(\mathbf{z},t)=0. \tag{1.11}$$

Let us consider the case of a system made by N identical hard spheres of diameter σ and mass m: the potential $U(r)$ is defined as

$$U(r)=\begin{cases}0 & r>\sigma,\\ +\infty & r<\sigma,\end{cases} \tag{1.12}$$

where r is the distance between two particles. $U(r)$ is a discontinuous potential, which makes collisions instantaneous: indeed, when particles i and j collide, their precollisional velocities $(\mathbf{v}_i,\mathbf{v}_j)$ abruptly change to postcollisional velocities $(\mathbf{v}_i',\mathbf{v}_j')$. In *elastic* collisions, momentum and energy conservation respectively read

$$m\mathbf{v}_i'+m\mathbf{v}_j'=m\mathbf{v}_i+m\mathbf{v}_j, \tag{1.13a}$$

$$\frac{1}{2}mv_i'^2+\frac{1}{2}mv_j'^2=\frac{1}{2}mv_i^2+\frac{1}{2}mv_j^2. \tag{1.13b}$$

Those equations can be easily solved moving to the center of mass frame, considering the total velocity $\mathbf{V}=\frac{1}{2}(\mathbf{v}_1+\mathbf{v}_2)$ and the relative velocity $\mathbf{v}_{ij}=\mathbf{v}_i-\mathbf{v}_j$; indeed, Eqs. (1.13) yield the conservation of the total momentum and of the modulus of the relative velocity. In the smooth hard spheres case, the velocities are reflected after a collision with the rule

$$\mathbf{V}'=\mathbf{V}, \tag{1.14a}$$

$$\mathbf{v}_{ij}'=-\mathbf{v}_{ij}, \tag{1.14b}$$

So, in the laboratory frame the postcollisional velocities read

$$\mathbf{v}_i'=\mathbf{v}_i-\hat{\mathbf{n}}\left[\hat{\mathbf{n}}\cdot(\mathbf{v}_i-\mathbf{v}_j)\right], \tag{1.15a}$$

$$\mathbf{v}_j'=\mathbf{v}_j+\hat{\mathbf{n}}\left[\hat{\mathbf{n}}\cdot(\mathbf{v}_i-\mathbf{v}_j)\right]. \tag{1.15b}$$

being $\hat{\mathbf{n}}=(\mathbf{r}_i-\mathbf{r}_j)/|\mathbf{r}_i-\mathbf{r}_j|$ the unit vector connecting the center of the sphere i with the center of the sphere j, see Fig. 1.8. With the present rule, the collisions can be reintroduced into the Liouville equation by imposing the boundary condition

$$\mathcal{P}(\mathbf{z}',t)=\mathcal{P}(\mathbf{z},t) \tag{1.16}$$

where $\mathbf{z}'$ is the postcollisional configuration after particles i and j have collided. An instantaneous collision occurs when particles are in contact and the relative velocity $\mathbf{v}_{ij}$ has opposite direction of $\hat{\mathbf{n}}_{ij}=(\mathbf{r}_i-\mathbf{r}_j)/\sigma$: the latter requirement is known as *kinematic constraint*, i.e. the particles must move toward each to collide. The last requirement is fundamental to guarantee that immediately after a collision

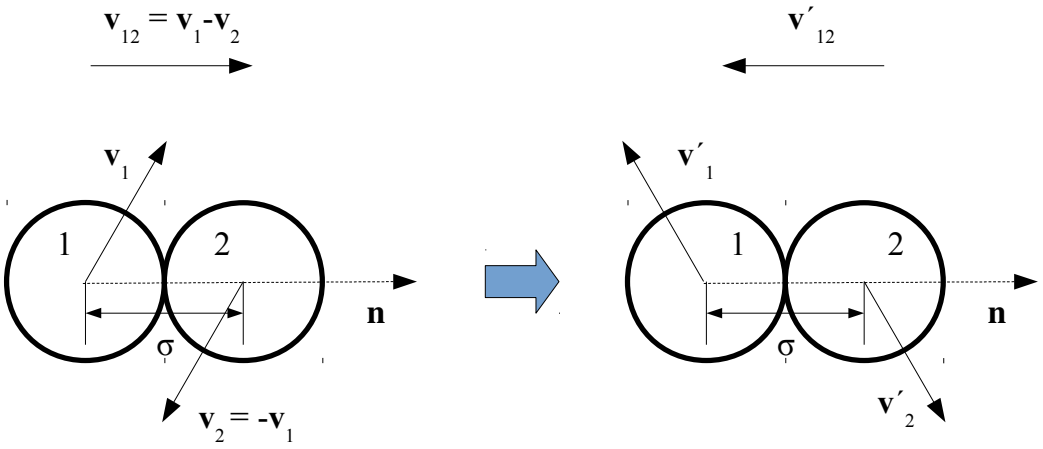

Figure 1.8. Elastic collision of identical hard spheres in the center of mass frame: pre- and post-collisional velocities have equal modulus and opposite direction. The relative velocity is parallel to the direction of collision, and is reflected after the collision. The velocity components perpendicular to the relative velocity are not affected by the collision.

the particles do not collide any more, since their velocities then point away from each other. Namely,

$$r_{ij} = \sigma, \tag{1.17a}$$
$$\mathbf{v}_{ij} \cdot \hat{\mathbf{n}}_{ij} < 0. \tag{1.17b}$$

In this case, the postcollisional phase space configuration reads

$$\mathbf{z}' = (\mathbf{r}_1, \mathbf{v}_1, \ldots, \mathbf{r}_i', \mathbf{v}_i', \ldots, \mathbf{r}_j', \mathbf{v}_j', \ldots, \mathbf{r}_N, \mathbf{v}_N) \tag{1.18a}$$
$$\mathbf{r}_i' = \mathbf{r}_i \tag{1.18b}$$
$$\mathbf{r}_j' = \mathbf{r}_j \tag{1.18c}$$

and $\mathbf{v}_i'$, $\mathbf{v}_j'$ follow the collisional rule in Eq. (1.15).

Since hard spheres cannot overlap, the effect of excluded volume changes the phase space: there is an excluded region consisting of the occupied volume called Γ_{ov} so that the actual phase space is $\Gamma = V^N \times \mathbb{R}^N - \Gamma_{ov}$, where

$$\Gamma_{ov} = \left\{ \mathbf{z} \in V^N \times \mathbb{R}^N \mid \exists\, i, j \in \{1, 2, \ldots, N\} \ : \ |\mathbf{r}_i - \mathbf{r}_j| < \sigma \right\}. \tag{1.19}$$

With the previous condition, the Liouville equation reads

$$\frac{\partial}{\partial t}\mathcal{P}(\mathbf{z}, t) = \left(-\sum_i \mathbf{v}_i \cdot \frac{\partial}{\partial \mathbf{r}_i} \right) \mathcal{P}(\mathbf{z}, t) \qquad \text{when } \mathbf{z} \in \Gamma, \tag{1.20a}$$
$$\mathcal{P}(\mathbf{z}, t) = \mathcal{P}(\mathbf{z}', t) \qquad \text{when } \mathbf{z} \in \partial\Gamma, \tag{1.20b}$$

where $\partial\Gamma$ is the boundary of the phase space Γ. The interaction term has been resumed in the time-discontinuous boundary condition in the second line, while between two collisions the particles undergo free motion at constant speed $\mathbf{v}_i$.

The discontinuity introduced prevents the use of formal perturbation expansion such as the ones usually employed in many-body theory. It can be shown [68] that an alternative expression for the streaming operator can be written in terms of binary collision operators: indeed one can write S_t for two particles labeled 1 and 2 as

$$S_t(1,2) = S_t^0(1,2) + \int_0^t \mathrm{d}\tau\, S_\tau^0(1,2) T_+(1,2) S_{t-\tau}^0(1,2) \tag{1.21}$$

where S_t^0 is the free flow operator and $T_+(1,2)$ a collisional operator

$$T_+(1,2) = \sigma^2 \int\limits_{\mathbf{v}_{12}\cdot\hat{\mathbf{n}}<0} \mathrm{d}\hat{\mathbf{n}}\, |\mathbf{v}_{12}\cdot\hat{\mathbf{n}}|\, \delta\left(\mathbf{r}_1 - \mathbf{r}_2 - \sigma\hat{\mathbf{n}}\right)\, (b_c - 1), \tag{1.22}$$

being $\mathbf{v}_{12} = \mathbf{v}_1 - \mathbf{v}_2$ and b_c a substitution operator which replaces precollisional velocities with postcollisional ones, $(\mathbf{v}_1, \mathbf{v}_2) \to (\mathbf{v}_1', \mathbf{v}_2')$. Eq. (1.21) can be interpreted as evolution of 2-particles dynamics during time t, consisting in a free flow term (no collisions) plus a convolution term considering all eventual collisions at time $0 < \tau < t$. Since two spheres alone cannot collide more than once, one notices that $T_+(1,2)S_\tau^0(1,2)T_+(1,2) = 0$ and therefore Eq. (1.21) is equivalent to

$$S_t(1,2) = \exp\left\{t\, \left[L_0(1,2) + T_+(1,2)\right]\right\}. \tag{1.23}$$

Generalizing the above equation to the N-particles streaming operator (here in the case of infinite volume) one has

$$S_{\pm t}(\mathbf{z}) = \exp\left\{\pm t\, \left[L_0(\mathbf{z}) \pm \sum_{i<j} T_\pm(i,j)\right]\right\}, \tag{1.24}$$

where $T_-(1,2)$ represents a backward collisional operator, i.e.

$$T_-(1,2) = \sigma^2 \int\limits_{\mathbf{v}_{12}\cdot\hat{\mathbf{n}}>0} \mathrm{d}\hat{\mathbf{n}}\, |\mathbf{v}_{12}\cdot\hat{\mathbf{n}}|\, \delta\left(\mathbf{r}_1 - \mathbf{r}_2 - \sigma\hat{\mathbf{n}}\right)\, (b_c - 1). \tag{1.25}$$

$S_{\pm t}(\mathbf{z})$ is defined as the *pseudo-streaming operator*. Now, a continuous-time Liouville equation can be written by means of the adjoint of $S_{\pm t}$, considering the adjoint operators of $T_\pm(1,2)$ which read

$$T_\pm^\dagger(1,2) = \sigma^2 \int\limits_{\mathbf{v}_{12}\cdot\hat{\mathbf{n}}\lessgtr 0} \mathrm{d}\hat{\mathbf{n}}\, |\mathbf{v}_{12}\cdot\hat{\mathbf{n}}|\, \left[\delta\left(\mathbf{r}_1 - \mathbf{r}_2 - \sigma\hat{\mathbf{n}}\right) b_c - \delta\left(\mathbf{r}_1 - \mathbf{r}_2 + \sigma\hat{\mathbf{n}}\right)\right]. \tag{1.26}$$

At last, the pseudo-Liouville equation can be written

$$\frac{\partial}{\partial t}\mathcal{P}(\mathbf{z},t) = \left(-\sum_i L_i^0 + \sum_{i<j} T_-^\dagger(i,j)\right)\mathcal{P}(\mathbf{z},t). \tag{1.27}$$

which represents the analogue of Eq. (1.10) for elastic hard spheres. It replaces Eqs. (1.20) and will be the starting point to write the granular pseudo-Liouville equation when considering inelastic collisions.

The first step to derive the Boltzmann equation representing the evolution of the one-particle distribution $P(\mathbf{r}, \mathbf{v}, t)$ is to consider the marginalized distribution P_s defined as

$$P_s(\mathbf{r}_1, \mathbf{v}_1, \dots, \mathbf{r}_s, \mathbf{v}_s; t) = \int\limits_{V^{N-s} \times \mathbb{R}^{3(N-s)}} \left(\prod_{j=s+1}^{N} \mathrm{d}\mathbf{r}_j \mathrm{d}\mathbf{v}_j \right) \mathcal{P}(\mathbf{r}_1, \mathbf{v}_1, \dots, \mathbf{r}_N, \mathbf{v}_N; t). \tag{1.28}$$

Integrating over $\left(\prod_{j=s+1}^{N} \mathrm{d}\mathbf{r}_j \mathrm{d}\mathbf{v}_j\right)$ both sides of Eq. (1.20a) and implementing boundary conditions in (1.20b), it can be shown [164] that P_s follows the evolution equation

$$\frac{\partial P_s}{\partial t} + \sum_{i=1}^{s} \mathbf{v}_i \cdot \frac{\partial P_s}{\partial \mathbf{r}_i} = (N-s)\sigma^2 \sum_{i=1}^{s} \int\limits_{\mathbb{R}^3} \int\limits_{S^+} (P'_{s+1} - P_{s+1}) |\mathbf{V}_i \cdot \hat{\mathbf{n}}| \mathrm{d}\hat{\mathbf{n}} \mathrm{d}\mathbf{v}_* \tag{1.29}$$

where $\mathbf{V}_i = \mathbf{v}_i - \mathbf{v}_*$, S_+ is the hemisphere of $\hat{\mathbf{n}}$ having $\mathbf{V}_i \cdot \hat{\mathbf{n}} > 0$ and P'_{s+1} is defined as

$$P'_{s+1} = P'_{s+1}(\mathbf{r}_1, \mathbf{v}_1, \dots, \mathbf{r}_i, \mathbf{v}_i - \hat{\mathbf{n}}(\hat{\mathbf{n}} \cdot \mathbf{V}_i), \dots, \mathbf{r}_s, \mathbf{v}_s, \mathbf{r}_i - \sigma\hat{\mathbf{n}}, \mathbf{v}_* + \hat{\mathbf{n}}(\hat{\mathbf{n}} \cdot \mathbf{V}_i)). \tag{1.30}$$

The interpretation of Eq. (1.29) is straightforward : its lhs represents the evolution of P_s under the free s-particles flow, while the rhs represents the gain and loss terms of the s-particles configuration due to collisions with one of the remaining $N - s$ particles, which probability is given by the P_{s+1} distribution. The system of Eqs. (1.29) is known as *BBGKY hierarchy*[1]: indeed, starting from the one-particle distribution P_1, its evolution equation contains P_2, as well as the evolution equation of P_2 contains P_3 and so on... Clearly, this set of equations is closed only if one considers all the marginalized distribution functions up to $P_N \equiv \mathcal{P}(\mathbf{z})$, but this means coming back to the original Liouville equation.

This theoretical limit can be overcome in the case of a rarefied gas, which applies when considering a box of volume 1 cm^3 at atmospheric pressure and room temperature, for which one has $N \sim 10^{20}$, $\sigma \sim 10^{-18}$ cm, hence for small s $(N-s)\sigma^2 \sim N\sigma^2 \sim 1\text{m}^2$; furthermore, the difference between $\mathbf{r}_i$ and $\mathbf{r}_i + \sigma\hat{\mathbf{n}}$ can be neglected compared with system size, as well as the occupied volume $N\sigma^3 \sim 10^{-4}$ cm^3, so that the collision between two *selected* particles can be considered a rare event. These considerations lead to the so-called *Boltzmann-Grad limit*, which consists in taking $N \to \infty$ and $\sigma \to 0$ while $N\sigma^2$ remains finite. It is remarkable that the scattering cross section for two hard spheres is $\pi\sigma^2$, so that in a system with volume and typical velocities of order 1 the total cross section multiplied by N reads $N\pi\sigma^2$: the Boltzmann-Grad limit states that the single particle collision probability must vanish while the total number of collisions remains of order 1. So, Eq. (1.29)

[1] from Bogoliubov, Born, Green, Kirkwood and Yvon

can be modified changing $(N-s)\sigma^2 \to N\sigma^2$ and putting $\sigma = 0$ into (1.30).

The last but crucial assumption to obtain the Boltzmann equation is the *Molecular Chaos assumption*, namely

$$P_2(\mathbf{r}_1, \mathbf{v}_1, \mathbf{r}_2, \mathbf{v}_2; t) = P_1(\mathbf{r}_1, \mathbf{v}_1, t) P_1(\mathbf{r}_2, \mathbf{v}_2, t) \tag{1.31}$$

for particles that are about to collide, i.e. when $\mathbf{r}_2 = \mathbf{r}_1 - \sigma\hat{\mathbf{n}}$ and $\mathbf{v}_{12} \cdot \hat{\mathbf{n}} < 0$. The Molecular Chaos assumption states that the *pre*collisional velocities of the colliding particles are uncorrelated: it relies on Boltzmann-Grad limit, for which we already saw that a collision between two selected particles i, j is a rare event, hence between two collisions of the same particles they will have collided many times with other particles of the system, "forgetting" the possible correlation induced by the precedent collision. It is important to stress that Molecular Chaos states that *pre*collisional velocities are uncorrelated, but doesn't say anything about *post*collisional velocities distribution. This assumption can be clearly justified only in dilute gases and will be heavily used in Part II of this Thesis.

The Molecular Chaos assumption in (4.14) immediately closes BBGKY hierarchy at $s = 1$: the first equation of the hierarchy then reads (writing $P = P_1$ and omitting time dependence)

$$\frac{\partial P(\mathbf{r}, \mathbf{v})}{\partial t} + \mathbf{v} \cdot \frac{\partial P(\mathbf{r}, \mathbf{v})}{\partial \mathbf{r}} = N\sigma^2 \int_{\mathbb{R}^3} \int_{S^+} \left[P(\mathbf{r}, \mathbf{v}') P(\mathbf{r}, \mathbf{v}'_*) - P(\mathbf{r}, \mathbf{v}) P(\mathbf{r}, \mathbf{v}_*) \right] |\mathbf{V} \cdot \hat{\mathbf{n}}| \mathrm{d}\mathbf{v}_* \mathrm{d}\hat{\mathbf{n}} \tag{1.32}$$

with $\mathbf{v}' = \mathbf{v} - \hat{\mathbf{n}}(\mathbf{V} \cdot \hat{\mathbf{n}})$, $\mathbf{v}'_* = \mathbf{v}_* + \hat{\mathbf{n}}(\mathbf{V} \cdot \hat{\mathbf{n}})$ and $\mathbf{V} = \mathbf{v} - \mathbf{v}_*$. Eq. (1.32) is the *Boltzmann equation* for hard spheres. Its lhs contains the time evolution given by the free flow in phase space coordinates and its rhs the instantaneous evolution given by collisions. It is here evident that the first (positive) term into the integral is accounting for all the collisions where one particle has the postcollisional velocity $\mathbf{v}$ and therefore comes into phase space region around $(\mathbf{r}, \mathbf{v})$, whereas the second (negative) term is accounting for all the collisions where one of the particles has the precollisional velocity $\mathbf{v}$, and therefore after a collision it escapes from the phase space region measured by $P(\mathbf{r}, \mathbf{v})$.

Actually, it is not unusual to find the evolution equation for the single-particle distribution P directly written without considering the full phase space distribution $\mathcal{P}$ but rather computing the gain/loss terms through probabilistic considerations, see for instance [94]. Although this alternative derivation is well-based and legitimate, the full information about the physical system considered is given by $\mathcal{P}(\mathbf{z}, t)$, while $P(\mathbf{r}, \mathbf{v}, t)$ contains less information and its derivation from Liouville equation (1.10) has shown the assumptions needed. However, for many practical purposes, P is the main quantity of interest, as it will be seen in Part II.

1.4.2 Inelastic Collisions and granular Boltzmann Equation

The aim of the present paragraph is to derive a Boltzmann equation for inelastic smooth hard spheres, which are a fundamental modelization of granular particles.

Before doing that, the inelastic collisions need to be well-defined: conversely from elastic collisions, the former conserve momentum but dissipate energy, namely Eqs. (1.13) become

$$m\mathbf{v}_i' + m\mathbf{v}_j' = m\mathbf{v}_i + m\mathbf{v}_j, \tag{1.33a}$$

$$\frac{1}{2}mv_i'^2 + \frac{1}{2}mv_j'^2 < \frac{1}{2}mv_i^2 + \frac{1}{2}mv_j^2. \tag{1.33b}$$

In order to quantify the energy loss during a collision, it is common to introduce the *restitution coefficient* $0 \leq \alpha < 1$; after a collision, the relative velocity in the center of mass frame reads

$$\mathbf{v}_{ij}' = -\alpha\mathbf{v}_{ij}. \tag{1.34}$$

The last equation defines α and states that after a collision the relative velocity along the collision direction is reflected *and rescaled* by a factor α: when $\alpha = 0$, the postcollisional velocity vanishes and the colliding particles get stuck together, as when a ripe tomato crushes falling on the ground (sticky collision); conversely when $\alpha = 1$ the collision is elastic, and the previous paragraph's theory with Eqs. (1.13), (1.14) and (1.15) is recovered. Energy dissipation is absent when $\alpha = 1$ and increases as α decreases towards its minimum $\alpha = 0$, where energy dissipation is maximal.
Setting a restitution coefficient equivalent for each particle and collision event is clearly an idealization, as well as considering all particles as spheres having the same diameter: indeed, during a collision, kinetic energy of particles is mainly dissipated into work deforming the particles themselves - which cannot be exactly spherical anymore -, and in real collisions the dissipation ratio $\Delta E/E$ depends on the shape of the particles and the collision point on their surfaces as well as their relative velocity. Actually, there are granular models considering velocity-dependent restitution coefficient $\alpha(v)$ [99, 35], but their description is beyond the aim of this thesis. Furthermore, there are no tangential frictional forces (smooth grains) which may be taken into account considering also the rotational degree of freedom of particles: the simplest model satisfying this condition is the rough hard spheres gas [84]. For our purpose, a constant restitution coefficient is a good approximation.

The collisional rule for identical inelastic smooth hard spheres now reads

$$\mathbf{v}_i' = \mathbf{v}_i - \frac{1+\alpha}{2}\hat{\mathbf{n}}\left[\hat{\mathbf{n}}\cdot(\mathbf{v}_i - \mathbf{v}_j)\right], \tag{1.35a}$$

$$\mathbf{v}_j' = \mathbf{v}_j + \frac{1+\alpha}{2}\hat{\mathbf{n}}\left[\hat{\mathbf{n}}\cdot(\mathbf{v}_i - \mathbf{v}_j)\right]. \tag{1.35b}$$

and the energy dissipation is

$$\Delta E = E' - E = -\frac{1-\alpha^2}{4}\left|\hat{\mathbf{n}}\cdot(\mathbf{v}_i - \mathbf{v}_j)\right|^2. \tag{1.36}$$

Some fundamental features of inelastic collisions deserve to be underlined.

1. *Inelastic collisions are not invariant under time-reversal*. Eq. (1.27) is invariant under time-reversal: indeed, the elastic collision rule (1.15) states that $(\mathbf{v}_i, \mathbf{v}_j) \to (\mathbf{v}'_i, \mathbf{v}'_j)$ as well as $(-\mathbf{v}'_i, -\mathbf{v}'_j) \to (-\mathbf{v}_i, -\mathbf{v}_j)$. On the contrary, in inelastic collisions energy is dissipated, and the reversed collision should increase energy to reach the original precollisional state: indeed, precollisional velocities can be obtained from postcollisional ones with the rule

$$\mathbf{v}_i = \mathbf{v}_i - \frac{1+\alpha}{2\alpha}\hat{\mathbf{n}}\left[\hat{\mathbf{n}}\cdot\left(\mathbf{v}'_i - \mathbf{v}'_j\right)\right], \tag{1.37a}$$

$$\mathbf{v}_j = \mathbf{v}_j + \frac{1+\alpha}{2\alpha}\hat{\mathbf{n}}\left[\hat{\mathbf{n}}\cdot\left(\mathbf{v}'_i - \mathbf{v}'_j\right)\right], \tag{1.37b}$$

which corresponds to the original collisional rule (1.35) when transforming $\alpha \to 1/\alpha$: the only invariant case is the elastic collision with $\alpha = 1$. Fig. 1.9 geometrically shows the elastic case versus the inelastic one.

2. *Velocities align after a collision*. The inelastic collisional rule shrinks the velocity component parallel to the relative velocity, $\mathbf{v}^{\parallel} = \hat{\mathbf{n}}\cdot\mathbf{v}$ but conserves the transverse component $\mathbf{v}^{\perp} = \mathbf{v} - \mathbf{v}^{\parallel}$. Therefore, after a collision the transverse component weight is increased with respect to the parallel one: the relative angle between particles' velocities reduces and their velocities get more aligned, see Fig. 1.9 for geometrical visualization. This feature has a great importance in momentum transfer, because the velocities tend to get correlated at a microscopic level. In granular flows, velocity alignment cre-

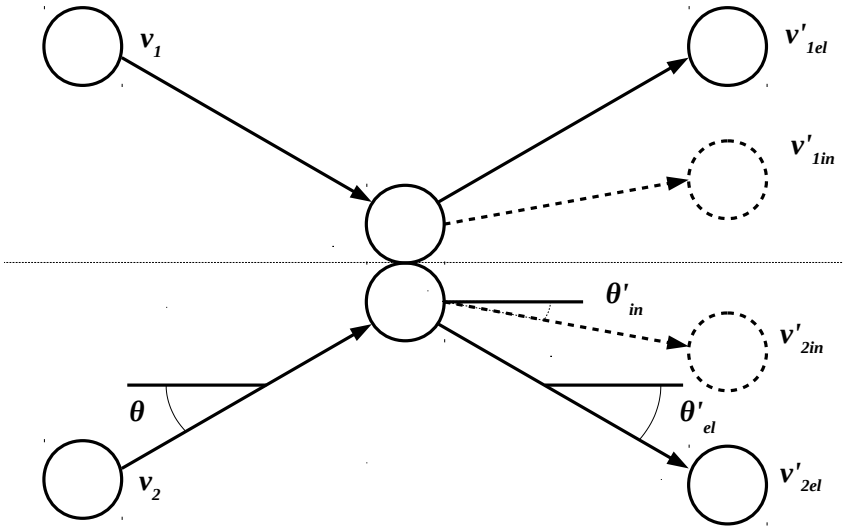

Figure 1.9. Elastic *vs.* inelastic collision: elastic trajectories (continuous lines) are reflected with a postcollisional angle $\theta'_{el} = \theta$ equivalent to the precollisional one - time reversal invariance -, while in the inelastic collision (dashed lines) velocities get more aligned because $\theta'_{in} < \theta$.

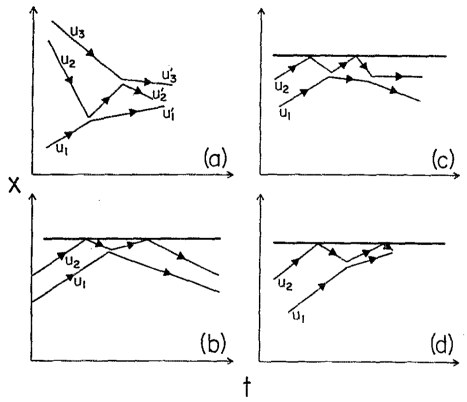

(a) Schematic trajectories showing inelastic collapse. (a) Three particle collapse: without surrounding walls, collapse occurs when $\alpha < \alpha_c = 7 - 4\sqrt{3} \sim 0.0718$. (b) Two particles collide between themselves and a wall, but do not collapse since $\alpha > 0.346015$. (c) At critical $\alpha = 0.346015$, the inner particle is stationary after two collisions with the outer one.(d) For $\alpha < 3 - 2\sqrt{2} \sim 0.17157$ there is inelastic collapse [141].

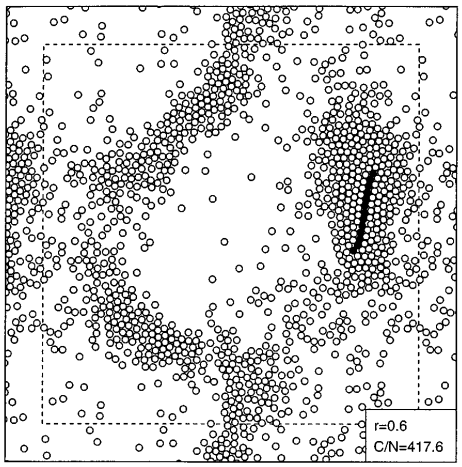

(b) A snapshot from a MD simulation of cooling inelastic hard spheres in a square box with periodic boundary conditions, with $\alpha = 0.6$ and $N = 1024$ particles. C/N=417.6 is the total number of collisions per particle at the time the simulation is stopped. Black particles are the one involved in the last two hundred collision: the linear arrangement characteristic of inelastic collapse is evident [143]

Figure 1.10. Inelastic collapse

ates groups of particles collectively moving with almost the same velocities.

3. *Inelastic collapse*. In Sec. 1.3.1 it has been already introduced how clustering is connected with inelastic collapse: the simplest example is the case of three particles on a line [141], see top left panel of Fig. 1.10a. When outer particles move monotonically toward each other, the central one bounces with them from both sides. In the elastic case at least one of the outer particles would be rejected from the collision and no more collisions occur unless a wall redirects the particles toward each other. In the inelastic case, if dissipation is strong enough the outer particles don't change their direction and they ceaselessly collide with the central one with geometrically smaller space and time scales at each successive cycle. The critical value of the dissipation is $\alpha < \alpha_c = 7 - 4\sqrt{3} \sim 0.0718$ [141]. When $\alpha > \alpha_c$, inelastic collapse can occur in presence of an inelastic wall, see Fig. 1.10a, if the number of particles is sufficiently high. In more than 1 dimension, inelastic collapse can be realized in a large cluster, see Fig. 1.10b. This phenomenon has dramatical consequences on inelastic hard spheres simulations: indeed, since time and space scales between two collisions geometrically decrease, the assumption of binary collisions will fail. Furthermore, the time between two collisions

will become exponentially small and event-driven simulation time steps will dramatically slow down, until at a certain time the simulation stops running as an infinite number of collisions occur in finite time. A snapshot of this situation in $2d$ is plotted in Fig. 1.10b, where collapsed particles are highlighted. To avoid the inelastic collapse, some models consider a velocity-dependent restitution coefficient, becoming more and more elastic as the relative velocity tends to zero, in agreement with experimental observations. This description is generally known as *viscoelastic model*. Simulations of such models have shown that the inelastic collapse is removed, suggesting that it is an artificial consequence of fixing a constant restitution coefficient.

Having considered the deep qualitative differences between elastic and inelastic collisions, now the Boltzmann equation for granular gases can be derived. Pseudo-Liouville equation (1.27) holds, provided that the binary collision $T_-^\dagger(1,2)$ is now written in terms of inelastic collision rules, Eqs. (1.35) and (1.37). Since direct and inverse transformation do not coincide anymore as in the $\alpha = 1$ case, the operator b_c in T_- and $T_-^\dagger$ which exchanges precollisional velocities with postcollisional ones must be exchanged with its inverse b_c'. The adjoint of inverse binary inelastic collision operator therefore reads

$$T_-^\dagger(1,2) = \sigma^2 \int\limits_{\mathbf{v}_{12}\cdot\hat{\mathbf{n}}>0} \mathrm{d}\hat{\mathbf{n}}\,|\mathbf{v}_{12}\cdot\hat{\mathbf{n}}| \left[\frac{1}{\alpha^2}\delta\left(\mathbf{r}_1 - \mathbf{r}_2 - \sigma\hat{\mathbf{n}}\right) - \delta\left(\mathbf{r}_1 - \mathbf{r}_2 + \sigma\hat{\mathbf{n}}\right)\right] \tag{1.38}$$

Deriving the BBGKY hierarchy and considering the first equation for one-particle distribution, the Molecular Chaos assumption gives the Boltzmann equation for granular gases

$$\left(\frac{\partial}{\partial t} + L_1^0\right) P(\mathbf{r}_1, \mathbf{v}_1, t) = N\sigma^2 Q(P,P) \tag{1.39a}$$

$$Q(P,P) = \int \mathrm{d}\mathbf{v}_2 \int\limits_{\mathbf{v}_{12}\cdot\hat{\mathbf{n}}>0} \mathrm{d}\hat{\mathbf{n}}\,|\mathbf{v}_{12}\cdot\hat{\mathbf{n}}| \left[\frac{1}{\alpha^2} P(\mathbf{r}_1, \mathbf{v}_1^*, t) P(\mathbf{r}_1, \mathbf{v}_2^*, t) - P(\mathbf{r}_1, \mathbf{v}_1, t) P(\mathbf{r}_1, \mathbf{v}_2, t)\right] \tag{1.39b}$$

where $\mathbf{v}_1$ and $\mathbf{v}_2^*$ indicate the precollisional velocities required to have $\mathbf{v}_1$ and $\mathbf{v}_2$ as postcollisional ones, see Eq. (1.37).

As a first approach, this equation can be studied in the spatially homogeneous case (therefore $L_1^0 = 0$), including the Enskog correction $\Xi(\sigma, n)$, which has been introduce to account for velocity correlations under some assumptions, and acts as a multiplicative factor correcting Molecular Chaos approximation [164]. The homogeneous equation reads

$$\frac{\partial}{\partial t} P(\mathbf{v}_1, t) = \Xi(\sigma, n) n \sigma^2 Q(P,P), \tag{1.40}$$

where n is the average number density; the last equation has been studied by Goldshtein and Shapiro [84] and by Ernst and van Noije [188]. This is the first step to derive dynamical equations of granular quantities, as will be done in the next paragraph.

1.4.3 The Homogeneous Cooling State and Haff's law

From now on only the spatially homogeneous case is considered.
The granular cooling has no stationary state, since the energy keeps dissipating because of the collisions all along the trajectory. Therefore, it is useful to define the rescaled velocity distribution $\tilde{f}$ as

$$NP(\mathbf{v},t) = \frac{n}{v_T^3(t)}\tilde{f}(\mathbf{v}/v_T(t)) \tag{1.41}$$

where the temperature $T(t) = m\langle v^2\rangle/3 = mv_T^2(t)/2$ defines the thermal velocity $v_T(t)$. It can be shown that $N^2Q \to n^2 v_T^2 \tilde{Q}$, with

$$\tilde{Q} = \int \mathrm{d}\mathbf{c}_2 \int\limits_{\mathbf{c}_{12}\cdot\hat{\mathbf{n}}>0} \mathrm{d}\hat{\mathbf{n}}\,|\mathbf{c}_{12}\cdot\hat{\mathbf{n}}| \left[\frac{1}{\alpha^2}\tilde{f}(\mathbf{c}_1^*,t)\tilde{f}(\mathbf{c}_2^*,t) - \tilde{f}(\mathbf{c}_1,t)\tilde{f}(\mathbf{c}_2,t)\right], \tag{1.42}$$

defining a rescaled velocity $\mathbf{c} = \mathbf{v}/v_T$. The collisions cause the temperature decay: from Eq. (1.36), one expects that collisions reduce energy by a quantity proportional to kinetic energy itself. The temperature evolution equation reads

$$\frac{\mathrm{d}}{\mathrm{d}t}\left(\frac{3}{2}nT\right)\bigg|_{coll} = \int \mathrm{d}\mathbf{v}\,\frac{mv^2}{2}\sigma^2 N^2 Q(P,P) \tag{1.43}$$

$$= \sigma^2 n^2 v_T \frac{mv_T^2}{2}\int \mathrm{d}\mathbf{c}_1 c_1^2 \tilde{Q} = -\sigma^2 n^2 v_T T \mu_2, \tag{1.44}$$

being

$$\mu_p = -\int \mathrm{d}\mathbf{c}_1 c_1^p \tilde{Q}. \tag{1.45}$$

Therefore

$$\frac{\mathrm{d}T}{\mathrm{d}t}\bigg|_{coll} = -\zeta(t)T(t). \tag{1.46}$$

where

$$\zeta(t) = \frac{2\sqrt{2}}{3}n\sigma^2\mu_2\sqrt{\frac{T(t)}{m}} \tag{1.47}$$

Eq. (1.46) rules the Homogeneous Cooling State (HCS). Since the density is constant and any global velocity can be put to 0 by means of a Galilean transformation, the temperature field is the only hydrodynamic relevant field in the HCS. Because of these simplifications, the HCS is usually the starting point to study granular flows and instabilities, see Sec. 3.1.2 and Part II.

Throughout homogeneous cooling all the particles continuously lose energy by means on inelastic collisions with uniform distribution in space, which makes the granular temperature homogeneously decreasing after having initialized the system with some non-trivial velocity distribution. This is the reason why $\tilde{f}$ has been introduced: indeed $P(\mathbf{v})$ necessarily tends to a Dirac delta $\delta(\mathbf{v})$. The dissipation coefficient $\zeta(t)$ is time-dependent, i.e. $\zeta(t) \propto \sqrt{T(t)}$: this is the effect of a hard-core potential, which makes the collision frequency proportional to the thermal velocity,

$$\omega_c \sim v_T \sim \sqrt{T} \tag{1.48}$$

where $\omega_c \mathrm{d}t$ is the probability that a given particle undergoes a collision between t and $t + \mathrm{d}t$.

When computing the rescaled distribution time-derivative, additional contributions appear

$$\frac{\partial NP}{\partial t} = \frac{n}{v_T^3}\frac{\partial \tilde{f}}{\partial t} + \left(-\frac{3n}{v_T^4}\tilde{f} + \frac{n}{v_T^3}\frac{\partial \tilde{f}}{\partial c_1}\frac{\partial c_1}{\partial v_T}\right)\frac{\mathrm{d}v_T}{\mathrm{d}t}, \tag{1.49}$$

leading to the following evolution equation

$$\frac{1}{v_T}\frac{\partial \tilde{f}}{\partial t} - \frac{1}{v_T^2}\frac{\partial(\mathbf{c}_1\tilde{f})}{\partial \mathbf{c}_1}\frac{\mathrm{d}v_T}{\mathrm{d}t} = \sigma^2 n\tilde{Q}. \tag{1.50}$$

The second term in the lhs can be computed through Eqs. (1.46) and (1.45),

$$\frac{1}{v_T^2}\frac{\mathrm{d}v_T}{\mathrm{d}t} = \sqrt{\frac{m}{2T}}\frac{1}{2T}\frac{\mathrm{d}T}{\mathrm{d}t} = -\frac{1}{3}\sigma^2 n\mu_2 \tag{1.51}$$

which prove it to be time-independent.

Assuming the existence of a scaling stationary solution, namely $\tilde{f}_{HCS}$ such that $\partial \tilde{f}_{HCS}/\partial t = 0$, this must satisfy

$$\frac{\mu_2}{3}\frac{\partial(\mathbf{c}_1\tilde{f}_{HCS})}{\partial \mathbf{c}_1} = \tilde{Q}. \tag{1.52}$$

The latter equation defines the Homogeneous Cooling State. Finally, in the HCS the solution of the temperature equation reads

$$T_{HCS}(t) = \frac{T(0)}{\left(1 + \frac{\zeta(0)t}{2}\right)^2}, \tag{1.53}$$

which is known as the Haff's law [88] and has the remarkable property of being independent of the initial temperature in the long time limit, namely

$$T(t) \sim 4(\bar{\zeta}t)^{-2} \tag{1.54}$$

with

$$\bar{\zeta} = \frac{\zeta(T_{HCS}(t))}{T_{HCS}^{1/2}(t)} = \frac{\zeta_0 v_T(t)}{l T_{HCS}^{1/2}(t)} \tag{1.55}$$

where $l \propto 1/(n\sigma^2)$ is the mean free path and ζ_0 is the dimensionless cooling rate, a physical parameter of the system.

1.4.4 Steady State Representation

Eq. (1.47) and Haff's law in (1.54) says that for long times

$$\omega_c(t) \sim \frac{2}{\bar{\zeta}t} \quad \Rightarrow \quad N_c(t) \sim \ln(\bar{\zeta}t/2) \tag{1.56}$$

where $N_c(t)$ is the number of cumulated collisions after a time t. A new time-scale can now be introduced

$$\tau(t) = \tau_0 \ln \frac{t}{t_0}, \tag{1.57}$$

with arbitrary τ_0 and t_0; Eq. (1.57) gives the trend of the mean intercollisional time τ at time t. In this new time scale, the number of collisions in a time interval $\mathrm{d}\tau$ is constant. This yields

$$\frac{\partial}{\partial t} = \frac{\tau_0}{t}\frac{\partial}{\partial \tau} \tag{1.58}$$

therefore for long times one has

$$\frac{1}{v_T(t)}\frac{\partial}{\partial t} \sim \frac{\overline{\zeta}\tau_0}{2}\frac{\partial}{\partial \tau} \tag{1.59}$$

Finally, the evolution equation of the one particle distribution in the new time scale τ reads

$$\frac{\partial \tilde{f}}{\partial \tau} + \frac{n\sigma^2\mu_2}{3}\frac{\partial(\mathbf{c}_1\tilde{f})}{\partial \mathbf{c}_1} = \sigma^2 n\tilde{Q} \tag{1.60}$$

which is equivalent to the Boltzmann equation of particles subjected to an external force

$$\mathbf{F} = \frac{n\sigma^2\mu_2}{3}\mathbf{c} \tag{1.61}$$

acting like a *positive* viscosity. Actually, this equivalence makes sense as long as the state remains homogeneous; in Sec. 3.1.2 it will be shown how the HCS is unstable for long wavelengths perturbations [83].

Eq. (1.60) is the Boltzmann equation in the *steady state representation* [33]: indeed, it has been seen how looking at the system in terms of the rescaled velocity $\mathbf{c}$ is equivalent to adding a *propulsive* continuous force, increasing the energy of the system. The meaning is evident: velocity rescales and as the new time scale τ slows down when t increases, the new velocity reads

$$\mathbf{w}(\tau) = \frac{\mathrm{d}\mathbf{x}}{\mathrm{d}\tau} = \frac{\mathrm{d}\mathbf{x}}{\mathrm{d}t}\frac{\mathrm{d}t}{\mathrm{d}\tau} = \frac{t}{\tau_0}\mathbf{v}(t) \tag{1.62}$$

so the effect of the propelling force is to inject back in the particles the same average quantity of energy lost by collisions, which follow the same rule (1.35) because they are instantaneous and not affected by time rescaling.

In this representation, Eq. (1.60) provides a new evolution equation for the rescaled homogeneous temperature $\tilde{T}_H(\tau) = m\langle w^2\rangle/3$ [33]

$$\left(\frac{\mathrm{d}}{\mathrm{d}\tau} - \frac{2}{\tau_0}\right)\tilde{T}_H(\tau) = -\overline{\zeta}\tilde{T}_H^{3/2}(\tau). \tag{1.63}$$

which solution reads

$$\tilde{T}_H(\tau) = \left(\frac{2}{\tau_0\overline{\zeta}}\right)^2\left[1 + \left(\frac{2}{\tau_0\overline{\zeta}\tilde{T}_H^{1/2}(0)} - \right)e^{-\tau/\tau_0}\right]. \tag{1.64}$$

The rescaled temperature hence tends to a stationary value given by

$$\tilde{T}_{st} = \left(\frac{2}{\tau_0 \bar{\zeta}}\right)^2 \tag{1.65}$$

From Eq. (1.55), it can be shown that $\tau_0 \tilde{v}_{T,st}$ is independent from τ_0 and proportional to the dimensionless cooling rate ζ_0, an intrinsic property of the system.
So, when considering rescaled variables, the steady state representation shows how the HCS forgets of its initial condition after sufficiently long times and tend to a value determined by the parameters of the system, regardless of the initial velocity distribution. The steady state representation provides a mapping between a granular cooling, where no stationary state is possible, to a system where energy is dissipated and injected at the same rate, leading to the stationary values described above.

1.4.5 Driven Granular Systems

A granular fluid can reach a stationary state when power is supplied in order to balance the energy lost because of collisions. There are two main theoretical description of driven granulars:

1. imposing boundary conditions like in a sheared or shaken granular, which is typically done in hydrodynamic description - see Sec. 3.1.2 - and implemented in numerical simulations - see Sec. 4 ;

2. driving the granular in the bulk, i.e. supplying energy to all the particles in their microscopic dynamics. This is the case discussed in this section.

I report the randomly driven granular gas model [166, 167], consisting of a gas made by N identical hard objects of mass m and diameter D moving inside a d-dimensional box of volume $V - L^d$, being L the side of the box. The dynamic of the gas is ruled by the interplay between two physical phenomena: a continuous interaction with the environment (Langevin process) and inelastic collisions among the grains. The equations of motion read

$$\frac{\mathrm{d}}{\mathrm{d}t}\mathbf{x}_i(t) = \mathbf{v}_i(t), \tag{1.66a}$$

$$m\frac{\mathrm{d}}{\mathrm{d}t}\mathbf{v}_i(t) = -\gamma_b \mathbf{v}_i(t) + \sqrt{2\gamma_b T_b}\boldsymbol{\xi}_i(t) + \mathbf{F}_i(t). \tag{1.66b}$$

So, the grains are coupled with a thermal bath, calling $\tau_b = m/\gamma_b$ and T_b respectively the characteristic time and temperature of the bath. The function $\boldsymbol{\xi}_i(t)$ is a standard Wiener process, i.e. $\langle \boldsymbol{\xi}_i(t) = 0$ and $\langle \xi_i^\alpha(t)\xi_j^\beta(t')\rangle = \delta(t-t')\delta_{ij}\delta_{\alpha\beta}$. The noise coefficient $\sqrt{2\gamma_b T_b}$ satisfies the Einstein fluctuation-dissipation relation. Inelastic collisions are taken into account by $\mathbf{F}_i(t)$: they occur instantaneously with a mean intercollisional time τ_c.

Therefore, the parameters defining the dynamics are the restitution coefficient α and the ratio between the characteristic time scales, $\rho = \tau_b/\tau_c$. Depending on these (adimensional) parameters, one can define three limit cases of the dynamics

- the elastic limit $\alpha \to 1^-$;
- the collisionless limit $\rho \to 0 \quad (\tau_c \gg \tau_b)$;
- the cooling limit $\rho \to \infty \quad (\tau_c \ll \tau_b)$.

In $d > 1$, the elastic limit is smooth and one can take $\alpha = 1$: this is equivalent to consider an elastic gas, where collisions contribute to the relaxation towards an homogeneous particle distribution in space and a Maxwellian distribution of velocities, with temperature T_b. In $d = 1$ the situation is different because in elastic collisions particles exchange their velocities *exactly*, so there is no mixing because a collision is equivalent to an exchange of labels, namely $(v_i, v_j) \to (v_j, v_i)$ and the initial set of velocities is conserved in time.

In the collisionless limit $\tau_c \gg \tau_b$, therefore collisions are very rare and the gas can be considered as a gas of non-interacting random Brownian walkers, which sometimes collide between them but then relax toward a Maxwellian distribution with temperature T_b and homogeneous density.

Finally, in the cooling limit $\tau_c \ll \tau_b$ and collisions dominate: between two collisions particles move almost ballistically. The bath is heating the granular but this effect can be seen only for time scales greater than τ_b: for intermediate observation times $\tau_c \ll t \ll \tau_b$ the gas behaves like a cooling granular gas.

1.4.6 Inelastic Maxwell Molecules

The last part of this chapter is devoted to *inelastic Maxwell molecules*: this is a category of particles which collision integral *does not* depend on the flux term $|\mathbf{v}_{12} \cdot \hat{\mathbf{n}}|$ [67]. Kinetic theory calculations show that this is approximately the case for particles in d dimensions subject to a power law repulsion interaction potential $U(r) \sim r^{-2(d-1)}$ [164]. The Boltzmann equation for Maxwell molecules is greatly simplified, and in the inelastic $1d$ case reads

$$\frac{\partial}{\partial \tau} P(v,\tau) + P(v,\tau) = \beta \int \mathrm{d}u P(u,\tau) P(\beta v + (1-\beta)u, \tau) \tag{1.67}$$

where $\beta = 2/(1+\alpha)$ and τ is the number of collisions per particle. For Maxwell molecules the collision frequency ω_c is constant, i.e. it doesn't depend from the thermal velocity as for hard spheres, hence τ is linear with t and they can be used alternatively. Otherwise, one can take the flux term $|v - v'|$ in $1d$ hard rods to be proportional to the thermal velocity, $\sqrt{T}$; by means of a time reparametrization $\tau(t)$, the latter factor can be eliminated and the Boltzmann equation reduces to Eq. (1.67). This description is called *pseudo-Maxwell* model [25].

Eq. (1.67) implies that at each time step an arbitrary couple of particles is selected and their velocities are transformed following the collisional rule (1.35) in $d = 1$. This model was applied by in 1999 [13] as a traffic flow model, and further analyzed in [14]: essentially, it analyzes the dynamics of Maxwell molecules in mean field case, i.e. disregarding spatial structure. In the homogeneous case of zero total momentum (i.e. in the center of mass frame) the authors obtained an

exponential decay of velocity moments, namely

$$\langle v^n \rangle \sim e^{-a_n \tau}, \tag{1.68}$$

but with decay rates $a_n \neq n a_2/2$, arguing the presence of a *multiscaling* behavior, namely that higher-order moments cannot be written as function of the second moment. The authors in [14] consequently exclude the existence of a rescaled asymptotic distribution $P(v,\tau) \to f(v/v_T(\tau))/v_T(\tau)$ in the long time limit. On the contrary, it has been shown [6] that the rescaled distribution function

$$f(v/v_0(\tau)) = \frac{2}{\pi \left[1 + (v/v_0(\tau))^2\right]^2} \tag{1.69}$$

is a physical asymptotic solution of Eq. (1.67) when considering inelastic hard rods on a lattice. Since it has the form of a power law with $f(c) \sim c^{-4}$ for high c, moments $\langle v^n \rangle$ with $n \geq 3$ diverge and therefore do not scale with the second moment. Remarkably, the scaling velocity distribution form in (1.69) does not depend on the restitution coefficient α: the dynamics is completely contained in the thermal velocity $v_0(\tau)$. Furthermore, Eq. (1.68) leads to a new version of Haff's law (1.53) for Maxwell molecules, namely

$$T(t) \sim e^{-a_2 \tau} \tag{1.70}$$

so that the temperature exponentially decays in function of the collisional clock τ. Further studies have shown that the multiscaling behavior yields non-stationary total energy fluctuations [51]

$$\frac{\langle E^2(\tau) \rangle - \langle E(\tau) \rangle^2}{\langle E(\tau) \rangle^2} = \frac{1}{N} \left[A + B \exp(2\zeta^2 t) \right] \tag{1.71}$$

where $E(\tau) = \sum_{i=1}^{N} v_i^2(\tau)$ is the total energy, $2\zeta^2 = 2a_2 - a_4$ and A and B depend on the initial velocity distribution. Energy fluctuations vanish in the large-size limit since they scale as $1/\sqrt{N}$ and so a thermal capacity can always be defined, but it grows with time. This property will be discussed in Sec. 5.3 for the granular lattice model introduced in Chapter 4.

A great deal of attention has been focused on Maxwell molecules over the last years, because the simplification of Maxwell particles allows the derivation of several analytical results. Lattice Maxwell models will be described in more detail in Sec. 3.3.2, and will be one of the subject of this thesis analyzed in Chapter 4.

Walk on, through the wind
Walk on, through the rain
Though your dreams be tossed and blown
Walk on, walk on
With hope in your heart
And you'll never walk alone

2 Active Matter

This chapter is an introduction to the physics of *active matter*. In the first section 2.1 some active matter phenomena and physical systems will be reviewed, mainly distinguishing between living and non-living active matter. The second section 2.2 is dedicated to physical models of active matter, introducing their essential ingredients and reviewing some of the most important and successful models. The last section 2.3 investigates a possible comparison and symmetry between granular and active matter, in the light of what has been presented in the first two chapters.

2.1 What is active matter

Many biological living units have the ability to move themselves in a fluid medium, converting stored energy into kinetic energy by means of some biochemical process: this is what we call an *active particle*. When considering physical systems, one usually determines the motion of a particle through the resultant of the forces acting on it, thinking at the particle as a passive unity; on the contrary, active particles typically generate on their own a force to attain a certain state of motion: this force is called *self-propulsion*. Self-propulsion is made possible by the interaction of the active particle with a substrate or a surrounding fluid: actually, the momentum of an active unit is not conserved during its motion, but it must be so when considering both the particle and the environment. For instance, human beings are active particles: we convert our chemical energy stored as ATP into kinetic energy through our muscular activity, being able to change our velocity intensity and orientation, but we can do it only in presence of a reacting medium, i.e. when walking on the ground or when swimming in the water, unless there is some mass exchange acting like a jet propulsion, which will be disregarded here. This principle obviously holds for any kind of active particle that we will see below, such as animals, bacteria, robots and so on.

When many active particles move together in a united system we talk about

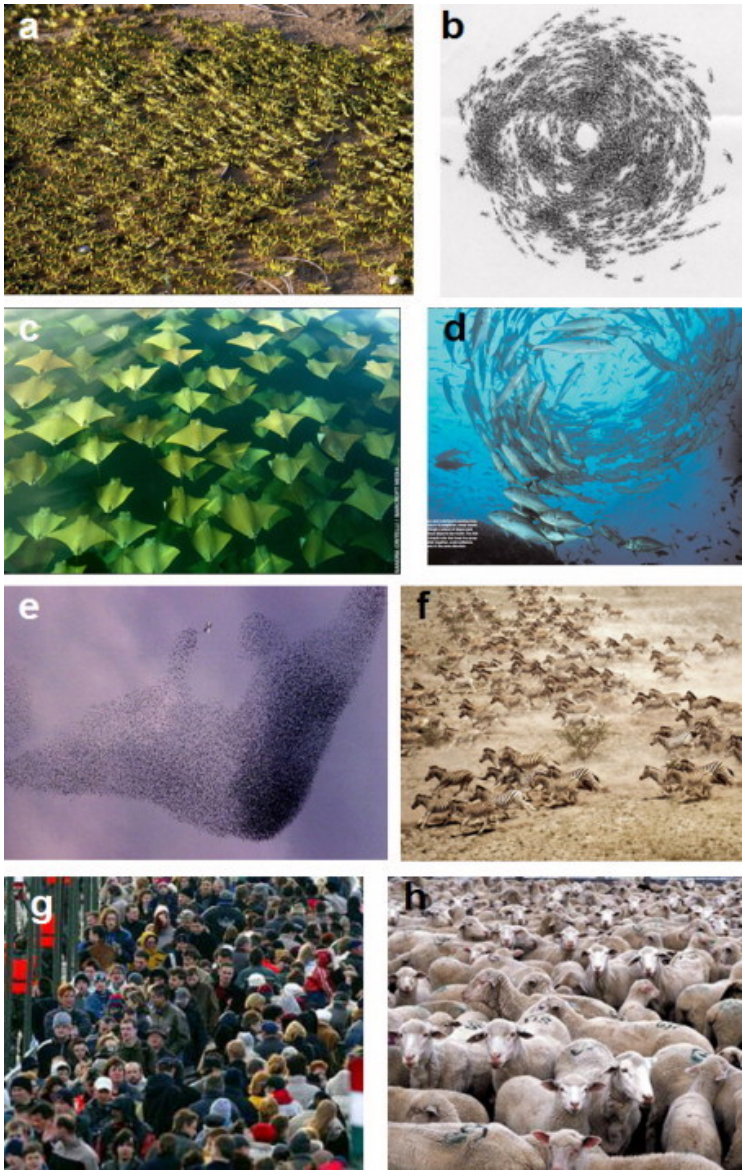

Figure 2.1. Several examples of collective behavior in living systems: (a) locusts, (b) army ants, (c) golden rays, (d) fishes forming a vortex, (e) starlings flocking, (f) a herd of zebra, (g) people walking in a street, (h) sheep hanging around [192].

active matter. In this case the particles are not just self-propelling themselves but also interacting among them. Active matter can be observed in several circumstances in everyday life: bird flocks fly together in the sky; fish schools swim almost like a single object, defending from predators; sheep herds graze together, and also human beings use to walk together in more or less crowded environments, see Fig. 2.1. The interactions between active particles give rise to *collective motion*, i.e. individual units coherently move and form outstanding patterns and shapes: this phenomenon is also known as *flocking*, a general notion standing for the formation of order in an active matter system. Biological systems with active

behavior are ubiquitous, and their complete review is far beyond the aim of this thesis. Some reviews already exist [168, 135, 192, 12] where a wider and more detailed outlook on active systems, phenomenology and models is given. A list of the most experimentally studied systems includes macromolecules, bacteria colonies, amoeba, cells, insects, fishes, birds, mammals and humans [192]. Furthermore, active matter can be also composed by *non-living* units: actually, there exist several systems [192, 12] where particles absorb energy from a substrate where chemical, thermal or electrostatic gradients are induced; or where particles are activated by some external field (typically the electromagnetic field); or where particles contain stored energy that can be converted in kinetic energy; or finally where the walls of the substrate are shaken and the asymmetry of the particles' geometry induces a self-propulsion mechanism [12]. The main goal of all these setups is to generate a self-propulsion mechanism mimicking the self-propulsion characteristic of living systems. In the last subsection 2.1.3 some of these systems are reviewed, like Janus particles, nano-swimmers, simple robots or vibrated polar granular particles: the latter represent a bridge between granular and active matter, which will be examined carefully. In Appendix C a collection of links to videos is reported to show the experimental behavior of some discussed systems.

2.1.1 Active phenomenology

It is useful to introduce the typical phenomena of collective motion before presenting the most studied active systems: indeed, a quantitative characterization of collective behavior is needed to analyze it and compare several phases and systems. An important feature is the presence of phase transitions, which are expected in active matter even though the system is out of equilibrium. Phase transitions occur when a macroscopic quantity named *order parameter* suddenly changes under a variation of an external parameter, usually called *control parameter*. Typical examples of phase transitions at equilibrium are the condensation of a gas turning into liquid or the spontaneous magnetization of a ferromagnet, both happening if the temperature is decreased below a *critical value*. In these cases, the order parameters are respectively the mass density and the magnetization, while the control parameter is the temperature. Liquid-gas transition is called a *first-order* transition, because the order parameter discontinuously changes at the critical point; on the contrary, spontaneous magnetization is called a *second-order* transition, because the order parameter continuously decreases with the temperature. What kind of phases are observed in active matter, and what are the order parameters involved?

First of all, many active systems show **swarming**, that is when a macroscopic fraction of the units move with the same orientation of the velocity. Such a state can be reached in interacting systems where, after an interaction, the particles tend to correlate their velocities aligning their orientations. An order parameter indicating the presence of swarming is given by [192]

$$r = \frac{1}{N v_0} \left| \sum_{i=1}^{N} \mathbf{v}_i \right| \tag{2.1}$$

where N is the number of the particles, v_0 the average absolute velocity and $\mathbf{v}_i$ the velocity of the i-th particle. The swarming parameter r vanishes for disordered

motion (uniform distribution of velocity orientations, particles go in all directions as in a molecular gas) while $r = 1$ for perfect swarming, i.e. active units move together in the same direction without fluctuations. The particles spontaneously align their velocities in a given direction, breaking the continuous rotational symmetry of the system, similarly to what happens in the Heisenberg model of ferromagnetism. Here, the transition from disorder to swarming is governed by the competition between an aligning mechanism and the noise of the process: while aligning interactions force the system towards a swarming, ordered state (as ferromagnetic interaction in Ising or Heisenberg models), the noise given by self-propulsion or interactions with the surroundings increases disorder. This competition will be clarified in Sec. 2.2.

The swarming state implies a strong correlation between the velocity orientation of the active units. Furthermore, even without formation of collective motion, interactions of active units can give rise to a **leader-follower** behavior, consisting in an asymmetric relation between units when the motion of unit i (the leader) anticipates the motion of another unit j (the follower). This behavior can be observed through the directional correlation function

$$c_{ij}(\tau) = \langle \mathbf{v}_i(t) \cdot \mathbf{v}_j(t+\tau) \rangle \tag{2.2}$$

quantifying the degree of correlation between the velocity of unit i and j after a time delay τ, where the average $\langle \cdots \rangle$ is over the starting time t. The time τ^*_{ij} at which the directional correlation function shows a maximum is the *time delay* of the particle j with respect to the motion of particle i. If $\tau^*_{ij} > 0$ one can identify the unit i as the leader and j as the follower, and vice versa for $\tau^*_{ij} < 0$, recalling that $c_{ij}(\tau) = c_{ji}(-\tau)$ [192].

Another typical active phase is **clustering**: as discussed for granular materials, also active systems can form clusters during their motion. Indeed, even in presence of purely repulsive interactions, two colliding particles can get blocked by the persistence of their motion. When a third particle collides with them, they grow into a cluster which is attractive under certain conditions [12]. Particles become very correlated because of continuous interactions between them. A measure of local spatial ordering can be given by the radial distribution function $g(r)$

$$g(r) = \frac{V}{4\pi r^2 N^2} \left\langle \sum_{i \neq j} \delta(r - r_{ij}) \right\rangle, \tag{2.3}$$

giving the unit density ρ at distance r from a particle placed at the origin, namely $\rho(r) = ng(r)$, being n the averaged number density $n = N/V$ [192]. When a cluster grows in a dilute system, the local density sharply increases and deviates from n. The radial density distribution moves from a single-peaked to a double-peaked shape, signaling the presence of a dense clustered region and a dilute region, which is called a *phase separation* (see below) [77, 169]. An order parameter C can be defined as

$$C = \frac{\langle N_c \rangle}{N} \tag{2.4}$$

where N_c is the number of units belonging to the larger cluster, so that $C \ll 1$ in absence of clustering and $C \to 1$ when clustering is present [38]. Clustered

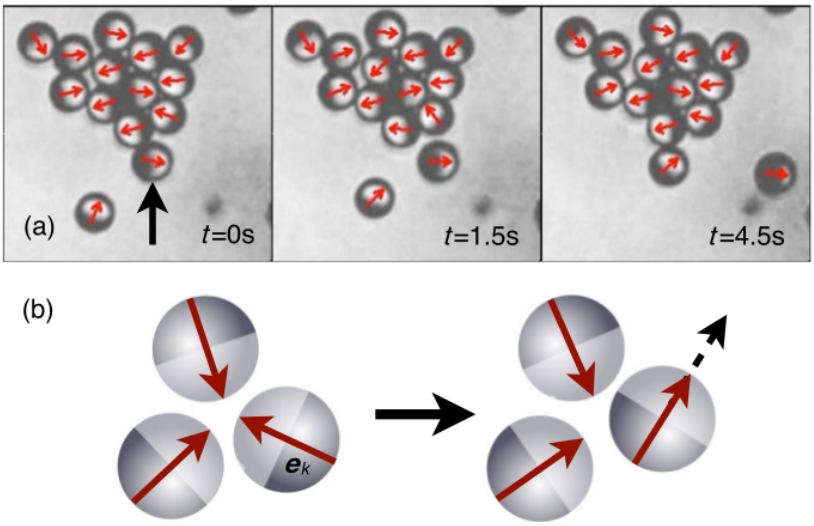

Figure 2.2. Clustering of self-propelled Janus rods. Top panel: snapshots of experimental system where the projected orientations of the caps are resolved (red arrows). Bottom panel: sketch of the self-trapping mechanism (left). Rotational diffusion is the only way that particles have to escape from the cluster [38].

units can move together in the same direction, giving rise to a swarming state, or form a static cluster where they ceaselessly collide and the excluded volume prevent them to escape the cluster. In the latter case, self-clustering can lead also to **self-jamming** [12]: particles get stuck together in one or more regions behaving like a solid: they become able to support a shear, and a probe particle in the active medium feels a dramatical increase of viscosity when moving from a dilute to a jammed zone. The viscosity exhibits strong spatial fluctuations signaling the presence of jamming.

Phase separation in active matter is the consequence of an intrinsically non-equilibrium mechanism called **motility-induced phase separation** (MIPS), which is absent for Brownian motion of particles at thermal equilibrium or for colloidal particles without attractive interactions. It has been shown [171] that for some kind of isotropic active particles one has a stationary one-particle distribution $P_s(\mathbf{r}, \mathbf{u}) \propto 1/v(\mathbf{r})$, being $\mathbf{u}$ the velocity orientation and $v(\mathbf{r})$ the space-dependent average speed field, which is the effect of self-propulsion. Therefore, the local density $\rho(\mathbf{r})$ decreases as self-propulsion increases and one can define a constitutive relation $v(\rho)$. Slower particles tend to accumulate and MIPS arises when the decrease of the speed with the density is steep enough to make an uniform suspension unstable, leading to a coexistence of an active motile gas with a dense liquid of low motility [41].

Finally, as it has been stated in the Introduction, active systems are far from thermodynamical limit, and therefore fluctuations play an important role in their dynamics. A common phenomenon observed are **giant number fluctuations** (GNF): for some systems of self-propelled units, the fluctuations of the number of particles linearly scale with the number of units N of an increasing region, in contrast with

classic fluctuations in equilibrium systems scaling as $\sqrt{N}$ [168].

2.1.2 Living systems

There exist a plethora of active systems studied in the last decades by physicist and biologists, exhibiting many other features beyond the ones above introduced; the present section contains an overview of the most studied, specifying how the phenomena explained above are actually observed in living systems.

- **Bacteria**: bacterial colonies are one of the simplest systems made of a large number of interacting organisms and displaying a non-trivial macroscopic behavior. *Escherichia coli* is one of the most studied bacteria since the observation of traveling bands when seeking an optimal environment [105]. Further studies observed the presence of collective motion patterns such as super-diffusion, rotating and highly-correlated turbulent states.

  The motion of *E. coli* has shown for the first time another important dynamics, which is known as *run-and-tumble* motion [12]: bacteria follow a ballistic, constant speed motion (run) until they suddenly change their direction of motion (tumble), starting with another run in the new direction. This motion has been studied in several models and will be described in Sec. 2.2.3.

  Further experiments on a morphotype of *Bacillus subtilis* at high concentration showed the existence of a collective phase called "Zooming BioNematics" [49], where cells cluster move together in a swarming state at speeds larger than the average speed of a single bacterium. Giant number fluctuations are present. Some species spread very efficiently in a medium: this ability has been investigated experimentally [197], and it has been found that certain bacteria (*Myxococcus xanthus*) regularly reverse their direction, coming back to the colony and thus walking against a density gradient. This

Figure 2.3. Collective dynamics of swimming *B. subtilis* cells.[49]

behavior, a waste of energy and time at first sight, actually contributes to the alignment of swarming cells, reducing the probability of collisions and consequently the "active viscosity" of the medium.

- **Fishes**: fishes are commonly known to form *shoals* or *schools*, two different collective behaviors. The former indicates when fishes aggregate together, moving without a collective order (no swarming) and many species can be included. In the latter, fishes coherently move in the same direction (swarming), and can be then considered a special case of shoal. A shoal can also suddenly organize into a school and vice versa depending on the momentary activity, such as escaping predators, feeding, resting or traveling [92].

  Recording the trajectories of individual fishes in schools, both individual and collective behavior have been studied. Depending on the density of units, a transition from disorder to correlated motion has been found [11]. Also, observations on *Notemigonus Crysoleucas* trajectories produced data about the structure of the interactions in schools: the last don't seem to be governed by an alignment rule but rather by a speed regulation which is the crucial ingredient of interactions, while alignment only modulates the strength of speed regulation. Furthermore, it has been claimed that fish interactions are not pairwise, but rather multiple-bodies interactions more suitable to explain the observed dynamics [104].

  Fish schools are a system of great interest for *decision making processes* into collective motion, e.g. trying to understand if there is a leader fish or a kind of consensus, and how the size of the school influence decision making. Some experiments have shown the ability of groups of fishes to influence the entire school, or that individual fish responded when a threshold number of conspecifics performed a particular behavior (*quorum responses*). Nevertheless, decision making and leader-follower behavior is still under debate.

- **Bird flocks**: birds flying together usually form spectacular flocks exhibiting great order in their collective behavior, giving rise to highly-coordinated motion patterns. These have been studied for thirty years, but in the last decade the most important experimental observations have been carried out on *Sturnus vulgaris*, European Starlings, observing flocks containing up to 2 600 units: tracking the position and velocity of each bird, it was possible to reconstruct the dynamics of the network through the spatial distribution of nearest neighbors of each bird, which is represented in Fig. 2.4b. In the same experiment [8], it has been observed that birds interact with their 6-7 closest neighbors - "topological interaction" - instead of those within a certain distance - "metrical interaction". Different kinds of interaction give rise to different models, especially concerning the role of density in flocks. On the contrary, further experiments concerning various species [37] suggested that the range of interaction did not change with density. Further experiments focused on velocity correlations unveiled that these follow a power law decay with a unexpectedly small exponent, meaning that every bird may have an effective perception range much larger than the distance with its first neighbors [42]. All these points are still under debate and further simulations and

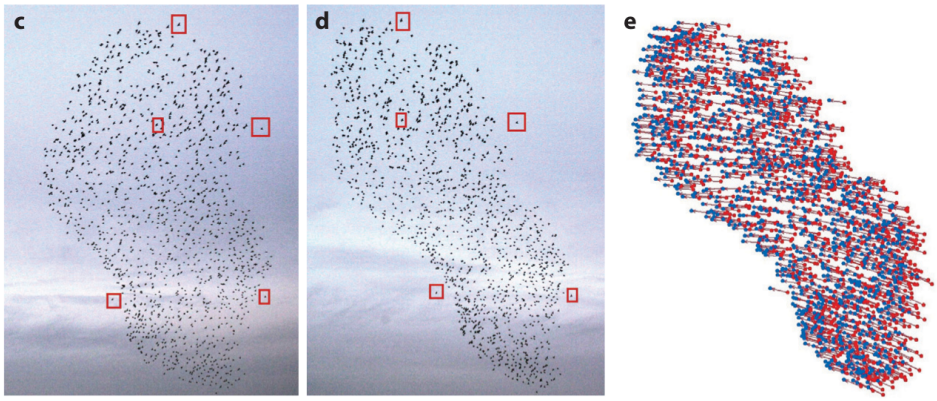

(a) Bird flocking and the representation of their $3d$ observed velocities.

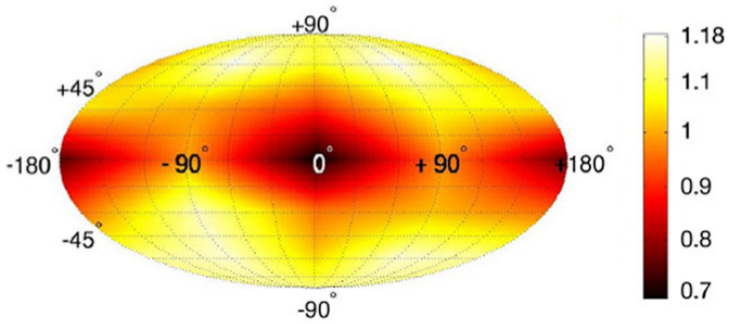

(b) Angular distribution of the birds' nearest neighbors. The distribution is strongly anisotropic and there is a lack of neighbors in the direction of motion.

Figure 2.4. Bird flocks

observations are needed.

- **Humans** can be considered active matter as well. Indeed, when a large number of people are present, self-organization takes place: for instance in the growth of settlements, traffic dynamics or pedestrian movement. At the end of 90s some studies started using collective motion methods to describe human behavior in these cases. Comparison between models and experiments have been related to motion of human trail systems [91] and escape panic [90], leading to possible prescriptions on architectural and urban structures to facilitate human motion and prevent accidents.

  Further experiments focused on the role of consensus and leadership in human crowds, where a randomly chosen person had the goal of guiding the group towards a random target without explicit communication: providing none or some information about the presence of a leader, the group always reached the target but with a less accurate motion when no information about the leader where given, and with a high accurate motion when the group knew of its presence (even without knowing its identity) [75].

2.1.3 Non-living systems

As said before, active systems can be also realized out of biological context. A kind of particles extensively studied in the field are **Janus particles**: their name come from the two-faced roman God Janus, because they consist of particles made by two or more parts having different chemical or physical properties. Thus, even a spherical particle can break geometrical rotational invariance and when a particle is at contact with the environment the different reactions on its surface generate a net force acting as a self-propulsion [12]. Janus spherical particles can be made for instance by a hydrophilic hemisphere separated from a hydrophobic one; in Fig. 2.2 the cluster formation of Janus particles is shown.

Janus particles are a special kind of non-living active particles called **artificial microswimmers**, i.e. artificially generated particles exploiting some kind of symmetry breaking to self-propel themselves. There are two main categories of propulsion mechanisms: local conversion of energy (such as catalytic processes) or driving by an external field (e.g. electric, magnetic, acoustic); it is important to stress that there is a deep difference between particles that are internally driven active matter and particles brought out of equilibrium by the action of external fields: though there exist similar effective models describing both categories, they show quite different microscopic details. An extended catalogue of such particles has been reviewed in [12]. A category of artificial active systems made of macroscopic units are **collective robotics**, namely groups of robots moving on a plane (and sometimes in a $3d$ region), able to sense obstacles, localize themselves with respect to a static frame and broadcast information with the other units. The very interesting feature of collective robotics is that interaction rules and individual behavior can be externally driven by humans, so they can represent a practical guide to understand how collective behavior stems from individual propulsion and local interactions. Also for collective robotics, several collective motions have been classified, like marching, oscillations, wandering and swarming [177]. There is a huge field of possible applications of collective robotics, such as localization of hazardous emission sources, surveillance in hostile or dangerous places, optimization of telecommunication networks. Last but not least, **driven granulars** have been studied in the framework of active particles in the last decade. Actually, a granular particle moving on a vibrated, rough plate feels the action of a *mechanical* driving mechanism able to sustain its state of motion: this feature can be correctly interpreted as a self-propulsion mechanism. Experiments on vibrated granular rods

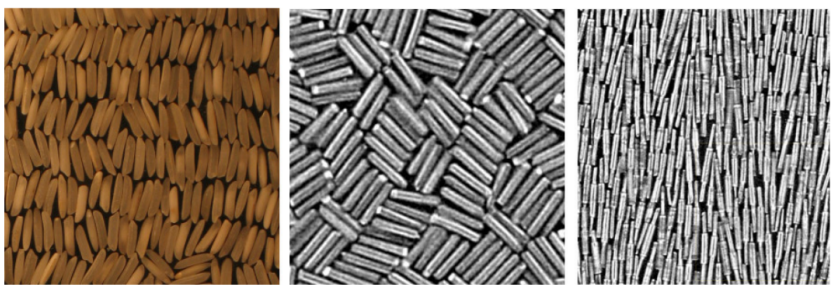

Figure 2.5. Orientational order in apolar granular rods: [149]

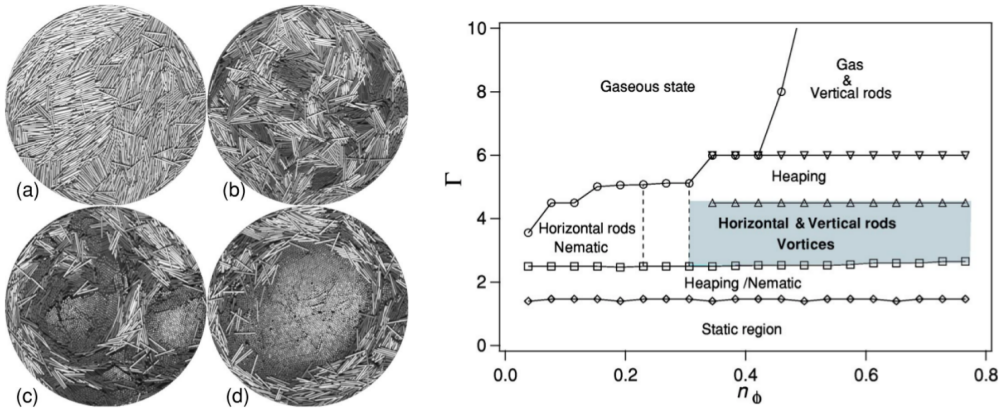

Figure 2.6. Active phases in vertically vibrated granular rods. Left panel, pattern formation: (a) nematiclike state, (b) moving domains of near vertical rods, (c) multiple vortices and (d) large vortex. See [26] for experimental details. Right panel: phase diagram. All the realizations have frequency $f = 50$ Hz. Vortices appear for sufficiently high density n and vibration amplitude Γ.

showed the presence of collective motion: when considering apolar, symmetric rods, nematic order and persisting swirling have been found [149], together with giant number fluctuations; moreover, varying the shape of granular rods several patterns of orientational ordering have been found, see Fig. 2.5. Also vortices can appear, when ordered domains made by nearly vertical granular rods coherently swirl and grow in time (coarsening), depending on packing fraction and vibration amplitude [26] (see Fig. 2.6). Conversely, apolar rods (with a head and a tail) have also been studied, displaying local ordering, aggregating at side walls and clustering; when the shaking amplitude is increasing, a collective swirling motion is observed [114]. Collective behavior and pattern formation in granular matter has been reviewed in [3]. Many of these features suggested a comparison between driven granular and active matter, at least from a phenomenological point of view because of pattern formation, clustering, and so on. Experiments mostly concentrated on the shape of grains, arguing that an oriented shape (like rods instead of disks or spheres) was necessary to create anisotropic relations and thus an aligning mechanism. At the end of this chapter, it will be shown how this is not necessary and that inelasticity can play a crucial role in collective dynamics.

2.2 Active models

Collective phenomenology introduced in the above section raised a series of questions about its theoretical description: as we saw, there are many kind of collective motion exhibited by several living and non-living systems. Hence, a good modelization of active matter is very difficult if one wants to replicate *all* the observed features in a single, universal model, and it is rather preferable to seek for essential ingredients of motion leading to the emergence of collective behavior. Statistical mechanics is a powerful tool to develop a theoretical representation of active mat-

ter: many models start from Brownian motion and add some prescriptions about interactions and self-propulsion. These are the main ingredients of active matter models and, before introducing the most established, it is useful to give a short classification of active systems.

Active systems can be **dense or dilute**: in human made systems density is a control parameter which can be easily tuned, but biological, self-organized systems show characteristic densities that change their motion properties. Density affects interactions and observed phases: indeed at higher densities the effect of excluded volume gets more important, and self-trapping becomes more probable. Also, in dense systems particles are more likely to interact continuously between the same ones, and Molecular Chaos assumption - as stated in Eq. (4.14) - often does not give a good approximation.

Interactions can also be produced by several different mechanisms, as it has been described before, and have various physical features. Vicsek and Zafeiris classified them as [192]

- physical, chemical, visual or medium-mediated
- isotropic or anisotropic, polar or apolar
- metrical or topological
- short or long-range

For instance, driven granulars collide between themselves (physical interaction) while birds in flocks almost never do it, probably interacting through a visual mechanism. Generally speaking, the shape and symmetries of the units affect the typology of the interactions: for instance, granular rods are nematic and apolar particles, while Janus spheres are isotropic and polar. Any combination of these properties is possible, accounting for several possible interactions. It has been shown that the notion of distance in collective motion is ambiguous: birds in a flock seem to interact through a topological rather than metrical distance, as said in Sec. 2.1.2. The case of medium-mediated or long-range interactions deserves a specific consideration: until now, self-propulsion mechanism has always been considered as a momentum and energy injection in a unity able to convert internal energy into kinetic energy, or to generate a non-trivial motion in presence of external fields. However, the role of surrounding medium (excluding external fields) was generally neglected. Actually, neglecting external forces such as gravity active particles can change their motion only by interacting with the surrounding fluid: the total momentum of the fluid and the active unit *does not change* in the self-propulsion reaction, because particles moving in some direction push the fluid in the opposite one, as we do when we swim or we row on a boat. Particles generally create a force dipole, which can have various shapes depending on self-propulsion mechanism and propagates across the fluid, see Fig. 2.7, and reaches other units at long-range distances [10, 135]. These are called *hydrodynamic interactions* and motivate two kinds of active models: **dry or wet active matter**. In the latter, it is not always necessary to consider the coupled evolution of the swimmers and the surrounding fluid, but one can consider the fluid as a mediator of interactions between active particles, transmitted for instance by means of hydrodynamic waves. These

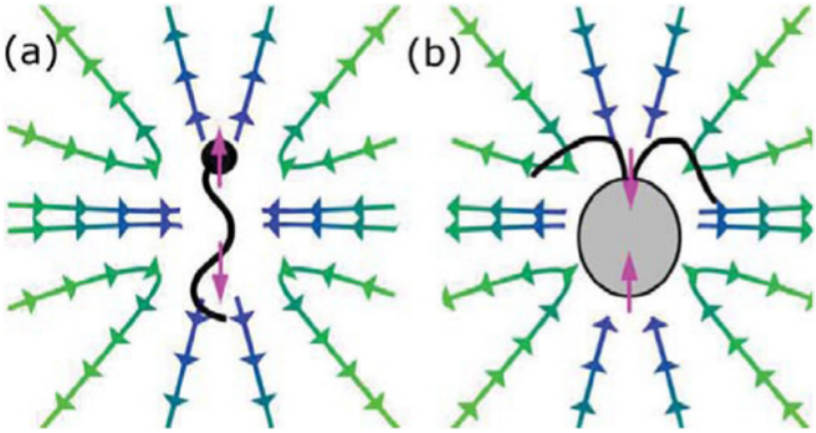

Figure 2.7. Force dipoles in a fluid medium generated by microswimmers, namely called (a) *pushers* or (b) *pullers*, depending on the polarity of their swimming mechanism: purple arrows display the self-propelling forces [66].

particles are called *microswimmers* and have been reviewed in [66, 12]. It can be summarized that in dry models self-propulsion is an individual force, which any particle feels independently and momentum is not conserved; in the other hand, in wet models the self-propulsion is always coupled with a momentum transport, which propagates in the medium and is transmitted to surrounding particles, and the *total* momentum is always conserved.

The role of **equilibrium** in active matter description and models is very important and currently under debate: it is physically clear that active matter is *out of equilibrium* because of continuous energy dissipation and injection occurring in the single active units, and that non-conservative interactions are acting. However, many studies on active matter use an equilibrium description, defining an effective Hamiltonian, temperature and free energy leading to equilibrium phase transitions [178, 23, 174, 152]. For instance, aligning interactions inspired a modeling of birds flock as ferromagnetic models, inspired from Ising, Heisenberg or XY models [57, 47, 82, 175, 147]. This approach is clearly motivated by the wide and self-consistent progresses made by equilibrium statistical physics and critical phenomena through the last century. However, its application needs some justifications: these have been studied in the very last years and related to the characteristic *time scales* of the system. Indeed, if a scale separation is present between equilibrium and out-of equilibrium mechanisms, a *local equilibrium approximation* can be made to consider the local time behavior of the system as an equilibrium process. In 2016, Mora *et al.* [147] studied the case of bird flocks using a ferromagnetic model, driven out of equilibrium by network rearrangement, typical of active matter. The experimental comparison between the alignment relaxation time τ_r and network rearrangement time τ_n showed that $\tau_r \ll \tau_n$, therefore interactions occur at almost fixed network: this result justifies a local equilibrium approximation for the model purposed. Furthermore, few weeks before Fodor *et al.* published a study with the aim of *quantifying* the non-equilibrium properties of an active matter model, namely the Active Ornstein-Uhlenbeck Particles model (see Sec. 2.2.4).

In this model, active particles feel a self-propelling persistent velocity with a correlation time τ: the authors have shown that the entropy production is of order $\mathcal{O}(\tau^2)$ for small τ, and therefore argued that there exists a regime where direct and reversed trajectories have the same probabilities, entropy production vanishes and the system relaxes towards an effective Boltzmann distribution [78]. In both cases, some specific models have been used to give a quantitative analysis of non-equilibrium properties and justify the local equilibrium approximations made; a general response about the limits of equilibrium properties in active matter is still under investigation [137].

It is now evident that an active model is composed by two ingredients: a **self-propulsion** mechanism and an **interaction** rule. Their qualitative properties, especially for interactions, have been overviewed in this paragraph; the following paragraphs are dedicated to successful models that headed the study of active matter in the last decades. It has to be stressed that self-propulsion and interactions can be considered separately, and that the self-propulsion mechanism of a model can be combined with the interaction rule of another model. So, two models of interactions will be introduced: the Kuramoto model and the Vicsek model, respectively in Sec. 2.2.1 and 2.2.2. In further sections self-propulsion models will be introduced. Any realistic model of active particles requires an implementation of both ingredients.

2.2.1 Kuramoto model

Kuramoto model, introduced in 1975 [117, 118], is one of the most successful models describing collective *synchronization* of coupled rotators. Its success consisted in an essential description of transition to order by means of "aligning" interactions, tuned by the coupling strength as the control parameter of the system. A complete review of the model can be found in [1]; for the need of this thesis, also the analysis in [16, 17] is sufficient.

Consider a set of N coupled rotators of phase θ_j, with quenched random frequencies ω_j: the standard Kuramoto model dynamics is given by

$$\dot{\theta_j} = \omega_j + \frac{K}{N} \sum_{k=1}^{N} \sin(\theta_k - \theta_j). \tag{2.5}$$

This evolution equation describes a system of overdamped rotators moving at a fixed and random individual frequency ω_j modified by a sort of elastic interaction among all of them, with fixed intensity K/N: each rotator feels the phase difference with other rotators as an attractive force to the synchronized state where $\theta_k = \theta_j$ for all j, k. The transition to synchronization can be analyzed in few steps: first, one sees that the global motion of phases evolves through the deterministic equation

$$\frac{1}{N} \sum_{j=1}^{N} \dot{\theta}_j = \frac{1}{N} \sum_{j=1}^{N} \omega_j = \Omega \tag{2.6}$$

where the last equivalence defines the global frequency Ω: it is convenient to define a sort of "center of mass" frame, where $\theta \to \theta - \Omega t$ and $\omega \to \omega - \Omega$: evolution

equation (2.5) is invariant under this translation and the new global frequency of the system vanishes, i.e. $\sum_j \omega_j = 0$.

Synchronization can be observed through the complex order parameter

$$re^{i\psi} = \frac{1}{N}\sum_{j=1}^{N} e^{i\theta_j} \tag{2.7}$$

which is finite in the large size limit, defining the *coherence* r and the *global phase* ψ. Their meaning is evident if one considers the swarming phase described in Sec. 2.1.1: when $r \approx 0$, rotators move with random, disordered phases and no global order is observed; conversely, when $r \approx 1$, rotators are locked to the same phase oscillating with the same frequency and acting as a unique, giant rotator. By means of the complex order parameter, evolution equation of the single rotator can be written as

$$\dot{\theta}_j = \omega_j + Kr\sin(\psi - \theta_j) \tag{2.8}$$

where r and ψ generally depend on time.

In the large size limit, we call $g(\omega)$ the density of natural frequencies ω_j, normalized to one and assumed even for simplicity and symmetry reasons. The probability distribution of the phase θ for an rotator of given frequency ω is called $\rho(\theta|\omega, t)$, and evolves according to

$$\frac{\partial\rho}{\partial t} + \frac{\partial}{\partial\theta}\left[(\omega + Kr\sin(\psi - \theta))\,\rho\right] = 0 \tag{2.9}$$

which stems from Eq. (2.8) and must be completed by the initial condition $\rho(\theta|\omega, 0)$. In the infinite N limit, the complex order parameter can be computed as

$$re^{i\psi} = \langle e^{i\theta}\rangle = \int_{-\pi}^{\pi} \mathrm{d}\theta \int_{-\infty}^{+\infty} \mathrm{d}\omega\, e^{i\theta}\rho(\theta|\omega, t)g(\omega). \tag{2.10}$$

The last equation has a stationary uniform solution $\rho(\theta|\omega) = 1/(2\pi)$ for all values of coupling constant K: the solution yields $r = 0$ and uniform distribution of phases, i.e. no synchronization. Synchronized solutions can be found looking at fixed points of Eq. (2.8): assuming $r > 0$ and $\psi = 0$ without loss of generality, if $|\omega| < Kr$ one has a stable fixed point $\theta_0 = \sin^{-1}(\omega/Kr)$; otherwise, for $|\omega| > Kr$ there are no fixed points. Therefore a stationary distribution of rotator's phases can be piecewise defined as

$$\rho(\theta|\omega) = \begin{cases} \delta\left[\theta - \sin^{-1}(\omega/Kr)\right] & |\omega| < Kr \\ \\ \frac{1}{2\pi}\frac{\sqrt{\omega^2 - (Kr)^2}}{|\omega - Kr\sin\theta|} & |\omega| > Kr \end{cases} \tag{2.11}$$

where the second line is given by Eq. (2.9) with $\partial_t = 0$. The coherence r can be computed through Eq. (2.10), and the only non-vanishing term is the one for $|\omega| < Kr$ [176]. So,

$$r = \int_{-\pi}^{\pi} \mathrm{d}\theta \int_{-Kr}^{Kr} \mathrm{d}\omega\, e^{i\theta}\delta[\theta - \sin^{-1}(\omega/Kr)]g(\omega). \tag{2.12}$$

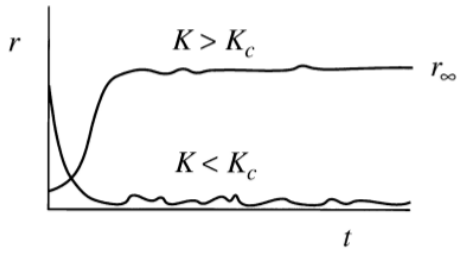

(a) Coherence in function of time for trajectories above and below the critical coupling K_c.

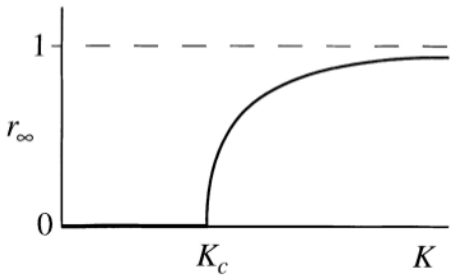

(b) Steady-state coherence in function of critical coupling K.

Figure 2.8. Synchronization in Kuramoto model [176]

The latter has a consistent solution only if

$$K > K_c = \frac{2}{\pi g(0)} \tag{2.13}$$

having assumed that frequency distribution $g(\omega)$ has a maximum in 0. Therefore, K_c is the critical value of the coupling strength above which synchronization occurs, see Fig. 2.8. If $g(\omega)$ is regular up to ω^2 terms around $\omega = 0$, the coherence parameter scales as $r \sim (K - K_c)^{1/2}$.

Kuramoto model has been studied and generalized accounting for inertia of rotators, friction force, non-uniform couplings K_{kj} and noise terms; the latter is generally introduced adding a Gaussian White Noise (GWN) term $\eta_j(t)$ to evolution equation (2.5), with $\langle \eta_j(t) \rangle = 0$ and $\langle \eta_k(t)\eta_j(t') \rangle = 2D\delta_{kj}\delta(t - t')$. Noise introduces a second control parameter competing with coupling strength K, because the former leads the system away from order while the latter is accounting for synchronization: a more detailed discussion on oscillators phases and their linear stability can be found in [1].

2.2.2 Vicsek model

The Vicsek model is a milestone in the theoretical description of self-propelled particles. Introduced in 1995 by Vicsek *et al.* [191], the model aims at reproducing the self-ordering of active systems. The original model consists of N point particles moving on a periodic square cell of linear size L, with positions $\mathbf{x}_j(t)$ and velocities $\mathbf{v}_j(t)$ of constant modulus v. Velocities are described only by their orientation $\theta_j(t)$ and equations of motion in discrete time read

$$\mathbf{x}_j(t + \Delta t) = \mathbf{x}_j(t) + \mathbf{v}_j(t)\Delta t \tag{2.14a}$$

$$\theta_j(t + \Delta t) = \langle \theta(t) \rangle_R + \xi_j(t) \tag{2.14b}$$

with $\Delta t = 1$, being $\langle \theta(t) \rangle_R$ the average direction of particles' velocities within a circle of radius R from the focusal particle j, which is included in the average, namely

$$\langle \theta(t) \rangle_R = \tan^{-1}\left(\frac{\langle \sin\theta(t) \rangle_R}{\langle \cos\theta(t) \rangle_R} \right). \tag{2.15}$$

The term $\xi_j(t)$ is a random number drawn with uniform distribution in the interval $[-\eta/2, \eta/2]$. Since particles have no volume, without loss of generality the interaction radius can be taken $R = 1$. The free parameters of the system are then η (noise), $\rho = N/L^2$ (number density) and v (speed, i.e. the distance run by a particle between two updates); self-propulsion is guaranteed by the constant speed v. Varying the parameters η and ρ several phases can be observed - see Fig. 2.9. Especially, at high density and small noise a global ordered swarming state arises. Fixing the speed at $v = 0.03$, the authors looked at the swarming order parameter

$$v_a = \frac{1}{Nv} \left| \sum_{j=1}^{N} \mathbf{v}_j \right| \tag{2.16}$$

and observed a non-equilibrium transition when the noise is reduced below a critical value $\eta_c(\rho)$, or alternatively when the density is increased above $\rho_c(\eta)$. The transition is studied for several number of particles and gets sharper for large N, see Fig. 2.10. Thus, even in a non-equilibrium system as the one studied a phase transition occurs which is quite similat to an equilibrium transition. From previous results the authors argue that in the thermodynamic limit the swarming parameter

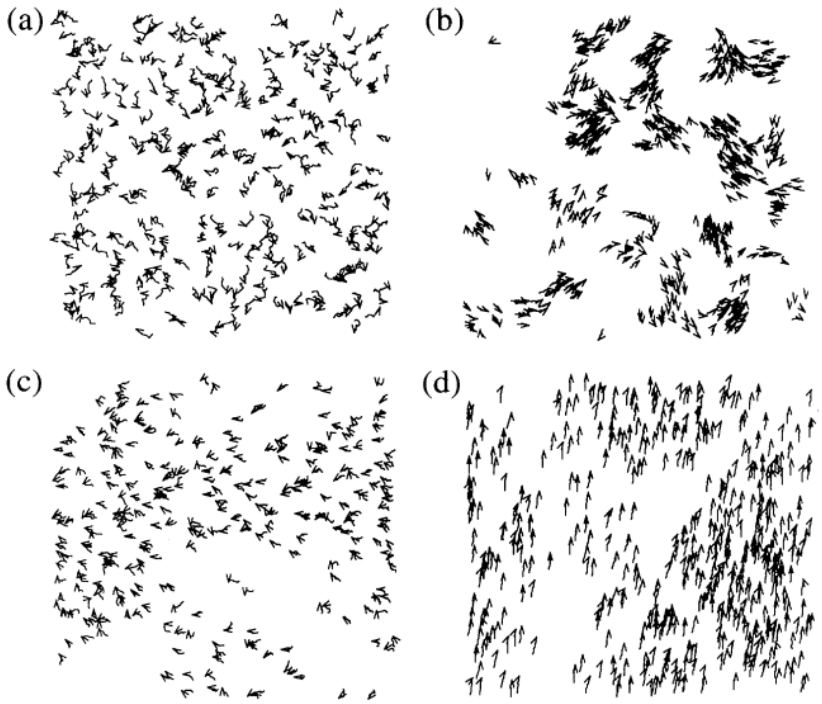

Figure 2.9. Snapshots of the Vicsek model with $N = 300$ particles: velocities are indicated by a small arrow and trajectories for the last 20 time steps is shown by a short continuous curve. Panels show (a) initial disordered configuration at $L = 7$ and $\eta = 2.0$, (b) formation of coherent motion groups for small densities and noise, $L = 25$ and $\eta = 0.1$, (c) randomly moving particles with some correlation for high density and noise, $L = 7$ and $\eta = 2.0$ and (d) collective swarming for high densities and small noise, $L = 5$ and $\eta = 0.1$ [191].

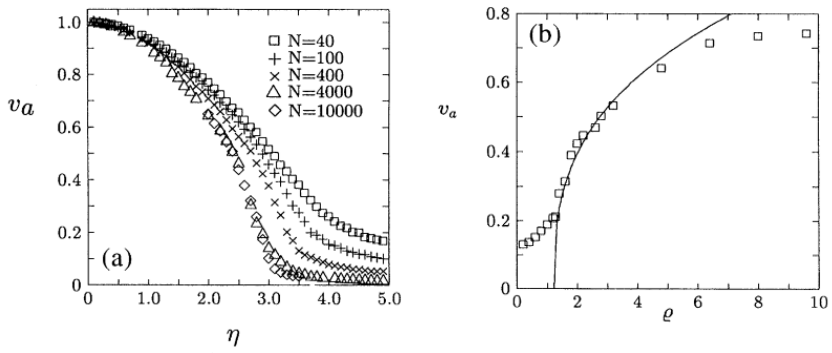

Figure 2.10. Swarming parameter v_a in function of noise η (left) and density ρ (right). In left panel, density is kept constant and cell size is varied according to legend; in right panel, noise is constant and cell size is $L = 20$ [191].

scales as

$$v_a \sim [\eta_c(\rho) - \eta]^{\beta} \qquad , \qquad v_a \sim [\rho - \rho_c(\eta)]^{\delta} \, , \tag{2.17}$$

defining the critical exponents β and δ. Numerical fits give $\beta = 0.45 \pm 0.07$ and $\delta = 0.35 \pm 0.06$. Combined results are the basis to build a phase diagram in the plane $\eta - \rho$: the critical line has been numerically found as

$$\eta_c(\rho) \sim \rho^{\kappa} \tag{2.18}$$

with $\kappa = 0.45 \pm 0.05$ [56].

A first application of Vicsek model has been the description of hydrodynamics and vortex formation in bacteria colonies for the case of *Bacillus subtilis* [55]. Further analysis on the Vicsek model showed the presence of moving clusters, a strong connection with XY model especially at low speed $v \ll 1$, and a similar behavior when considering different shapes of the surface [57]; Vicsek model has been enhanced and modified considering nematic (apolar) particles, adding cohesion and introducing the role of surrounding fluid [47]. Moreover, a strong connection between Kuramoto and Vicsek model has been found, because the two models show a similar bifurcation behavior under variation of control parameters [48]: indeed, synchronization in Kuramoto model is the equivalent of swarming in Vicsek model. The success of Vicsek model is basically resumed in the sentence

> We have chosen this realization because of its simplicity, however, there may be several more interesting alternatives of implementing the main rules of the model. In particular, the absolute value of the velocities does not have to be fixed, one can introduce further kind of particle interactions and or consider lattice alternatives of the model. [191]

Actually, Vicsek model is a very commonly used starting point to observe collective motion from microscopic behavior of self-propelled interacting particles, and many subsequent models are variations of this one [192].

2.2.3 Active Brownian Particles and Run-and-Tumble Dynamics

After having considered Kuramoto and Vicsek model as a starting point to introduce ordering interactions in a system of active particles, the most used models of self-propelled particles will be introduced. The goal of all the following descriptions is to introduce a self-propulsion mechanism accounting for two properties

- keep the particle in a constant state of motion, avoiding cooling because of dissipative collisions or interactions with the environment
- describe the changes of direction in particle's motion.

In this section only *dry* particles are considered, which means that self-propulsion does not conserve momentum as it has been discussed above.

Active Brownian particles (ABP) are one of the most general model of active particles [12]: each unit is a Brownian particle performing active motion, generated by internal energy storing or nonlinear velocity-dependent friction [170]. ABPs equations of motion for a particle of unit mass $m = 1$ generally read

$$\dot{\mathbf{r}} = \mathbf{v} \tag{2.19a}$$

$$\dot{\mathbf{v}} = \mathbf{F}_d(\mathbf{r}, \mathbf{v}) - \nabla U(\mathbf{r}) + \boldsymbol{\xi}(t) \tag{2.19b}$$

where $\mathbf{F}_d(\mathbf{r}, \mathbf{v})$ is a position and velocity-dependent dissipation force, $U(\mathbf{r})$ an external potential and $\boldsymbol{\xi}(t)$ a stochastic force acting on the particle. For $F_d = -\gamma\mathbf{v}$ and $\boldsymbol{\xi}(t)$ GWN satisfying the Einstein relation $\langle \xi_\alpha(t)\xi_\beta(t')\rangle = 2\gamma T\delta_{\alpha\beta}\delta(t-t')$, one recovers the classical Brownian motion at equilibrium. On the contrary, a different choice of dissipation is sufficient to have a self-propulsion force: a suitable choice is to define a velocity dependent friction $\mathbf{F}_d = -\gamma(\mathbf{v})\mathbf{v}$, e.g.

$$\gamma(\mathbf{v}) = -a + bv^2 = a\left(\frac{v^2}{v_0^2} - 1\right) \tag{2.20}$$

leading the particles to the stable fixed point $v_0 = \sqrt{a/b}$: nonlinear friction *accelerates* the particle in its direction of motion for $v < v_0$ and slows it down for high speed $v > v_0$. This velocity-dependent friction is called Rayleigh-Helmoltz friction. An exact solution of Eq. (2.19b) without noise or external potential is given in Appendix B.1. Without noise or interactions, no changing of orientation is possible. When the noise is Gaussian and white with variance $2D$, the probability density $P(\mathbf{r}, \mathbf{v}, t|\mathbf{r}_0, \mathbf{v}_0, t_0)$ of this process follows the Kramers' Equation [80]

$$\frac{\partial P}{\partial t} + \mathbf{v}\cdot\nabla P - \nabla U(\mathbf{r})\cdot\frac{\partial P}{\partial \mathbf{v}} = \frac{\partial}{\partial \mathbf{v}}\left[\gamma(\mathbf{v})\mathbf{v}P + D\frac{\partial P}{\partial \mathbf{v}}\right] \tag{2.21}$$

which in the homogeneous case $\nabla = 0$ (no spatial gradients) has a stationary solution

$$P_0(\mathbf{v}) = \mathcal{N}\exp[-\Phi(\mathbf{v})/D] \tag{2.22}$$

where $\Phi(\mathbf{v})$ is a velocity-dependent effective potential, namely $\Phi(\mathbf{v}) = \int^{\mathbf{v}} \mathrm{d}\mathbf{v}'\gamma(\mathbf{v}')\mathbf{v}'$, holding for a general choice of $\gamma(\mathbf{v})$; for Rayleigh-Helmoltz viscosity, one has $\Phi(\mathbf{v}) = -\frac{a}{2}v^2 + \frac{b}{4}v^4$. Depending on the sign of a particles motion is *passive* ($a < 0$) or *active*

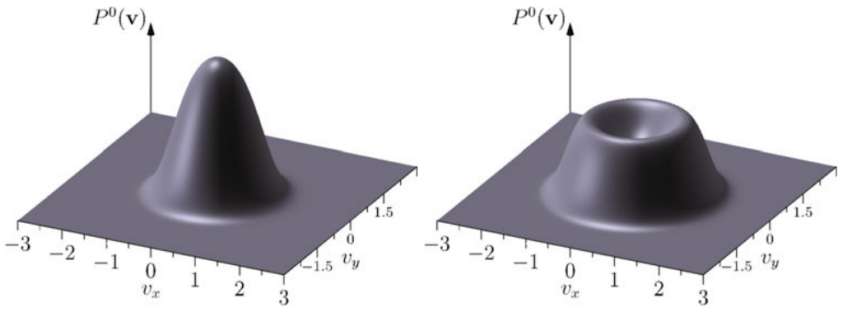

Figure 2.11. Stationary velocity distribution $P_0(\mathbf{v})$ (2.22) in the Cartesian plane for Rayleigh-Helmoltz friction. Left panel: passive regime with $a = -0.1$. Right panel: active regime with $a = 1.0$. In both cases $b = 1.0$ and $D = 0.5$ [170].

$a > 0$; active particles potential has the typical mexican hat shape, leading to a continuous set of minima with speed $|\mathbf{v}| = v_0$, see Fig. 2.11; there is spontaneous symmetry breaking in each trajectory where particles travel along a given direction, which is what one observes when looking at experiments and simulation on swarming particles.

The stationary distribution in Eq. (2.22) has a limit value for the high dissipation regime: if $b/D \to \infty$ while $v_0 = \sqrt{a/b}$ remains finite, the distribution converges to a delta function

$$P_0(\mathbf{v}) = \delta(|\mathbf{v}| - v_0). \tag{2.23}$$

The latter applies when the relaxation time towards the fixed point v_0 is extremely small compared to the characteristic time of rotational diffusion. Therefore, particles can be considered at constant speed $\mathbf{v} = v_0$ and their motion is described by the angular orientation $\theta(t)$. Two possible dynamics are **angular diffusion** [17] or **run-and-tumble dynamics** [171, 178], frequently used to describe active systems, especially for crowded environments such as bacteria colonies [12]. In the former, the orientation evolves gradually, following a Wiener process with diffusion coefficient D_R, namely

$$\dot{\theta} = \sqrt{2D_R}\xi(t) \tag{2.24}$$

where now $\xi(t)$ is a GWN of unit variance; on the other side, run-and-tumble dynamics consists of particles following a ballistic, straight motion and undergoing instantaneous scattering events $\theta \to \theta + \eta$ at a rate λ per unit time, where η is a random angular variable with distribution $p(\eta)$. Both dynamics can be expressed by the Fokker-Planck equation

$$\frac{\partial P}{\partial t} + v_0 \mathbf{e}(\theta) \cdot \nabla P = I[P] \tag{2.25}$$

where $\mathbf{e}(\theta)$ is the unit vector in the direction θ and the functional $I[P]$ accounts for diffusion rule, which for angular diffusion reads

$$I[P] = D_R \frac{\partial^2 P}{\partial \theta^2} \tag{2.26}$$

while for run-and-tumble dynamics one has [17]

$$I[P] = -\lambda P(\mathbf{r}, \theta, t) + \lambda \int_{-\infty}^{+\infty} \mathrm{d}\eta p(\eta) P(\mathbf{r}, \theta - \eta, t) \tag{2.27}$$

Both angular diffusion and run-and-tumble particles reproduce the tendency of active particles to explore space by changing their orientation, for instance when seeking nutrients. It is usual to read of active Brownian particles as a synonym of angular diffusion motion. Angular diffusion is often used to describe the motion of self-propelling Janus colloids, while run-and-tumble dynamics has been introduced to describe the motion of *E. coli* bacteria [12]. It has been shown that, despite the two models follow quite different microscopic dynamics, their diffusion properties for long times are equivalent [40]; an effective equilibrium regime has been found and can be applied for both models if angular diffusion and tumbles act on the same time scale [174].

2.2.4 Active Ornstein-Uhlenbeck Particles

Another interesting modelization of self-propelling particles is the Active Ornstein-Uhlenbeck Particles model (AOUPs), introduced in the last years [109, 74, 130, 136]. Its simplest version consists of particles following the overdamped motion equation

$$\dot{\mathbf{r}} = -\mu \nabla U(\mathbf{r}) + \mathbf{v}(t) \tag{2.28}$$

where μ is the mobility, $U(\mathbf{r})$ an external or interaction potential, and $\mathbf{v}(t)$ a noise term which is persistent rather than white in time, namely

$$\langle \mathbf{v}(t) \rangle = 0, \tag{2.29a}$$
$$\langle v_\alpha(t) v_\beta(t') \rangle = \delta_{\alpha\beta} \Gamma(t - t'). \tag{2.29b}$$

The memory term is often taken as $\Gamma(t) = \frac{D}{\tau} e^{-|t|/\tau}$. In this case, the noise $\mathbf{v}(t)$ is an Ornstein-Uhlenbeck process [80], and the equation of motion (2.28) can be written as

$$\dot{\mathbf{r}}(t) = -\mu \nabla U(\mathbf{r}) + \mathbf{v}(t) \tag{2.30a}$$
$$\tau \dot{\mathbf{v}}(t) = -\mathbf{v}(t) + \sqrt{2D}\xi(t) \tag{2.30b}$$

where $\xi(t)$ is GWN of unit variance. AOUPs model is often called *Gaussian Colored Noise* model (GCN). Motion persistence produces a self-propulsion mechanism; in the limit $\tau \to 0$, memory effects vanish and Eqs. (2.30) reduce to overdamped Brownian motion equations. Persistence time τ is driving the system out of equilibrium, and can be considered as a *distance* from the latter [78]. An effective equilibrium description can be developed also for AOUPs [109, 136]. The model has been used to describe active colloids behavior [109] and motility-induced phase separation [74]; moreover, it turned to be a useful approach to describe accumulation of active particles around obstacles, i.e. walls, and a good approximation for the pressure generated by active matter [130].

Looking at Eq. (2.28), it is fundamental to clarify that in this case $\dot{\mathbf{r}} \neq \mathbf{v}$: the variable $\mathbf{v}$ is *not* the actual velocity of the units, feeling the action of potential $U(\mathbf{r})$

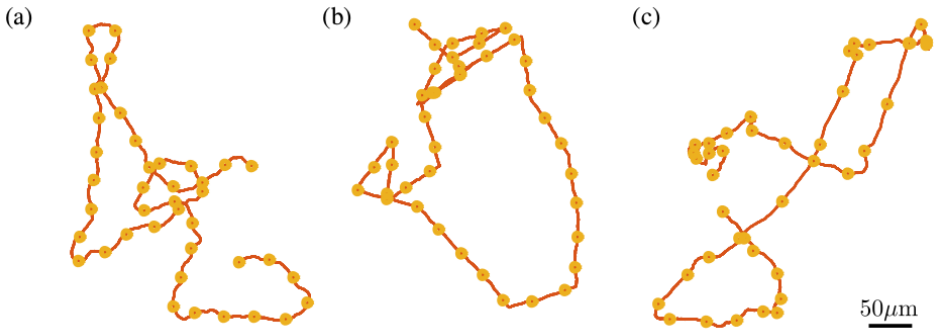

Figure 2.12. Sample trajectories illustrating three kinds of active motion of a single particle: (a) angular diffusion dynamics, (b) run-and-tumble dynamics, (c) active Ornstein-Uhlenbeck particle. The position of the particle (dots) is sampled every 5 s [12].

because of the overdamping, but rather an *active velocity* which represents an internal stochastic mechanism driving the particles to a certain speed and energy. Actually, the active velocity becomes the physical velocity of the unit when no external potential or interactions are present, i.e. the unit is free to move with velocity $\dot{\mathbf{r}} = \mathbf{v}$, so one may interpret the velocity $\mathbf{v}$ as an "intentional" velocity.

Although the discussed models have been developed to describe systems showing different behaviors at a microscopic scale, it is tempting to find a unified description of their behavior at a mesoscopic or macroscopic scale; while angular diffusion and run-and-tumble dynamics have shown an equivalent behavior at a macroscopic scale, it is still under debate if AOUPs model shares the same macroscopic properties. [12].

2.3 Grains and active particles

In Sec. 2.1.3 it has been shown how granular matter has been used to produce systems of active particles, when energy dissipation is balanced through some driving mechanism. Some questions arise: can active particles and driven granulars be considered two manifestations of the same physical phenomena? Is it possible to build a unified theory describing both of them?

Experiments on polar or anisotropic vibrated granular particles have shown the collective behavior illustrated in Sec. 2.1.3. To understand how granular collisions can lead to collective motion even for apolar and isotropic particles, we now consider the model of Grossman, Aranson and Ben Jacob [87]. In 2008, the authors examined a model of self-propelled smooth disks of unit mass moving on a $2d$ frictionless surface. Interactions between particles are inelastic and passive: they actually are a variation of granular collision rule (1.15), allowing overlap between particles. The degree of inelasticity is measured by a restitution coefficient α, analogously with granular collisions. At each time step, units also undergo a self-propulsion force compensating energy lost during collisions; the self-propelling force is constant in the direction of motion if $v < 1$, and vanishes for $v > 1$.

The model has been numerically studied under many conditions, varying the

number of particles, the number density and the restitution coefficient. Also, both reflecting and periodic boundary conditions have been implemented, and the model has been simulated with different confined geometries (circular, squared and elliptic). The main observation is the formation of vortices and collective migration - swarming - depending on boundary conditions and physical parameters of the system. In Fig. 2.13 the evolution of the swarming order parameter and snapshots of the system displaying swarming formation are shown. Furthermore, when a stochastic angular noise is added into motion equations - analogously to Vicsek angular noise - the competition between noise and density yields an apparent first-

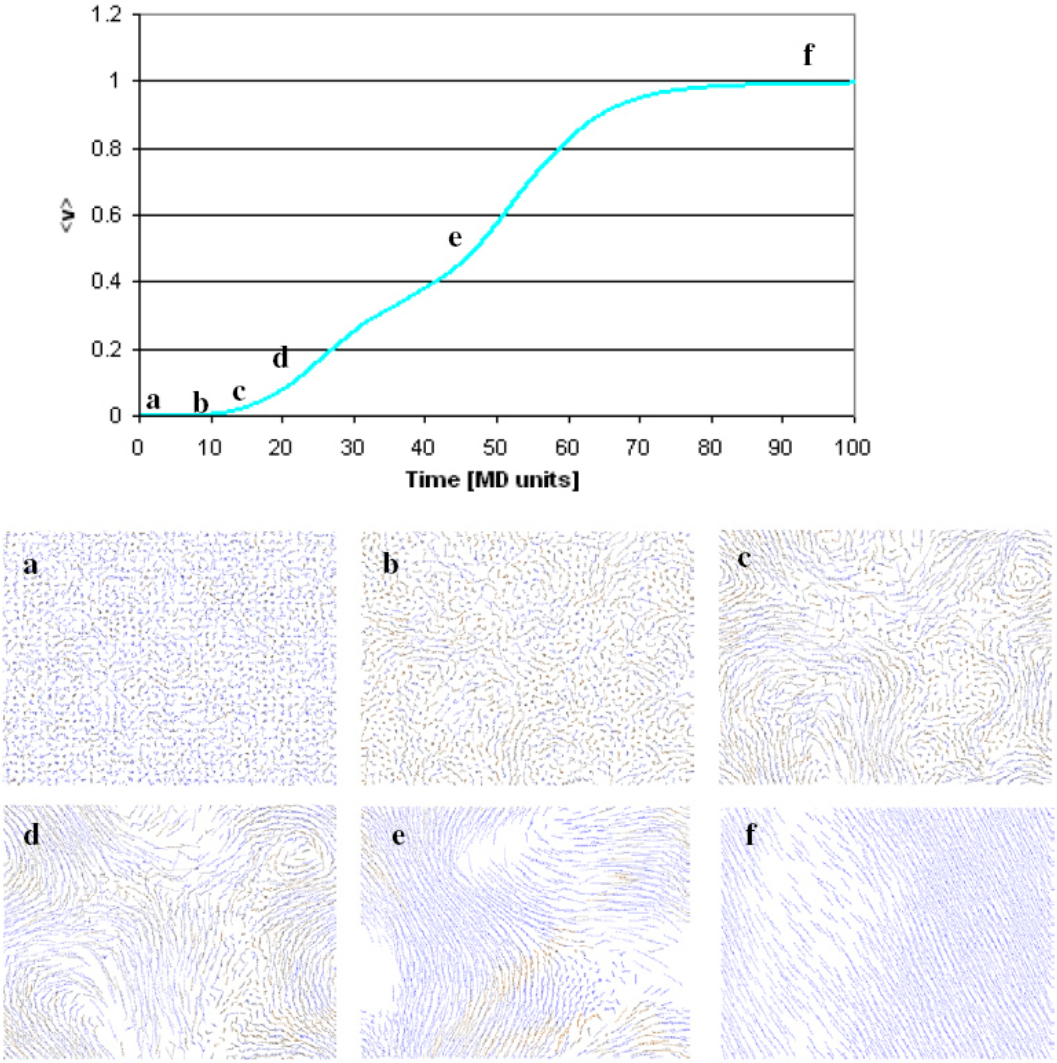

Figure 2.13. Evolution of Grossman *et al.* model [87] with periodic boundary conditions, $N = 1600$ particles, number density $n = 0.6$ and restitution coefficient $\alpha = 0.93$. Top panel: time evolution of swarming order parameter $\langle v \rangle = \frac{1}{N} \left| \sum_j \mathbf{v}_j \right|$. Bottom panel: snapshots of the system showing swarming formation. The letter of each snapshot corresponds to the time indicated in top panel.

order transition from disorder to swarming, as it had been observed by Vicsek *et al.* [191].

So, even a system of isotropic and apolar particles without steering or sensing capabilities has shown the presence of collective, ordered motion. The authors claim that

> [...] the results can be interpreted as if the inelastic interaction coupled with the self-propagation serves the equivalent role of the traditional velocity alignment force in the biologically inspired agent models.[...]
>
> The underlying reason why coherent motion is attained in our model is that simple inelastic collisions between isotropic particles create an increase in velocity correlation each time two particles collide. [87]

Therefore the *inelasticity*, increasing correlations between the particles, is playing the role of an effective aligning force, because after inelastic collisions velocities tend to increase their alignment (see Fig. 1.9). Active matter studies often distinguish between interactions with *explicit* or *implicit alignment rule* [192], where repulsion - like in the above-examined model - is considered a non-aligning force. This is true when considering elastic repulsion, but in the granular case the inelastic collisions have the same effect of aligning interactions: once the self-propelling force is increased enough to consider the speed v as a constant, the model of Grossman *et al.* is in every aspect a granular version of Vicsek model. In the last years, experiments on vibrated granular layers confirmed and studied the presence of collective motion for polar disks [195, 64] and a binary mixture of polar rods and spherical beads [116].

Granular and active matter have been frequently associated and studied together. Indeed, the continuous energy injection and dissipation mechanisms underlying their dynamics are quite similar, especially when considering bulk driven granular matter - see Sec. 1.4.5. Granular and active matter share similar practical applications, one of the most interesting being *Brownian motors* or *ratchets* [164, 12], namely the possibility of building devices where the random motion of granular or active particles is converted into directed, drifting motion of a bigger unit called the motor, thanks to the asymmetry under time reversal characteristic of out of equilibrium systems. However, while on one hand kinetic theory of granular matter has been developed in a systematic way in the last decades, on the other hand a systematic and general kinetic theory of active matter is missing. A framework where comparisons between granular and active matter can be done is the *hydrodynamic description*, which will be analyzed in the next chapter.

Quei giorni perduti a rincorrere il vento

3

Hydrodynamic description and lattice models

When a fluid is flowing for instance under the action of gravity or a pressure gradient, its motion can be described introducing the continuous *hydrodynamic fields* such as density $\rho(\mathbf{x}, t)$, velocity $\mathbf{u}(\mathbf{x}, t)$ and temperature $T(\mathbf{x}, t)$, measuring the *local* mechanical and thermodynamical properties of the fluid at the position $\mathbf{x}$ and time t. Hydrodynamic fields generally depend on time and space, and hydrodynamic equations aim at describing their time evolution, affected by spatial gradients and external forces.

Kinetic theory is the basis of hydrodynamic description. Although Euler and Navier-Stokes hydrodynamic equations were derived through continuum mechanics arguments, kinetic theory allows a derivation based on a clear separation of time and space scales: indeed, hydrodynamics is well-defined if the typical length of variation of the fields is much bigger than the mean free path of the particles between two collisions. In this chapter, the classical derivation of elastic hydrodynamics will be given in the first section, 3.1.1; then, hydrodynamic descriptions of granular matter - Sec. 3.1.2 - and active matter - Sec. 3.1.4 - will be overviewed. Sec. 3.2 will be devoted to *fluctuating hydrodynamics*, namely a hydrodynamic theory where the role of statistical fluctuations cannot be neglected as in classical hydrodynamics.

The second part of this chapter, Sec. 3.3, will be dedicated to the study of *lattice models*. Actually, the formulation of hydrodynamics presents many technical difficulties and needs many physical assumptions and approximations to derive a consistent set of equations. On the contrary, lattice models developed in the last decades can both describe hydrodynamic behavior and yield exact results also on fluctuating hydrodynamics. For this reason, they have become a powerful tool in nonequilibrium statistical mechanics, and have been a guide for the development of this thesis.

3.1 Hydrodynamics

3.1.1 Conservative interactions

Our starting point is the Boltzmann Eq. (1.32), which in presence of external forces $\mathbf{F}$ reads

$$\frac{\partial f}{\partial t} + \mathbf{v} \cdot \frac{\partial f}{\partial \mathbf{r}} + \frac{\mathbf{F}}{m} \cdot \frac{\partial f}{\partial \mathbf{v}} = Q(f, f) \tag{3.1a}$$

$$Q(f, f) = C \int_{\mathbb{R}^3} \int_{S^+} (f' f'_* - f f_*) \, |\mathbf{V} \cdot \hat{\mathbf{n}}| \, \mathrm{d}\mathbf{v}_* \mathrm{d}\hat{\mathbf{n}} \tag{3.1b}$$

where the Enskog correction in (1.40) has been neglected and the probability density $P(\mathbf{r}, \mathbf{v}, t)$ has been rescaled to give $f(\mathbf{r}, \mathbf{v}, t)$ so that

$$n(\mathbf{r}, t) = \int_{\mathbb{R}^3} f(\mathbf{r}, \mathbf{v}, t) \mathrm{d}\mathbf{v} \tag{3.2a}$$

$$N = \int_V \int_{\mathbb{R}^3} f(\mathbf{r}, \mathbf{v}, t) \mathrm{d}\mathbf{r} \mathrm{d}\mathbf{v} \tag{3.2b}$$

where N is the number of particles in volume V, and $n(\mathbf{r}, t) = \frac{1}{m}\rho(\mathbf{r}, t)$ is the number density with particles of mass m. The collisional term $Q(f, f)$ is equivalent to the one introduced in Eq. (1.40), where the C factor includes $N\sigma^2$ and other factors coming from the rescaling from P to f.

When considering a fluid flow on a macroscopic volume, the possibility of a continuum description relies on the smoothness of the hydrodynamic fields, i.e. the fields and their gradients must not diverge. This is possible thanks to the fact that total density, momentum and energy of two particles are conserved during collisions. Indeed, it can be proven [94] that if a generic observable $\chi(\mathbf{r}, \mathbf{v})$ satisfies

$$\chi_1 + \chi_2 = \chi'_1 + \chi'_2 \tag{3.3}$$

then the following relation holds

$$\int_{\mathbb{R}^3} \mathrm{d}\mathbf{v} \chi(\mathbf{r}, \mathbf{v}) Q(f, f) = 0 \tag{3.4}$$

where the primed variables indicate as usual the postcollisional observable. Thus, multiplying Eq. (3.1a) by $\chi(\mathbf{r}, \mathbf{v})$ and integrating by $\mathrm{d}\mathbf{v}$ one gets

$$\int_{\mathbb{R}^3} \mathrm{d}\mathbf{v} \chi(\mathbf{r}, \mathbf{v}) \left[\frac{\partial f}{\partial t} + \mathbf{v} \cdot \frac{\partial f}{\partial \mathbf{r}} + \frac{\mathbf{F}}{m} \cdot \frac{\partial f}{\partial \mathbf{v}} \right] = 0. \tag{3.5}$$

Integrating by parts and assuming that $f(\mathbf{r}, \mathbf{v}, t) \underset{v \to \infty}{\to} 0$ and that external forces do not depend on velocity, one gets the conservation theorem

$$\frac{\partial}{\partial t} \langle n\chi \rangle + \frac{\partial}{\partial \mathbf{r}} \cdot \langle n\mathbf{v}\chi \rangle - n \left\langle \mathbf{v} \cdot \frac{\partial \chi}{\partial \mathbf{r}} \right\rangle - n \left\langle \mathbf{f} \cdot \frac{\partial \chi}{\partial \mathbf{v}} \right\rangle = 0 \tag{3.6}$$

where the average is performed over the velocities and is local in space and time, namely $\langle A \rangle (\mathbf{r}, t) = \int \mathrm{d}\mathbf{v} A(\mathbf{r}, \mathbf{v}) f(\mathbf{r}, \mathbf{v}, t)$ and $\mathbf{f} = \mathbf{F}/m$ is the external force per mass unit.

Elastic collisions conserve density, momentum and energy, so one can take respectively $\chi = m, m\mathbf{v}, \frac{1}{2}mv^2$ or, equivalently, a combination of them. Introducing the average velocity

$$\mathbf{u}(\mathbf{r},t) = \langle \mathbf{v} \rangle \tag{3.7}$$

and the temperature as (being always in $d = 3$)

$$k_B T(\mathbf{r},t) = \frac{1}{3} m \left\langle |\mathbf{v}-\mathbf{u}|^2 \right\rangle \tag{3.8}$$

the conservation theorem (3.6) leads to

$$\frac{\partial \rho}{\partial t} + \nabla \cdot (\rho \mathbf{u}) = 0 \qquad \text{(mass conservation)} \tag{3.9a}$$

$$\rho \left(\frac{\partial}{\partial t} + \mathbf{u} \cdot \nabla \right) \mathbf{u} = \rho \mathbf{f} - \nabla \cdot \mathsf{P} \qquad \text{(momentum conservation)} \tag{3.9b}$$

$$\rho \left(\frac{\partial}{\partial t} + \mathbf{u} \cdot \nabla \right) T = -\frac{2m}{3} \left(\nabla \cdot \mathbf{q} + \mathsf{P} : \nabla \mathbf{u} \right) \qquad \text{(energy conservation)} \tag{3.9c}$$

where the following quantities have been defined

$$\mathbf{q}(\mathbf{r},t) \equiv \frac{1}{2} \rho \left\langle (\mathbf{v}-\mathbf{u}) \, |\mathbf{v}-\mathbf{u}|^2 \right\rangle \qquad \text{(heat flux)} \tag{3.10}$$

$$P_{ij} \equiv \rho \left\langle (v_i - u_i)(v_j - u_j) \right\rangle \qquad \text{(pressure tensor)} \tag{3.11}$$

and it has been taken $k_B = 1$. The term $\nabla \mathbf{u}$ is the velocity gradient tensor of components $\partial u_i / \partial x_j$, and the : operator in Eq. (3.9b) is the scalar product between tensors, namely $\mathsf{P} : \nabla u \equiv \sum_{i,j} P_{ij} \partial u_i / \partial x_j$.

Hydrodynamic equations (3.9) have only a formal value because heat flux and pressure tensor are determined by the distribution function $f(\mathbf{r}, \mathbf{v}, t)$, solution of the Boltzmann equation. Since f is generally unknown, we need to make some assumption about its behavior.

As it has been stated above, we expect the hydrodynamic fields to be almost constant over microscopic length scales, which correspond to the *mean free path* λ. Therefore, if L is a characteristic length of the macroscopic system, one expects that there is a scale separation whether

$$\mathrm{Kn} = \frac{\lambda}{L} \ll 1, \tag{3.12}$$

having defined the *Knudsen number* Kn, an adimensional parameter indicating the validity of a hydrodynamic approach. In this limit, hydrodynamic equations (3.9) can be closed assuming that heat flux and pressure tensor can be expressed in terms of the uniform fields and their gradients, so [34]

$$\mathbf{q} = -\kappa \nabla T, \tag{3.13a}$$

$$P_{ij} = p \delta_{ij} - \eta \left(\frac{\partial u_i}{\partial x_j} + \frac{\partial u_j}{\partial x_i} - \frac{2}{3} \delta_{ij} \nabla \cdot \mathbf{u} \right). \tag{3.13b}$$

The last expressions define the *hydrostatic pressure* p and the transport coefficients η and κ, respectively the *shear viscosity* and the *thermal conductivity*. Their values

are unknown until we find a way to derive them from the Boltzmann Equation. The pressure tensor P is the sum of a diagonal, isotropic part $p\delta_{ij}$ and a symmetric and traceless part, to the first order in the velocity gradients.

The pressure tensor and heat flux obtained can be placed back in Eqs. (3.9); however, since we are introducing linearized terms with respect to the gradients into exact equations, the perturbative approach must be carried out carefully. This is done by the *Chapman-Enskog* procedure [46, 76]: the space scales separation when $\epsilon \ll 1$ [1] physically means that a particle in volume of macroscopic size $\sim L$ will undergo an enormous number of collisions with other particles on the region, thermalizing to some *local* velocity distribution: the fundamental assumption of Chapman-Enskog procedure is that macroscopic gradients scale with Knudsen parameter, i.e. $\nabla \sim \epsilon$, $\nabla^2 \sim \epsilon^2 \ldots$. Therefore, the distribution function can be expanded as

$$f = f^{(0)} + \epsilon f^{(1)} + \epsilon^2 f^{(2)} + \cdots . \tag{3.14}$$

where $f^{(0)}$ denotes the homogeneous unperturbed solution (no gradients), $f^{(1)}$ the linear approximation with respect to field gradients, and so on. Obviously, the zeroth order solution $f^{(0)}$ is the Maxwell-Boltzmann distribution, as will be proved below.

Furthermore, the collisional invariants introduce a separation of *fast* variables from *slow* variables: while velocities of the particles change abruptly during a collision, conserved variables should change only over long scales of space and time. Therefore, one assumes that Boltzmann Equation admits a *normal solution*

$$f(\mathbf{r}, \mathbf{v}, t) = f\left[\mathbf{v} | n(\mathbf{r}, t), \mathbf{u}(\mathbf{r}, t), T(\mathbf{r}, t))\right] \tag{3.15}$$

where the dependence in time and space comes from the hydrodynamic (slow) fields, and the only fast variable is the velocity $\mathbf{v}$. The normal assumption (3.15) yields the time derivative

$$\frac{\partial f}{\partial t} = \frac{\partial f}{\partial n}\frac{\partial n}{\partial t} + \frac{\partial f}{\partial \mathbf{u}} \cdot \frac{\partial \mathbf{u}}{\partial t} + \frac{\partial f}{\partial T}\frac{\partial T}{\partial t}. \tag{3.16}$$

The last equation can be approached because time derivatives of $n = \rho/m, \mathbf{u}$ and T can be evaluated through Eqs. (3.9). Substituting the expression of pressure and heat flux from (3.13) and marking the gradients with the corresponding power of ϵ, one gets

$$\frac{\partial \rho}{\partial t} = -\epsilon \nabla \cdot (\rho \mathbf{u}) \tag{3.17a}$$

$$\frac{\partial \mathbf{u}}{\partial t} = -\epsilon \left(\mathbf{u} \cdot \nabla \mathbf{u} - \mathbf{f} + \frac{1}{\rho}\nabla p \right) + \epsilon^2 \frac{\eta}{\rho} \left(\nabla^2 \mathbf{u} + \frac{1}{3}\nabla \left(\nabla \cdot \mathbf{u} \right) \right) \tag{3.17b}$$

$$\frac{\partial T}{\partial t} = -\epsilon \left(\mathbf{u} \cdot \nabla T + \frac{2}{3n} p (\nabla \cdot \mathbf{u}) \right) + \epsilon^2 G \tag{3.17c}$$

where the external force has been assumed to be of first order in ϵ, consistently with a conservative force, $\mathbf{F} = -\nabla\phi$. The term G reads

$$G = \frac{2\eta}{3n} \left[\frac{\partial u_i}{\partial x_j}\frac{\partial u_j}{\partial x_i} + \frac{\partial u_i}{\partial x_j}\frac{\partial u_i}{\partial x_j} - \frac{2}{3} \left(\nabla \cdot \mathbf{u} \right)^2 \right] + \frac{2\kappa}{3n} \nabla^2 T \tag{3.18}$$

[1] from now on we call ϵ the Knudsen number to be consistent with literature

where the usual sum over repeated indices is implied.

When writing Eqs. (3.17), we retained only the first two orders in ϵ: this is the so-called *Navier-Stokes* order of the hydrodynamic description. Adding ϵ^3 terms, one gets a next order description named *Burnett* order. Substituting Eqs. (3.17) into (3.16), the time derivative of the distribution function is given as a series of terms at several powers of ϵ. This behavior suggests the need for a *multiple-scale analysis*, a procedure well described in [15]: assuming a scale separation also when considering characteristic times of the system, the time derivative can be expanded as

$$\frac{\partial}{\partial t} = \frac{\partial^{(0)}}{\partial t} + \epsilon \frac{\partial^{(1)}}{\partial t} + \epsilon^2 \frac{\partial^{(2)}}{\partial t} + \cdots . \tag{3.19}$$

A rigorous derivation of the procedure can be found in [76]. The physical meaning of multiple-scale analysis in this context is the requirement that the higher the order of the space gradient, the slower the time variation it causes [34].

Thus, Boltzmann Eq. (3.1) can be perturbatively solved at each order, writing a *local* Boltzmann equation (where the time and space dependence occurs only through the slow fields, Eq. (3.15)) supplemented by hydrodynamic equations (3.9). At first order, they read

$$\frac{\partial^{(0)}}{\partial t} f^{(0)} = Q(f^{(0)}, f^{(0)}) \tag{3.20a}$$

$$\frac{\partial^{(0)} n}{\partial t} = 0 \tag{3.20b}$$

$$\frac{\partial^{(0)} \mathbf{u}}{\partial t} = 0 \tag{3.20c}$$

$$\frac{\partial^{(0)} T}{\partial t} = 0 \tag{3.20d}$$

Since all the fields are constant at this order, from Eq. (3.16) one has $Q(f^{(0)}, f^{(0)}) = 0$; therefore, the homogeneous solution $f^{(0)}$ is the Maxwell-Boltzmann distribution

$$f^{(0)} = n^{(0)} [m/(2\pi m T^{(0)})]^{3/2} \exp\left[-\frac{m}{2T^{(0)}} |\mathbf{v} - \mathbf{u}^{(0)}|^2 \right] \tag{3.21}$$

where $n^{(0)}$, $\mathbf{u}^{(0)}$ and $T^{(0)}$ are in principle arbitrary functions of space and time, satisfying the self-consistency equations

$$n^{(0)} = \int \mathrm{d}\mathbf{v} f^{(0)}, \tag{3.22a}$$

$$\mathbf{u}^{(0)} = \int \mathrm{d}\mathbf{v} \mathbf{v} f^{(0)}, \tag{3.22b}$$

$$T^{(0)} = \int \mathrm{d}\mathbf{v} \frac{1}{3} |\mathbf{v} - \mathbf{u}|^2 f^{(0)}. \tag{3.22c}$$

which can be taken as the *actual* local hydrodynamic fields $n(\mathbf{r}, t)$, $\mathbf{u}(\mathbf{r}, t)$ and $T(\mathbf{r}, t)$ [76].

Going at the next order in the expansion, one finds

$$\frac{\partial^{(0)}}{\partial t} f^{(1)} + \left(\frac{\partial^{(1)}}{\partial t} + \mathbf{u} \cdot \nabla \right) f^{(0)} = Q(f^{(0)}, f^{(1)}) + Q(f^{(1)}, f^{(0)}), \tag{3.23a}$$

$$\frac{\partial^{(1)} \rho}{\partial t} = -\nabla \cdot (\rho \mathbf{u}), \tag{3.23b}$$

$$\left(\frac{\partial^{(1)}}{\partial t} + \mathbf{u} \cdot \nabla \right) \mathbf{u} = \mathbf{f} - \frac{1}{\rho} \nabla p, \tag{3.23c}$$

$$\left(\frac{\partial^{(1)}}{\partial t} + \mathbf{u} \cdot \nabla \right) T = -\frac{2}{3} (\nabla \cdot \mathbf{u}) T. \tag{3.23d}$$

The third equation is known as the Euler equation and for this reason this is called the *Euler order* of hydrodynamics. Some remarks have to be done: first, Eq. (3.23b) accounts for mass conservation at the first order. This is called *continuity equation*, and it holds at *any* order. The Euler equation for the velocity is the equation for a flow induced by external acceleration $\mathbf{f}$ and pressure field p in absence of viscosity. The last can be derived at this order using the Maxwell-Boltzmann distribution, and for dilute systems reads $p = nT$ [94]. Finally, the fourth equation describes the evolution of the temperature, and substituting $\nabla \cdot \mathbf{u}$ from Eq. (3.23b) one gets

$$\left(\frac{\partial^{(1)}}{\partial t} + \mathbf{u} \cdot \nabla \right) \left(\rho T^{-3/2} \right) = 0 \tag{3.24}$$

which is the equation of state for an adiabatic transformation; indeed, at Euler order the heat flux vanishes and the local evolution of the fluid is adiabatic. Finally, when $\mathbf{F} = -\nabla \phi$ is a conservative force, Euler equation gives the *Bernoulli Equation* which holds for an inviscid flow [94]

$$\nabla \left(\frac{1}{2} u^2 + \frac{1}{\rho} p + \frac{1}{m} \phi \right) = 0. \tag{3.25}$$

The viscosity and heat flux can be recovered in the hydrodynamic equations moving to the next order of the expansion; the first step is to derive the form of $f^{(1)}$ from Eq. (3.23a) knowing $f^{(0)}$; the former accounts for spatial gradients and through a quite long procedure leads to a closed expression of transport coefficients in terms of hydrodynamic fields [76]. For elastic hard spheres of mass m and diameter σ, those read [34]

$$\eta = \frac{5}{16 \sigma^2} \sqrt{\frac{mT}{\pi}}, \tag{3.26}$$

$$\kappa = \frac{75}{64 \sigma^2} \sqrt{\frac{T}{\pi m}} \tag{3.27}$$

A remarkable result of hydrodynamic derivation of viscosity is that it doesn't depend on the density of the fluid, contrarily to our physical intuition.

The ϵ dependence in Eqs. (3.17) can now be reabsorbed into the gradients taking $\epsilon = 1$ and recovering the Navier-Stokes order of hydrodynamic equations, which

finally read

$$\left(\frac{\partial}{\partial t}+\mathbf{u}\cdot\nabla\right)\rho=0 \tag{3.28a}$$

$$\left(\frac{\partial}{\partial t}+\mathbf{u}\cdot\nabla\right)\mathbf{u}=\mathbf{f}-\frac{1}{\rho}\nabla p+\nu\left[\nabla^2\mathbf{u}+\frac{1}{3}\nabla\left(\nabla\cdot\mathbf{u}\right)\right] \tag{3.28b}$$

$$\left(\frac{\partial}{\partial t}+\mathbf{u}\cdot\nabla\right)\mathbf{u}T=-\frac{2}{3n}p(\nabla\cdot\mathbf{u})+\frac{2\kappa}{3n}\nabla^2T+\frac{4\eta}{3n}\left[\mathsf{D}:\mathsf{D}-\frac{1}{3}\left(\nabla\cdot\mathbf{u}\right)^2\right] \tag{3.28c}$$

where D is the symmetrized velocity gradient tensor $D_{ij}\equiv(\partial_{x_i}u_j+\partial_{x_j}u_i)/2$ and $\nu\equiv\eta/\rho$ is the kinematic viscosity.

The equations display the fundamental features of hydrodynamic behavior. In the lhs it always appears the *material derivative* $\partial_t+\mathbf{u}\cdot\nabla$, representing the time variation of hydrodynamic fields in a frame comoving with the local fluid stream $\mathbf{u}$. Therefore, Eq. (3.28a) implies that density is conserved along the streaming lines because of incompressibility, $\nabla\cdot\mathbf{u}=0$. The velocity equation (3.28b) is the balance equation for velocity, corresponding to Newton's law $\mathbf{F}=m\mathbf{a}$ for a volume element of fluid; the velocity Laplacian on the rhs is given by viscosity and leading to *velocity diffusion*. In the temperature evolution equation (3.28c), the first term of the rhs is responsible for *temperature diffusion*, and the equation actually gets back to heat equation when the fluid is at rest, i.e. $\mathbf{u}=0$. The last term is increasing the temperature when a shear (namely a velocity gradient) is present in a viscous fluid: this phenomenon is called *viscous heating* and it is the consequence of frictional effects dissipating kinetic energy into heat when the fluid is sheared.

3.1.2 Granular hydrodynamics

The successful results obtained on conservative hydrodynamics inspired the formulation of granular hydrodynamics. Since kinetic theory has been consistently defined for granular matter, the same approach can be implemented in the case of inelastic collisions. The main difference consists in energy dissipation: mass and momentum are still conserved by collisions while energy is not, then the conservation theorem (3.6) cannot be rigorously applied to the latter. However, one can always derive the continuity equations (3.9) simply by integrating over $1,\mathbf{v},v^2$; while the equations for mass density and average velocity do not change, the evolution of temperature now reads [34]

$$\rho\left(\frac{\partial}{\partial t}+\mathbf{u}\cdot\nabla\right)T=-\zeta T-\frac{2m}{3}\left(\nabla\cdot\mathbf{q}+\mathsf{P}:\nabla\mathbf{u}\right). \tag{3.29}$$

The appearance of the term ζT, known as *sink term*, is given by the energy dissipation which is acting at the *microscopic level* during each collision. The parameter ζ is the *cooling coefficient* already encountered in Sec. 1.4.3, which stems from the rhs of Boltzmann Equation (3.1a) multiplied by $mv^2/2$ and integrated over $\mathbf{v}$, i.e.

$$\int\mathrm{d}\mathbf{v}\frac{mv^2}{2}Q(f,f)\equiv-\frac{3}{2}nT\zeta \tag{3.30}$$

yielding [34]

$$\zeta(\mathbf{r},t)=\frac{\pi m\sigma^2}{24nT}(1-\alpha^2)\int\mathrm{d}\mathbf{v}\mathrm{d}\mathbf{v}_*\,V^3f(\mathbf{r},\mathbf{v},t)f(\mathbf{r},\mathbf{v}_*,t). \tag{3.31}$$

The zeroth order Chapman-Enskog equations now read

$$\frac{\partial^{(0)}}{\partial t} f^{(0)} = Q(f^{(0)}, f^{(0)}) \tag{3.32a}$$

$$\frac{\partial^{(0)} n}{\partial t} = 0 \tag{3.32b}$$

$$\frac{\partial^{(0)} \mathbf{u}}{\partial t} = 0 \tag{3.32c}$$

$$\frac{\partial^{(0)} T}{\partial t} = -\zeta^{(0)} T \tag{3.32d}$$

where the zeroth order cooling coefficient $\zeta^{(0)}$ can be calculated through Eq. (3.31) with the homogeneous distribution function $f^{(0)}$, which for a constant restitution coefficient α reads

$$f^{(0)} = \frac{n}{v_T^3} \tilde{f}^{(0)} \left(\frac{\mathbf{v} - \mathbf{u}}{v_T} \right) \tag{3.33}$$

as in Eq. (1.41), yielding

$$\zeta^{(0)} = \frac{2\sqrt{2}}{3} n \sigma^2 \mu_2 \sqrt{\frac{T}{m}} \tag{3.34}$$

where μ_2 has been defined in Eq. (1.45), and the zeroth order of ζ naturally coincides with the HCS result of Eq. (1.47). The Chapman-Enskog procedure can be carried on exactly as before: the only difference from the elastic case of Sec. 3.1.1 is the presence of the sink term and that the heat flux expressed in function of linear gradients now reads

$$\mathbf{q} = -\kappa \nabla T - \mu \nabla n \tag{3.35}$$

where the coefficient μ relates the heat flux with the density gradient and is non vanishing only for $\alpha < 1$, as well as cooling coefficient ζ [29]. All the transport coefficients can be analogously computed for granular hydrodynamics: their explicit expressions, which can be found in [34], show that in the elastic limit $\alpha \to 1$ conservative hydrodynamics values are recovered.

This last feature is the qualitative difference between granular and elastic particles. Actually, energy dissipation occurs from the zeroth order of expansion, therefore one cannot assume a local equilibrium behavior of the system as stated above. However, if the dissipation is small enough so that the cooling coefficient can be compared with the gradients in Chapman-Enskog procedure, local equilibrium can be recovered. This is known as the *quasielastic limit* and will be widely used in Chapter 4. Finally, we can write the Navier-Stokes hydrodynamic equations substituting 3.29 and 3.35 in Eqs. (3.17), obtaining for a compressible fluid ($\nabla \cdot \mathbf{u} \neq 0$)

$$\left(\frac{\partial}{\partial t} + \mathbf{u} \cdot \nabla \right) n = -n \nabla \cdot \mathbf{u} \tag{3.36a}$$

$$\left(\frac{\partial}{\partial t} + \mathbf{u} \cdot \nabla \right) \mathbf{u} = -\frac{1}{nm} \nabla p + \frac{\eta}{nm} \left(\nabla^2 \mathbf{u} + \frac{1}{3} \nabla \left(\nabla \cdot \mathbf{u} \right) \right) \tag{3.36b}$$

$$\left(\frac{\partial}{\partial t} + \mathbf{u} \cdot \nabla \right) T = -\zeta T - \frac{2}{3n} p (\nabla \cdot \mathbf{u}) + \frac{2}{3n} \left[\kappa \nabla^2 T + \mu \nabla^2 n + \eta \left(2\mathsf{D} : \mathsf{D} - \frac{2}{3} \left(\nabla \cdot \mathbf{u} \right)^2 \right) \right] \tag{3.36c}$$

3.1.3 Hydrodynamic instabilities and the HCS

As for conservative hydrodynamics, the equations for n, $\mathbf{u}$ and T are coupled and nonlinear, therefore a solution can be found only under suitable conditions. When a stationary solution is present, one can look at its *linear stability*. Linear stability analysis is widely used in dynamical systems [44]: when a dynamical observable is evolving under the evolution equation $\dot{x}(t) = F(x(t))$, the dynamics can be linearized around a fixed point x^* such that $F(x^*) = 0$, so a perturbation near x^* evolves as

$$\frac{\mathrm{d}}{\mathrm{d}t}\delta x(t) = \lambda \delta x \tag{3.37}$$

where $x(t) = x^* + \delta x(t)$ and $\lambda = dF/dx|_{x^*}$. Thus, the perturbation diverges when $\lambda > 0$ (unstable fixed point) and vice versa vanishes when $\lambda < 0$ (stable fixed point). For $d > 1$ case, Eq. (3.37) is a vectorial relation

$$\frac{\mathrm{d}}{\mathrm{d}t}\delta x_i(t) = \sum_{j=1}^{d} L_{ij}\delta x_j(t) \tag{3.38}$$

so one has to find the eigenvalues of the stability matrix $L_{ij} \equiv \partial F_i/\partial x_j|_{\mathbf{x}^*}$. The fixed point $\mathbf{x}^*$ is now stable if the real part of its eigenvalues is always negative [44].

The same linearization can be carried out for hydrodynamic equations (3.17): hydrodynamic instabilities are an important research field in fluid dynamics, as they have been introduced to describe the departure of hydrodynamics from a stationary state [119, 65]. In Appendix C the reader will find some links to videos describing the most studied. Looking at the granular case, one starts from Eqs. (3.36). One of the basic granular states is, again, the HCS, which is known to be unstable to linear perturbations [83]. Spatially dependent perturbation of the homogeneous HCS read

$$n(\mathbf{r},t) = n + \delta n(\mathbf{r},t)\,, \quad \mathbf{u}(\mathbf{r},t) = \delta\mathbf{u}(\mathbf{r},t)\,, \quad T(\mathbf{r},t) = T_{HCS}(t) + \delta T(\mathbf{r},t) \tag{3.39}$$

where $n = N/V$ is the constant and homogeneous number density, and $T_{HCS}(t)$ is the homogeneous Haff's law from Eq. (1.53). As discussed in Sec. 1.4.3, the HCS has no stationary state because of continuous energy dissipation, so one looks at the rescaled hydrodynamic fields

$$\tilde{n} \equiv \frac{\delta n}{n} \ll 1\,; \quad \tilde{\mathbf{u}} \equiv \frac{\delta\mathbf{u}}{\sqrt{T_{HCS}(t)}}\,, \ |\tilde{\mathbf{u}}| \ll 1\,; \quad \tilde{T} \equiv \frac{\delta T}{T_{HCS}(t)} \ll 1 \tag{3.40}$$

The mechanism of cluster formation, qualitatively explained in Sec. 1.3.1, is the cause of homogeneous density instability. Furthermore, inelastic collisions are correlating the particles, reducing the outgoing angle with respect to the incoming angle of collision and yielding an aligning mechanism - see Sec. 2.3. This mechanism accounts for vortex formation, which will be explained below.

The linear stability of hydrodynamic equations can be better analyzed in Fourier space, defining the Fourier transform of a generic observable $\mathbf{a}(\mathbf{r},t)$ and its inverse as

$$\begin{aligned} \mathbf{a}_\mathbf{k}(t) &= \frac{1}{\sqrt{V}}\int \mathrm{d}\mathbf{r}\, e^{-i\mathbf{k}\cdot\mathbf{r}}\mathbf{a}(\mathbf{r},t) \\ \mathbf{a}(\mathbf{r},t) &= \frac{1}{\sqrt{V}}\sum_\mathbf{k} e^{i\mathbf{k}\cdot\mathbf{r}}\mathbf{a}_\mathbf{k}(t) \end{aligned} \tag{3.41}$$

where $V = L^3$ is the volume of the system, and $\mathbf{k}$ are the discrete wave vectors $\mathbf{k} = \frac{2\pi}{L}(n_x, n_y, n_z)$, with $n_i \in \mathbb{Z}$. With all these transformations and changing the time t into the mean collisional time $\tau(t)$ defined in (1.57), we get the linearized equations [34]

$$\frac{\partial \tilde{n}_{\mathbf{k}}}{\partial \tau} = -i\mathbf{k}\cdot\tilde{\mathbf{u}}_{\mathbf{k}} \tag{3.42a}$$

$$\frac{\partial \tilde{\mathbf{u}}_{\mathbf{k}}}{\partial \tau} = \frac{1}{4}\zeta^*\tilde{\mathbf{u}}_{\mathbf{k}} - \frac{1}{2}i\mathbf{k}\left(\tilde{n}_{\mathbf{k}} + \tilde{T}_{\mathbf{k}}\right) - \eta^*\left[k^2\tilde{\mathbf{u}}_{\mathbf{k}} + \frac{1}{3}\mathbf{k}\left(\mathbf{k}\cdot\tilde{\mathbf{u}}_{\mathbf{k}}\right)\right] \tag{3.42b}$$

$$\frac{\partial \tilde{T}_{\mathbf{k}}}{\partial \tau} = -\frac{1}{4}\zeta^*(\tilde{T}_{\mathbf{k}} + 2\tilde{n}_{\mathbf{k}}) - \frac{5}{2}k^2(\kappa^*\tilde{T}_{\mathbf{k}} + \mu^*\tilde{n}_{\mathbf{k}}) - \frac{2}{3}\left(i\mathbf{k}\cdot\tilde{\mathbf{u}}_{\mathbf{k}}\right) \tag{3.42c}$$

where the coefficients ζ^*, η^*, κ^* and μ^* are the transport coefficients computed in the HCS. Eqs. (3.42) can be written in a compact form as

$$\frac{\partial \boldsymbol{\Psi}}{\partial \tau} = \mathsf{L}\boldsymbol{\Psi} \tag{3.43}$$

where L is the stability matrix defined in Eq. (3.38) and $\boldsymbol{\Psi} = (\tilde{n}_{\mathbf{k}}, \tilde{\mathbf{u}}_{\mathbf{k}}, \tilde{T}_{\mathbf{k}})$ is a five-dimensional vector containing all the hydrodynamic fields. The eigenvectors $\boldsymbol{\Psi}_l$ of the stability matrix are called *hydrodynamic modes*, where $l = 1, \ldots, 5$: if their corresponding eigenvalues $\lambda_l(\mathbf{k})$ satisfy $\mathrm{Re}\left[\lambda_l(\mathbf{k})\right] < 0$, the hydrodynamic mode is stable, otherwise it is not. This analysis can be applied to any hydrodynamic state.

Looking at the HCS linearized equations (3.42), it is convenient to separate the rescaled velocity into a longitudinal component $\tilde{\mathbf{u}}_{\mathbf{k}}^{\parallel} = \tilde{\mathbf{u}}_{\mathbf{k}}\cdot\mathbf{k}/k$ and a transverse component $\tilde{\mathbf{u}}_{\mathbf{k}}^{\perp} = \tilde{\mathbf{u}}_{\mathbf{k}} - \tilde{\mathbf{u}}_{\mathbf{k}}^{\parallel}$. Since

$$i\mathbf{k}\cdot\tilde{\mathbf{u}}_{\mathbf{k}}^{\perp} = 0\,, \quad i\mathbf{k}\cdot\tilde{\mathbf{u}}_{\mathbf{k}}^{\parallel} = ik\tilde{u}_{\mathbf{k}}^{\parallel} \tag{3.44}$$

Eq. (3.42b) gives a decoupled equation for the transverse component

$$\frac{\partial \tilde{\mathbf{u}}_{\mathbf{k}}^{\perp}}{\partial \tau} = \left(\frac{1}{4}\zeta^* - \eta^*k^2\right)\tilde{\mathbf{u}}_{\mathbf{k}}^{\perp} \tag{3.45}$$

so the transverse velocity is a hydrodynamic mode with the eigenvalue

$$\lambda_{\perp}(\mathbf{k}) = \frac{1}{4}\zeta^* - \eta^*k^2. \tag{3.46}$$

The last equation gives the *shear instability* criterion in the HCS, revealing the existence of a threshold wavelength

$$k_{\perp}^*(\alpha) = \frac{1}{2}\sqrt{\frac{\zeta^*(\alpha)}{\eta^*(\alpha)}} \propto \sqrt{1-\alpha^2}. \tag{3.47}$$

Thus, for short-wave perturbations (large k) shear modes are stable and decay rapidly, while long-wave modes (low k) grow exponentially. The critical equation (3.47) leads to a critical value of the size $L^*(\alpha)$: indeed, since $k \geq 2\pi/L$, the instability arises only when the size of the system exceed a critical value

$$L^*(\alpha) = \frac{2\pi}{k_{\perp}^*(\alpha)} \propto \frac{1}{\sqrt{1-\alpha^2}} \tag{3.48}$$

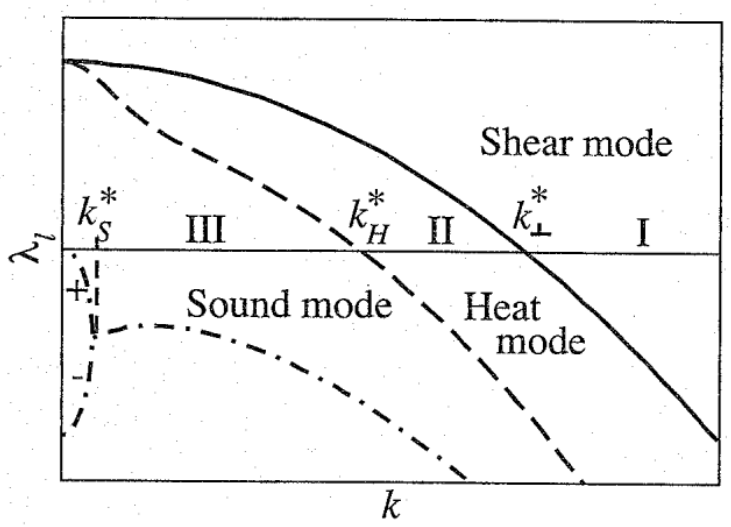

Figure 3.1. Plot of the real part of the eigenvalues of the hydrodynamic modes in function of the wave vector k. The marginal values $k_\perp^*$, k_H^* and k_S^* are shown, indicating respectively the regions of stability of the shear mode, of the heat mode and of the propagating sound modes [34].

depending on the restitution coefficient α, responsible for dissipation. Actually, when the system size increases over $L^*(\alpha)$ unstable modes wavelengths are smaller than system size and can be amplified by the dynamics of the system. The critical values of k and L are coupled to α, and as expected the instability is absent for $\alpha = 1$; at fixed size of the system, one may recover unstable modes also increasing the dissipation over a critical value α^*.

Shear instability is responsible for vortex formation: indeed, the shear creates long-ranged waves of transversally aligned particles. When two shear waves cross each other, particles on the x direction wave are moving in the y direction, where they encounter the flux of the perpendicular shear wave and therefore they start rotating their velocity. A clear representation of the phenomenon is given in [34]. It must be stressed that vortex formation is observed in the *rescaled* variables, i.e. vortices are growing when compared with the thermal velocity $v_T(t)$, which is decreasing with Haff's law; they act on velocity scales rapidly decreasing, while the total energy is decreasing because of collisions. Finally, the meaning of the minimal size allowing the formation of structure is controversial and still object of debate [34].

Cluster formation can be analyzed analogously, underlining that the rescaled density $\tilde{n}$ has a different physical meaning with respect to rescaled velocity and temperature, because the homogeneous density is not decaying in time. From the stability analysis of Eqs. (3.42), excluding shear modes which are independent from the rest of the system, one finds three eigenstates corresponding to the *heat mode* with real eigenvalue $\lambda_H(\mathbf{k})$ and two *sound modes* of complex eigenvalues $\lambda_{S1/2}(\mathbf{k})$; their behavior is shown in Fig. 3.1. The heat eigenvalue λ_H changes sign at $k_H^*(\alpha)$, a new critical value below which a combination of density, temperature and longitudinal velocity grow exponentially; therefore density grows exponen-

tially and clustering is occurring. The critical value $k_H^*(\alpha)$ yields another critical size of the system. However, one has $k_H^*(\alpha) < k_\perp^*(\alpha)$, so three scenarios are possible depending on the size of the system

- $L < 2\pi/k_\perp^*(\alpha)$: no vortex or cluster formation. The HCS is stable
- $2\pi/k_\perp^*(\alpha) < L < 2\pi/k_H^*(\alpha)$: vortices are present, but no clusters. The shear mode of maximum wavelength dominates the system. The HCS linearized equations are no longer valid
- $L > 2\pi/k_H^*(\alpha)$: vortices (sooner) and clusters (later) form. The final state is strongly inhomogeneous

As it can be seen, the first instability observed when increasing the system size is the shear instability: this observation will motivate the first model purposed in this thesis, which will be analysed in Chapter 4.

3.1.4 Active hydrodynamics

Active hydrodynamics has not yet reached the same level of systematic development of conservative and granular hydrodynamics. The main reason is that an active kinetic theory is still under development, because of the relevant differences between active particles and passive molecules. The interactions between active particles and fluid can be very complex and strongly dependent on the considered system [135]. Furthermore, as shown in Sec. 2.2, dry active systems do not conserve their total momentum, and thus both energy and momentum do not obey the conservation law (3.5). In the last years some studies derived a Boltzmann Equation for particular models of active particles, leading to a hydrodynamic description as discussed above for the elastic and granular case [18, 19, 153].

The first attempts to derive an active hydrodynamics have been strictly connected with the development of microscopic models such as Vicsek model. A milestone of active hydrodynamics is the continuum field description of orientation density in an active fluid, introduced by Toner and Tu in 1995 [184, 185]. The model is based on the continuum equations

$$\frac{\partial \rho}{\partial t} + \nabla \cdot (\rho \mathbf{u}) = 0 \tag{3.49a}$$

$$\frac{\partial \mathbf{u}}{\partial t} + \lambda_1(\mathbf{u}\cdot\nabla)\mathbf{u} + \lambda_2(\nabla\cdot\mathbf{u})\mathbf{u} + \lambda_3\nabla(|\mathbf{u}|^2) = \tag{3.49b}$$
$$\alpha\mathbf{u} - \beta|\mathbf{u}|^2\mathbf{u} - \nabla P + D_B\nabla(\nabla\cdot\mathbf{u}) + D_T\nabla^2\mathbf{u} + D_2(\mathbf{u}\cdot\nabla)^2\mathbf{u} + \mathbf{f}$$

$$P = P(\rho) = \sum_{n=1}^{\infty} \sigma_n(\rho - \rho_0)^n \tag{3.49c}$$

where β, D_B, D_T and D_2 are all positive, and $\mathbf{f}$ is a GWN force. A transition from disorder to order is present when α becomes positive: indeed the first two terms of the rhs are equivalent to the Rayleigh-Helmoltz friction described in Sec. 2.2.3, and the equations have an homogeneous fixed point at density ρ_0 and velocity $u = \sqrt{\alpha/\beta}$. The equations are *not* derived through a coarse-graining procedure from a Boltzmann Equation as in previous sections, but rather wrote down as the

most general continuum equations of motion for velocity and density consistent with the symmetries ad conservation laws of the system, namely rotation invariance and number of particles conservation [192]. On the contrary, Galilean invariance doesn't hold because of lack of momentum conservation: for these reason, in principle all the convective coefficients λ in lhs are present, while in the Galilean case one has $\lambda_2 = \lambda_3 = 0$ and $\lambda_1 = 1$. The pressure P is expanded around the uniform density ρ_0, forcing the system to the uniform density case. The symmetry arguments used to derive Eqs. (3.49) are very powerful; however, within this approach the transport coefficients cannot be derived from microscopic dynamics as we have seen in previous sections, and one must derive them from other arguments.

The authors concentrated on the broken symmetry ordered phase with $\alpha > 0$, looking at the velocity component perpendicular to the direction of motion $\mathbf{u}_\perp$ and the density fluctuations $\delta\rho = \rho - \rho_0$. By means of renormalization group method they performed a scaling analysis leading to the scaling exponents of the model. The analysis of the model is strongly supported by a comparison with ferromagnetic models, especially XY model, with the big difference that the swarming transition breaks the rotational *continuous* symmetry also in $2d$, which is forbidden in short-range equilibrium systems [186].

Recently, a derivation of active hydrodynamics from kinetic theory has been carried out by Bertin *et al.* [18, 19]. The authors derived a Boltzmann Equation for a system of N pointlike particles, combining binary collisions mimicking Vicsek interactions with run-and-tumble dynamics: when two particles are closer than a given distance d_0, their orientations change as $\theta_i \to \theta_i' = \overline{\theta} + \eta_i$, where $\overline{\theta} = \mathrm{Arg}[e^{i\theta_i} + e^{i\theta_j}]$ is the average orientation of the two particles, and η_i are identically distributed, independent GWN with distribution $p(\eta)$ and variance σ^2. Boltzmann Equation for this model reads

$$\frac{\partial f}{\partial t}(\mathbf{r}, \theta, t) + \mathbf{e}(\theta) \cdot \nabla f(\mathbf{r}, \theta, t) = I_{dif}[f] + I_{col}[f, f] \tag{3.50}$$

which is the extension of Eq. (2.25) to the interacting case, where in the rhs the diffusion functional $I_{dif}[f]$ and the collision functional $I_{col}[f, f]$ account for run-and-tumble dynamics and interactions, respectively. Following a coarse-graining and scale separation procedure, the authors find the hydrodynamic equation for momentum $\mathbf{w} \equiv \rho\mathbf{v}$

$$\frac{\partial \mathbf{w}}{\partial t} + \gamma(\mathbf{w} \cdot \nabla)\mathbf{w} = -\frac{1}{2}\nabla(\rho - \kappa\mathbf{w}^2) + (\mu - \xi)|\mathbf{w}|^2)\mathbf{w} + \nu\nabla^2\mathbf{w} - \kappa(\nabla \cdot \mathbf{w})\mathbf{w} \tag{3.51}$$

recovering several features observed in Toner and Tu Eq. (3.49b). The kinetic model allows the computation of transport coefficients from microscopic parameters. Again, the homogeneous disordered and ordered phase are present, respectively when $\mu < 0$ and $\mu > 0$; the authors recover a noise-dependent threshold density $\rho^*(\eta)$ above which the ordered phase becomes stable *under homogeneous perturbations*, showing the transition to collective motion. Taking into account space-dependent perturbations, the homogeneous disordered state is found to be stable for any $\rho < \rho^*$. On the other hand, the homogeneous flow state is unstable for long-wave longitudinal fluctuations near the transition line, while it gets

stable at high densities $\rho \gg \rho^*$: this phenomenon is called *restabilization*, a delicate result because in this region the system is far from the validity domain of the hydrodynamic description [19]. The linear stability must be analyzed through the Boltzmann Equation, which confirms the stability for high densities, an interesting result because it shows how hydrodynamic equations are predictive beyond their validity domain. An agreement with numerical simulations of agent-based models has been found [19]. This model was further analysed and modified in [97], where multibody interactions have been reintroduced following Vicsek model's scheme: this correction allowed to recover the phase diagram of Vicsek *et al.* in the continuum mode. Finally, these studies proved that Toner and Tu theory is actually the continuum limit of Vicsek model under a suitable choice of transport coefficients, confirming the generality claim in the formulation of the model.

In the last years, active hydrodynamics models have been developed also from overdamped, microscopic Langevin equations leading to Smoluchowski dynamics for the density function and then to hydrodynamic equations in the coarse-grained case. Studying the density ρ, momentum $\mathbf{w}$ and alignment tensor $\mathsf{Q} = \hat{\mathbf{u}}\hat{\mathbf{u}} - \frac{1}{d}\mathsf{I}$ [135, 9, 174, 89], similar results have been found with respect to above-mentioned models, typically differing in transport coefficients because of the microscopic rules defining the model. A rich variety of models is still under development and debate; in Chapter 6, it will be shown how an hydrodynamic description of active matter can be derived from microscopic rules, reproducing on a lattice the kinetic behavior of active particles in the case of a dilute system with short-range interactions.

3.2 Fluctuating hydrodynamics

Hydrodynamic theory described in the last section is *deterministic*: hydrodynamic fields are averaged quantities and fluctuations are not observable when the number of particles in a fluid volume element is very large (for instance of the order of Avogadro's number). However, we know that granular and active matter are *small* systems, and the number of active units or grains generally is in the range $10^2 \div 10^4$. This means that fluctuations become measurable: their description is the goal of fluctuating hydrodynamics. To do this, one generally can write hydrodynamic deterministic equations as in the previous section and add a noise source directly in the equations.

In general, noise can be thought as the result of a coarse-graining of the system. For instance, for a conservative system with Hamiltonian $H(\mathbf{p}, \mathbf{q})$ one can include the effect of an external reservoir adding a noise and dissipation term, i.e.

$$\begin{aligned} \dot{\mathbf{q}} &= \frac{\partial H}{\partial \mathbf{p}} \\ \dot{\mathbf{p}} &= -\frac{\partial H}{\partial \mathbf{q}} - \gamma \mathbf{p} + \boldsymbol{\xi}(t) \end{aligned} \tag{3.52}$$

where $\boldsymbol{\xi}(t)$ is a GWN satisfying $\langle \xi_\alpha(t)\xi_\beta(t')\rangle = D\delta_{\alpha\beta}\delta(t-t')$. For a canonical Hamiltonian $H = p^2/2m + V(\mathbf{q})$, the probability distribution $f(\mathbf{q}, \mathbf{p}; t)$ follows the Fokker-

Planck equation

$$\frac{\partial f}{\partial t} = -\frac{\partial}{\partial \mathbf{q}} \cdot \left(\frac{\mathbf{p}}{m} f\right) + \frac{\partial}{\partial \mathbf{p}} \cdot \left[\left(\nabla V(\mathbf{q}) + \gamma \mathbf{p}\right) f\right] + \frac{D}{2} \frac{\partial^2 f}{\partial p^2} \tag{3.53}$$

which under a change of variables leads to the Kramers' Equation [80]. The noise and friction term generally stem from fast variables with respect to Hamiltonian coordinates $\mathbf{p}$ and $\mathbf{q}$. So, dissipation and noise comes from the same coarse-graining mechanism, and *at equilibrium* they are related by Einstein relation, which in this specific case reads $D = 2m\gamma k_B T$. This crucial relation between diffusivity and mobility provides that the Boltzmann distribution $f(\mathbf{p}, \mathbf{q}) \sim \exp[-H(\mathbf{p}, \mathbf{q})/k_B T]$ is a stationary solution of Eq. (3.53). Therefore, if Einstein relation is satisfied fluctuations can be reintroduced into Hamiltonian dynamics leaving the equilibrium Boltzmann distribution unchanged.

The procedure described above relies on the *fluctuation-dissipation relations* between linear response of an observable to a perturbation and its autocorrelation in time [138]. It must be stressed that the particular relation depends on the coarse-graining applied: indeed, viscous friction $-\gamma \mathbf{p}$ acts instantaneously on the particle without any memory effect of its trajectory; when memory effects are present, the noise $\boldsymbol{\xi}$ must be modified as well to recover the equilibrium Boltzmann distribution [112]. The main idea of *Landau-Lifschitz* fluctuating hydrodynamics is the following [119]: given the deterministic hydrodynamic equations $\partial_t \boldsymbol{\Psi} = \mathcal{F}[\boldsymbol{\Psi}]$, being $\boldsymbol{\Psi}(\mathbf{x}, t)$ the vectorial density, momentum and temperature field and $\mathcal{F}$ the deterministic average hydrodynamic evolution operator, the fluctuating equations should be written

$$\partial_t \boldsymbol{\Psi}(\mathbf{x}, t) = \mathcal{F}[\boldsymbol{\Psi}(\mathbf{x}, t)] + \boldsymbol{\xi}(\mathbf{x}, t). \tag{3.54}$$

where the deterministic hydrodynamic operator $\mathcal{F}$ is taking into account only the average, deterministic terms and all the fluctuations are contained in $\boldsymbol{\xi}$. Now, $\mathcal{F}$ already defines dissipative terms such as viscosity and heat diffusion: therefore, in the case of conservative interactions one may directly introduce a Gaussian noise $\boldsymbol{\xi}$ which correlation properties are determined by equilibrium fluctuation-dissipation relations, avoiding the ambiguity of the coarse-graining described above.

For out of equilibrium systems, the situation is more complicated because the distribution function is generally unknown and differs from Boltzmann distribution. This lack of information removes the constraint on noise definition. Thus, nonequilibrium methods are necessary to derive the correct fluctuations at a mesoscopic scale.

In 1969, a seminal paper of Bixon and Zwanzig [24] introduced the *Boltzmann-Langevin* Equation: the one-particle distribution function is written as

$$f(\mathbf{x}, \mathbf{v}; t) = \sum_{j=1}^{N} \delta(\mathbf{x}_j(t) - \mathbf{x}) \delta(\mathbf{v}_j(t) - \mathbf{v}) \tag{3.55}$$

where $\mathbf{x}_j(t)$ and $\mathbf{v}_j(t)$ are the position and velocity of the j-th particle in the system, with $j = 1, \ldots, N$. The field f is a dynamical, *fluctuating* observable, which averaged over initial conditions give the one-particle marginalized distribution defined in Eq. (1.28), which we here call $\overline{f}$. Thus, the distribution deviation $\phi = (f - \overline{f})/\overline{f}$

in linear approximation evolves through a Boltzmann-Langevin Equation, namely a Boltzmann Equation modified by some noise term

$$\frac{\partial \phi}{\partial t} + \mathbf{v} \cdot \nabla \phi - J\phi = F(\mathbf{r}, \mathbf{v}, t) \tag{3.56}$$

where J is the linearized collision operator and F a random noise term, whose average over initial conditions must vanish. The noise term is an *effective* term coming from the contribution of 2-particles distribution $F_2(\mathbf{x}_1, \mathbf{v}_1, \mathbf{x}_2, \mathbf{v}_2; t)$: its contribution is an effect of the second equation of Boltzmann hierarchy. Velocity moments of Eq. (3.56) lead to hydrodynamic equations through the usual Chapman-Enskog procedure, but the pressure tensor and heat flux are now written as a sum of a deterministic and a fluctuating component. At equilibrium, the averaged distribution is the Maxwell-Boltzmann distribution $\overline{f} = f_{MB}$ and the Einstein relations are recovered, validating Landau-Lifschitz theory.

The work of Bixon and Zwanzig inspired the study of fluctuating hydrodynamics in inelastic materials. Indeed, when equilibrium doesn't hold, kinetic theory is the starting point to obtain macroscopic predictions from microscopic features. Fluctuating hydrodynamics has been applied to the case of granular materials [30, 164]. Generally speaking, the deviation of microscopic density leads to deviation in any general hydrodynamic field $\psi(\mathbf{x}, t)$, which can be written as $\psi^{\text{av}}(\mathbf{x}, t) + \delta\psi(\mathbf{x}, t)$, separating the average term $\psi^{\text{av}}(\mathbf{x}, t)$ from the zero-average fluctuations $\delta\psi(\mathbf{x}, t)$. The latter follow a generalized Langevin equation: its solution leads to the correlation properties of hydrodynamic fluctuations, namely $\langle \delta\psi(\mathbf{x}, t)\delta\psi(\mathbf{x}', t')\rangle$.

To see a real example, let's focus on the shear mode, a particular hydrodynamic mode [164]. The fluctuating transverse velocity field in Fourier space is defined as

$$u_\perp(k, t) \equiv \sum_{j=1}^{N} v_{y,j}(t) e^{-ikx_j(t)} \tag{3.57}$$

where k is the wave number of the mode, $x_j(t)$ is the x-coordinate and $v_{y,j}(t)$ is the y-velocity of particle j at time t. The shear mode is the analytically simplest mode, as it has been shown to decouple from other modes in linearized hydrodynamics. We aim at describing the rescaled autocorrelation function

$$C_\perp(k, t) \equiv \frac{\langle u_\perp(k, 0) u_\perp^*(k, t)\rangle}{2T} \tag{3.58}$$

where $u_\perp^*$ is the complex conjugate of $u_\perp$ and T is the (isotropic) temperature of the system, corresponding to room temperature for elastic fluids or granular temperature for granular materials. Both equilibrium case and HCS can be studied. In the former, the Landau-Lifschitz fluctuating hydrodynamics predicts the stochastic equation

$$\frac{\partial}{\partial t} u_\perp(k, t) = -\nu k^2 u_\perp(k, t) + \xi(k, t) \tag{3.59}$$

where ν is the kinematic viscosity. Einstein relation corresponds to

$$\langle \xi(k, t)\xi(k', t')\rangle = \delta_{k,-k'}\delta(t - t') 2TN\nu k^2 \tag{3.60}$$

which are of order N because $u_\perp$ is an extensive field, so the noise associated to the intensive field $u_\perp/N$ is scaling as $1/N$. Eq. (3.59) leads to

$$C_\perp(k,t) = \frac{N}{2} e^{-\nu k^2 t} \tag{3.61}$$

In the inelastic case, the evolution equation for transverse velocity can be written as

$$\frac{\partial}{\partial t} u_\perp(k,t) = -\nu(T(t)) u_\perp(k,t) + \xi(k,t) \tag{3.62}$$

Here, the temperature is decaying following Haff's law, so noise correlations must be time-dependent. as well. A first approximation can be derived using the granular temperature instead of the room temperature, and writing an Einstein relation in the granular case [189]. The evolution equation for rescaled fields, Eq. (3.45), can be written as

$$\frac{\partial}{\partial \tau} \tilde{u}_\perp(k,\tau) = -z(k) \tilde{u}_\perp(k,\tau) + \tilde{\xi}(k,\tau) \tag{3.63}$$

with $z(k) = qk^2 - \zeta/2$, where $q = \nu(T(t))/\omega_c(T(t))$ is the time-independent ratio between kinematic viscosity and collision rate, and ζ is the cooling coefficient, from $T(\tau) \sim \exp(-\zeta\tau)$. The coefficient $z(k)$ is now constant and so are noise correlations. Analogously with the equilibrium case, one can now write

$$\langle \xi(k,t)\xi(k',t') \rangle = \delta_{k,-k'} \delta(t-t') 2TNqk^2 \tag{3.64}$$

where T is now the granular temperature The HCS is stable for $z(k) > 0$: for stable modes, with this choice of the stationary autocorrelation reads

$$C_\perp(k,\tau) = \frac{N}{2} \frac{qk^2}{z(k)} e^{-z(k)\tau} \tag{3.65}$$

which in the elastic case $\zeta = 0$ is equivalent to the equilibrium correlation in (3.61).

This result has been obtained following the physical intuitive analogy between granular temperature in granular fluids and physical temperature in molecular fluids, and assuming the validity of a local Einstein relation. However, a rigorous derivation of noise correlations must follow the Boltzmann-Langevin derivation described above. In this case, noise correlations can be computed and give [30]

$$\left\langle \tilde{\xi}(k,\tau)\tilde{\xi}(k',\tau') \right\rangle = \delta_{k,-k'} 2Nk^2 G(|\tau - \tau'|) \tag{3.66}$$

where $G(s) \neq \delta(s)$. So, memory terms are present and confirmed by numerical simulations. The stationary autocorrelation is no longer a simple exponential, but it has an exponential tail for long times: Eq. (3.63) with the above prescription leads to

$$\begin{aligned} C_\perp(k,0) &= \frac{N}{2} \frac{q_1 k^2}{z(k)} \\ C_\perp(k,\tau) &= \frac{N}{2} \frac{(q_1+q_2)k^2}{z(k)} e^{-z(k)\tau} \qquad \tau \gg 1 \end{aligned} \tag{3.67}$$

where q_1 and q_2 have been computed in [30]. The time-dependent expression is valid after a transient, indeed the value at $\tau = 0$ is not the limit of the time-dependent expression. In the elastic limit $\zeta \to 0$, $q_1 \to q$ and $q_2 \to 0$, so the equilibrium result of Eq. (3.61) is recovered. While the initial value and transient are different, for long times the correlations derived from kinetic theory get the same temperature decay of correlations derived with the Einstein-Landau prescription in Eq. (3.64). This result confirms that the latter is a good approximation for long times correlations, while memory terms observables for short times can be obtained through kinetic theory. Einstein-Landau prescription is predictive also in the case of driven granular gases, both for bulk [190] or boundary driving [52]. Numerical results are in fair agreement with the theory, and again the Einstein-Landau approach has been recovered as a limit of kinetic derivation. The case of a bulk driven granular medium including external viscosity has been analyzed theoretically [166, 85] and experimentally: it has been shown that this is a good description of a quasi-$2d$ vibrated granular on a horizontal plate [86].

The shear mode is one of the simplest cases of fluctuating hydrodynamics, because it is decoupled from the others and then can be treated individually; nevertheless, this "simplicity" leads to complicated analytical calculations. Heat and sound modes are coupled and the derivation of fluctuating hydrodynamics from kinetic theory is a very hard challenge. For this reasons, further methods to describe fluctuating hydrodynamics are an important goal in current research.

Hydrodynamic fluctuations have been studied in the last years also in the framework of *Macroscopic Fluctuation Theory* (MFT), which has been derived to describe macroscopic fluctuations of hydrodynamic quantities in non-equilibrium steady states (NESS) [20, 21]. The general procedure considers a hydrodynamic density field $\rho(\mathbf{x}, t)$ and its associated current $\mathbf{j}(\mathbf{x}, t)$, satisfying

$$\partial_t \rho + \nabla \cdot \mathbf{j} = 0 \tag{3.68a}$$

$$\mathbf{j}(\mathbf{x}, t) = \mathbf{J}([\rho]; \mathbf{x}, t) \tag{3.68b}$$

respectively the continuity equation and the constitutive relation for the current $\mathbf{j}$ depending on the field ρ and eventually on time and space through the functional $\mathbf{J}$. For driven diffusive systems, the latter generally reads

$$\mathbf{J}([\rho]; \mathbf{x}, t) = -D(\rho)\nabla\rho + \chi(\rho)E(\mathbf{x}, t) \tag{3.69}$$

defining the diffusivity $D(\rho)$ and the mobility $\chi(\rho)$ under the action of an external field $E(\mathbf{x}, t)$. Under these assumptions, one can compute the probability of a trajectory (ρ, j) between time t_0 and t_1 as

$$\begin{aligned} \mathbb{P}_{\rho_0} &\approx \exp[-\epsilon^{-d}\mathcal{I}_{[t_0,t_1]}(\rho, j)] \\ \mathcal{I}_{[t_0,t_1]}(\rho, j) &= \frac{1}{4}\int_{t_0}^{t_1} \mathrm{d}t \int \mathrm{d}\mathbf{x}\, [\mathbf{j} - \mathbf{J}([\rho]; \mathbf{x}, t)] \cdot \chi^{-1}(\rho) \cdot [\mathbf{j} - \mathbf{J}([\rho]; \mathbf{x}, t)] \end{aligned} \tag{3.70}$$

where $\epsilon \ll 1$ is an adimensional parameter such that $\epsilon \to 0$ when $N \to \infty$, where N is the number of particles of the system, and trajectories are constrained to satisfy continuity equation (3.68a) and initial condition $\rho(t_0) = \rho_0$. The rate functional

$\mathcal{I}_{[t_0,t_1]}(\rho, j)$ acts as a *large deviation functional* [193], and the average hydrodynamic field and current correspond to the optimal path $\rho_{\rm av}(\mathbf{x}, t), \mathbf{j}_{\rm av}(\mathbf{x}, t)$ defined by

$$\min_{(\rho,j)} \mathcal{I}_{[t_0,t_1]}(\rho, j) = \mathcal{I}_{[t_0,t_1]}(\rho_{\rm av}, j_{\rm av}). \tag{3.71}$$

The theory derives back the deterministic hydrodynamic equations and obtains the hydrodynamic fluctuations beyond the linear approximation which has been used in the previous part of the section, necessarily leading to Gaussian fluctuations. The theory represents also a bridge between nonequilibrium fluctuation relations [79, 101, 123, 138], stochastic thermodynamics [172] and hydrodynamic theory.

MFT ha been recently applied to study fluctuating hydrodynamics of active systems, when comparing ABP and Run-and-Tumble dynamics [174] or investigating lattice models of interacting bacteria [181]. MFT found a successful field of application in *lattice models*, where a derivation of macroscopic hydrodynamic equations (3.68) from microscopic dynamics can be done in a transparent and rigorous way [62]. Lattice models have actually developed in the last 40 years as a tool to investigate several out-of-equilibrium processes, deriving their essential macroscopic features from minimal microscopic dynamics. The most important lattice models will be reviewed in the following of this chapter, as they have been a guide to introduce the granular and active lattice models in Part II which are the fundamental result of this thesis.

3.3 Lattice Models

Lattice models have been widely used in statistical physics in the last century because of the great simplifications that they introduce and consequently the possibility of many analytical calculations. The most famous lattice models have been developed for equilibrium systems, especially describing ferromagnetic behavior as in Ising, Heisenberg or XY model. Nevertheless, these models introduce an universal behavior and they can be adopted to describe several physical systems, such as lattice gases and binary alloys [94]. The reason of their success is the capability to reproduce complex physical behavior such as phase transitions by means of few essential, microscopic rules and yielding new theoretical predictions; furthermore, the investigation on lattice models usually doesn't need equilibrium assumption but rather relies on microscopic dynamics of the system. Therefore, the analysis is generally developed out of equilibrium, recovering the equilibrium case by a suitable choice of boundary conditions [140].

A plethora of lattice models have been developed in the last years, and a single model can lead to many others simply through a slight variation of its rules. Here a selection of the most significant models is presented, starting in Sec. 3.3.1 from the Kipnis-Marchioro-Presutti (KMP) model describing heat conduction in a chain of harmonic oscillators, and the simple exclusion processes (SEP) describing the diffusion of hopping particles on a linear chain. Both these models have *conservative* interactions and can be either in or out of equilibrium, depending on the boundary conditions. Subsequently, in Sec. 3.3.2 the case of dissipative models will

be introduced, for which *inelastic* interactions necessarily drive the system out of equilibrium.

3.3.1 Conservative models

In 1982, Kipnis, Marchioro and Presutti introduced a lattice model to describe the time evolution and heat flux of a linear chain of L mechanically uncoupled oscillators coupled with two thermal reservoir at both extremities [108]. A configuration of the system is given by $\{q_i, p_i\}$, i.e. the set of coordinates and momenta of all the sites, with $i = -L, \dots, L$. The energy at each site reads $\varepsilon_i = q_i^2 + p_i^2$. The system undergoes a stochastic evolution: at each discrete time step, two nearest-neighbors sites are chosen and exchange their energy redistributing it randomly, namely

$$\varepsilon_i' = p(\varepsilon_i' - \varepsilon_{i+1}'), \quad \varepsilon_{i+1}' = (1-p)(\varepsilon_i' - \varepsilon_{i+1}') \tag{3.72}$$

so that the microscopic evolution conserves the total energy. At sites $i = \pm L$ the oscillators thermalize with the reservoirs at temperatures T_+ $(+L)$ and T_- $(-L)$, i.e. they exchange energy with oscillators having a random energy with corresponding Boltzmann distribution.

The authors derive a mathematically rigorous expression for the evolution equation of the energy distribution $P(\{\varepsilon\}, t)$, and prove that in the stationary limit it converges to the local equilibrium distribution

$$f(\varepsilon; x, t) = \frac{1}{k_B T(x)} e^{-\varepsilon / k_B T(x)}, \tag{3.73}$$

where f is the one-site distribution and $P(\{\varepsilon\}, t) = \prod_x f(\varepsilon; x, t)$, x is the site index $x = i/L \in [-1, 1]$ which is continuous in the hydrodynamic limit $L \to \infty$, and $T(x)$ the temperature profile

$$T(x) = T_- \frac{1-x}{2} + T_+ \frac{1+x}{2}. \tag{3.74}$$

So, after a transient time the oscillators have thermalized and developed a temperature profile depending on bath temperatures. Although the system is out of equilibrium for $T_+ \neq T_-$, the local equilibrium holds *exactly* for the system.

The heat flux q can be defined as the energy transferred from oscillator i to $i+1$, and therefore it is a stochastic quantity. Its average behavior can be written as

$$q_i(t) = \int_0^\infty \mathrm{d}^L \varepsilon P(\{\varepsilon\}, t) \int_0^1 \mathrm{d}p \left[\varepsilon_i(t) - p(\varepsilon_i(t) + \varepsilon_{i+1})\right], \tag{3.75}$$

therefore, in the steady state local equilibrium holds and one has

$$q(x) = -\frac{k_B}{2} \frac{\mathrm{d}T}{\mathrm{d}x} \tag{3.76}$$

which is the Fourier's law with diffusion coefficient $D = k_B/2$. The stochastic energy current can be generally defined as $J(x,t) = q(x,t) + \xi(x,t)$, and the evolution equation of the local energies can be written as

$$\partial_t \varepsilon = -\partial_x J(x) = -\partial_x (-\frac{k_B}{2} \partial_x \varepsilon + \xi) \tag{3.77}$$

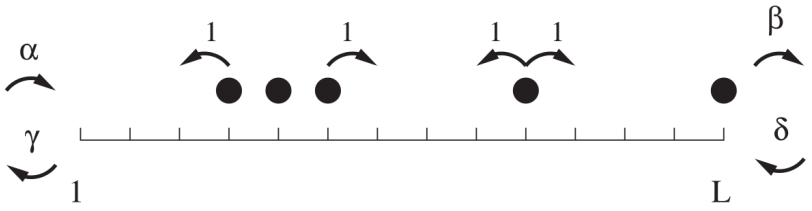

Figure 3.2. A sketch of the SSEP model [62]

which is the fluctuating hydrodynamics equation for the energy field $\varepsilon(x,t)$, namely a stochastic diffusion equation. Now, the noise amplitude and correlations can be computed directly through the local equilibrium distribution in (3.73); moreover, noise appears in the current in Eq. (3.77), which is a continuity equation also at a stochastic level, because energy conservation exactly holds in microscopic interactions, and mesoscopic equation (3.77) must respect it.

The model has been a milestone for lattice models of nonequilibrium statistical physics, since it shows how fundamental features such as heat diffusion can be rigorously recovered from lattice models, and the nonequilibrium probability distribution can be derived through the dynamics of the system. There is no need to define an effective Hamiltonian, or an equilibrium distribution, or to assume an Einstein relation: the local equilibrium approximation is the asymptotic limit of a nonequilibrium process. The local equilibrium found allows to derive the current fluctuations without the need to guess them from equilibrium dynamics.

The KMP model can be interpreted as well as the diffusion of particles on a chain, or diffusion of excitations on a linear system. Lattice models have indeed been applied from the beginning to describe density diffusion, magnetic models, fermionic systems, vibrations on a harmonic chain or electrical lines [2]. Among them, we will concentrate on models of *hopping* particles on a lattice. Random walk on a lattice is very well known, leading to the diffusion equation for the average density $\partial_t \rho = D\partial_x^2 \rho$ and the diffusive relation $\overline{x^2(t)} \sim t$. It has been shown that, when a particle jumps on heterogeneous medium (where the hopping rates depend on the position and they can be asymmetric), several regimes of motion arise depending on the statistical properties of the hopping rates [63, 61]. The *simple exclusion processes* (SEP) aims at describing the motion of particles moving on a linear chain with excluded volume interactions. The system is made by a random number of particles placed on L sites: each site $i = 1, \dots, L$ is occupied or not depending on the *occupation number* $n_i = 1, 0$. The hops are a Poissonian process: at each continuous time interval of length $\mathrm{d}\tau$, a particle on i can jump either to site $i-1$ or $i+1$ only if the site is empty and with probability $\mathrm{d}\tau$ for both directions (*symmetric* process, SSEP). The chain is coupled with two reservoirs of particles at the extremities, analogous to the thermal baths of KMP model: if the site $i = 0$ (L) is empty, a particle can enter the system with probability $\alpha \mathrm{d}\tau$ ($\delta \mathrm{d}\tau$); otherwise, if the site i (L) is occupied, the particle can leave the chain with probability $\gamma \mathrm{d}\tau$ ($\beta \mathrm{d}\tau$); the full dynamics of the SSEP is represented in Fig. 3.2. Thus, the system is Markovian and it is possible to write the evolution equations for the average

density $\langle n_i(t)\rangle$ in the limit $\mathrm{d}\tau \to 0$, which read [62]

$$\begin{aligned}
\frac{\mathrm{d}\langle n_1\rangle}{\mathrm{d}\tau} &= -\langle n_1\left[\gamma + (1-n_2)\right]\rangle + \langle (1-n_1)(\alpha + n_2)\rangle && \text{(3.78a)}\\
&= \alpha - (\alpha+\gamma+1)\langle n_1\rangle + \langle n_2\rangle \\
\frac{\mathrm{d}\langle n_i\rangle}{\mathrm{d}\tau} &= -\langle n_1\left[(1-n_{i-1}) + (1-n_{i+1})\right]\rangle + \langle (1-n_1)(n_{i-1}+n_{i+1})\rangle && \text{(3.78b)}\\
&= \langle n_{i-1}\rangle - 2\langle n_i\rangle + \langle n_{i+1}\rangle \qquad \text{for} \quad i = 2,\dots,L \\
\frac{\mathrm{d}\langle n_L\rangle}{\mathrm{d}\tau} &= -\langle n_L\left[\beta + (1-n_{L-1})\right]\rangle + \langle (1-n_L)(\delta + n_{L-1})\rangle && \text{(3.78c)}\\
&= \langle n_{L-1}\rangle - (\beta+\delta+1)\langle n_L\rangle + \delta
\end{aligned}$$

Eqs. (3.78a),(3.78c) are the boundary conditions of the system, while the bulk evolution is given by Eq. (3.78b). The derivation of a *closed* set of equations for the density has been made possible by the *exact* cancellation of two-point correlations $\langle n_i n_{i+1}\rangle$, which vanish in Eqs. (3.78) regardless of their value. The stationary solution can be found imposing $\mathrm{d}\langle n_i\rangle/\mathrm{d}\tau = 0$, yielding

$$\langle n_i\rangle = \frac{\rho_a(L + 1/(\beta+\delta) - i) + \rho_b(i - 1 + 1/(\alpha+\gamma))}{L + 1/(\alpha+\gamma) + 1/(\beta+\delta) - 1} \tag{3.79}$$

with $\rho_a = \alpha/(\alpha+\gamma)$ and $\rho_b = \delta/(\beta+\delta)$. In the hydrodynamic limit $L \to \infty$, it is natural to introduce once again the continuum position $x = i/L$, for which the stationary density reads

$$\langle n_i\rangle \equiv \rho_s(x) = \rho_a(1-x) + \rho_b x \tag{3.80}$$

which has the same form of KMP equation for temperature profile, except that here $x \in [0,1]$ whereas for KMP $x \in [-1,1]$ (I kept the original choice of the authors). So, ρ_a and ρ_b are the densities of the reservoirs, and if particles carry an energy ε the reservoirs become heat baths with temperatures T_a and T_b, satisfying

$$\exp\left[\frac{\varepsilon}{k_B T_a}\right] = \frac{\alpha}{\gamma} \quad , \quad \exp\left[\frac{\varepsilon}{k_B T_b}\right] = \frac{\delta}{\beta} \tag{3.81}$$

As for Eq. (3.78), the evolution equation of the average current and two-points correlations can be computed; their steady state reads

$$\langle J\rangle \equiv \langle n_i(1-n_{i+1}) - n_{i+1}(1-n_i)\rangle \simeq \frac{\rho_a - \rho_b}{L} \tag{3.82}$$

$$\langle n_i n_j\rangle_c \equiv \langle n_i n_j\rangle - \langle n_i\rangle\langle n_j\rangle = -\frac{x(1-y)}{L}(\rho_a - \rho_b)^2 \tag{3.83}$$

where $x = i/L$ and $y = j/L$. Eq. (3.82) gives the Fick's law for the SSEP model. These results show that currents and correlations are nonvanishing only when a density gradient $\rho_a \neq \rho_b$ is applied, and they are both finite-size effects $\sim 1/L$. One may say that these can therefore be easily neglected when $L \to \infty$, however this can be done only in first approximation as it will be shown in Chapter 4. Moreover, when considering macroscopic quantities such as the fluctuations of the total

number of particles N in the system, one sees that

$$\begin{aligned}\langle N^2\rangle - \langle N\rangle^2 &= \sum_i \left[\langle n_i\rangle - \langle n_i\rangle^2\right] + 2\sum_{i<j}\langle n_i n_j\rangle_c \\ &\simeq L\left[\int_0^1 \mathrm{d}x \rho_s(x)(1-\rho_s(x)) - 2(\rho_a-\rho_b)^2\int_0^1 \mathrm{d}x\int_0^1 \mathrm{d}y x(1-y)\right]\end{aligned} \tag{3.84}$$

so the correlations contribute at the leading order to the macroscopic fluctuations of the system.

The above results have been derived for the discrete set of microscopic configurations $\{n_i\}$; however, from Eqs. (3.78) it is tempting to move to a continuum description in the hydrodynamic limit $L \to \infty$. This is possible when assuming that averaged fields slowly vary with position, i.e. making the smoothness ansatz

$$\langle n_{i\pm1}\rangle \equiv \rho(x\pm\Delta x,\tau) = \rho(x,\tau) \pm \Delta x \left.\frac{\partial\rho}{\partial x}\right|_{x,t} + \frac{1}{2}(\Delta x)^2 \left.\frac{\partial^2\rho}{\partial x^2}\right|_{x,\tau} + \mathcal{O}((\Delta x)^3) \tag{3.85}$$

so the $\langle n_{i\pm1}\rangle$ terms in Eqs. (3.78) can be expanded and one has

$$\begin{aligned}\partial_\tau\rho(x=0,t) &= \alpha - (\alpha+\gamma)\rho(0,t) + \Delta x\,\partial_x\rho(x=0) \\ \partial_\tau\rho(x,t) &= (\Delta x)^2\partial_x^2\rho(x,t) \\ \partial_\tau\rho(x=1,t) &= \beta - (\beta+\delta)\rho(0,t) + \Delta x\,\partial_x\rho(x=1)\end{aligned} \tag{3.86}$$

Now, the lattice spacing $\Delta x = 1/L$ enters explicitly in the equations in the continuum limit $L \to \infty$: this implies that a macroscopic, *hydrodynamic time* must be defined as

$$t = (\Delta x)^2\tau \tag{3.87}$$

for this model, yielding $\partial_\tau = (\Delta x)^2\partial_t$ and canceling the explicit Δx dependence. By matching the equations at the leading orders in Δx, one has the evolution equation

$$\begin{aligned}\partial_t\rho(x,t) &= \partial_x^2\rho(x,t) \\ \rho(0) = \rho_a\,, &\quad \rho(1) = \rho_b\end{aligned} \tag{3.88}$$

which has the stationary solution of Eq. (3.80). The time rescaling defined in Eq. (3.87) is called *hydrodynamic scaling*, and will be widely used in Part II: its physical meaning is that hydrodynamic phenomena are evolving with characteristic times L^2 times bigger than the characteristic time of microscopic evolution, say the mean time between two hops. This is related with the scale separation introduced in the Chapman-Enskog procedure, and the ratio between microscopic and hydrodynamic times is equivalent to the Knudsen number for this model. The scaling $t = (\Delta x)^2\tau$ is called a *diffusive* scaling: indeed, in this case a diffusive behavior has been derived, see Eqs. (3.88). On the contrary, when $t = \Delta x\,\tau$ the scaling is said to be *ballistic*, because a tracer in the system follows a ballistic motion $\overline{x^2(t)} \sim t^2$. A fluctuating hydrodynamic description of the model has been made possible, mainly applying the Macroscopic Fluctuation Theory described in Sec. 3.2 [62].

The SSEP model can be modified by changing one of the hopping rates in the bulk from 1 to q: this case is known as the asymmetric simple exclusion process (ASEP). This asymmetry typically represents the effect of a driving force applied to the system, which can be gravity acceleration, electrical field, and so on. The ASEP model reproduces the essential features of driven diffusive models, and has been used as a model of traffic, growth and polymer dynamics [62]. Equations for the mean density eolution can be derived as in (3.78), but now the correlation terms do not vanish and must be treated carefully. The large scale ASEP behavior presents shock waves whereas the SSEP is purely diffusive.

Those two models have been both investigated in the framework of MFT to derive fluctuating hydrodynamics predictions. Their great utility is the possibility to derive several theoretical results far from equilibrium, and coming back to the equilibrium case when no gradient is applied at the boundaries. Their generalization to arbitrary dimensions is straightforward [62].

3.3.2 Dissipative models

The last models have been a useful guide to study fluctuating hydrodynamics of driven and diffusive conservative systems. However, this is not the case of granular or active matter systems, where dissipation is present in the bulk dynamics because of inelastic collisions and or self-propulsion. Granular models have been often developed on a lattice; especially, granular models in one dimension have been used to develop a rigorous hydrodynamic description [5, 7]. A granular lattice model can be introduced as a linear chain of L grains with velocities v_i, with $i = 1, \dots, L$; at each discrete time step $p \in \mathbb{N}$, a pair $i, i+1$ of nearest-neighbors is drawn and collide according to the inelastic collision rule in Eq. (1.35), which in 1d reads

$$\begin{aligned} v_i' &= v_i - \frac{1+\alpha}{2}(v_i - v_{i+1}) \\ v_{i+1}' &= v_{i+1} + \frac{1+\alpha}{2}(v_i - v_{i+1}) \end{aligned} \tag{3.89}$$

Similar models have been studied to find the asymptotic scaling distribution in the HCS or investigate the multiscaling properties described in Sec 1.4.6. The collision probability P_i of the pair $i, i+1$ plays a crucial role: indeed this can be chosen uniformly, $P_i = 1/L$, corresponding to Maxwell molecules dynamics; or it can contain a kinematic constraint $P_i \propto \Theta(v_i - v_i + 1)$, which implies that particles collide only when their velocities point towards each other; or there can be a flux term $P_i \propto |v_i - v_{i+1}|$, analogous with flux term in collisional operator of Boltzmann Equation for hard spheres (1.39b), increasing the collision probability with the magnitude of the relative velocity. When the last two terms are taken together, the system behaves as a $1d$ channel of inelastic hard rods, exchanging their velocities by means of collisions, with a perfect exchange when $\alpha = 1$ (elastic case) and slight reduction of speeds for $\alpha < 1$. It is worth stressing that in the elastic case $\alpha = 1$ the system is not really evolving in time: once given the set of initial velocities $\{v\}_{t=0}$, collisions only exchange labels, say $v_i' = v_{i+1}$ and $v_{i+1}' = v_i$, so the empirical velocity distribution is *invariant* in time. The model leads to a hydrodynamic description and several regimes of temperature decay are found, especially

in the case of high dissipation $\alpha \approx 0$: indeed, when $\alpha = 0$, after a collision two particles move with the same velocities and don't collide any more until a third particle change their velocity once again. Shock waves have been observed when the kinematic constraint is included, both in molecular dynamics (MD) of inelastic hard rods and in simulations of the lattice model; similarly, a $2d$ model has shown the presence of vortices spontaneously arising in the dynamics of the system [7]. It must be underlined that in this model the particles are *not* moving: indeed, all the sites are occupied, there are no hops and their velocities do not represent their motion but rather the dynamical observable involved in collisions, more or less like in the KMP model where we disregarded the physical meaning of position q_i and momentum p_i to concentrate only on the energy ε_i, which could be taken as the energy level of the site.

The first attempt to make a fluctuating hydrodynamics from dissipative lattice models has been done in 2011 by Prados, Lasanta and Hurtado [161, 162]: inspired from KMP model, they introduced a model of driven dissipative media, made by a chain on L particles each carrying an energy ρ_i, and coupled with two heat baths at the boundaries. The dynamics is equivalent to KMP model, but with a slightly modified interaction rule

$$\rho_i' = z_p \alpha(\rho_i + \rho_{i+1}) \,, \quad \rho_{i+1}' = (1 - z_p)\alpha(\rho_i + \rho_{i+1}) \tag{3.90}$$

where z_p is a random uniform number drawn at ecach time step between 0 and 1, and $\alpha \in [0, 1)$ is the inelasticity coefficient analogous to the restitution coefficient in granular collisions; the particles can be extracted uniformly or according to a distribution which typically depends from the total energy of the pair, i.e.

$$P_i(\{\rho\}) = \frac{f(\Sigma_i)}{L\Omega(L)} \,, \quad \Omega(L) = \sum_{i=1}^{L} f(\Sigma_i) \tag{3.91}$$

being $\{\rho\}$ the configuration of the system, $\Sigma_i \equiv \rho_i + \rho_{i+1}$ the total energy of the colliding particles and $f(\Sigma)$ a projection function which, together with collisional rule (3.90), determines the dynamics of the system. The time dependence of variables ρ_i has been omitted for simplicity. Without the need of specifying the collisional probability $f(\Sigma)$, the authors derived the hydrodynamic equations in the large-size limit

$$\partial_t \rho_{\text{av}}(x,t) = -\partial_x J_{\text{av}}(x,t) + d_{\text{av}}(x,t) \tag{3.92}$$

where the "av" fields are averaged fields such $\langle \rho \rangle = \rho_{\text{av}}$. The energy current J and dissipation rate d can be computed through the local equilibrium approximation, i.e. taking a Gaussian the energy distribution on a site i and assuming that $F_2(\rho_i, \rho_{i+1}; t) \approx F_1(\rho_i, t) F_1(\rho_{i+1}, t)$. So, one can write

$$J_{\text{av}}(x,t) = -D(\rho_{\text{av}})\partial_x \rho_{\text{av}} \tag{3.93}$$

$$d_{\text{av}}(x,t) = \nu R(\rho_{\text{av}}) \tag{3.94}$$

defining a diffusion coefficient $D(\rho)$, a transport coefficient $R(\rho)$ related to dissipation and a mesoscopic dissipation coefficient $\nu = (1 - \alpha^2)/2L^2$. The latter is non-vanishing in the large size limit only if $\alpha = 1 - \mathcal{O}(L^{-2})$ for large L: this is

called *quasielastic limit* and will be assumed as well in Chapter 4, being strictly connected with local equilibrium assumption. While the scaling of $1-\alpha$ is needed to match the current and dissipation terms in Eq. (3.92), we have already seen that for the KMP model ($\alpha = 1$) the asymptotic distribution was the Boltzmann distribution, so we expect that the asymptotic distribution in the quasielastic limit may be a perturbation of the equilibrium one.

The transport coefficients can be computed for a general f and read

$$D(\rho) = \frac{1}{6}\int_0^{+\infty} \mathrm{d}r\, r^7\, f(\rho r^2) e^{-r^2} \tag{3.95a}$$

$$R(\rho) = \rho \int_0^{+\infty} \mathrm{d}r\, r^5\, f(\rho r^2) e^{-r^2} \tag{3.95b}$$

under the local equilibrium assumption. Hydrodynamic equation (3.92) can be written in the fluctuating form

$$\partial_t \rho(x,t) = -\partial_x J(x,t) + d(x,t) \tag{3.96}$$

with $J(x,t) = \widetilde{J}(x,t) + \xi(x,t)$ and $d(x,t) = \widetilde{d}(x,t) + \eta(x,t)$. The idea is to split the fluctuating current and dissipation in two contributions: one from the average terms $\langle \widetilde{J} \rangle = J_{\mathrm{av}}$, $\langle \widetilde{d} \rangle = d_{\mathrm{av}}$, and the other from the noise as a zero-average fluctuations, ξ and η. Microscopic dynamics allows to compute the noise correlations, yielding at the leading order in $1/L$

$$\langle \xi(x,t)\xi(x',t') \rangle \sim \frac{1}{L}\sigma(\rho_{\mathrm{av}})\delta(x-x')\delta(t-t') \tag{3.97a}$$

$$\langle \eta(x,t)\eta(x',t') \rangle \sim \frac{1}{L^3}\nu^2\kappa(\rho)\delta(x-x')\delta(t-t') \tag{3.97b}$$

so, the dissipation fluctuations are much smaller than the current fluctuations and therefore are neglected in the following. The noises are proven to be Gaussian. Current noise amplitude is given by

$$\sigma(\rho) = 2\rho^2 D(\rho) \tag{3.98}$$

relating the mobility $\sigma(\rho)$ to the diffusivity $D(\rho)$. This is a kind of *fluctuation-dissipation* relation, which is connected with the quasielastic limit introduced above. Again, this relation has not been assumed from some equilibrium relation, but derived from the microscopic dynamics. Finally, for a specific choice of $f(\Sigma)$, the time evolution of energy in the HCS can be found, recovering Haff's law in the hard spheres case, $f(\Sigma) \propto \sqrt{\Sigma}$; in the heated case, the stationary profiles of energy, current and dissipation can be derived as well. The model has been analyzed in the framework of MFT, confirming previous results and leading to new theoretical prediction on his fluctuating hydrodynamics.

The model of Prados, Lasanta and Hurtado introduced above has been a key guide to develop this thesis. I did not report the technical calculations, because many of them will be explained for the granular sheared model of Chapter 4; a rigorous derivation can be found in [120]. Finally, lattice models have been developed also to describe active matter: in 1995, Csahók and Vicsek developed a lattice

model of active particles, interlacing the Vicsek model of collective motion with lattice gas methods [54]. More recently, in 2011 Thompson *et al.* introduced a $1d$ model of run-and-tumble bacteria, hopping on a lattice without excluded volume, aiming at reproducing the observed features in off lattice run-and-tumble dynamics and deriving the fluctuating hydrodynamics of the system [181]. As it has been shown, lattice models leads to a huge number of theoretical predictions, especially on fluctuating quantities. The analytical power together with the phenomenological realism inspired us to derive the models in Part II.

Part II

Fluctuating Hydrodynamics of Granular and Active Matter: Lattice Models

Jusqu'ici tout va bien

4

Granular lattice: fluctuating hydrodynamics

Inspired from the works of Baldassarri *et al.* [6] and Prados *et al.* [161], we formulated a granular lattice model to derive fluctuating hydrodynamics from microscopic ingredients under controlled assumptions, considering only shear modes on a granular linear chain [122]. The evolution of the system conserves momentum and dissipates energy, as in granular collisions. The new model is different from the previous proposals in a few crucial aspects. In [6], the velocity field evolved under the enforcement of the so-called kinematic constraint, which is disregarded here. In [161], only the energy field was considered, therefore momentum conservation was absent. The results I present especially focus on the hydrodynamic behavior of the model; the analysis of velocity distribution evolution and a detailed approach to a mesoscopic fluctuation theory of our model can be found respectively in [133, 155, 154].

The aim of the model is reproducing the shear hydrodynamics of a granular system and deriving its fluctuating behavior starting from microscopic rules. As it has been shown in Sec. 3.1.2, there is a range of sizes of granular systems such as the only linearly unstable mode in the HCS is the shear mode: this implies that the velocity field is incompressible and density does not evolve from its initial uniform configuration. Such a regime may be observed for a certain amount of time (longer and longer as the elastic limit is approached). In two dimensions, granular hydrodynamic equations (3.36) are obeyed with constant density and, for instance, $u_x = 0$ whereas the hydrodynamic fields u_y and T only depend on x, leading to

$$\partial_t u_y(x,t) = (nm)^{-1}\partial_x[\eta\partial_x u_y(x,t)], \tag{4.1a}$$

$$\partial_t T(x,t) = \frac{1}{n}\eta[\partial_x u_y(x,t)]^2 + \frac{1}{n}\partial_x[\kappa\partial_x T(x,t)] - \zeta T. \tag{4.1b}$$

In section 4.2 we will see that our lattice model is well described, in the continuum

limit, by the same equations.

It is interesting to put in evidence that (4.1) sustains also particular stationary solutions. Seeking time-independent solutions thereof, one finds

$$\partial_x[\eta\partial_x u_y^{(s)}(x)] = 0, \quad \eta[\partial_x u_y^{(s)}(x)]^2 = -\partial_x[\kappa\partial_x T^{(s)}(x)] + n\zeta T^{(s)}(x). \tag{4.2}$$

The general situation is that both the average velocity and temperature profiles are inhomogeneous: this is the so-called Couette flow state, which also exists in molecular fluids. Yet, in granular fluids, there appears a new steady state in which the temperature is homogeneous throughout the system, $T^{(s)}(x) = T$, and the average velocity has a constant gradient, $\partial_x u_y = a$: this is the Uniform Shear Flow (USF) state, characterized by the equations

$$\partial_x^2 u_y^{(s)}(x) = 0, \quad \eta[\partial_x u_y^{(s)}(x)]^2 = nk_B\zeta T^{(s)}. \tag{4.3}$$

Such a steady state is peculiar of granular gases where the viscous heating term is locally compensated by the energy sink term. In a molecular fluid, this compensation is lacking and viscous heating must be balanced by a continuous heat flow toward the boundaries, which entails a gradient in the temperature field, typical of the Couette flow.

The formal definition of the model is given in Sec. 4.1. In Sec. 4.2 the hydrodynamic equations are derived as the continuum limit of microscopic balance equations. Sec. 4.3 is devoted to the analysis of some relevant physical states such as the Homogeneous Cooling State (HCS), the Uniform Shear Flow (USF) and the Couette flow. In Sec. 4.4 the fluctuating currents are defined and their correlations are derived. Sec. 4.5 contains numerical analysis of hydrodynamic states and fluctuating currents discussed in previous sections.

4.1 Definition of the model

In this section, the granular model is introduced by means of a Markovian process, defining an evolution equation of the phase-space probability distribution P_N and later deriving the evolution equation of the single particle distribution P_1. In the rest of the chapter, these quantities will not be part of the analysis, as we will focus on hydrodynamic fields. Nevertheless, the present section shows that a "kinetic" derivation of hydrodynamic equation is possible, following the approach of Sec. 1.4. Furthermore, the Markovian description is transparent and without ambiguities, illustrating also the residence-time algorithm which will actually be used in simulations. In our work, the derivation of hydrodynamics from microscopic balance equations preceded in time the Markovian description; since the two procedures have shown to be equivalent, I present the microscopic balance equations in Appendix A.1 for the sake of completeness.

4.1.1 Master Equation for the lattice model

The model is defined on a $1d$ lattice with N sites, but it can be generalized to higher dimensions. In each site there is a scalar velocity v_i, so that a state of the system

is the vector $\mathbf{v} \in \mathbb{R}^N$. The evolution is a Markov jump process which - in general - takes place in continuous time τ, each jump representing a collision. Jumps (collisions) are counted by the integer $p \in \{0, 1, 2...\}$. The random time increment $\delta\tau_p$ between two collisions $p \to p+1$ is given by

$$\delta\tau_p = \Omega_p(L)^{-1} |\ln \chi|, \quad \Omega_p(L) = \omega \sum_{l=1}^{L} |v_{l,p} - v_{l+1,p}|^\beta, \tag{4.4}$$

in which χ is a stochastic variable homogeneously distributed in the interval $(0, 1)$, ω is a constant frequency that determines the time scale, and L is the number of pairs that can collide (i.e. $L = N$ when periodic boundary conditions are considered, or $L = N + 1$ when thermostatted boundaries are taken into account). The physical meaning of Eq. (4.4) is clear: $\Omega_p(L)$ is the total exit rate from the state of the system, as given by its velocity configuration $\mathbf{v}$, at time p, and the time increment $\delta\tau$ follows the distribution $P(\delta\tau) = \Omega_p(L) \exp[-\Omega_p(L)\delta\tau]$ as in a Poissonian process. We have introduced the parameter $\beta \geq 0$ that affects the collision rate. For $\beta = 0$, the collision rate is independent of the relative velocity, similarly to the case of pseudo-Maxwell molecules [6]. For this reason, we refer to $\beta = 0$ as the MM case, while $\beta = 1$ and $\beta = 2$ are analogous to the hard spheres (HS) [32] and "very hard-core" [67, 69] collisions, respectively.

It is convenient to define $\Delta_l = v_l - v_{l+1}$, and to introduce the operator $\hat{b}_l$, which evolves the vector $\mathbf{v}$ by colliding the pair $(l, l+1)$ according to granular collision rule (1.35), i.e.

$$\hat{b}_l(v_1, ..., v_l, v_{l+1}, ..., v_N) = \left(v_1, ..., v_l - \frac{1+\alpha}{2}\Delta_l, v_{l+1} + \frac{1+\alpha}{2}\Delta_l, ..., v_N\right), \tag{4.5}$$

where $\alpha \in [0, 1]$ is the restitution coefficient. After the p-th collision, momentum is conserved, $v_{l,p} + v_{l+1,p} = v_{l,p+1} + v_{l+1,p+1}$,, while energy, if $\alpha \neq 1$, is not:

$$v_{l,p+1}^2 + v_{l+1,p+1}^2 - v_{l,p}^2 - v_{l+1,p}^2 = (\alpha^2 - 1)\Delta_{l,p}^2/2 < 0. \tag{4.6}$$

Also, note that for a generic function of the velocities $f(\mathbf{v})$ one has

$$\int \mathrm{d}\mathbf{v}' |v_l' - v_{l+1}'|^\beta \delta(\mathbf{v} - \hat{b}_l\mathbf{v}') f(\mathbf{v}') = \frac{|\Delta_l|^\beta}{\alpha^{\beta+1}} f(\hat{b}_l^{-1}\mathbf{v}). \tag{4.7}$$

The operator $\hat{b}_l^{-1}$ is the inverse of $\hat{b}_l$, that is, it changes the post-collisional velocities into the pre-collisional ones when the colliding pair is $(l, l+1)$.

The continuous time Markov process is fully described by the two-time conditional probability $P_N(\mathbf{v}, \tau|\mathbf{v}_0, \tau_0)$ with $\tau \geq \tau_0$, which evolves according to the following forward Master Equation,

$$\partial_\tau P_N(\mathbf{v}, \tau|\mathbf{v}_0, \tau_0) = \int d\mathbf{v}' W(\mathbf{v}|\mathbf{v}') P_N(\mathbf{v}', \tau|\mathbf{v}_0, \tau_0) - \Omega(\mathbf{v}) P_N(\mathbf{v}, \tau|\mathbf{v}_0, \tau_0), \tag{4.8}$$

in which

$$W(\mathbf{v}'|\mathbf{v}) = \omega \sum_{l=1}^{N} |\Delta_l|^\beta \delta(\mathbf{v}' - \hat{b}_l\mathbf{v}), \quad \Omega(\mathbf{v}) = \int \mathrm{d}\mathbf{v}' W(\mathbf{v}'|\mathbf{v}) = \omega \sum_{l=1}^{N} |\Delta_l|^\beta. \tag{4.9}$$

The Master Equation can be simplified by making use of (4.7), with the final result

$$\partial_\tau P_N(\mathbf{v},\tau|\mathbf{v}_0,\tau_0) = \omega \sum_{l=1}^{L} |\Delta_l|^\beta \left[\frac{P_N(\hat{b}_l^{-1}\mathbf{v},\tau|\mathbf{v}_0,\tau_0)}{\alpha^{\beta+1}} - P_N(\mathbf{v},\tau|\mathbf{v}_0,\tau_0) \right]. \quad (4.10)$$

The conditional probability distribution $P_N(\mathbf{v},\tau|\mathbf{v}_0,\tau_0)$ is the solution of the above equation with the initial condition $P_N(\mathbf{v},\tau_0|\mathbf{v}_0,\tau_0) = \delta(\mathbf{v}-\mathbf{v}_0)$. On the other hand, the one-time probability distribution $P_N(\mathbf{v},\tau)$ verifies the same equation but with an arbitrary (normalized) initial condition $P_N(\mathbf{v},0)$.

Residence time algorithms that give a numerical integration of the master equation in the limit of infinite trajectories [27, 160] show that either (4.8) or (4.10) is the Master equation for a continuous time jump Markov process consisting in the following chain of events:

1. at time τ, a random "free time" $\tau_f \geq 0$ is extracted with a probability density $\Omega(\mathbf{v})\exp[-\Omega(\mathbf{v})\tau_f]$ which depends upon the state of the system $\mathbf{v}$;
2. time is advanced by such a free time $\tau \to \tau + \tau_f$;
3. the pair $(l, l+1)$ is chosen to collide with probability $\omega|\Delta_l|^\beta/\Omega(\mathbf{v})$;
4. the process is repeated from step 1.

The Master equation derived above can be considered our "Liouville equation", that is, it evolves the probability in full phase-space. It is tempting, from such equation, to derive a Lyapunov (or "H") functional which is minimized by the dynamics, as it is customary for Markov processes [103]. However, in the general case our system does not admit an asymptotic steady state, apart from the trivial zero, and therefore the usual H function (which relies upon the existence of the steady state) cannot be built. However, this programme can be carried on in the presence of appropriate boundary conditions, e.g. thermostats, which allow the system to reach a steady state [139, 60]. Very recently, an H-theorem for the driven system has been formulated and proven to hold under certain mathematical assumptions on the initial distribution. [156].

4.1.2 Physical interpretation

The model, if taken literally, implies that there is no mass transport, particles are at fixed positions and they only exchange momentum and kinetic energy. As discussed above, this can be a valid assumption in an *incompressible* regime which is expected when the velocity field is divergence free, for instance during the first stage of the development of the shear instability, or in the so-called Uniform Shear Flow. We are also disregarding the so-called kinematic constraint, which is fully considered in [6]: indeed a colliding pair is chosen independently of the sign of its relative velocity, while in a real collision only approaching particles can collide. Even without the kinematic constraint, our model has a straightforward physical interpretation: the dynamics occurs inside an elongated $2d$ or $3d$ channel, the lattice sites represent positions on the long axis, while the transverse (shorter) directions are ignored; the velocity of the particles do not represent their motion along the

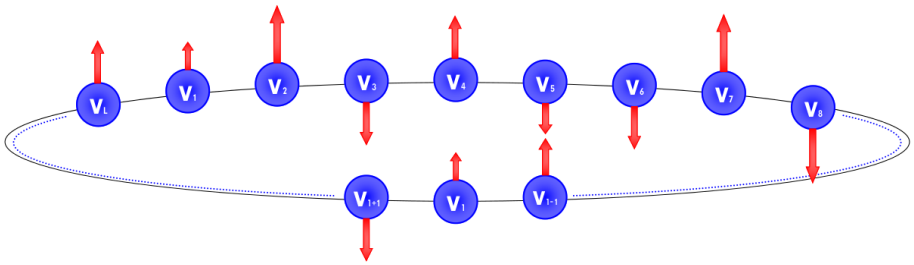

Figure 4.1. A sketch of the granular lattice model with periodic boundaries. The velocities are represented by red arrows.

lattice axis but rather along a perpendicular one. One may easily imagine that the (hidden) component along the lattice axis is of the order of the perpendicular component, but in random direction. On the one hand, this justifies the choice of disregarding the kinematic constraint, while on the other, the collision rate may still be considered proportional to some power β of the velocity difference (in absolute value). A fair confirmation of this interpretation comes from the average hydrodynamics equations derived in section 4.2, which, as anticipated in the introduction, replicate the transport equations (4.1) for granular gases in $d > 1$ restricted to the shear (transverse) velocity field.

4.1.3 Evolution equation for the one-particle distribution

Here, we apply the usual procedure of kinetic theory and map the Master equation into a BBGKY hierarchy. In particular, we focus on the evolution equation for the one-particle distribution function at site l and at time τ, which we denote by $P_1(v; l, \tau)$. The behavior of the one-particle distribution P_1 in our model will be deeply analyzed in [154]. By definition,

$$P_1(v; l, \tau) = \int \mathrm{d}\mathbf{v} P_N(\mathbf{v}, \tau)\delta(v_l - v). \tag{4.11}$$

It is easy to show that none of the terms in the sum (4.10) contribute to the time evolution of P_1 except those corresponding to $l-1$ and l, because the collisions involving the pairs $(l-1, l)$ and $(l, l+1)$ are the only ones which change the velocity at site l. Therefore,

$$\begin{aligned}
&\partial_\tau P_1(v; l, \tau) = \omega \times \\
&\left\{ \int_{-\infty}^{+\infty} \mathrm{d}v_{l-1} |\Delta_{l-1}|^\beta \left[\frac{P_2(\hat{b}_{l-1}^{-1}\{v_{l-1}, v\}; l-1, l, \tau)}{\alpha^{\beta+1}} - P_2(v_{l-1}, v; l-1, l, \tau) \right] \right. \\
&\left. + \int_{-\infty}^{+\infty} \mathrm{d}v_{l+1} |\Delta_l|^\beta \left[\frac{P_2(\hat{b}_l^{-1}\{v, v_{l+1}\}; l, l+1, \tau)}{\alpha^{\beta+1}} - P_2(v, v_{l+1}; l, l+1, \tau) \right] \right\},
\end{aligned} \tag{4.12}$$

where, for the sake of simplicity, we also denote by $\hat{b}_l^{-1}$ the backward collisional operator which acts on only the velocities of the colliding particles. In the equation above, we have the two-particle probability distribution $P_2(v, v'; l, l+1, \tau)$ for

finding the particles at the l-th and $(l+1)$-th sites with velocities v and v', respectively. For the special case $\beta = 0$, the evolution equation for P_1 can be further simplified, because the terms on the rhs of (4.12) coming from the loss (negative) terms of the master equation can be integrated. We get

$$\partial_\tau P_1(v;l,\tau) = \omega \left[-2P_1(v;l,\tau) + \frac{1}{\alpha}\int_{-\infty}^{+\infty} \mathrm{d}v_{l-1} P_2(\hat{b}_{l-1}^{-1}\{v_{l-1},v\};l-1,l,\tau) + \frac{1}{\alpha}\int_{-\infty}^{+\infty} \mathrm{d}v_{l+1} P_2(\hat{b}_{l}^{-1}\{v,v_{l+1}\};l,l+1,\tau) \right]. \quad (4.13)$$

The equation for P_1, either (4.12) for a generic β or (4.13) for $\beta = 0$, could be converted to a closed equation for P_1 by introducing the *Molecular Chaos* assumption, which in our present context means that

$$P_2(v,v';l,l+1,\tau) = P_1(v;l,\tau)P_1(v';l+1,\tau) + O(L^{-1}). \quad (4.14)$$

By neglecting the $O(L^{-1})$ terms in (4.14), we obtain a pseudo-Boltzmann or kinetic equation for P_1, which determines the evolution of the one-time and one-particle averages under the assumption of $O(L^{-1})$ correlations. Note that since $L/N \to 1$ for a large system, independently of the boundary conditions, orders of inverse powers of N and L are utterly equivalent. It is important to stress that the range of validity of assumption (4.14) is assessed in numerical simulations, see section 4.5. In Chapter 5 the conjecture that two-particle correlations scale with L^{-1} will be proven analytically. Note that this "smallness" of two-particle correlations do not prevent them from being long-ranged.

The structure of the kinetic equation for P_1 is thus much simpler for the MM case. In particular, we see along the next sections that the evolution equations for the moments are closed under the molecular chaos assumption, without further knowledge of the probability distribution P_1. This is the reason why, in the remainder of the paper, we restrict ourselves to the MM case $\beta = 0$, since the mathematical treatment needed for the $\beta \neq 0$ case is much more complicated and then is deferred to further studies.

4.2 Hydrodynamics

In the following section, we derive the hydrodynamic behavior for $\beta = 0$, in which the evolution equations for the averages are closed. Moreover, the MM case makes it possible to grasp the essential points.

4.2.1 Microscopic balance equations

From Eq. (4.8) it is straightforward to get the evolution rule for $v_{l,p}$ (for any site l) at collision index p:

$$v_{l,p+1} - v_{l,p} = -j_{l,p} + j_{l-1,p}, \quad (4.15)$$

where the momentum current, that is, the flux of momentum from site l to site $l+1$ at the p-th collision reads

$$j_{l,p} = \frac{1+\alpha}{2}\Delta_{l,p}\delta_{y_p,l}, \quad (4.16)$$

Here $\delta_{y_p,l}$ is Kronecker's δ and $y_p \in [1, L]$ is a random integer which selects the colliding pair.

The corresponding equation for the energy, obtained by squaring (4.15), reads

$$v_{l,p+1}^2 - v_{l,p}^2 = -J_{l,p} + J_{l-1,p} + d_{l,p}. \tag{4.17}$$

Again, we have defined an energy current from site l to site $l+1$ as

$$J_{l,p} = (v_{l,p} + v_{l+1,p}) j_{l,p}. \tag{4.18}$$

In addition, the energy dissipation at site l is

$$d_{l,p} = (\alpha^2 - 1)[\delta_{y_p,l}\Delta_{l,p}^2 + \delta_{y_p,l-1}\Delta_{l-1,p}^2]/4 < 0. \tag{4.19}$$

The total energy of the system at the p-th collision is $E_p = \sum_{l=1}^N v_{l,p}^2$.

It is customary to define, as relevant fields for hydrodynamics, the following local averages, at a given collision number p, over initial conditions and noise realizations:

$$u_{l,p} = \langle v_{l,p} \rangle, \qquad E_{l,p} = \langle v_{l,p}^2 \rangle, \qquad T_{l,p} = E_{l,p} - u_{l,p}^2. \tag{4.20}$$

A few words should be spent for commenting the choice of the relevant fields: in the usual conservative kinetic theory, the velocity and energy fields are naturally "slow" because of their global conservation (recall that there is no density transport in our model, as discussed before in section 4.1.2). For a granular gas, energy is not necessarily slow: however, when α approaches 1, as it is in many physical situations, the total energy evolves quite slowly and can be thought of as a *quasi-slow* variable. In the following, we show that the continuum limit necessary to get a hydrodynamic description requires $\alpha \to 1$ if dissipation of energy and diffusion take place over the same time scale. It is important to realize, however, that such an elastic limit is singular here: in $1d$, when $\alpha = 1$ the dynamics corresponds to a pure relabelling without mixing or ergodicity.

The microscopic equations for the evolution of averages at time (counted by collisions) p at site l are obtained by averaging equations (4.15) and (4.17):

$$u_{l,p+1} - u_{l,p} = -\langle j_{l,p} \rangle + \langle j_{l-1,p} \rangle, \tag{4.21}$$

$$E_{l,p+1} - E_{l,p} = -\langle J_{l,p} \rangle + \langle J_{l-1,p} \rangle + \langle d_{l,p} \rangle. \tag{4.22}$$

For the case of MM ($\beta = 0$, i.e. all sites collide with the same probability) we have that $\langle \delta_{y_p,l} f(\mathbf{v}_p) \rangle = L^{-1} \langle f(\mathbf{v}_p) \rangle$ and therefore we can write the averages as

$$\langle j_{l,p} \rangle = \frac{1+\alpha}{2L} \langle \Delta_{l,p} \rangle, \tag{4.23a}$$

$$\langle J_{l,p} \rangle = \frac{1+\alpha}{2L} \langle \Delta_{l,p}(v_{l,p} + v_{l+1,p}) \rangle, \tag{4.23b}$$

$$\langle d_{l,p} \rangle = \frac{\alpha^2 - 1}{4L} \langle \Delta_{l,p}^2 + \Delta_{l-1,p}^2 \rangle. \tag{4.23c}$$

From these equations, it is readily obtained that

$$\langle j_{l,p}\rangle = \frac{1+\alpha}{2L}\left(u_{l,p}-u_{l+1,p}\right) \tag{4.24a}$$

$$\langle J_{l,p}\rangle = \frac{1+\alpha}{2L}\left(T_{l,p}-T_{l+1,p}+u_{l,p}^2-u_{l+1,p}^2\right) \tag{4.24b}$$

$$\begin{aligned}\langle d_{l,p}\rangle = \frac{\alpha^2-1}{4L}\Big[&2T_{l,p}+T_{l+1,p}+T_{l-1,p}\\ &+2\left(u_{l,p}-\frac{u_{l+1,p}+u_{l-1,p}}{2}\right)^2+\frac{1}{2}(u_{l+1,p}-u_{l-1,p})^2\Big].\end{aligned} \tag{4.24c}$$

In order to write the average dissipation, we have neglected $O(L^{-1})$ terms, since we have made use of the molecular chaos approximation, more specifically of the equality $\langle v_{l,p}v_{l\pm1,p}\rangle = u_{l,p}u_{l\pm1,p}+O(L^{-1})$.

Had we considered $\beta \neq 0$, we would have had an extra factor $|\Delta_{l,p}|^\beta$ in the averages on the rhs of (4.23). This extra factor would have made it necessary, apart from the "molecular chaos" hypothesis, to use further assumptions about the one-particle distribution function. More specifically, we would have needed to know its shape, at least in some approximation scheme, to calculate the moments in the average currents and dissipation in terms of the hydrodynamic fields u and T, that is, the so-called constitutive relations.

4.2.2 Balance equations in the continuum limit

Now we assume that $u_{l,p}$ and $E_{l,p}$ are smooth functions of space and time and introduce a continuum, "hydrodynamic", limit (CL). First, the macroscopic space-time scales (x,t) are defined which are related to the microscopic ones (l,p) through size-dependent factors:

$$x = l/L, \quad t = p/L^3. \tag{4.25}$$

Note that both x and t are dimensionless variables. The choice of the above scalings is dictated by the aim of: (i) working with a "reduced" unit size to prevent L factors enter into the solutions through the boundary conditions, and (ii) matching the dominant L dependence on the right hand side and left hand side of the balance equations. With the identification $f_{l,p} = f(l/L, p/L^3)$, we say that $f(x,t)$ is a "smooth" function $f(x,t)$ if

$$f_{l\pm1,p} - f_{l,p} = \pm L^{-1}\partial_x f(x,t) + O\left(L^{-2}\right), \tag{4.26}$$

$$f_{l,p\pm1} - f_{l,p} = \pm L^{-3}\partial_t f(x,t) + O\left(L^{-6}\right). \tag{4.27}$$

It is natural, on the scales defined by the CL, to define the mesoscopic fields $u(x,t)$, $E(x,t)$ and $T(x,t)$ such that

$$u_{l,p} = u(l/L, p/L^3), \quad E_{l,p} = E(l/L, p/L^3), \quad T_{l,p} = T(l/L, p/L^3). \tag{4.28}$$

and assume them to be smooth.

Using these definitions and the smoothness assumption, one finds that each discrete spatial derivative in (4.21) and (4.22) introduces a L^{-1} leading factor. Then,

the difference between the current terms in the balance equations is of the order of L^{-3}, because the average currents $\langle j_{l,p}\rangle$ and $\langle J_{l,p}\rangle$ are of the order of L^{-2}, as we have discrete derivatives of the currents therein. Those terms, therefore, perfectly balance the $1/L^3$ dominant scaling on the left-hand side, i.e. the time-derivative. Since $\langle d_{l,p}\rangle$ is of the order of $(1-\alpha^2)/L$, to match the scaling $1/L^3$ of the other terms, we define the *macroscopic inelasticity*

$$\nu = (1-\alpha^2)L^2, \tag{4.29}$$

and assume it to be order 1 when the limit is taken. This choice implies that when $L \to \infty$ one has $\alpha \to 1$, that is, microscopic collisions are quasi-elastic.

From a mathematical point of view, the following results for the average hydrodynamic behavior become exact in the double limit $\alpha \to 1$, $L \to \infty$ but finite $\nu = (1-\alpha^2)L^2$, provided that the initial conditions are smooth in the sense given by (4.26). Nonetheless, for a large-size system, the following results will hold over a certain time window, which is expected to increase as its size L increases. An analysis of the limits of validity of our hydrodynamic equations is carried out in section 4.3.4.

By defining the average mesoscopic currents

$$j_{\rm av}(x,t) = \lim_{L\to\infty} L^2\langle j_{l,p}\rangle, \quad J_{\rm av}(x,t) = \lim_{L\to\infty} L^2\langle J_{l,p}\rangle \tag{4.30}$$

and the average mesoscopic dissipation of energy

$$d_{\rm av}(x,t) = \lim_{L\to\infty} L^3\langle d_{l,p}\rangle, \tag{4.31}$$

one gets the CL of (4.21) and (4.22), which are

$$\partial_t u(x,t) = -\partial_x j_{\rm av}(x,t), \tag{4.32a}$$
$$\partial_t E(x,t) = -\partial_x J_{\rm av}(x,t) + d_{\rm av}(x,t). \tag{4.32b}$$

Therein, the average currents and dissipation follow from (4.30), (4.31) and (4.24), with the result

$$j_{\rm av}(x,t) = -\partial_x u(x,t), \tag{4.33a}$$
$$J_{\rm av}(x,t) = -\partial_x \left[u^2(x,t) + T(x,t)\right], \tag{4.33b}$$
$$d_{\rm av}(x,t) = -\nu T. \tag{4.33c}$$

Note that (i) we have replaced $1+\alpha$ by 2, because $\alpha^2 = 1-\nu L^{-2}$, and we have already neglected L^{-1} terms and (ii) $J_{\rm av}(x,t) = -\partial_x E(x,t)$, with $E(x,t) = u^2(x,t) + T(x,t)$, consistently with (4.20).

Taking into account the above expressions, the following average hydrodynamic equations are obtained,

$$\partial_t u(x,t) = \partial_{xx} u(x,t), \tag{4.34a}$$
$$\partial_t T(x,t) = -\nu T(x,t) + \partial_{xx} T(x,t) + 2\left[\partial_x u(x,t)\right]^2. \tag{4.34b}$$

These equations must be supplemented with boundary conditions for the situation of interest. The identification with the granular Navier-Stokes hydrodynamic

equations (4.1) in the shear mode regime is immediate, particularized for the case of constant (time and space-independent) κ and η.

Additionally, the time evolution of higher central moments of the one-particle distribution function, such as

$$\mu_3 = \langle (v-u)^3 \rangle, \quad \mu_4 = \langle (v-u)^4 \rangle, \tag{4.35}$$

can be derived. These moments are particularly relevant to check deviations from the Gaussian behavior, since for a Gaussian distribution with variance T one has that $\mu_3 = 0$ and $\mu_4 = 3T^2$. Their evolution equations are

$$\partial_t \mu_3 = -\frac{3}{2}\nu\mu_3 + \partial_{xx}\mu_3 + 6\,(\partial_x u)\,(\partial_x T), \tag{4.36a}$$

$$\partial_t \mu_4 = -2\,\nu\mu_4 + \partial_{xx}\mu_4 + 8\,(\partial_x \mu_3)\,(\partial_x u) + 12T(\partial_x u)^2. \tag{4.36b}$$

Again, these evolution equations must be supplemented with appropriate boundary conditions, which depend on the physical situation of interest. It is important to stress that μ_3 and μ_4 are *not* hydrodynamic fields because $(v-u)^n$ with $n \geq 3$ is not conserved during collisions, not even in the quasielastic limit as considered in Sec. 4.2.1. The derivation of Eqs. (4.36b) is given in Appendix A.2.

4.3 Physically relevant states

In this section, always under the assumption $\beta = 0$, we analyze some physically relevant states that are typical of dissipative systems such as granular fluids. Specifically, we investigate the Homogeneous Cooling State (HCS), the Uniform Shear Flow (USF) state and the Couette Flow state. The theoretical results obtained throughout are compared to numerical results in section 4.5.

4.3.1 The Homogeneous Cooling State

We now focus our attention on the case of spatial periodic boundary conditions, with an initial "thermal condition": $v_{l,0}$ is a random Gaussian variable with zero average and unit variance, that is, $T_{l,0} \equiv T(x,0) = 1$. Starting from this condition, the system typically falls into the so-called Homogeneous Cooling State (HCS), where the total energy decays in time and the velocity and temperature fields remain spatially uniform. In this case, the solution of the average hydrodynamic equations (4.34) reads

$$u(x,t) = 0, \qquad T_{\text{HCS}}(x,t) = T(t=0)e^{-\nu t}. \tag{4.37}$$

The exponential decrease of the granular temperature is typical of MM, where the collision frequency is velocity-independent. It replaces the so-called Haff's law which was originally derived in the HS case, where $T_{\text{HCS}} \sim t^{-2}$ because $\dot{T} \propto -T^{3/2}$ [88].

The HCS is known to be unstable: as discussed in Sec. 3.1.2, it breaks down in too large or too inelastic systems. In our model and in the hydrodynamic limit,

this condition is expected to be replaced by a condition of large ν. The stability is studied by introducing rescaled fields $\tilde{u}(x,t) = u(x,t)/\sqrt{T_{HCS}(t)}$ and $\tilde{T} = T(x,t)/T_{HCS}(t)$ and by linearizing the hydrodynamic equations near the HCS, i.e. $T(x,t) = T_{HCS}(t) + \delta T(x,t)$ and $\tilde{u}(x,t) = \delta\tilde{u}(x,t)$. The analysis of linear equations becomes straightforward by space-Fourier-transforming, which gives

$$\partial_t \delta\tilde{u}(k,t) = \frac{\nu - 2k^2}{2}\delta\tilde{u}(k,t), \qquad \partial_t \delta\tilde{T}(k,t) = -k^2\delta\tilde{T}(k,t). \tag{4.38}$$

Therefore, $\delta\tilde{u}$ is unstable for wave numbers that verify $\nu - 2k^2 > 0$. In the continuous variables we are using, the system size is 1, so that the minimum available wavenumber is $k_{min} = 2\pi$. Thus, there is no unstable mode for ν (lengths) below a certain threshold ν_c (L_c), with

$$\nu_c = 8\pi^2, \qquad L_c = 2\pi\sqrt{2}\left(1-\alpha^2\right)^{-1/2}. \tag{4.39}$$

On the contrary, for $\nu > \nu_c$ ($L > L_c$), the HCS is unstable and the rescaled modes with wave numbers verifying $k < \sqrt{\nu/2}$ amplify with time. This instability mechanism is identical to the one found in granular gases for shear modes and described in Sec. 3.1.2. Theoretical predictions and simulations results perfectly agree, as plotted in Fig. 4.2. It is important to stress that the amplification appears in the rescaled velocity $\tilde{u}(x,t)$ and not in the velocity $u(x,t)$. The same result is found and compares well with simulations in the HS case. Numerical analysis of the HCS instability and the existence of a critical dissipation (length) ν_c (L_c) will be carried out in Sec. 4.5.

The one-particle velocity distribution has been derived; although of course $p(v) \to \delta(v)$ because of the cooling, when looking at rescaled variables it has been found that the shape of the initial distribution is not altered in the HCS: it only "shrinks" with the thermal velocity [133].

Perturbation of the HCS: Non-homogeneous cooling

The average hydrodynamic equations (4.34) are non-linear, but for the MM case we are considering they can be solved for general periodic initial conditions $u(x,0)$ and $T(x,0)$: the evolution of the velocity profile $u(x,t)$ is decoupled from the evolution of the temperature profile $T(x,t)$ and then $u(x,t)$ can be readily obtained. Afterwards, the evolution equation for $T(x,t)$ can be integrated, with the non-linear viscous heating term $(\partial_x u)^2$ playing the role of a inhomogeneity. Going to Fourier space, it is easily shown that

$$u(x,t) = \sum_{n=-\infty}^{+\infty} e^{-n^2\nu_c t/2} e^{ik_n x}\hat{u}(k_n,0), \tag{4.40}$$

being $\hat{u}(k,0)$ the Fourier-transform of the velocity at the initial time, and $k_n = 2\pi n$. This general results shows that the damping coefficient of the n-th shear mode is $\nu_c n^2/2$; therefore, the slowest decaying mode is the first mode $n = 1$, which yields the instability of the HCS for $\nu > \nu_c$. Note that $\hat{u}(k_0,0) = 0$, since in the center-of-mass frame we have that $\int_0^1 dx u(x,0) = 0$ and total momentum is conserved for periodic boundary conditions.

To be concrete, now we consider an initial perturbation that only excites one Fourier mode in the velocity field, whereas the temperature remains homogeneous. We derive the general solution for an arbitrary initial perturbation later in section 4.3.2. Thus,

$$u(x,0) = u_0 \sin(2\pi m\, x), \qquad T(x,0) = T_0. \tag{4.41}$$

being m an integer number. Then, on the one hand the velocity profile can be immediately written by making use of (4.40) and, on the other, the viscous heating term $(\partial_x u)^2$ gives rise to two Fourier modes in the evolution of the temperature, corresponding to $n = 2m$ and $n = 0$. Namely, we have

$$u(x,t) = e^{-m^2\nu_c t/2} u_0 \sin(2\pi m\, x), \tag{4.42a}$$

$$T(x,t) = T_0 e^{-\nu t} + e^{-m^2\nu_c t}\frac{u_0^2}{2} m^2\nu_c \times \left[\frac{1-e^{-(\nu-m^2\nu_c)t}}{\nu - m^2\nu_c} + \cos(4\pi m\, x)\frac{1-e^{-(\nu+m^2\nu_c)t}}{\nu + m^2\nu_c}\right]. \tag{4.42b}$$

The presence of a velocity gradient induces the development of a non-homogeneous temperature profile, through the local mechanism of viscous heating.

4.3.2 The Uniform Shear Flow steady state

Here we consider that our system is sheared at the boundaries: we impose a velocity difference a (shear rate) between the velocities at the left and right ends of the system. This is done by considering the Lees-Edwards boundary conditions [124]

$$u(1,t) - u(0,t) = a,\ u'(1,t) = u'(0,t),\ T(0,t) = T(1,t),\ T'(0,t) = T'(1,t), \tag{4.43}$$

in which the prime stands for the spatial derivative ∂_x.

With the above conditions, there is a steady solution of the hydrodynamic equations (4.34) characterized by a linear velocity profile and a homogeneous temperature:

$$u_s(x) = a(x - 1/2), \quad T_s = 2a^2/\nu. \tag{4.44}$$

This steady state is called Uniform Shear Flow and it is peculiar of dissipative systems, in which the continuous energy loss in collisions may compensate the viscous heating.

The USF state is expected to be globally stable, in the sense that the system tends to it from any initial condition compatible with the Lees-Edwards boundary conditions. This stems from the energy injection allowing the system to fully explore its phase space, which entails that the H-theorem for the master equation holds [103, 139, 60]. Therefore, the N-particle distribution $P_N(\mathbf{v}; x, t)$ approaches the steady solution of the master equation $P_N^{(s)}(\mathbf{v}; x)$ corresponding to the USF monotonically as time increases.

Contrarily from the HCS, where the initial shape of the rescaled velocity distribution was conserved in time, the velocity distribution of the USF tends to a Gaussian stationary distribution with average local velocity $u_s(x)$ and homogeneous temperature T_s [133]. In a recent paper, Plata and Prados showed that in the

USF the one-particle velocity distribution follows an H-theorem under some mathematical assumptions, which can be generalized to the bulk driven case [156].

Transient evolution towards the USF

In this section, we consider the hydrodynamic equations (4.34) with the Lees-Edwards boundary conditions (4.43), and look for the general time-dependent solution thereof.

To start with, we consider the deviations of the average velocity and temperature with respect to their USF values, by introducing

$$\delta u(x,t) = u(x,t) - u_s(x), \quad \delta T(x,t) = T(x,t) - T_s. \tag{4.45}$$

The Lees-Edwards boundary conditions for (u, T) are changed into periodic boundary conditions for $(\delta u, \delta T)$. The latter satisfy the equations

$$\partial_t \delta u = \partial_{xx}\delta u, \quad \partial_t \delta T = -\nu \delta T + \partial_{xx}\delta T + 4a\partial_x \delta u + 2(\partial_x \delta u)^2. \tag{4.46}$$

Since no linearization has been done when deriving the above equations from (4.34), they exactly describe the approach of the system to the USF state. Note that if we set $a = 0$ in (4.46), we reobtain the exact evolution equations for the deviations from the HCS. Therefore, the general solution for the hydrodynamic fields in the HCS correspond to putting $a = 0$ in the expressions derived below. Now, we go to Fourier space by defining

$$\delta u(x,t) = \sum_{n=-\infty}^{+\infty} \hat{u}(k_n,t) e^{ik_n x}, \quad \delta T(x,t) = \sum_{n=-\infty}^{+\infty} \hat{T}(k_n,t) e^{ik_n x}. \tag{4.47}$$

The initial values for the Fourier components $(\hat{u}, \hat{T})$ are given by

$$\hat{u}(k_n,0) = \int_0^1 dx\, \delta u(x,0) e^{-ik_n x}, \quad \hat{T}(k_n,0) = \int_0^1 dx\, \delta T(x,0) e^{-ik_n x}. \tag{4.48}$$

Recall that (i) $k_n = 2n\pi$ and (ii) $\hat{u}(k_0,t) = 0$ in the centre of mass frame.

The quadratic term in (4.46) that stems from viscous heating couples different Fourier modes. More specifically, the evolution equations in Fourier space read

$$\partial_t \hat{u}(k_n,t) = -k_n^2 \hat{u}(k_n,t), \tag{4.49a}$$

$$\partial_t \hat{T}(k_n,t) = -(\nu + k_n^2)\hat{T}(k_n,t) + 4iak_n \hat{u}(k_n,t) + \sum_{m=-\infty}^{+\infty} k_m(k_m - k_n)\hat{u}(k_m,t)\hat{u}^*(k_m - k_n,t). \tag{4.49b}$$

The solution of the equation for $\hat{u}(k_n,t)$ can be written straight away; afterwards, this solution is inserted into the equation for $\hat{T}(k_n,t)$ that is thus transformed into a closed non-homogeneous linear equation. Hence, we get

$$\hat{u}(k_n,t) = \hat{u}(k_n,0) e^{-k_n^2 t}, \tag{4.50a}$$

$$\hat{T}(k_n,t) = \hat{T}(k_n,0) e^{-(\nu+k_n^2)t} + 4iak_n \hat{u}(k_n,0) e^{-k_n^2 t} \frac{1 - e^{-\nu t}}{\nu} + 2e^{-k_n^2 t} \sum_{m=-\infty}^{+\infty} k_m(k_m - k_n)\hat{u}(k_m,0)\hat{u}^*(k_m - k_n,0) \frac{e^{-\nu t} - e^{-2k_m(k_m-k_n)t}}{2k_m(k_m - k_n) - \nu}. \tag{4.50b}$$

Note that there are no unstable modes in the USF of our model: when the denominators in (4.50) are zero, the numerators also vanish and the corresponding fractions remain finite. This is consistent with the (linear) stability of the USF state of a dilute granular gas of hard spheres described by the Boltzmann equation with respect to perturbations in the velocity gradient (the only possible ones in our model) [81]. Nevertheless, here the analysis is not restricted to small perturbations, at the level of the hydrodynamic equations the USF is globally stable.

4.3.3 The Couette Flow steady state

As introduced in Sec. 4.2.2, equation (4.34) yields a steady state solution when the system is coupled to reservoirs at its boundaries, e.g. when at sites 0 (L) and $N+1$ (R) we have two particles with independent normal velocity distributions, with average $u_{L/R}$ and variance $T_{L/R}$. Thus the system is no longer periodic, there are $L = N+1$ colliding pairs and the boundary conditions for the mesoscopic fields read $u(0) = u_L$, $u(1) = u_R$, $T(0) = T_L$ and $T(1) = T_R$. It must be stressed that momentum is no longer conserved for this choice of boundary conditions, since in general $u'(1,t) \neq u'(0,t)$.

The stationary solution for hydrodynamic equations (4.34), setting symmetric conditions

$$T_R = T_L = T_B, \qquad u_R = -u_L = a/2, \tag{4.51}$$

is

$$u(x) = a\left(x - \frac{1}{2}\right), \quad T(x) = \frac{2a^2}{\nu} + \left(T_B - \frac{2a^2}{\nu}\right)\frac{\cosh\left[\sqrt{\nu}\,(x-1/2)\right]}{\cosh\left(\sqrt{\nu}/2\right)}. \tag{4.52}$$

Here, we have put ourselves in the centre of mass frame by considering that $u_R = -u_L$, and we see that when $T_B = 2a^2/\nu$ the USF state described in section 4.3.2 is recovered. On the other hand, when $T_B \neq 2a^2/\nu$, the average velocity profile remains linear but the temperature develops a gradient, because the viscous heating that stems from the velocity gradient is not *locally* compensated by the energy sink, which is proportional to the temperature. In other words, when $T_B = 2a^2/\nu$, the velocity gradient a is exactly the one needed to satisfy (4.34) with an homogeneous temperature throughout the system. Otherwise, if the velocity gradient is smaller, the bulk temperature will be lower than that at the boundaries, and vice versa when the velocity gradient is steeper.

These results satisfy the energy balance (4.32b) required to have a stationary state, namely

$$J_{\text{av}}(x=0) - J_{\text{av}}(x=1) = \nu \int_0^1 \mathrm{d}x\, T(x) \tag{4.53}$$

where the lhs is the energy flow entering the system at the boundaries and the rhs is the energy loss in collisions.

The one-particle distribution function is not Gaussian in this steady state, except in the case $T_B = 2a^2/\nu$ for which we recover the USF. This can be readily seen by taking into account the time evolution of higher-order-than-two central moments of the velocity, the evolution of which is governed by (4.36). In the Couette case, we have Gaussian distributions at the boundaries and the appropriate

boundary conditions are $\mu_3(0,t) = \mu_3(1,t) = 0$, $\mu_4(0,t) = \mu_4(1,t) = 3T_B^2$. Equation (4.36a) shows clearly the point: if the term $\partial_x u\, \partial_x T \neq 0$, the third central moment μ_3 cannot be identically zero in the steady state and the one-particle distribution is non-Gaussian.

Therefore, the only steady state with a Gaussian probability distribution in the present model is the USF. We recall that the HCS is not a steady state, although the probability distribution for the rescaled velocity is a time-independent Gaussian if it starts from a Gaussian shape. We do not write down the theoretical expressions for μ_3 and μ_4 in Couette's steady state because they are not particularly illuminating.

4.3.4 Validity of the hydrodynamic description

There are some analogies between our expansion in terms of L^{-1} and the Chapman-Enskog expansion of the Boltzmann equation. In both cases, terms up to the second order in the gradients (of the order of k^2, being k the wave vector, in Fourier space) are kept. On the one hand, and from a purely mathematical point of view, in our model (4.34) becomes exact in the limit $L \to \infty$, but $\nu = (1-\alpha^2)L^2$ of the order of unity, as previously stated. On the other hand, on a physical basis, the hydrodynamic equations are approximately valid whenever the terms omitted upon writing them are negligible against the ones we have kept.

Following the discussion in the preceding paragraph, we must impose that $L \gg 1$. Moreover, we have also to impose that $t \ll L$ in order to have an approximate hydrodynamic description, which stems from the correlations $\langle v_i v_{i\pm1}\rangle$ being of the order of L^{-1} as compared to the granular temperature, see Sec. 5.1. For example, in the elastic case at equilibrium, the correlations $\langle v_i v_{i+k}\rangle$ do not depend on the distance k, and therefore $\langle v_i v_{i+k}\rangle = -T(L-1)^{-1}$, $\forall k \neq 0$. More specifically, the term proportional to the correlations in the evolution equation for the granular temperature over the microscopic time scale τ is of the order of $(1-\alpha^2)L^{-1}$, which must also be negligible against the second spatial derivative terms, of the order of L^{-2}. Then, $(1-\alpha^2)L \ll 1$ must be further imposed when the correlations are neglected in Equations (4.34). This condition, although less restrictive that $1-\alpha^2 = O(L^{-2})$, also implies that the microscopic dynamics is quasi-elastic. In Chapter 5 we discuss how to relax these conditions and take into account spatial correlations in the system.

4.4 Fluctuating hydrodynamics

4.4.1 Definition of fluctuating currents

The size of granular systems is limited both in real experiments and in numerical or theoretical studies, as discussed before, particularly when the instability of the HCS was analysed in section 4.3.1. Therefore, it is important to investigate finite size effects and the first way to take into account such effects is to develop a fluctuating hydrodynamic description, as introduced in Sec. 3.2: the microscopic currents are split in two terms, their "main" contribution that depends only on the hydrodynamic variables, and their corresponding "noises", with zero average.

The main physical idea under the fluctuating hydrodynamics approach is to calculate the averages that lead from the microscopic dynamics to the hydrodynamic equations in two steps. First, the average over the "fast" variables (namely y_p) is taken, conditioned to given values of the hydrodynamic fields. This defines the "main" contribution to the current, which is still a function of the "slow" hydrodynamic variables. The difference between the microscopic current and its main contribution is the noise of the current, which by definition has zero average: it is clear that the average value of the microscopic current (both over the "fast" and "slow" variables) coincides with the average of the main contribution (only over the "slow" variables). Specifically, each physical magnitude is written as $x = \overline{x} + \xi^{(x)}$, where $\overline{x}$ is its main contribution and $\xi^{(x)}$ is its noise.

Following the above discussion we start by splitting the microscopic currents in their main parts and their noises, namely

$$j_{l,p} = \overline{j}_{l,p} + \xi^{(j)}_{l,p}, \quad J_{l,p} = \overline{J}_{l,p} + \xi^{(J)}_{l,p}, \quad d_{l,p} = \overline{d}_{l,p} + \xi^{(d)}_{l,p}. \tag{4.54}$$

As stated above, overlined variables correspond to partial averages over the fast variables $y_{l,p}$ conditioned to given values of the slow ones $v_{l,p}$. We are considering the particular case of MM, that is, $\beta = 0$. Consequently,

$$\overline{j}_{l,p} = \frac{1+\alpha}{2L}\Delta_{l,p}, \tag{4.55a}$$

$$\overline{J}_{l,p} = \frac{1+\alpha}{2L}\Delta_{l,p}(v_{l,p} + v_{l+1,p}) \tag{4.55b}$$

$$\overline{d}_{l,p} = \frac{\alpha^2-1}{4L}(\Delta^2_{l,p} + \Delta^2_{l-1,p}). \tag{4.55c}$$

It is clear that such choices guarantee that all noises $\xi^{(j)}$, $\xi^{(J)}$ and $\xi^{(d)}$ have zero average.

4.4.2 Noise correlations

Noise correlations: momentum current

We start by studying the properties of the current noise correlation function $\xi^{(j)}_{l,p} = j_{l,p} - \overline{j}_{l,p}$, namely the moment $\langle \xi^{(j)}_{l,p}\xi^{(j)}_{l',p'}\rangle$, which reads

$$\langle \xi^{(j)}_{l,p}\xi^{(j)}_{l',p'}\rangle = \langle j_{l,p}j_{l',p'}\rangle - \langle \overline{j}_{l,p}\overline{j}_{l',p'}\rangle. \tag{4.56}$$

In order to obtain the noise correlations, we exploit a series of conditions. First, it is straightforward that $\langle \xi^{(j)}_{l,p}\xi^{(j)}_{l',p'}\rangle = 0$ for $p \neq p'$, because y_p and $y_{p'}$ are independent random numbers. For equal times, $p = p'$, the second term on the right hand of (4.56) is negligible because it is $O(L^{-2})$, while the leading behavior of the first term will be shown to be $O(L^{-1})$. Using now the definition (4.16) of the microscopic momentum current, we get

$$j_{l,p}j_{l',p'} = \frac{(1+\alpha)^2}{4}\Delta_{l,p}\delta_{y_p,l}\Delta_{l',p'}\delta_{y'_p,l'}. \tag{4.57}$$

Second, we take into account, setting again $\beta = 0$, that $\langle \delta_{y_p,l} \delta_{y_p,l'} \rangle = \delta_{l,l'} \langle \delta_{y_p,l} \rangle = L^{-1} \delta_{l,l'}$. Thus, for $p = p'$, we have

$$\langle \xi^{(j)}_{l,p} \xi^{(j)}_{l',p} \rangle = \frac{(1+\alpha)^2}{4L} \left\langle \Delta^2_{l,p} \right\rangle \delta_{l,l'} + O(L^{-2}). \tag{4.58}$$

At this point, we can make use of (i) the quasi-elasticity of the microscopic dynamics to substitute $(1+\alpha)/2$ by 1 (neglecting terms of order L^{-2}) and (ii) the molecular chaos assumption to obtain $\langle \Delta^2_{l,p} \rangle$, with the result

$$\langle \Delta^2_{l,p} \rangle = T_{l,p} + T_{l+1,p} + (u_{l,p} - u_{l+1,p})^2 + O(L^{-1}) \sim 2T_{l,p}, \tag{4.59}$$

because both $u_{l+1,p} - u_{l,p}$ and $T_{l+1,p} - T_{l,p}$ are of the order of L^{-1}. Therefore,

$$\langle \xi^{(j)}_{l,p} \xi^{(j)}_{l',p'} \rangle \sim 2L^{-1} T_{l,p}\, \delta_{l,l'}\, \delta_{p,p'}. \tag{4.60}$$

In the large size system, $j_{l,p}$ scales as L^{-2}, as given by (4.30) (an analogous scaling has been found in other simple dissipative models, see [162]). Therefore, the mesoscopic noise of the momentum current is defined as

$$\xi^{(j)}(x,t) = \lim_{L\to\infty} L^2 \xi_{l,p}, \quad j(x,t) = \overline{j}(x,t) + \xi^{(j)}(x,t) \tag{4.61}$$

in which, again, $\overline{j}(x,t) = \lim_{L\to\infty} L^2 \overline{j}_{l,p}$. Going to the continuous limit and remembering (4.25), which implies that $\delta_{l,l'}/\Delta x \sim \delta(x-x')$ and $\delta_{p,p'}/\Delta t \sim \delta(t-t')$, we derive the noise amplitude of the momentum current as

$$\langle \xi^{(j)}(x,t) \xi^{(j)}(x',t') \rangle \sim 2L^{-1}\, T(x,t)\, \delta(x-x') \delta(t-t'). \tag{4.62}$$

Noise correlations: energy current

As in the previous subsection, we start with (4.54). Again in this case we are interested in the correlation properties of the noise $\xi^{(J)}_{l,p} = J_{l,p} - \overline{J}_{l,p}$

$$\langle \xi^{(J)}_{l,p} \xi^{(J)}_{l',p'} \rangle = \langle J_{l,p} J_{l',p'} \rangle - \langle \overline{J}_{l,p} \overline{J}_{l',p'} \rangle. \tag{4.63}$$

Similarly to the case of the current noise, we have that (i) $\langle \xi^{(J)}_{l,p} \xi^{(J)}_{l',p'} \rangle = 0$ for $p \neq p'$, (ii) the second term on the right-hand side is $O(L^{-2})$ and thus subdominant in the limit $L \to \infty$ and (iii) the noise correlation is dominated by the contribution that stems from the first term on the rhs. Therefore, making use of (4.18), and again of the relation (for $\beta = 0$) $\langle \delta_{y_p,l} \delta_{y_p,l'} \rangle = \delta_{l,l'} \langle \delta_{y_p,l} \rangle = \frac{\delta_{l,l'}}{L}$, we obtain

$$\langle \xi^{(J)}_{l,p} \xi^{(J)}_{l',p'} \rangle \sim L^{-1} \left\langle \left(v^2_{l,p} - v^2_{l+1,p} \right)^2 \right\rangle \delta_{l,l'} \delta_{p,p'}. \tag{4.64}$$

In general, the moment $\left\langle \left(v^2_{l,p} - v^2_{l+1,p} \right)^2 \right\rangle$ is not a function of the hydrodynamic variables u and T, unless the one-particle distribution is Gaussian.

In order to obtain a closed fluctuating hydrodynamic description, we need to write $\langle (v^2_{l,p} - v^2_{l+1,p})^2 \rangle$ in terms of the hydrodynamic variables. Then, on top of the

molecular chaos assumption (factorization of the moments involving several sites), we introduce the so-called local equilibrium approximation (LEA): the one-particle distribution function P_1 is assumed to be the equilibrium distribution corresponding to the local values of the hydrodynamic variables, which in our case corresponds to a Gaussian distribution of the velocities. There is strong numerical evidence that the LEA gives a good quantitative description of the noise amplitudes in some dissipative models without momentum conservation [161, 162, 96, 121], as a consequence of the quasi-elasticity of the underlying microscopic dynamics. In our model, we know that the LEA is not an approximation but an exact result for some physical states, such as the HCS [1] or the USF. For other states like the Couette flow, it still remains an approximation, whose range of validity is a priori not known.

In the large system size limit, $J_{l,p}$ scales as L^{-2} and it is expected that the noise does too. Along the same lines as in the preceding section, after using the LEA and neglecting terms of the order of L^{-2}, we obtain the autocorrelation of the energy current noise,

$$\langle \xi^{(J)}(x,t)\xi^{(J)}(x',t')\rangle \sim 4L^{-1}T(x,t)[T(x,t)+2u^2(x,t)]\delta(x-x')\delta(t-t'). \quad (4.65)$$

Thus, the energy current noise is also white and its amplitude scales as L^{-1} with the system size L, accordingly with the physical intuition.

Noise correlations: dissipation field

Now we deal with the third "current" in the system, the dissipation field $d_{l,p}$ by repeating the same procedure as before. We are interested in the correlation properties of the noise $\xi^{(d)}_{l,p} = d_{l,p} - \overline{d}_{l,p}$.

Once more, $\langle \xi^{(d)}_{l,p}\xi^{(d)}_{l',p'}\rangle = 0$ for $p \neq p'$ and the dominant contribution for $p = p'$ comes from the dissipation correlation $\langle d_{l,p}d_{l',p}\rangle$. Making use of the definition of (4.19),

$$\begin{aligned}\langle d_{l,p}d_{l',p}\rangle &= \frac{(\alpha^2-1)^2}{16L}\Big[\delta_{l,l'}\langle (v_{l,p}-v_{l+1,p})^4+(v_{l-1,p}-v_{l,p})^4\rangle + \\ &\quad \delta_{l,l'-1}\langle (v_{l,p}-v_{l+1,p})^4\rangle + \delta_{l,l'+1}\langle (v_{l-1,p}-v_{l,p})^4\rangle\Big]. \quad (4.66)\end{aligned}$$

Therefore, by taking into account the LEA and neglecting $O(L^{-2})$ terms,

$$\langle \xi^{(d)}_{l,p}\xi^{(d)}_{l',p'}\rangle \sim \frac{3(\alpha^2-1)^2}{4L}T^2_{l,p}[2\delta_{l,l'}+\delta_{l,l'-1}+\delta_{l,l'+1}]\delta_{p,p'}. \quad (4.67)$$

In the large size system $d_{l,p}$ scales as L^{-3} and we expect the same scaling for the noise. Going to the continuous limit, we get

$$\langle \xi^{(d)}(x,t)\xi^{(d)}(x',t')\rangle \sim L^{-3}\,3\nu^2T(x,t)^2\delta(x-x')\delta(t-t'). \quad (4.68)$$

In summary, the noise of the dissipation is subdominant with respect to the moment and energy currents, its amplitude being proportional to L^{-3}, and therefore it is usually negligible.

[1] For the usual choice of an initial Gaussian distribution, see Sec. 4.3.1

4.4.3 Cross-correlations of the noises and Gaussianity

Interestingly, being in the presence of two fluctuating fields, correlations between different noises appear. The cross correlations between different noises are straightforwardly obtained, along similar lines:

$$\begin{aligned}\langle \xi^{(j)}(x,t)\xi^{(J)}(x',t')\rangle &= 4L^{-1}T(x,t)u(x,t)\delta(x-x')\delta(t-t'), \\ \langle \xi^{(j)}(x,t)\xi^{(d)}(x',t')\rangle &= 0, \quad \langle \xi^{(J)}(x,t)\xi^{(d)}(x',t')\rangle = 0,\end{aligned} \tag{4.69}$$

up to and including $O(L^{-1})$. Theoretical predictions for noise correlations, amplitudes and Gaussianity have been successfully tested in simulations, see section 4.5.

In the large system size limit $L \gg 1$, the current noise introduced in the subsection (4.4.1) is white. We can introduce a new noise field $\tilde{\xi}(x,t)$ by

$$\xi^{(j)}(x,t) = L^{-1/2}\tilde{\xi}(x,t) \tag{4.70}$$

and $\tilde{\xi}(x,t)$ remains finite in the large system size limit $L \to \infty$,

$$\langle \tilde{\xi}(x,t)\rangle = 0, \qquad \langle \tilde{\xi}(x,t)\tilde{\xi}(x',t')\rangle \sim 2\,T(x,t)\delta(x-x')\delta(t-t'). \tag{4.71}$$

Here we show that all the higher-order cumulants of $\tilde{\xi}(x,t)$ vanish in the thermodynamic limit as $L \to \infty$. Let us consider a cumulant of order n of the microscopic noise $\xi_{l,p}$ that is equal to the n-th order moment of the ξ plus a sum of nonlinear products of lower moments of ξ. A calculation analogous to the one carried out for the correlation $\langle \xi^{(j)}_{l,p}\xi^{(j)}_{l',p'}\rangle$ shows that the leading behavior of any moment is of the order of L^{-1}, which is obtained when all the times are the same. Therefore, the moment $\langle j_{l,p}j_{l',p'}...j_{l^{(n)},p^{(n)}}\rangle$ gives the leading behavior of the considered cumulant, which is thus of the order of L^{-1} for $p = p' = ... = p^{(n)}$; any other contribution to the cumulant is at least of the order of L^{-2}. We have that

$$\langle j_{l,p}j_{l',p'}\cdots j_{l^{(n)},p^{(n)}}\rangle \sim L^{-1}\langle C_{l,p}\rangle \delta_{l,l'}\delta_{l',l''}\delta_{l^{(n-1)},l^{(n)}}\cdots\delta_{p,p'}\delta_{p',p''}\delta_{p^{(n-1)},p^{(n)}}, \tag{4.72}$$

where $\langle C_{l,p}\rangle$ is certain average that remains finite in the large system size limit as $L \to \infty$. In the continuous limit, each current introduces a factor L^2 due to the scaling introduced in section 4.4. Moreover, we take into account the relationship between Kronecker and Dirac δ's in the continuum limit to write the cumulants $\langle\langle\cdots\rangle\rangle$ of the rescaled noise introduced in (4.70) as

$$\begin{aligned}\langle\langle \tilde{\xi}(x,t)\tilde{\xi}(x',t')\cdots\tilde{\xi}(x^{(n)},t^{(n)})\rangle\rangle &\sim L^{3\left(1-\frac{n}{2}\right)}\langle C(x,t)\rangle \times \\ &\delta(x-x')\delta(x'-x'')\delta(x^{(n-1)}-x^{(n)})\cdots\delta(t-t')\delta(t'-t'')\delta(t^{(n-1)}-t^{(n)}).\end{aligned} \tag{4.73}$$

Thus, in the limit as $L \to \infty$,

$$\langle \tilde{\xi}(x,t)\tilde{\xi}(x',t')\cdots\tilde{\xi}(x^{(n)},t^{(n)})\rangle = 0, \quad \text{for all } n > 2, \tag{4.74}$$

and the vanishing of all the cumulants for $n > 2$ means that the momentum current noise is Gaussian in the infinite size limit.

The same procedure can be repeated for the energy current noise, by defining $\xi^{(J)}(x,t) = L^{-1/2}\tilde{\eta}(x,t)$), with the result

$$\langle\langle\tilde{\eta}(x,t)\tilde{\eta}(x',t')\cdots\tilde{\eta}(x^{(n)},t^{(n)})\rangle\rangle \sim L^{3\left(1-\frac{n}{2}\right)}\langle D(x,t)\rangle \times \\ \delta(x-x')\delta(x'-x'')\delta(x^{(n-1)}-x^{(n)})\cdots\delta(t-t')\delta(t'-t'')\delta(t^{(n-1)}-t^{(n)}). \tag{4.75}$$

In the equation above, $\langle D(x,t)\rangle$ is a certain average, different from $\langle C(x,t)\rangle$, but also finite in the large system size limit. Thus, we have that

$$\langle\tilde{\eta}(x,t)\tilde{\eta}(x',t')\cdots\tilde{\eta}(x^n,t^n)\rangle = 0, \quad \text{for all } n>2, \tag{4.76}$$

and the energy current noise also becomes Gaussian in the continuum limit.

Note that the Gaussianity of the noises is independent of the validity of the local equilibrium approximation, which is only needed to write $\langle C(x,t)\rangle$ and $\langle D(x,t)\rangle$ in terms of the hydrodynamic fields $u(x,t)$ and $T(x,t)$. Besides, a similar procedure for the dissipation noise gives that the corresponding scaled noise vanishes in the continuum limit, since the power of L in the dominant contribution to the n-th order cumulant is $3-5n/2$ instead of $3-3n/2$. This means that the dissipation noise is subdominant as compared to the currents noises in the continuum limit, and can be neglected.

We conclude this section mentioning that, in general, our noise amplitudes do not seem to satisfy any "equilibrium-like" Fluctuation-Dissipation relation of the 2nd kind (see for instance [112]). This is however not surprising, considered that it is a non-conservative model.

4.5 Numerical results

4.5.1 General simulation strategy

Simulations have been made reproducing M times the phase-space trajectory of a system of N particles, each one carrying a velocity v_l and being at a definite position $l = 1,\ldots,L$, with $L = N$ for periodic or Lees-Edwards boundaries and $L = N+1$ for a thermostatted system. For each trajectory, the system starts with a random extraction of velocities v_l normally distributed with $\langle v_l\rangle = 0$ and $\langle v_l^2\rangle = T_0$, unless otherwise specified. Afterwards, we move to the centre of mass frame making the transformation $v_l \Rightarrow v_l' = v_l - \frac{1}{L}\sum_{l=1}^{L} v_l$, so that the total momentum of the system is zero.

We carry out Monte Carlo simulation of the system time-evolution through the residence time algorithm described in section 4.1.1 [27, 160]. This procedure allows us to compute the time-evolution of our model for every collision rate β, although we focus here only on the case $\beta = 0$ (MM).

4.5.2 Homogeneous and non-homogeneous cooling

Following the above-mentioned procedure, we have simulated the homogeneous cooling state described in section 4.3.1 a system made of 10^3 particles, with periodic

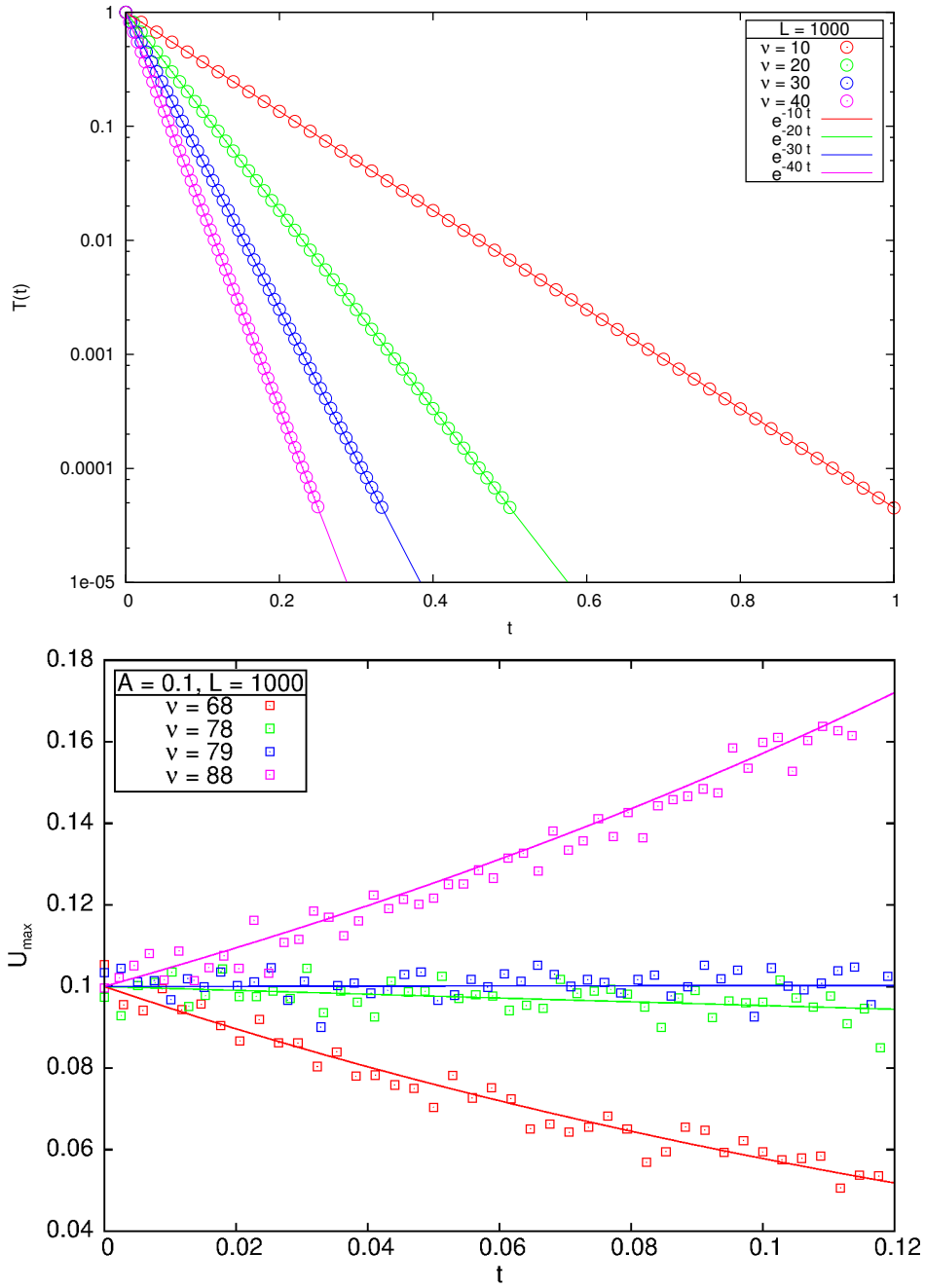

Figure 4.2. Top: Numerical results (circles) and theoretical predictions (lines) for HCS average temperature, $T(t) = \int \mathrm{d}x T(x,t)$, with $\nu = 10, 20, 30, 40$. and $N = 1000$. Bottom: Rescaled velocity profile maximum $U_{\max} = \tilde{u}(x_M, t)$ as a function of time, where $x_M = 1/4$. Trajectories start from a sinusoidal average velocity profile $u(x,0) = u_0 \sin(2\pi x)$ (here $u_0 = 0.1$), which gives hydrodynamic predictions $\tilde{u}(x,t) = u_0 \sin(2\pi x) e^{(\nu - \nu_c)t/2}$ (drawn as solid lines). The averages have been taken over $M = 10^5$ trajectories.

boundaries and starting from a flat velocity profile $u(x,0) \equiv 0$ with unit variance $T(x,0) \equiv T_0 = 1$. Theoretical predictions for average velocity and temperature de-

cay in (4.37) perfectly agree with simulations. The instability of the HCS has been investigated through the rescaled field of velocity for a perturbed initial condition

$$u(x,0) = A\sin(2\pi x) \tag{4.77}$$

introducing a small sinusoidal perturbation and measuring the time evolution of its rescaled amplitude $\tilde{u}$. Theory and simulations are compared in Fig. 4.2, where the existence of a threshold value of the dissipation around $\nu_c = 8\pi^2$ is evident. Also, we have performed simulations of non-homogeneous cooling, starting as in section 4.3.1 from a sinusoidal periodic average velocity profile $u(x,0) = u_0\sin(2\pi m x)$, with m integer, and a homogeneous temperature $T(x,0) = T_0 = 1$ as before. The simulations show the cooling of the system, as expected from (4.42), with the development of a temperature profile given by viscous heating. Comparisons between numerical results and theoretical predictions for the non-homogeneous case are displayed in figure 4.3.

4.5.3 Uniform Shear Flow state

The Uniform Shear Flow described in section 4.3.2 can be simulated by introducing appropriate boundary conditions in the simulations. When the pair $(1,N)$ is chosen to collide at time p, there are two separate collisions: particle 1 (N) undergoes a collision with a particle with velocity $v_{N,p} - a$ ($v_{1,p} + a$). These boundary collision rules introduce a shear rate a between the left and right ends of the system, and at the hydrodynamic level are represented by the Lees-Edwards conditions (4.43). This can be readily shown by considering the special evolution equations for $v_{1,p}$ and $v_{N,p}$ with the above boundary collision rules in the continuum limit.

We have tested our theoretical predictions in the USF state, given by (4.44), for the steady (i) profile of the average velocity and (ii) value of the temperature. We have done so in a system with $N = 500$ and three different values of ν, namely $\nu = 10$, 20 and 40. As seen in figure 4.4, the agreement is excellent in all cases.

Furthermore, in Figs. 4.5 and 4.6, we check the tendency of the hydrodynamic variables u and T towards their USF values, whose theory was developed in section 4.3.2. In both figures, we present the evolution of the velocity and temperature profiles towards its steady value from an initial state such that (i) $T(x,t=0) = T_0 = 1$ and (ii)

$$u(x,t=0) = u_s(x) + A\sin(2\pi x), \quad A = 1, \tag{4.78}$$

$$u(x,t=0) = u_s(x) + A\sin(2\pi x) + B\cos(2\pi x), \quad A = B = 1, \tag{4.79}$$

respectively. In both cases, there is only one Fourier mode: that corresponding to $n = 1$. However, an important physical difference should be stressed: the temperature profile is always horizontal at the boundaries in the left panel, but it is not in the right one. Therefore, there is heat flux at the system boundaries in the latter case but not in the former. Anyhow, the agreement between simulation and theory is excellent in both situations.

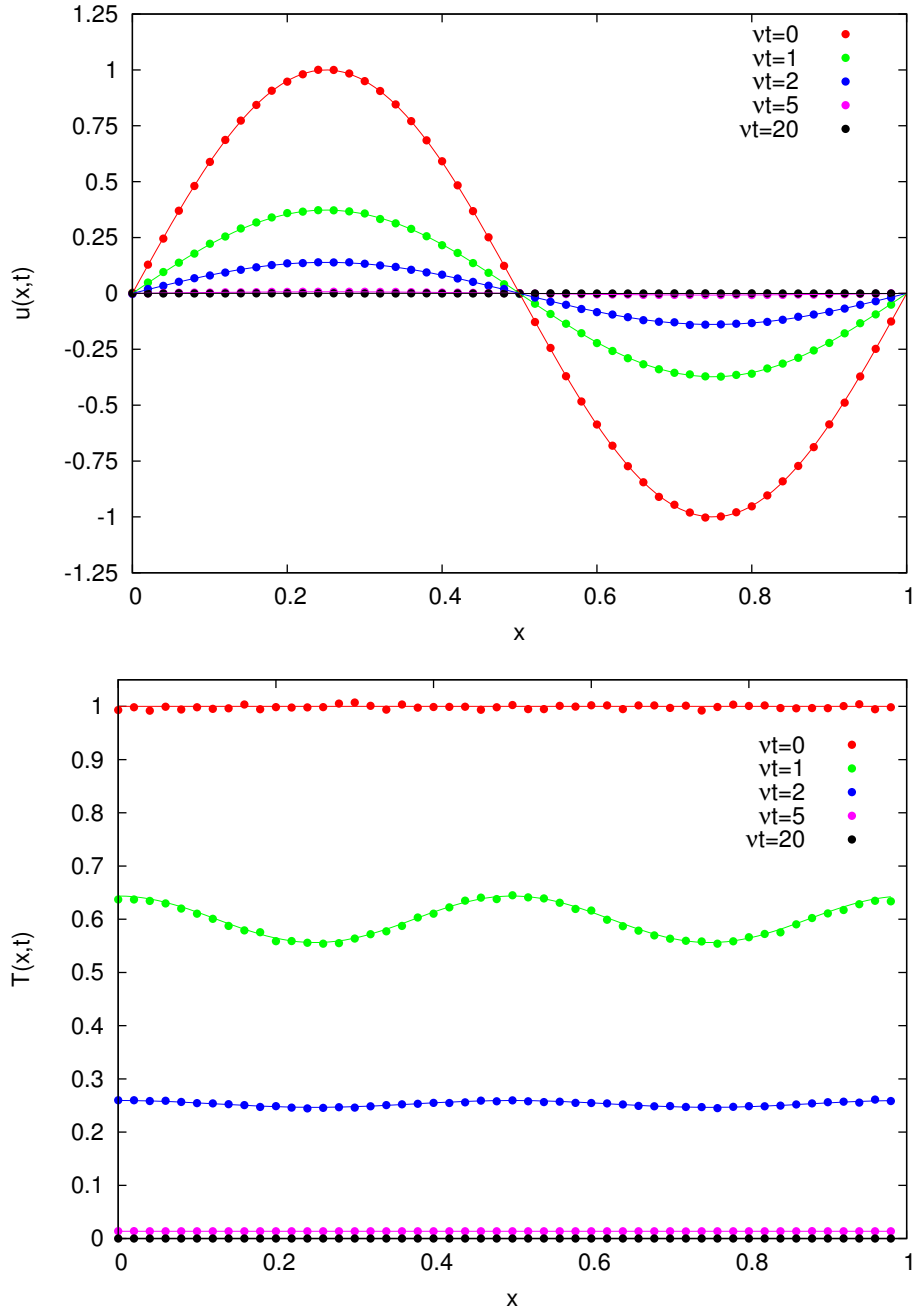

Figure 4.3. Top: Numerical results (points) and theoretical values (solid lines) for the average sinusoidal velocity profile $u(x,t)$, with $u_0 = 1$, $\nu = 40$, $N = 500$, $T_0 = 1$ and $m = 1$ for $\nu t = 0, 1, 2, 5, 20$. Bottom: Same plot for the temperature profile $T(x,t)$ of the system. Here, the averages have been taken over $M = 10^5$ trajectories.

4.5.4 The Couette flow state

Now we consider a system coupled to two reservoirs at both ends, as described in section 4.3.3. In the simulations, two "extra" sites 0 and $N + 1$ are introduced, so

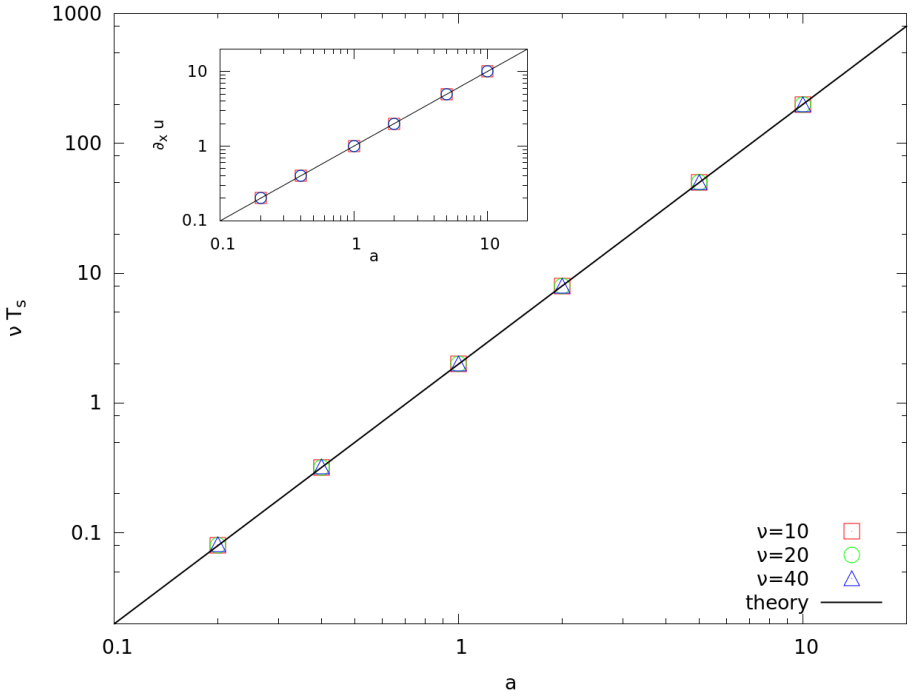

Figure 4.4. Steady temperature in the USF state as a function of the shear rate a. We consider three different values of ν in a system of size $N = 500$, with averages over $M = 10^5$ realizations. Specifically, we plot νT_s, the theoretical value of which is $2a^2$, as given by (4.44). In the inset, we show the numerical value of the velocity gradient $\partial_x u_s(x)$ as a function of the shear rate. Note the logarithmic scale in both axes.

that the number of colliding pairs is $L = N + 1$. When the pair to collide involves one boundary particle (that is, pairs $(0, 1)$ or $(N, N + 1)$), the same collision rule for the bulk pairs $(1, 2), \dots, (N - 1, N)$ is applied but the velocity of the "wall" particles is drawn from a Gaussian distribution with fixed average velocities $u_{L/R}$ and temperatures $T_{L/R}$. This is the only change in the simulations, which no longer correspond to periodic boundary conditions either in u or T. In particular, the non-periodicity of u' implies that momentum is not conserved in the time evolution of the system, conversely to the case of the HCS and USF states.

In figure 4.7, we report the comparison between simulations and theoretical predictions from (4.52), for different values of the parameter $g = 2a^2/(\nu T_B)$. The boundary conditions are chosen as $T_{L/R} = T_B = 1$, $u_R = -u_L = a/2$. It should be recalled that $g = 1$ corresponds to the case in which the Couette steady state coincides with the USF state and there is no heat current in the system. For $g > 1$ ($g < 1$), viscous heating is stronger (weaker) than that of the USF, and the steady temperature profile is concave (convex), that is, $T'' < 0$ ($T'' > 0$) and displays a maximum (minimum) at the centre of the system $x = 1/2$. Simulations start from a non-stationary profile, initial particle velocities are drawn from a Gaussian distribution with local average velocity $u(x, 0) = 0$ and temperature $T(x, 0) = 1$. An excellent agreement is found in all the cases.

Figure 4.8 depicts the third and fourth central moments of the one-particle ve-

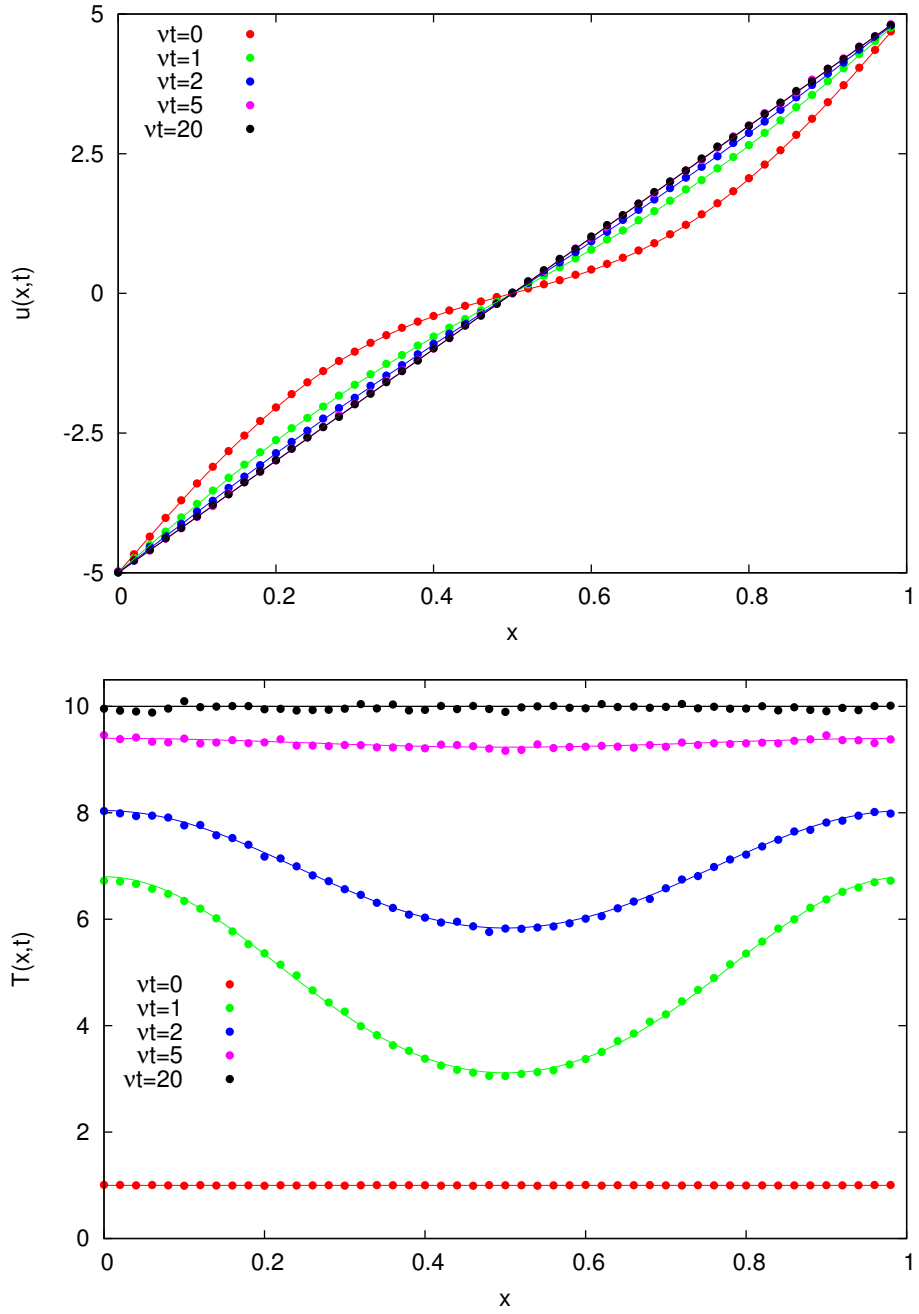

Figure 4.5. (Colour online) Transient evolution of the velocity (top) and the temperature (bottom) to their steady profiles in the USF state, for $a = 10$. The numerical curves are plotted with points, whereas the solid lines correspond to the theoretical expression (4.50). The agreement between simulation and theory is excellent in both cases. The system size is $N = 500$, the dissipation coefficient is $\nu = 20$, and the number of trajectories is $M = 10^5$. In this case, initial conditions correspond to 4.78, namely $A = 1$ and $B = 0$.

locity distribution, scaled with their corresponding powers of the temperature,

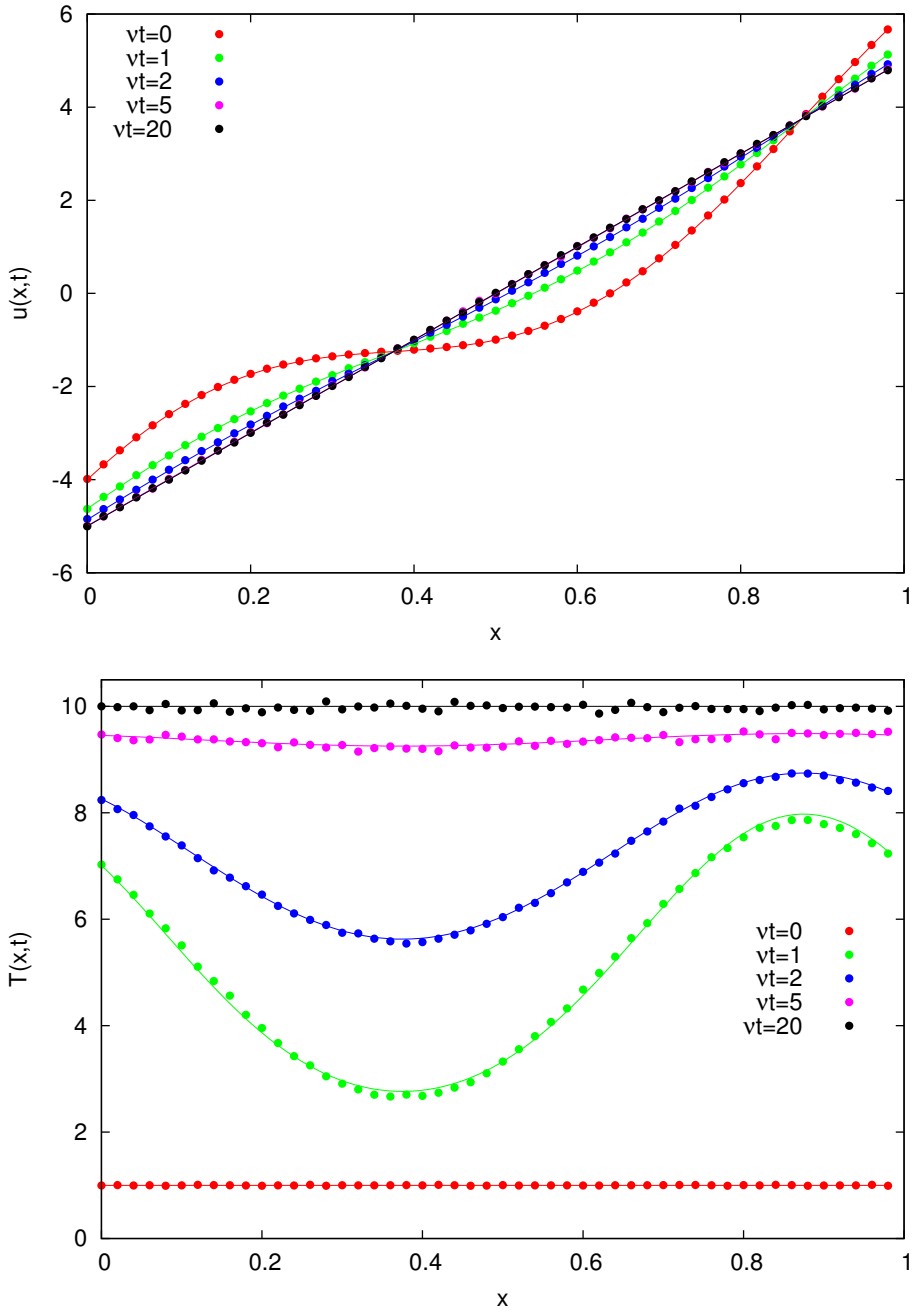

Figure 4.6. Same as in figure 4.5, but for initial conditions defined in (4.79), namely $A = B = 1$.

namely $\mu_3/T^{3/2}$ and μ_4/T^2. Both moments display a non-trivial structure. In particular, the non-vanishing third moment clearly shows that the one-particle distribution is not symmetric with respect to the average velocity u. It is evident that the distribution is non-Gaussian, except for the case $T_B = 2a^2/\nu$, which corresponds to the USF state.

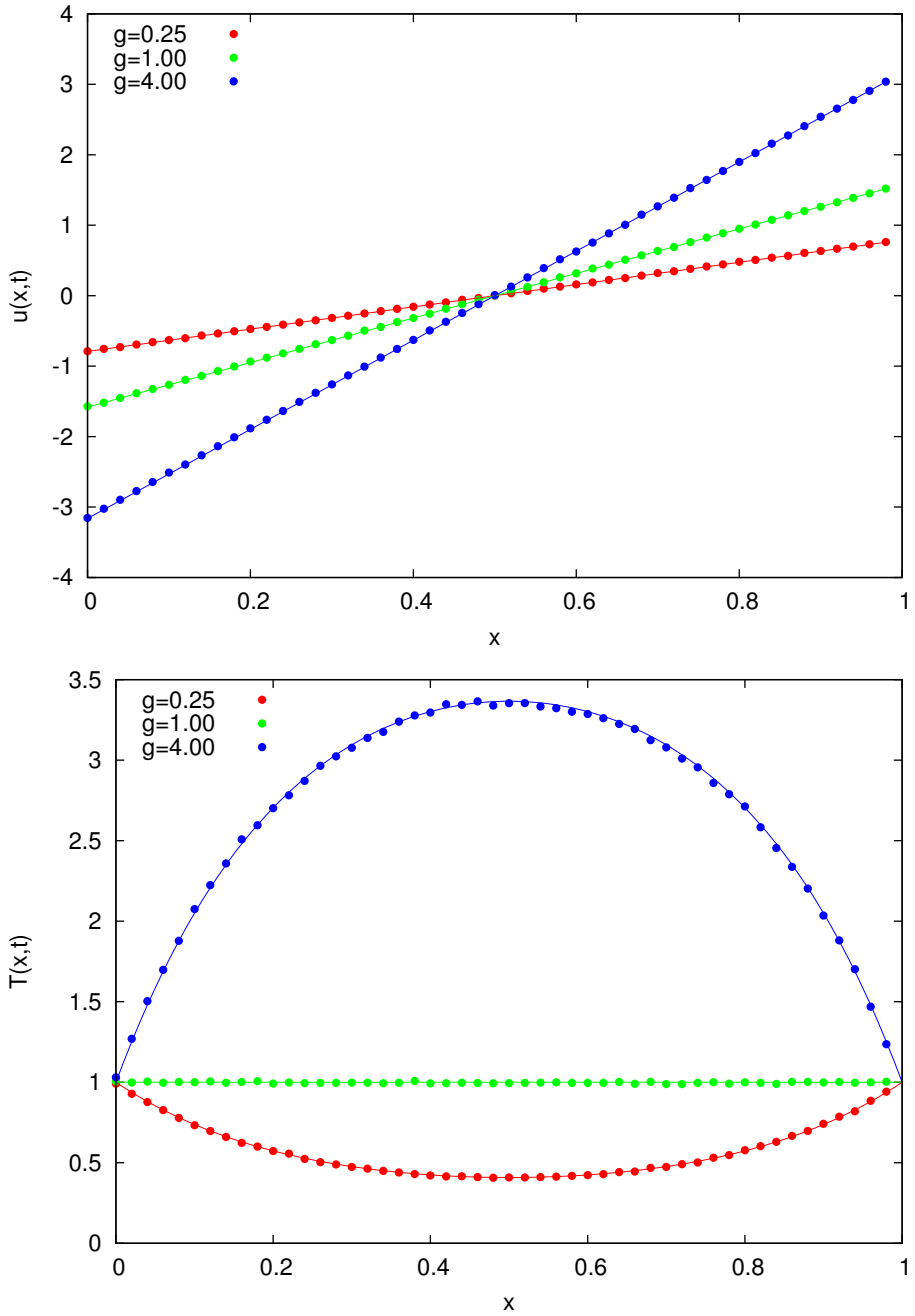

Figure 4.7. Numerical results (symbols) and theoretical values (solid lines) for the stationary velocity profile $u(x)$ (top) and the stationary temperature profile $T(x)$ (bottom) in the Couette state. The parameter values are $\nu = 20$, $N = 500$, $M = 10^5$, and we have considered several values of g. The profiles have been plotted at the final time $\nu t = 20$.

4.5.5 Fluctuating currents

A comparison for the amplitudes of noise for the velocity and energy currents is shown in Fig. 4.9. We carry it out in the USF state, in which the steady distribution

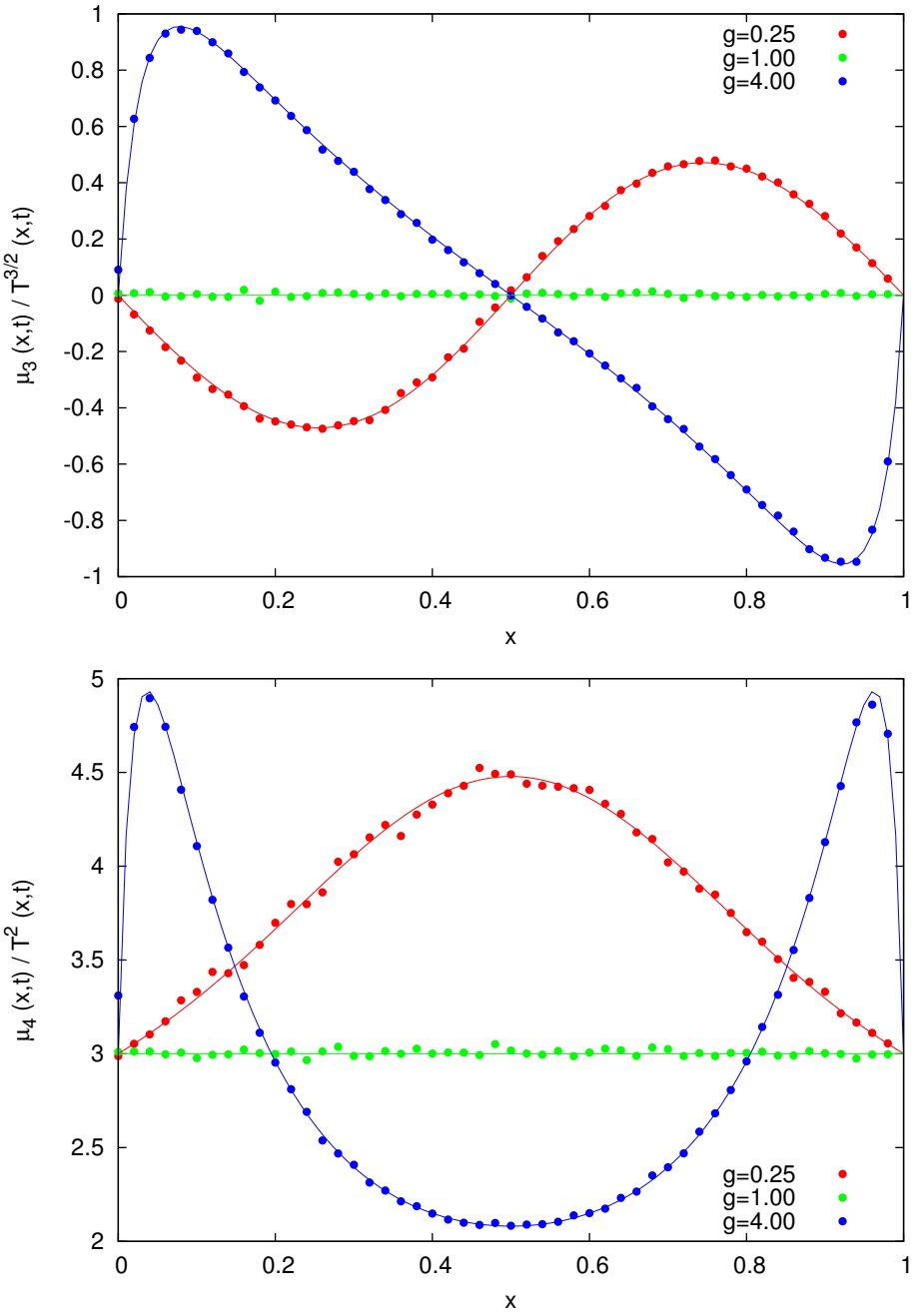

Figure 4.8. Third and fourth central moments μ_3 (top) and μ_4 (bottom) in the Couette steady state for the same simulation as in Fig. 4.7. Numerical results are shown with symbols whereas the lines stand for the theoretical prediction, i.e. the solutions of (4.36). We can see that, excluding the case $g = 1$, the one particle distribution is far from Gaussian in most of the spatial domain.

is Gaussian but the average velocity is not homogeneous. This allows us to make a more exigent test of the theoretical result for the amplitude of the energy current, as given by (4.65), which contains a term proportional to u^2. The agreement is

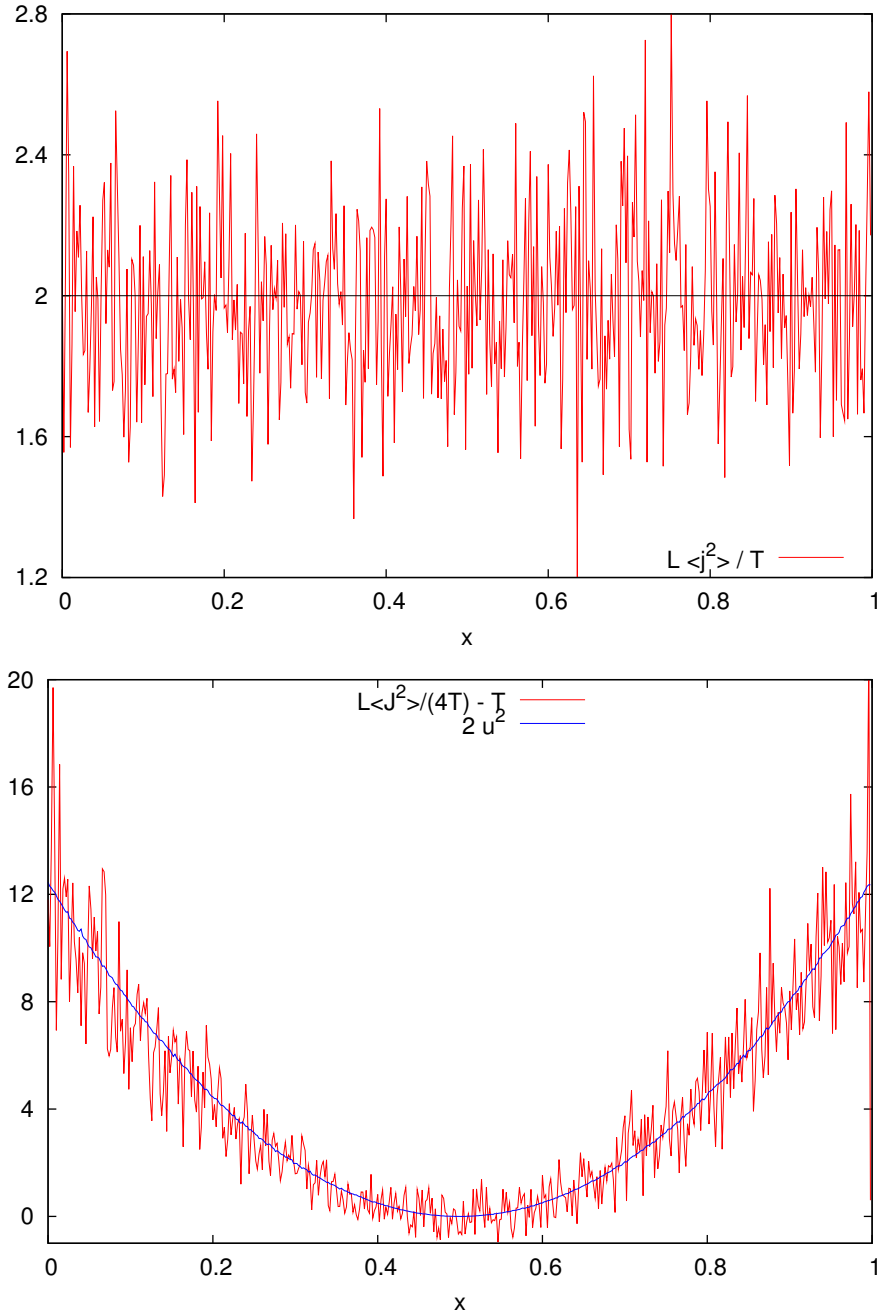

Figure 4.9. Top: Amplitude of the momentum current as a function of x in the USF state. Specifically, we plot the rescaled amplitude $L\langle j^2(x,t)\rangle/T_s$ in the simulations (red line) and the theoretical value 2 (black line). Bottom: Amplitude of the energy current as a function of x in the USF state. Here, we plot $L\langle J^2(x,t)\rangle/4T(x,t) - T(x,t)$ as measured in the simulations (red line) and the numerical value of $2u_s^2(x)$ (blue line). All the simulations have been done in a system with $N = 500$, $\nu = 20$, $a = 5$, and $M = 10^5$.

excellent for the amplitudes of both noises.

I'm looking for a complication
Looking cause I'm tired of trying
Make my way back home when I learn to fly high

5

Granular lattice: beyond Molecular Chaos

The hydrodynamic behavior derived in Chapter 4 and numerically analyzed in Sec. 4.5 has been obtained through the Molecular Chaos ansatz stated in (4.14), mathematically equivalent to the factorization of velocity correlations

$$\langle v_{l,p} v_{l',p} \rangle = \langle v_{l,p} \rangle \langle v_{l',p} \rangle \tag{5.1}$$

This approximation has been found acceptable when comparing the numerical data with the theoretical results. However, when looking at the time behavior of the rescaled temperature $\tilde{T}(t) = T(t)/T_{\text{HCS}}(t)$, this is found to diverge from the stationary solution $\tilde{T} = 1$ which is expected in the region of stability of the HCS, so Haff's law is violated as can be seen in Fig. 5.1. The main reason of this violation is the presence of velocity correlations between next-neighbor particles: in this section, we analyze the effect on the free cooling of the system introduced by the velocity correlations. Interestingly, for the case of Maxwell molecules we are considering in the paper, we can account for the effect of the correlations in the cooling of the system in quite a detailed way. It will be shown that long-range correlations arise in the system tending to a stationary value. A multiple scales analysis of temperature decay yields a "renormalized" mesoscopic dissipation coefficient ν^r, equivalent to ν in the limit $L \to \infty$. Finally, total energy rescaled fluctuations (expected to be stationary in the HCS) also have a divergent behavior in time: their time evolution is again derived from microscopic balance equations, showing the fact that two-particles energy correlations are not scaling with the square of the temperature and producing an increase of energy fluctuations with time. Numerical observations are shown together with analytical results.

5.1 Perturbative Solution for Temperature and Correlations

We assume that the system is in a spatial-translation-invariant state, such as the HCS. We define the set of spatial correlations of the velocity at time τ as

$$C_k(\tau) = \langle v_j(\tau) v_{j+k}(\tau) \rangle. \tag{5.2}$$

Here, k represents the distance between the involved sites in the correlation. Throughout this section, the microscopic *continuous* time τ will be used, being equivalent to the collisional discrete time p with $\langle \delta\tau_p \rangle = (\omega \Omega_p(L))^{-1}$, see Sec. 4.1.1. Note that the average temperature at any site j is given by C_0,

$$T(\tau) \equiv C_0(\tau) = \langle v_j^2(\tau) \rangle. \tag{5.3}$$

The evolution equations of these correlations are readily obtained from the Master Equation 4.10, namely

$$\omega^{-1}\partial_\tau C_0 = (\alpha^2 - 1)(C_0 - C_1), \tag{5.4a}$$

$$\omega^{-1}\partial_\tau C_1 = \frac{1-\alpha^2}{2}(C_0 - C_1) + (1+\alpha)(C_2 - C_1), \tag{5.4b}$$

$$\omega^{-1}\partial_\tau C_k = (1+\alpha)(C_{k+1} + C_{k-1} - 2C_k), \quad 2 \le k \le (L-1)/2, \tag{5.4c}$$

$$C_{\frac{L+1}{2}} = C_{\frac{L-1}{2}}, \quad \forall \tau. \tag{5.4d}$$

In the above equations, we have omitted the τ-dependence of the correlations to keep our notation simple. We have written them for odd L, because the "upper" boundary condition (for the maximum value of k) is simpler to write. Of course, this choice is irrelevant in the large system size limit. The same equations can be derived in discrete time p by averaging Eq. (4.17).

As a consequence of momentum conservation, in the center of mass frame we have the "sum rule"

$$C_0(\tau) + 2\sum_{k=1}^{\frac{L-1}{2}} C_k(\tau) = 0, \quad \forall \tau. \tag{5.5}$$

For a conservative ($\alpha = 1$) system at equilibrium, the correlations C_k do not depend on the distance between sites k and they are of the order $O(L^{-1})$: $C_k^{\text{eq}} = -T(L-1)^{-1}, \forall k > 0$. In a non-equilibrium state, we may have a non-trivial space structure in the correlations, but we still assume them to be of the order of L^{-1}. Then, we define the rescaled correlations $D_k(\tau)$ as

$$D_k(\tau) = L C_k(\tau), \tag{5.6}$$

which we assume to be of the order of unity in the infinite size limit as $L \to \infty$.

Let us write (5.4) in the large system size limit, in which we expect $D_k(\tau)$ to be a smooth function of space, in the sense that $D_{k+1}(\tau) - D_k(\tau) = O(L^{-1})$. Then, the typical hydrodynamic length and time scales are introduced as in (4.25), with

$$x = \frac{k-1}{L}, \quad t = \frac{\omega\tau}{L^2} = \frac{p}{L^3} \tag{5.7}$$

Keeping solely terms up to $O(L^{-1})$, we arrive at

$$\frac{dT(t)}{dt} = -\nu \left[T(t) - L^{-1}\psi(t)\right], \tag{5.8a}$$

$$\nu T(t) + 4\partial_x D(x,t)|_{x=0} = L^{-1}\left(\frac{d\psi(t)}{dt} + \nu\psi(t)\right), \tag{5.8b}$$

$$\partial_t D(x,t) = 2\,\partial_{xx} D(x,t), \tag{5.8c}$$

$$\partial_x D(x,t)|_{x=1/2} = \frac{1}{2}L^{-1}\frac{d\chi(t)}{dt} \tag{5.8d}$$

in which we have introduced the notations

$$\psi(t) = \lim_{x\to 0} D(x,t), \quad \chi(t) = \lim_{x\to \frac{1}{2}} D(x,t). \tag{5.9}$$

These equations are exact up to times such that $t \ll L^2$, since the lowest order terms that have been neglected are of the order of L^{-2}, for instance the fourth-spatial-derivative term in the diffusion equation (5.8b) for the correlations. In (5.8a), we have a L^{-1} correction to the cooling rate, brought about by the nearest-neighbor velocity correlation.

Of course, these equations are compatible with the sum rule (5.5). When we retain only terms up to and including $O(L^{-1})$, we have

$$T(t) + 2\int_0^1 dx\, D(x,t) + L^{-1}\left[\psi(t) - 2\chi(t)\right] = O(L^{-2}), \tag{5.10}$$

as shown in Appendix A.3. The lhs of (5.10) is a constant of motion, as can be readily shown by using the evolution equations (5.8).

In order to solve the above system, it is useful to define the scaled (tilde) fields with their corresponding power of $T_{\text{HCS}}(t)$. Namely, we define

$$\tilde{T}(t) = \frac{T(t)}{T_{\text{HCS}}(t)}, \quad \widetilde{D}(x,t) = \frac{D(x,t)}{T_{\text{HCS}}(t)}. \tag{5.11}$$

These rescaled fields obey the equations

$$\frac{d\tilde{T}(t)}{dt} = \nu L^{-1}\tilde{\psi}(t), \tag{5.12a}$$

$$\nu\tilde{T}(t) + 4\partial_x \widetilde{D}(x,t)|_{x=0} = L^{-1}\frac{d\widetilde{\psi}(t)}{dt}, \tag{5.12b}$$

$$\partial_t \widetilde{D}(x,t) = \nu\widetilde{D}(x,t) + 2\,\partial_{xx}\widetilde{D}(x,t), \tag{5.12c}$$

$$\partial_x \widetilde{D}(x,t)|_{x=1/2} = \frac{1}{2}L^{-1}\left(\frac{d\widetilde{\chi}(t)}{dt} - \nu\widetilde{\chi}(t)\right). \tag{5.12d}$$

The system above is linear in $(\tilde{T}, \widetilde{D})$, so it is possible to seek the exact solution thereof: this has been done in [155, 154]. Here, we are interested in finding the corrections to the cooling rate introduced by the velocity correlations, so we look for a solution of (5.12) by means of a perturbative approach. This can be performed by expanding all functions of time in powers of L^{-1},

$$\tilde{T}(t) = \tilde{T}_0(t) + L^{-1}\tilde{T}_1(t) + O(L^{-2}), \tag{5.13a}$$

$$\widetilde{D}(x,t) = \widetilde{D}_0(x,t) + L^{-1}\widetilde{D}_1(x,t) + O(L^{-2}), \tag{5.13b}$$

with analogous expansions for $\widetilde{\psi}(t)$ and $\widetilde{\chi}(t)$.
To the lowest order, we have

$$\frac{\mathrm{d}}{\mathrm{d}t}\tilde{T}_0 = 0, \tag{5.14a}$$
$$\nu\tilde{T}_0 + 4\partial_x\widetilde{D}_0|_{x=0} = 0, \tag{5.14b}$$
$$\partial_t\widetilde{D}_0 = \nu\widetilde{D}_0 + 2\,\partial_{xx}\widetilde{D}_0, \tag{5.14c}$$
$$\partial_x\widetilde{D}_0|_{x=1/2} = 0. \tag{5.14d}$$

From (5.14a), we have that $\tilde{T}_0 = 1$ is a constant. Moreover, in the limit $t \gg 1$, the scaled correlations tend to a stationary value, which is given by

$$\widetilde{D}_0(x) = -A\cos\left[\pi\sqrt{\frac{\nu}{\nu_c}}(1-2x)\right], \quad A = \pi\sqrt{\frac{\nu}{\nu_c}}\csc\left(\pi\sqrt{\frac{\nu}{\nu_c}}\right). \tag{5.15}$$

Looking for the first order corrections, for our purposes we only need to write the evolution equation for $\tilde{T}_1(t)$,

$$\frac{\mathrm{d}}{\mathrm{d}t}\tilde{T}_1(t) = \nu\widetilde{\psi}_0(t) \tag{5.16}$$

hence when the correlations reached the stationary profile (5.15) we have that

$$\frac{\mathrm{d}}{\mathrm{d}t}\tilde{T}_1(t) = \nu\psi_{\text{HCS}} \tag{5.17}$$

defining ψ_{HCS} as

$$\psi_{\text{HCS}} \equiv -\pi\sqrt{\frac{\nu}{\nu_c}}\cot\left(\pi\sqrt{\frac{\nu}{\nu_c}}\right). \tag{5.18}$$

Therefore, for $t \gg 1$ the rescaled temperature is linearly diverging as

$$\tilde{T}(t) \sim 1 + \frac{\nu\psi_{\text{HCS}}}{L}t + O(L^{-2}) \tag{5.19}$$

neglecting the transient terms for $\tilde{T}_1$. This result explains the divergence of rescaled temperature from HCS value $\tilde{T} = 1$ and has been compared with simulations in figure 5.1. It is worth underlining the presence of a transition at $\nu = \nu_\psi = 2\pi^2$, for which $\psi_{\text{HCS}} = 0$ and first-order corrections to Haff's law vanish.

We have also checked the theoretical prediction (5.15) for the velocity correlations in the HCS in figure 5.2. Thus, we plot the simulation value of the nearest-neighbors rescaled correlation $\widetilde{\psi}(t)$ as a function on time, approaching the stationary value ψ_{HCS}, and the amplitude A as a function of ν, and compare them with (5.15). Trajectories start from a homogeneous mesoscopic velocity profile with zero average, $u(x,0) \equiv 0$. Once more, a very good agreement is found.

We already commented that the result in (5.19) is valid only for $\psi_{\text{HCS}}\nu t/L \ll 1$, while in this section we used the stationary value of the correlations supposing $t \gg 1$. Depending on the value of ν and L, these conditions on time may be either consistent or inconsistent. In fact, numeric data in figure 5.2 show an excellent agreement with the theoretical prediction in (5.19) for $\nu < 60$, while for higher dissipation the nearest-neighbor correlations do not seem to have reached their stationary value. Therefore, longer trajectories should be observed and this leads to the divergence of the first order perturbation $O(t/L)$.

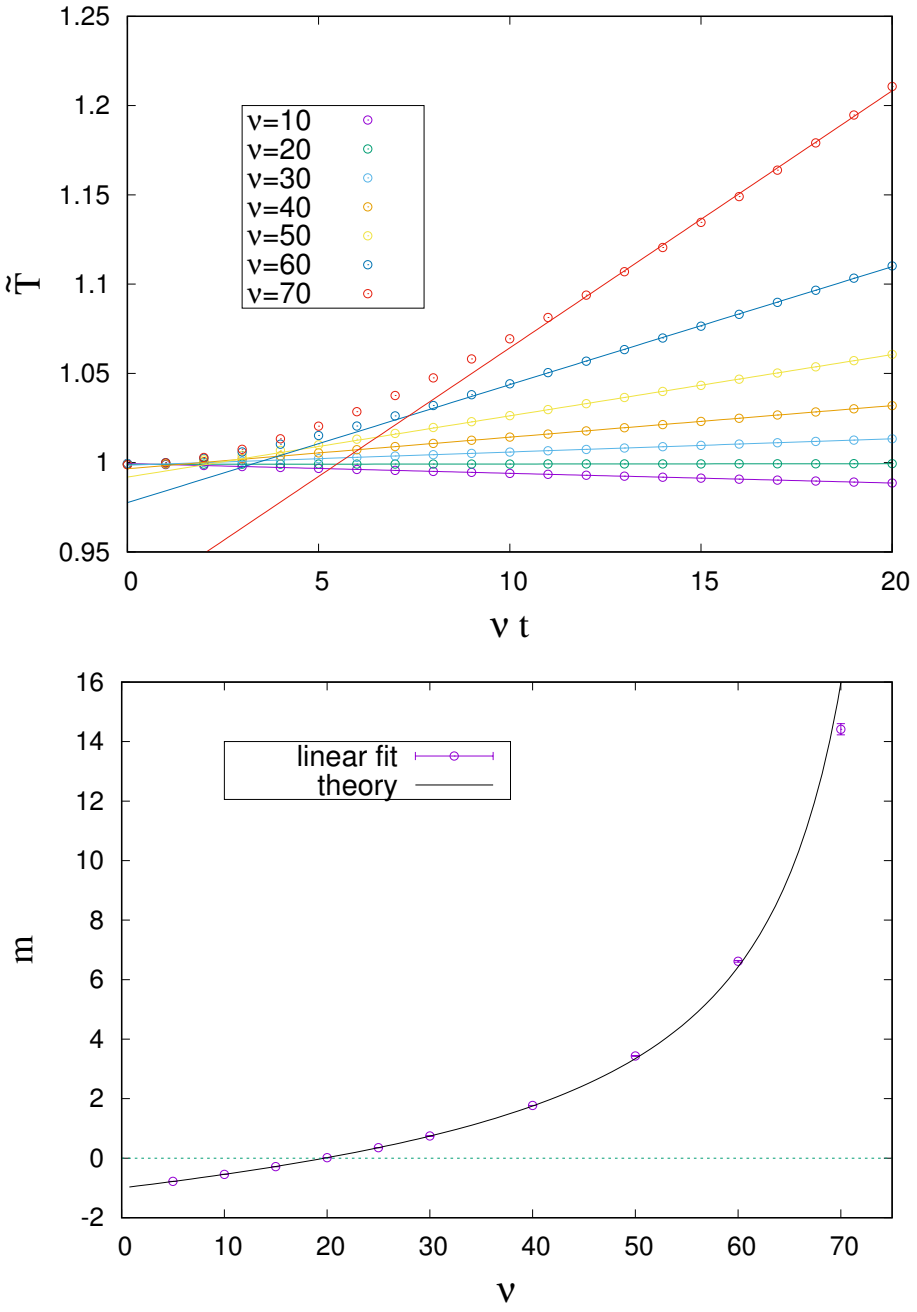

Figure 5.1. Top panel: rescaled temperature $\tilde{T}$ as a function of time. We compare the numerical values of $\tilde{T}$ (circles) and the linear fits (lines) in the second part of the trajectory, for several values of ν (see legend). Bottom panel: Plot of the slope $m = L\, d\tilde{T}/d(\nu t)$ as a function of ν. We compare the fitted slopes in the top panel (circles) and their theoretical values, as given by $\psi_{\rm HCS}$ in (5.16) (blue line). The transition at $\nu_\psi = 2\pi^2$ is marked by the horizontal dashed line. We have used a system of size $L = 1000$.

5.2 Temperature and Correlations Evolution: Multiple-Scale Analysis

In order to build up a theory which give a consistent picture for long times, we introduce a multiple-scale perturbative solution of (5.12). Equation (5.12a) suggests the introduction of two distinct time scales: apart from t, we define a slow time scale σ,

$$s = t,\ \sigma = L^{-1}t, \quad \partial_t{=}\partial_s + L^{-1}\partial_\sigma. \tag{5.20}$$

Our notation makes it possible to distinguish between ∂_t (with constant x) and ∂_s (with constant x and σ). All functions of time are expanded in powers of L^{-1} as before and considered to depend on both time scales (s,σ). So, to the lowest order we have

$$\partial_s \tilde{T}_0(s,\sigma) = 0, \tag{5.21a}$$
$$\nu\tilde{T}_0 + 4\partial_x \widetilde{D}_0|_{x=0} = 0, \tag{5.21b}$$
$$\partial_s \widetilde{D}_0 = \nu\widetilde{D}_0 + 2\,\partial_{xx}\widetilde{D}_0, \tag{5.21c}$$
$$\partial_x \widetilde{D}_0|_{x=1/2} = 0. \tag{5.21d}$$

which has the same form of (5.14) but now $\tilde{T}_0$ depends also on the slow time scale σ; more precisely, from (5.21a) we have that it depends only on σ, $\tilde{T}_0(\not{s},\sigma) = \tilde{T}_0(\sigma)$. Note that $\tilde{T}_0(\sigma)$ remains undetermined at the lowest order. Also, (5.21) leads now to a pseudo-stationary solution for $\widetilde{D}_0(x,\not{s},\sigma)$ for long time scales $s \gg 1$ but finite σ, namely

$$\widetilde{D}_0(x,\sigma) = -\tilde{T}_0(\sigma)A\cos\left[\pi\sqrt{\frac{\nu}{\nu_c}}(1-2x)\right], \tag{5.22}$$

which differs from (5.15) because of the σ dependence of $\tilde{T}_0(\sigma)$. As is usual in multiple-scale analysis, the latter can be obtained by writing down the equations for the first order corrections. In fact, for the purposes of the present paper, it suffices to write the evolution equation for $T_1(s,\sigma)$,

$$\partial_s\tilde{T}_1 + \frac{d}{d\sigma}\tilde{T}_0 = \nu\widetilde{\psi}_0, \qquad \widetilde{\psi}_0 = \tilde{T}_0\psi_{\text{HCS}}. \tag{5.23}$$

Since the rescaled energy should not contain linear terms in time (see [155, 154] for a rigorous proof), the first lhs term of (5.23) must vanish, and

$$\nu\psi_{\text{HCS}}\tilde{T}_0(\sigma) - \frac{\mathrm{d}}{\mathrm{d}\sigma}\tilde{T}_0 = 0 \ \Rightarrow\ \tilde{T}_0(\sigma) = e^{\nu\psi_{\text{HCS}}\sigma}, \tag{5.24}$$

where we have taken into account that $\tilde{T}_0(t=0) = 1$. Going back to the unscaled variables, what we have shown is that

$$T(t) = T(0)\exp\left[-\nu^r_{\text{HCS}}t\right] + O(L^{-1}), \qquad \nu^r_{\text{HCS}} = \nu\left(1 - L^{-1}\psi_{\text{HCS}}\right). \tag{5.25}$$

Equation (5.25) tells us that the cooling rate in Haff's law has a finite size correction. Of course, if we consider that $\sigma = t/L \ll 1$ and retain only the linear terms in L^{-1}, we reobtain the results in (5.19).

We check the renormalization of Haff's law predicted by (5.25) in figure 5.3: simulations made over long times $\nu t \psi_{\text{HCS}} \sim L$ show that the rescaled temperature has an exponential behavior, as predicted from the multiple-scale analysis. The exponential slope has been fitted and numerical results are in good agreement with the theoretical prediction (5.24). Nearest-neighbor correlations have been studied as before: figure 5.3 shows that for $\nu = 50, 60$ they converge to their expected value after a very short transient, whereas for $\nu = 70$ they also converge but to a stationary value smaller than the expected one. This effect is probably given by next order corrections which are becoming relevant when approaching the critical dissipation ν_c, where we know that ψ_{HCS} is divergent.

5.3 Total energy fluctuations and multiscaling

A typical question in granular systems concerns the distribution of the extensive energy $E(\tau) = \sum_l v_l^2(\tau)$: usually, granular models present non-Gaussian distributions that can be mostly characterized by the study of its fluctuations [28]. Within the same spirit of section 5.1, we now aim to derive the total energy rescaled fluctuations $\Sigma(\tau)$ defined as

$$\Sigma^2(\tau) = \frac{\langle E^2(\tau)\rangle - \langle E(\tau)\rangle^2}{\langle E(\tau)\rangle^2}. \tag{5.26}$$

The Local Equilibrium Approximation (LEA) gives the straightforward result $\Sigma^2(\tau) = 2/L$. However, numerical results in figure 5.4 show a time-dependent behavior of $\Sigma^2(\tau)$ which clearly diverges from the LEA prediction.

Such anomalous behavior is generally considered an evidence of multiscaling in the moments [14], i.e. the moments are not scaling proportionally to the granular temperature $T(\tau) = \langle v^2(\tau)\rangle$. Notwithstanding, this phenomenon can also be explained by a well-defined scaled distribution function with some divergent moments [6, 51]. Following the same approach of section 5.1, we look for a direct calculation of the energy fluctuations by means of the evolution equations for the 4-th order moments and correlations.

In the homogeneous case, we can write

$$\begin{aligned}
\left\langle E^2(\tau)\right\rangle &= \sum_{l=1}^{L}\left\langle v_l^4(\tau)\right\rangle + \sum_{l=1}^{L}\sum_{k=1}^{L-1}\left\langle v_l^2(\tau)\, v_{l+k}^2(\tau)\right\rangle \\
&= L\left\langle v^4(\tau)\right\rangle + L\left[(L-1)T^2(\tau) + 2\sum_{k=1}^{(L-1)/2} C_k^{2,2}(\tau)\right], \qquad (5.27a)\\
\langle E(\tau)\rangle &= LT(\tau), \qquad (5.27b)
\end{aligned}$$

where we have defined the two-particle squared velocity correlation function

$$C_k^{2,2}(\tau) = \left\langle v_l^2(\tau) v_{l+k}^2(\tau)\right\rangle - T^2(\tau), \quad k \neq 0. \tag{5.28}$$

Therefore, the energy fluctuations dynamics is given by the dynamics of $T(\tau)$, $q(\tau) = \langle v^4(\tau)\rangle$ and $C_k^{2,2}(\tau)$ altogether.

Rescaled energy fluctuations hence read

$$L\Sigma^2(t) = 2 + a_2(t) + \frac{2}{T^2(t)} \int_0^{\frac{1}{2}-\frac{3}{2L}} D^{2,2}(x,t)dx, \tag{5.29}$$

using the hydrodynamic scaling defined in (5.7) and introducing the excess kurtosis field $a_2(t) = q(t)/T^2(t) - 3$. Analogously with the scaling used in section 5.1, we define $D^{2,2} = LC^{2,2}$, where the evolution equations for these fields can be computed from the microscopic dynamics (4.15). By means of a perturbative approach, a set of equations is derived, similar to (5.14), coupling all the one-particle and two-particle fourth-degree fields, namely $q(t)$, $D^{2,2}(x,t)$ and $D^{3,1}(x,t)$. The latter is the large-size limit of $D_k^{3,1}(\tau) = L\,\langle v_l^3(\tau)\, v_{l+k}(\tau)\rangle$. Also, the three-particle correlation $C_{i,j}^{1,2,1}(\tau) = \langle v_{l-i}(\tau)\, v_l^2(\tau)\, v_{l+j}(\tau)\rangle$ appears in these equations: to get a closed set, we make use of the *clustering ansatz*, that is, we perform a cluster expansion of the latter and neglect purely correlated terms, specifically

$$\begin{aligned} C_{i,j}^{1,2,1}(\tau) &= \left\langle v_l^2(\tau)\right\rangle \langle v_{l-i}(\tau)\, v_{l+j}(\tau)\rangle + 2\,\langle v_l(\tau)\, v_{l-i}(\tau)\rangle\,\langle v_l(\tau)\, v_{l+j}(\tau)\rangle \\ &\quad + \mathcal{O}(L^{-3}) = \frac{1}{L}T(\tau)D_{|i+j|}(\tau) + \frac{2}{L^2}D_i(\tau)D_j(\tau) + \mathcal{O}(L^{-3}). \end{aligned} \tag{5.30}$$

The derivation from microscopic dynamics is lengthy and painful but conceptually easy to understand: it relies on the expansion of correlation fields and moments, analogous to the one defined in Eqs. (5.13). here we present a concise version going directly to the final results; in Appendix A.4 the reader will find the detailed calculations to obtain the results presented in the section.
Starting from the microscopic dynamics defined in (4.15) and moving to the continuum limit, with the clustering ansatz one gets to the lowest order

$$\frac{d}{dt}\tilde{q}_0(t) = 0, \tag{5.31a}$$
$$\nu\left[\tilde{q}_0(t) + 3\tilde{T}_0^2\right] + 8\partial_x \widetilde{D}_0^{3,1}|_{x=0} = 0, \tag{5.31b}$$
$$\partial_t \widetilde{D}_0^{3,1} = \frac{\nu}{2}\left(\widetilde{D}_0^{3,1} + \tilde{T}_0\widetilde{D}_0\right) + 2\,\partial_{xx}\widetilde{D}_0^{3,1}, \tag{5.31c}$$
$$\partial_x \widetilde{D}_0^{3,1}|_{x=1/2} = 0, \tag{5.31d}$$
$$\partial_x \widetilde{D}_0^{2,2}|_{x=0} = 0, \tag{5.31e}$$
$$\partial_t \widetilde{D}_0^{2,2} = 2\,\partial_{xx}\widetilde{D}_0^{2,2}, \tag{5.31f}$$
$$\partial_x \widetilde{D}_0^{2,2}|_{x=1/2} = 0. \tag{5.31g}$$

These equations can be readily solved. Assuming for instance the initial distribution to be Gaussian, we have at any time $\tilde{q}_0 = 3\,\tilde{T}_0^2$. Moreover, in the long time limit $t \gg 1$, we obtain the stationary fields

$$\widetilde{D}_0^{3,1}(x) = 3\,\widetilde{D}_0(x), \qquad \widetilde{D}_0^{2,2}(x) = 0, \tag{5.32}$$

recalling that $\tilde{T}_0 = 1$. However, these results do not give rise to any multiscaling effect such as the one observed into the simulations.

In light of the above, we move on to compute the next perturbative order. The equations needed from the definition (5.29) are those for $\tilde{q}_1$ and $\widetilde{D}_1^{2,2}$, i.e.

$$\frac{\mathrm{d}}{\mathrm{d}t}\tilde{q}_1(t) = 2\nu\widetilde{\psi}_0^{3,1}(t), \tag{5.33a}$$

$$\nu\tilde{T}_0\tilde{\psi}_0 + \partial_x\widetilde{D}_1^{2,2}|_{x=0} = 0, \tag{5.33b}$$

$$\partial_t\widetilde{D}_1^{2,2} = 2\,\partial_{xx}\widetilde{D}_1^{2,2} + 4\,\nu\tilde{D}_0^2, \tag{5.33c}$$

$$\partial_x\widetilde{D}_1^{2,2}|_{x=1/2} = 0. \tag{5.33d}$$

where $\widetilde{\psi}^{3,1}(t) = \lim_{x\to 0}\widetilde{D}^{3,1}(x,t)$. Equation (5.33a) is immediately solvable for long times since $\tilde{D}_0^{3,1}(x,t)$ is known from (5.32), yielding

$$\tilde{q}_1(t) = 2\nu\psi_0^{3,1} = 6\nu\psi_{\text{HCS}}. \tag{5.34}$$

Looking at the $\tilde{D}_1^{2,2}$ field from (5.29), all we need is to compute the integral $\Delta_1(t) = \int_0^1 dx\,\tilde{D}_1^{2,2}(x,t)$. Taking into account (5.33), we have that

$$\frac{d}{dt}\Delta_1(t) = 4\nu\left[\psi_0(t) + \int_0^1 dx\,\widetilde{D}_0^2(x,t)\right], \tag{5.35}$$

where we have used the boundary condition $\partial_x\widetilde{D}_1^{2,2}|_{x=1^-} = -\partial_x\widetilde{D}_1^{2,2}|_{x=0^+}$. Therefore, in the long time limit we use the stationary correlation profile $\tilde{D}(x)$ from (5.15) to get the stationary growth

$$\frac{d}{dt}\Delta_1(t) = 2\nu\left[\frac{\pi\sqrt{\nu/\nu_c}}{\sin\left(\pi\sqrt{\nu/\nu_c}\right)}\right]^2\left[1 - \frac{\sin\left(2\pi\sqrt{\nu/\nu_c}\right)}{2\pi\sqrt{\nu/\nu_c}}\right]. \tag{5.36}$$

Now, we have all the ingredients to compute the energy fluctuations in (5.29). To the first order, (5.34) and (5.16) yield that the excess kurtosis $a_2(t)$ vanishes for all times if it did initially, $a_2(t) = O(L^{-2})$. This implies that the steady-state linear divergence of the energy fluctuations (to the first order) is given by the $D^{2,2}$ correlations term in (5.36). Specifically, for $t \gg 1$, we have

$$\frac{d}{dt}\Sigma^2(t) = \frac{1}{L}\frac{d}{dt}\Delta_1(t) = \frac{\nu}{L}m_\Sigma(\nu). \tag{5.37}$$

We have introduced $m_\Sigma(\nu) = d\Delta_1/d(\nu t)$, which is the slope of the energy fluctuations as a function of the dimensionless time νt.

In conclusion, the observed energy multiscaling seems to stem from the multiscaling of two-particles and three-particles correlation fields, while the single-particle fourth moment still scales with the granular temperature squared. We have compared this theoretical result with simulations in figure 5.5. Although some discrepancies are apparent, especially for high ν, we see that they both exhibit a similar trend over three decades of m_Σ values. Keeping the clustering ansatz in (5.30), a multiple scale analysis has also been performed, analogous to that in section 5.2. Nevertheless, it does not improve the agreement with the numerics. Therefore, it seems that the most probable source for this discrepancy is the clustering ansatz that is used in both cases.

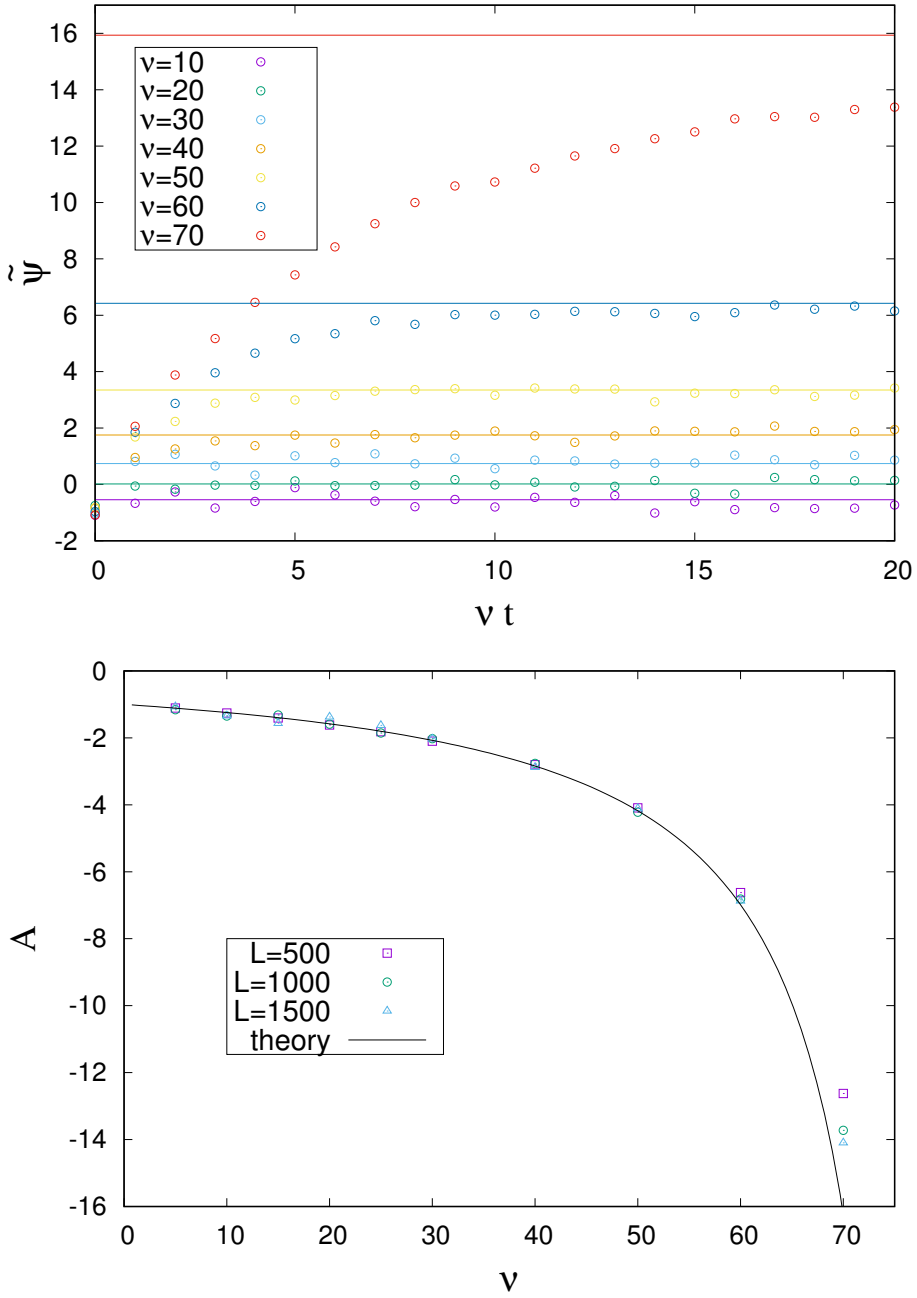

Figure 5.2. Top panel: Time evolution of nearest-neighbor rescaled correlations $\widetilde{\psi}(t)$. We plot their numerical values (circles) for several ν (see legend) and $L = 1000$ particles as a function of the dimensionless time νt, and their theoretical stationary values, given by (5.18). In the plotted time window, the correlations reach their stationary value for all $\nu \leq 60$, while they do not for $\nu = 70$. This discrepancy will be analyzed in figure 5.3. Bottom panel: Correlation amplitude A, defined in (5.15), as a function of ν. We plot both its numerical value, computed in simulations for $L = 250, 500, 1000$ (symbols), and its theoretical expectation (black line). A very good agreement is found for all $\nu < 70$.

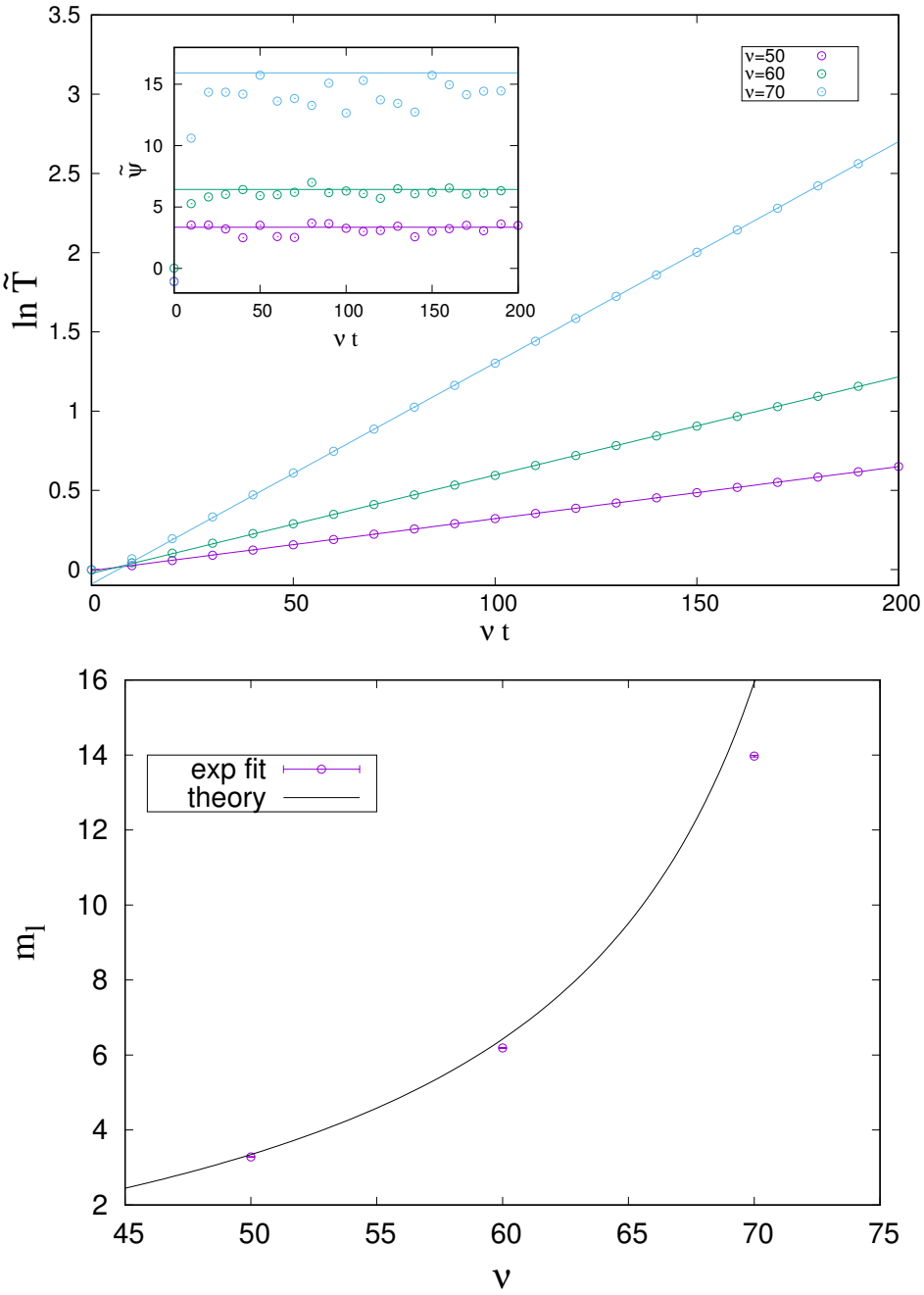

Figure 5.3. Top panel: Log-linear plot of the rescaled temperature. The simulation values are plotted for $\nu = 50, 60, 70$ (circles), and also the fits made upon the second part of the long trajectories (lines). The time evolution is clearly exponential as predicted from (5.24). Inset: Time evolution of the nearest-neighbor rescaled correlations $\widetilde{\psi}(t)$ for long trajectories. We have plotted the simulation curves (circles) and their corresponding theoretical stationary values (lines). Bottom panel: Slope m_l of the time evolution of $\ln \tilde{T}$. The fitting values from the top panel (squares) are plotted together with the theoretical prediction (5.24) (black line). All the trajectories have been done with $L = 1000$ particles up to a maximum time $\nu t = 200$.

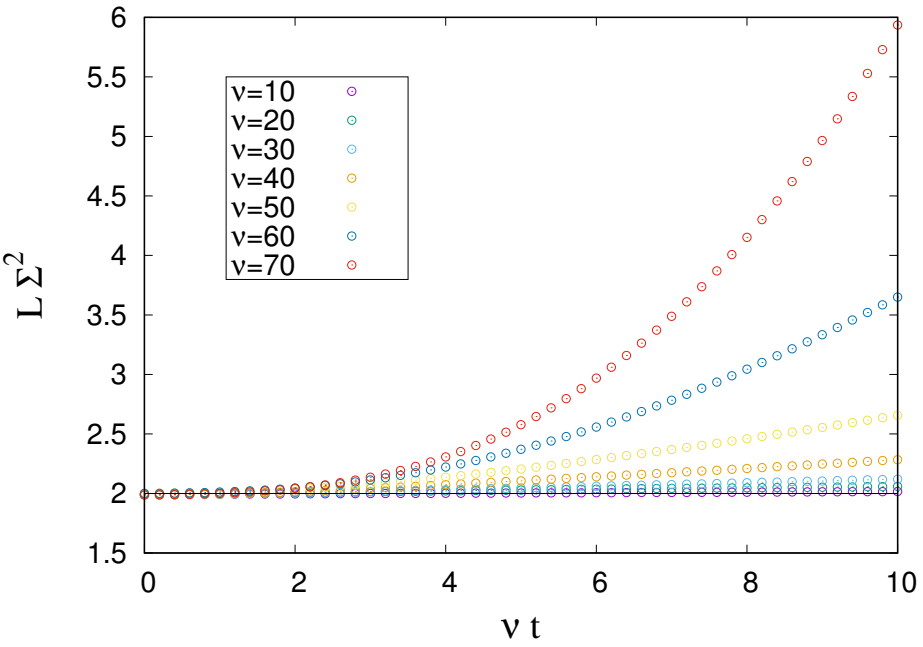

Figure 5.4. Total energy rescaled fluctuations as a function of dimensionless time νt. We have plotted the simulation curves for $\nu = 10, 20, \ldots, 70$, always with $L = 1000$. The divergence from the expected LEA value is evident and grows with ν.

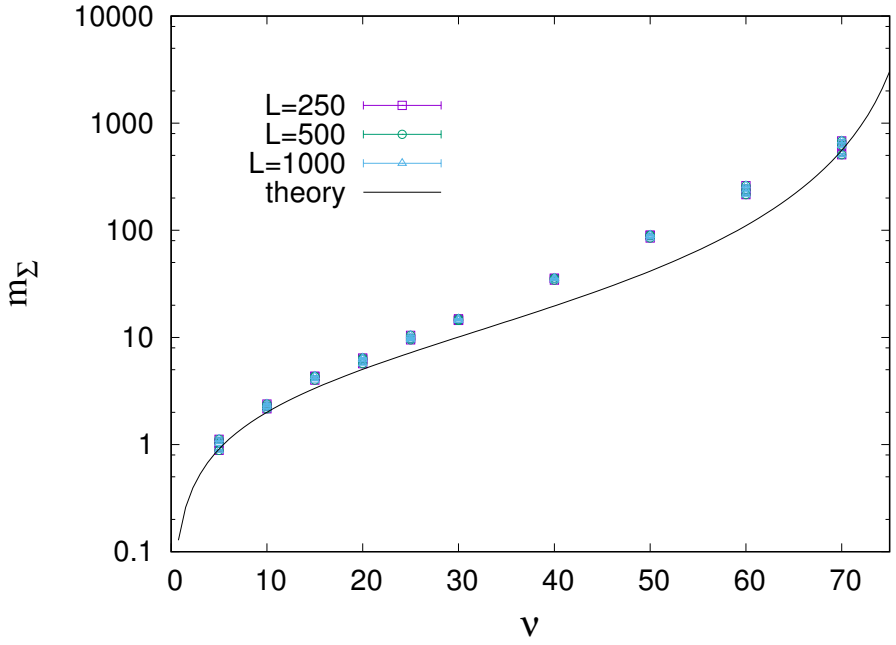

Figure 5.5. Slope of the energy fluctuations vs. time curves. We compare the fitted values (symbols) in the second part (long time) of the trajectories for $L = 250, 500, 1000$ with the theoretical prediction $m_\Sigma(\nu)$ in (5.37) (black line). Simulations are carried out as in figure 5.4.

It don't mean a thing
if it ain't got that swing

6

Active lattice fluctuating hydrodynamics

The granular lattice model analyzed in the last chapters has shown to reproduce realistic physical phenomena and to lead towards new analytical results on nonequilibrium fluctuating hydrodynamics. The generality of the method brought us to the formulation of a lattice model of active matter, which will be developed along the same lines [134].

Here we introduce a model of granular active particles (GAP) on the lattice where pairwise interactions combine excluded volume and dissipative alignment, quite similarly to the off-lattice model in [87] described in Sec. 2.3. Our main result is a set of hydrodynamic equations for the density, momentum and energy fields with fluctuating currents and source terms, in analogy with granular lattice results in Chapter 4. An application of these general equations is given in the dilute limit, assuming local equilibrium [147], where they describe a gas-swarming phase transition through the linear instability of the homogeneous disordered state. The homogeneous swarming state arises when either the noise amplitude is small enough or the aligning force is strong enough. Numerical simulations agree well with the theory - including predictions of the macroscopic noise amplitudes - for packing fraction smaller than 10%: they also suggest that the instability is discontinuous in the large volume limit. Simulations also display the emergence of clustering and phase separation at higher packing fraction, where our assumptions fail.

6.1 Definition of the model

6.1.1 Microscopic ingredients

We consider a square lattice in d dimensions of volume $V = L^d$, with $1 \ll N \leq V$ self-propelled particles moving on it. A lattice site $\mathbf{i} = (i_1, i_2, \ldots, i_d) \in \{1, L\}^d = \Lambda$ can be occupied at most by one particle (excluded volume) and is described by its occupation number $n_{\mathbf{i}} \in \{0, 1\}$ and its "active velocity" $\mathbf{v}_{\mathbf{i}} \in \mathbb{R}^d$ (the meaning of

this variable is discussed later). The elementary moves that constitute the microscopic evolution of each particle, see Fig. 6.1, amount to

- hopping
- nearest-neighbors interactions
- self-propulsion
- noise

Hopping means that a particle at site $\mathbf{i}$ can move to an adjacent site $\mathbf{i} + \sigma\mathbf{e}_l$, being $\mathbf{e}_l$ the unit vector in the l-th direction and $\sigma = \pm 1$ the orientation of the hop, with $l = 1, \dots, d$. The probability of hopping per unit of time can generally be velocity-dependent.

Pairwise interactions are represented by a contact force: when two particles with active velocities $\mathbf{v}$ and $\mathbf{v}'$ are nearest-neighbors, they act on each other with a force

$$\mathbf{f}^{(2)}(\mathbf{v}, \mathbf{v}') = -\mathbf{f}^{(2)}(\mathbf{v}', \mathbf{v}) \tag{6.1}$$

where $\mathbf{f}^{(2)}(\mathbf{v}, \mathbf{v}')$ represents the force transmitted from particle with velocity $\mathbf{v}$ to particle with velocity $\mathbf{v}'$. The above relation implies the conservation of total momentum during interactions. The force can be dissipative or conservative; from Sec. 6.2 on we will focus on the dissipative case, in analogy with granular collisions.

Self-propulsion consists in a velocity-dependent force $\mathbf{f}^{(1)}(\mathbf{v})$: indeed, the speed of active particles $v = |\mathbf{v}|$ is not fixed and the self-propulsion acts to maintain the state of motion of the particles, typically pushing them towards a fixed point of speed v_s. Self-propulsion is combined with a vectorial Wiener process $\Delta\mathbf{W}_\mathbf{i}(t)$ independently acting upon each component of the velocity of each particle, with a velocity-diffusion tensor $\mathsf{B}(\mathbf{v})$.

The state of the system is completely identified by its microscopic configuration $\{n_\mathbf{i}, \mathbf{v}_\mathbf{i}\}$. The system evolves with a discretized time. The index $p \in \mathbb{N}$ denotes the number of performed time steps. Physical time reads $t = p\Delta t \in \mathbb{R}$, where Δt will go to zero when taking the continuum limit, as well as the physical distance between two lattice sites Δx.

6.1.2 Physical interpretation

The model possesses the main features of active matter models described in Sec. 2.2. The interplay between an interaction rule and a self-propulsion is present, combined with a noise term which can be interpreted as the effect of hidden degrees of freedom like the action of surrounding fluid or the random exploration of space performed by active units. Conversely from the granular case, now particles do *move* on the lattice when hopping, similarly with exclusion processes described in Sec. 3.3.1. Additionally, particles hop from one site to another depending on the active velocity degree of freedom directly entering in the hopping probabilities: indeed, with the "natural active velocity" hopping probability defined in the next subsection, a probe particle on an empty lattice follows a ballistic motion with

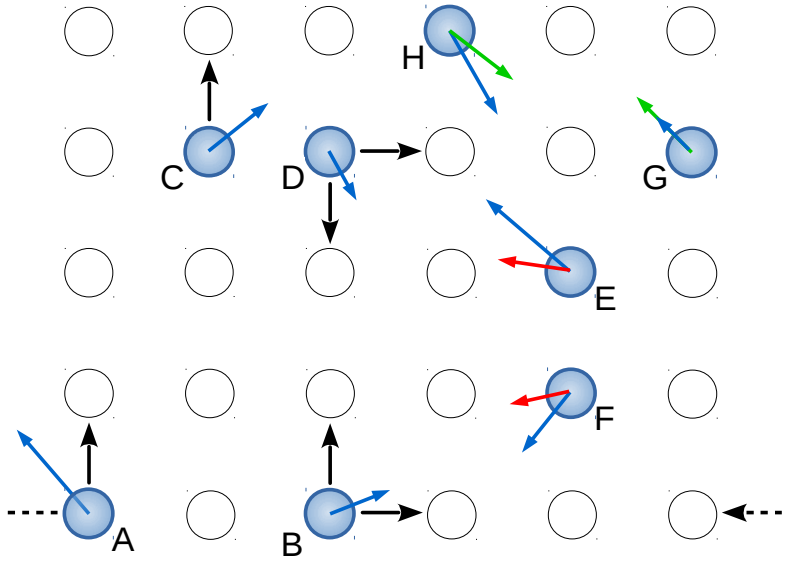

Figure 6.1. Sketch of active particles in a $2d$ lattice. Particles A-D show hopping (black arrows) to neighbor sites according to the directions of their active velocity (blue arrows), including periodic conditions (A) and excluded volume (C,D). Next-neighbors interact (E,F), with a force which aligns velocities (from blue to red arrows). Self-propulsion acts in the direction of the velocity and brings the speed toward a fixed value (G, from blue to green arrow). The velocity of a particle can be modified also by external noise (H, from blue to green).

$\langle \mathbf{x}(t) - \mathbf{x}(0) \rangle = \mathbf{v}\, t$, where $\mathbf{v}$ is constant in absence of self-propulsion, noise and interactions. However, this is not the case in a crowded environment: when all the adjacent sites are occupied, a particle with a non-vanishing active velocity does not move at all because of excluded volume. This is why we call $\mathbf{v_i}$ the *active velocity* of a particle in the site $\mathbf{i}$: it represents the tendency of active particles to move with a given direction and speed *provided that the direction of motion is not occupied by other particles*. This behavior may reproduce the clustering behavior of bacteria or Janus particles, when they all point towards the same direction and therefore self-clustering arises. So, in our model it is generally wrong to say that $\dot{\mathbf{x}} = \mathbf{v}$, as in the case of Active Ornstein-Uhlenbeck particles introduced in Sec. 2.2.4. However, in the latter model this was the consequence of an overdamping of the motion equations; here, it directly stems from the presence of excluded volume: the equations for our model are *not overdamped* in any considered case.

intensively

6.1.3 Microscopic balance equations

We now write the microscopic evolution equations for occupation $n_{\mathbf{i}}$, momentum $n_{\mathbf{i}}\mathbf{v_i}$ and energy $e_{\mathbf{i}} \equiv \frac{1}{2} n_{\mathbf{i}} \sum_k v_{\mathbf{i},k}^2$. From now on, the index l is associated to the direction of hopping while the index k indicates a general component of vectorial quantities.

At each infinitesimal time step p two random vectors are extracted: the random

site $\boldsymbol{\xi}_p \in \Lambda$, determining the hopping particle, and the random direction $\boldsymbol{\zeta}_p = \pm\mathbf{e}_l$ determining the direction and orientation of the hop. The probability of extraction satisfies

$$\overline{\delta_{\boldsymbol{\xi}_p,\mathbf{i}}\delta_{\boldsymbol{\zeta}_p,\sigma\mathbf{e}_l}} = n_{\mathbf{i},p}(1 - n_{\mathbf{i}+\sigma\mathbf{e}_l,p})g(\sigma v_{l,p})\frac{\Delta t}{\Delta x}, \tag{6.2}$$

where $\sigma = \pm 1$ and $\overline{\cdots}$ represents the average over the fast variables $\boldsymbol{\xi}_p$, $\boldsymbol{\zeta}_p$ conditioned by the actual microscopic configuration $\{n_{\mathbf{i},p}, \mathbf{v}_{\mathbf{i},p}\}$ at time p. The first two factors in the rhs guarantee that hopping can only occur from an occupied to an empty site, as for SEP models. The projection function relates the active velocity component l with the hopping probability in the l-th direction: since $g(\sigma v_{l,p})\Delta t/\Delta x$ must be dimensionless, g must have the dimension of a velocity. In our model, we will choose it as proportional to the projection of $\mathbf{v}_i$ along the direction l, namely

$$g(\sigma v_l) = \Theta(\sigma v_l)|\sigma v_l| \tag{6.3}$$

where $\Theta(x)$ is the Heaviside step function. We call this rule the "natural active velocity" prescription. Eqs. (6.2) and (6.3) provides that a free particle follows an average ballistic motion with $\langle\dot{\mathbf{x}}\rangle = \mathbf{v}$ if all the forces are absent. The hopping probability (6.2) also includes a constraint $\Delta t \ll \Delta x$ which will be analyzed later. The total hopping probability is generally under-normalized, i.e. there can be no hops during a time step.

The evolution of microscopic variables is given by *balance equations*: for each of the quantities above defined, we can compute the gain and loss terms at each time step. For instance, the occupation number $n_{\mathbf{i}}$ increases by 1 if a particle from an adjacent side hops into it, and vice versa if the occupying particle hops away from it. So,

$$n_{\mathbf{i},p+1} = n_{\mathbf{i},p} + \sum_{l=1}^{d}\sum_{\sigma=\pm1}\left(\delta_{\boldsymbol{\xi}_p,\mathbf{i}-\sigma\mathbf{e}_l}\delta_{\boldsymbol{\zeta}_p,\sigma\mathbf{e}_l} - \delta_{\boldsymbol{\xi}_p,\mathbf{i}}\delta_{\boldsymbol{\zeta}_p,\sigma\mathbf{e}_l}\right). \tag{6.4}$$

The discrete continuity equation for occupation number reads

$$\Delta n_{\mathbf{i}} = -\sum_{l=1}^{d}\left(\mathbf{j}_{\mathbf{i}} - \mathbf{j}_{\mathbf{i}-\mathbf{e}_l}\right)_l \tag{6.5}$$

where $\Delta n_{\mathbf{i}} \equiv n_{\mathbf{i},p+1} - n_{\mathbf{i},p}$ and the time dependence from now on is omitted because every variable in the rhs is evaluated at time p. Eq. (6.5) defines the *density current* vector as

$$j_{\mathbf{i},l} \equiv \delta_{\boldsymbol{\xi}_p,\mathbf{i}}\delta_{\boldsymbol{\zeta}_p,\mathbf{e}_l} - \delta_{\boldsymbol{\xi}_p,\mathbf{i}+\mathbf{e}_l}\delta_{\boldsymbol{\zeta}_p,-\mathbf{e}_l} \tag{6.6}$$

which is either 1 if the particle is leaving the site $\mathbf{i}$ in the "positive" direction (right, top...) or -1 if a particle is incoming from the same direction. The particles can not be created or destroyed, so the occupation number obey an exact continuity equation.

Analogously, the evolution of active velocity can be obtained through active momentum balance, i.e.

$$\begin{aligned}\Delta(n_{\mathbf{i}}\mathbf{v}_{\mathbf{i}}) = \sum_{l=1}^{d}\sum_{\sigma=\pm1}\Big[&\delta_{\boldsymbol{\xi}_p,\mathbf{i}-\sigma\mathbf{e}_l}\delta_{\boldsymbol{\zeta}_p,\sigma\mathbf{e}_l}\mathbf{v}_{\mathbf{i}-\sigma\mathbf{e}_l} - \delta_{\boldsymbol{\xi}_p,\mathbf{i}}\delta_{\boldsymbol{\zeta}_p,\sigma\mathbf{e}_l}\mathbf{v}_{\mathbf{i}} + \\ &+ n_{\mathbf{i}}n_{\mathbf{i}-\sigma\mathbf{e}_l}\mathbf{f}^{(2)}\left(\mathbf{v}_{\mathbf{i}-\sigma\mathbf{e}_l}, \mathbf{v}_{\mathbf{i}}\right)\Delta t\Big] + n_{\mathbf{i}}\left[\mathbf{f}^{(1)}(\mathbf{v}_{\mathbf{i}})\Delta t + \mathsf{B}(\mathbf{v}_{\mathbf{i}})\cdot\Delta\mathbf{W}_{\mathbf{i}}(t)\right]\end{aligned} \tag{6.7}$$

or, writing explicitly the components,

$$\Delta(n_{\mathbf{i}} v_{\mathbf{i},k}) = -\sum_{l=1}^{d} \left(\mathsf{J}_{\mathbf{i}} - \mathsf{J}_{\mathbf{i}-\mathbf{e}_l}\right)_{kl} + n_{\mathbf{i}} \left[f_k^{(1)}(\mathbf{v}_{\mathbf{i}})\Delta t + \sum_{l=1}^{d} B_{kl}(\mathbf{v}_{\mathbf{i}})\Delta W_{\mathbf{i},l}(t) \right] \tag{6.8}$$

accounting for momentum transport through hopping and pairwise interactions and momentum injection by means of self-propulsion $\mathbf{f}^{(1)}$ and random force $\mathsf{B}(\mathbf{v}_{\mathbf{i}}) \cdot \Delta\mathbf{W}_{\mathbf{i}}$ acting on the unit. The transported momentum defines the *momentum current* tensor J, namely

$$J_{\mathbf{i},kl} \equiv \delta_{\boldsymbol{\xi}_p,\mathbf{i}}\delta_{\boldsymbol{\zeta}_p,\mathbf{e}_l} v_{\mathbf{i},k} - \delta_{\boldsymbol{\xi}_p,\mathbf{i}+\mathbf{e}_l}\delta_{\boldsymbol{\zeta}_p,-\mathbf{e}_l} v_{\mathbf{i}+\mathbf{e}_l,k} + n_{\mathbf{i}} n_{\mathbf{i}+\mathbf{e}_l} f_k^{(2)}(\mathbf{v}_{\mathbf{i}}, \mathbf{v}_{\mathbf{i}+\mathbf{e}_l})\Delta t \tag{6.9}$$

representing the momentum in direction k transported in direction l.

The evolution of microscopic kinetic energy reads

$$\begin{aligned}
\Delta e_{\mathbf{i}} =& (n_{\mathbf{i}}\mathbf{v}_{\mathbf{i}}) \cdot \Delta(n_{\mathbf{i}}\mathbf{v}_{\mathbf{i}}) + \frac{1}{2}\left[\sum_{l,\sigma}\left(\delta_{\boldsymbol{\xi}_p,\mathbf{i}-\sigma\mathbf{e}_l}\delta_{\boldsymbol{\zeta}_p,\sigma\mathbf{e}_l}\mathbf{v}_{\mathbf{i}-\sigma\mathbf{e}_l} - \delta_{\boldsymbol{\xi}_p,\mathbf{i}}\delta_{\boldsymbol{\zeta}_p,\sigma\mathbf{e}_l}\mathbf{v}_{\mathbf{i}}\right)\right]^2 \\
&+ \frac{1}{2}\left[n_{\mathbf{i}}\sum_{l=1}^{d} B_{kl}(\mathbf{v}_{\mathbf{i}})\Delta W_{\mathbf{i},l}(t)\right]^2 \\
=& -\sum_{k,l}(n_{\mathbf{i}} v_{\mathbf{i},k})\left(\mathsf{J}_{\mathbf{i}} - \mathsf{J}_{\mathbf{i}-\mathbf{e}_l}\right)_{kl} + \sum_{k=1}^{d}\left[(n_{\mathbf{i}} v_{\mathbf{i},k})\left(f_k^{(1)}(\mathbf{v}_{\mathbf{i}})\Delta t + \sum_{l=1}^{d} B_{kl}(\mathbf{v}_{\mathbf{i}})\mathrm{d}W_{\mathbf{i},l}(t)\right)\right. \\
&\left. + \frac{1}{2}\sum_{l,\sigma}\left(\delta_{\boldsymbol{\xi}_p,\mathbf{i}-\sigma\mathbf{e}_l}\delta_{\boldsymbol{\zeta}_p,\sigma\mathbf{e}_l} v^2_{\mathbf{i}-\sigma\mathbf{e}_l,k} + \delta_{\boldsymbol{\xi}_p,\mathbf{i}}\delta_{\boldsymbol{\zeta}_p,\sigma\mathbf{e}_l} v^2_{\mathbf{i},k}\right) + \frac{1}{2} n_{\mathbf{i}} \sum_{l=1}^{d}[B_{kl}(\mathbf{v}_{\mathbf{i}})]^2\Delta t\right] \\
=& -\sum_{l=1}^{d}\left(\mathbf{J}_{\mathbf{i}} - \mathbf{J}_{\mathbf{i}-\mathbf{e}_l}\right)_l + n_{\mathbf{i}}\mathbf{v}_{\mathbf{i}} \cdot \mathsf{B}(\mathbf{v}_{\mathbf{i}}) \cdot \Delta\mathbf{W}_{\mathbf{i}}(t) + D_{\mathbf{i}}\,\Delta t
\end{aligned} \tag{6.10}$$

defining the energy current $\mathbf{J}_{\mathbf{i}}$ as

$$\begin{aligned}
\mathbf{J}_{\mathbf{i}} &= \mathbf{J}_{\mathbf{i}}^{(\mathrm{hops})} + \mathbf{J}_{\mathbf{i}}^{(\mathrm{int})} \\
J_{\mathbf{i},l}^{(\mathrm{hops})} &= \delta_{\boldsymbol{\xi}_p,\mathbf{i}}\delta_{\boldsymbol{\zeta}_p,\mathbf{e}_l} e_{\mathbf{i}} - \delta_{\boldsymbol{\xi}_p,\mathbf{i}+\mathbf{e}_l}\delta_{\boldsymbol{\zeta}_p,-\mathbf{e}_l} e_{\mathbf{i}+\mathbf{e}_l} \\
J_{\mathbf{i},l}^{(\mathrm{int})} &= \frac{1}{2} n_{\mathbf{i}} n_{\mathbf{i}+\mathbf{e}_l}(\mathbf{v}_{\mathbf{i}} + \mathbf{v}_{\mathbf{i}+\mathbf{e}_l}) \cdot \mathbf{f}^{(2)}(\mathbf{v}_{\mathbf{i}}, \mathbf{v}_{\mathbf{i}+\mathbf{e}_l})\,\Delta t
\end{aligned} \tag{6.11}$$

and the energy injection/dissipation terms

$$\begin{aligned}
D_{\mathbf{i}} &= D_{\mathbf{i}}^{(\mathrm{int})} + D_{\mathbf{i}}^{(\mathrm{self})} + D_{\mathbf{i}}^{(\mathrm{noise})} \\
D_{\mathbf{i}}^{(\mathrm{int})} &= -\frac{1}{2}\sum_{l,\sigma} n_{\mathbf{i}} n_{\mathbf{i}+\sigma\mathbf{e}_l}(\mathbf{v}_{\mathbf{i}} - \mathbf{v}_{\mathbf{i}+\mathbf{e}_l}) \cdot \mathbf{f}^{(2)}(\mathbf{v}_{\mathbf{i}}, \mathbf{v}_{\mathbf{i}+\mathbf{e}_l}) \\
D_{\mathbf{i}}^{(\mathrm{self})} &= n_{\mathbf{i}}\mathbf{v}_{\mathbf{i}} \cdot \mathbf{f}^{(1)}(\mathbf{v}_{\mathbf{i}}) \\
D_{\mathbf{i}}^{(\mathrm{noise})} &= \frac{1}{2} n_{\mathbf{i}} \sum_{k,l}^{1,d}[B_{kl}(\mathbf{v}_{\mathbf{i}})]^2 \equiv \frac{1}{2} n_{\mathbf{i}} B(\mathbf{v}_{\mathbf{i}})
\end{aligned} \tag{6.12}$$

where the contributions from hopping, interactions, self-propulsion and noise have been written separately.

Eqs. (6.5), (6.8) and (6.10) are the microscopic balance equations of the system. Their validity is not restricted to any equilibrium approximation or hypothesis on the configuration distribution function. At this stage, they are equivalent to Eqs. (4.15) and (4.17) of the granular model.

6.2 Hydrodynamic limit

The derivation of the hydrodynamic equations for the model can be done through a continuum limit of microscopic balance equations derived in the previous section. The hydrodynamic fields considered are density, momentum and temperature. The probability of a configuration $\{n_\mathbf{i}, \mathbf{v_i}\}$ at time t is defined as $\mathcal{P}(\{n_\mathbf{i}, \mathbf{v_i}\}; t)$. The 2-sites $(\mathbf{i}, \mathbf{j})$ and 1-site $(\mathbf{i})$ marginalized distributions are respectively given by $P^{(2)}_{\mathbf{i},\mathbf{j}}(n_\mathbf{i}, n_\mathbf{j}, \mathbf{v_i}, \mathbf{v_j}; t)$ and $P^{(1)}_\mathbf{i}(n_\mathbf{i}, \mathbf{v_i}; t)$. Locally averaged fields are defined as

$$\rho_\mathbf{i}(t) = \langle n_\mathbf{i} \rangle \tag{6.13a}$$

$$\rho_\mathbf{i}(t) u_{\mathbf{i},k}(t) = \langle n_\mathbf{i} v_{\mathbf{i},k} \rangle \tag{6.13b}$$

$$\rho_\mathbf{i}(t) T_\mathbf{i}(t) = \frac{1}{d} \langle n_\mathbf{i} |\mathbf{v_i} - \mathbf{u_i}|^2 \rangle, \tag{6.13c}$$

where

$$\langle f(n_\mathbf{i}, \mathbf{v_i}) \rangle = \prod_{\mathbf{i} \in \Lambda} \left(\sum_{n_\mathbf{i}=0,1} \int_{\mathbb{R}} d\mathbf{v_i} \right) \mathcal{P}(\{n_\mathbf{i}, \mathbf{v_i}\}; t) f(n_\mathbf{i}, \mathbf{v_i}) \tag{6.14}$$

and in Eq. (6.13c) we assumed isotropy of local temperature. From now on we make only use of continuous time $t = p\Delta t$. Temperature is related to energy through the relation

$$T_\mathbf{i}(t) \equiv \frac{1}{d} \left\langle |\mathbf{v} - \mathbf{u}|^2 \right\rangle_\mathbf{i} = \frac{1}{d} \left(\frac{2}{\rho_\mathbf{i}(t)} \langle e_\mathbf{i}(t) \rangle - u^2_\mathbf{i}(t) \right). \tag{6.15}$$

We move to a large volume limit $L \to \infty$, $N \to \infty$ at constant number density $\phi = N/V$. In this limit the physical spacing between two adjacent lattice sites is sent to 0 as $\Delta x = 1/L$, such that a spatial position in the system is denoted by a continuous $\mathbf{x} \in [0, 1]^d$.

To get a closed set of equations, we make use of two assumptions

1. Molecular Chaos (expected to be valid in the dilute limit $\phi \to 0$) with isotropic velocity factorization:

$$P^{(2)}_{\mathbf{i},\mathbf{j}}(n_\mathbf{i}, n_\mathbf{j}, \mathbf{v_i}, \mathbf{v_j}; t) = P^{(1)}_\mathbf{i}(n_\mathbf{i}, \mathbf{v_i}; t) P^{(1)}_\mathbf{j}(n_\mathbf{j}, \mathbf{v_j}; t), \tag{6.16}$$

$$P^{(1)}_\mathbf{i}(n_\mathbf{i}, \mathbf{v_i}; t) = p_\mathbf{i}(n_i; t) \prod_{k=1}^{d} P_{\mathbf{i},k}(v_{\mathbf{i},k}; t); \tag{6.17}$$

2. smoothness in space of averages of generic observables $F(n, v)$:

$$\langle F\rangle_{\mathbf{i}\pm\mathbf{e}_l,t} = \langle F\rangle(\mathbf{x},t) \pm \frac{1}{L}\frac{\partial}{\partial x_l}\langle F\rangle|_{(\mathbf{x},t)} + O(1/L^2), \tag{6.18}$$

being l a Cartesian direction $l \in \{1, d\}$.

With the hypothesis just stated, it is straightforward to perform averages and limits of the currents. At the first order, these read

$$\langle \mathbf{j}_{\mathbf{i},p}\rangle \to \frac{\Delta t}{\Delta x}\mathbf{j}^{\mathrm{av}}(\mathbf{x},t) \tag{6.19a}$$

$$\mathbf{j}^{\mathrm{av}}(\mathbf{x},t) = \rho(\mathbf{x},t)\left[1-\rho(\mathbf{x},t)\right]\mathbf{G}^{(0)}(\mathbf{x},t), \tag{6.19b}$$

$$\langle \mathsf{J}_{\mathbf{i},p}\rangle \to \frac{\Delta t}{\Delta x}\mathsf{J}^{\mathrm{av}}(\mathbf{x},t) \tag{6.20a}$$

$$\mathsf{J}^{\mathrm{av}}(\mathbf{x},t) = \rho(\mathbf{x},t)\left[1-\rho(\mathbf{x},t)\right]\mathsf{G}^{(1)}(\mathbf{x},t), \tag{6.20b}$$

$$\langle \mathbf{J}_{\mathbf{i},p}\rangle \to \frac{\Delta t}{\Delta x}\mathbf{J}^{\mathrm{av}}(\mathbf{x},t) \tag{6.21a}$$

$$\mathbf{J}^{\mathrm{av}}(\mathbf{x},t) = \rho(\mathbf{x},t)\left[1-\rho(\mathbf{x},t)\right]\mathbf{G}^{(2)}(\mathbf{x},t), \tag{6.21b}$$

where $\mathbf{G}^{(0)}$, $\mathsf{G}^{(1)}$ and $\mathbf{G}^{(2)}$ are defined as the hop vectors and tensor, respectively accounting for transport of particles, momentum and energy. They read

$$G_l^{(0)}(\mathbf{x},t) \equiv \int \mathrm{d}\mathbf{v} P(\mathbf{v};\mathbf{x},t) h(v_l), \tag{6.22a}$$

$$G_{kl}^{(1)}(\mathbf{x},t) \equiv \int \mathrm{d}\mathbf{v} P(\mathbf{v};\mathbf{x},t) h(v_l) v_k, \tag{6.22b}$$

$$G_l^{(2)}(\mathbf{x},t) \equiv \int \mathrm{d}\mathbf{v} P(\mathbf{v};\mathbf{x},t) h(v_l) \frac{1}{2}v^2. \tag{6.22c}$$

with $h(v_l) \equiv g(v_l) - g(-v_l)$.

We also take the averages of the gain/loss terms, which read

$$\left\langle n\mathbf{f}^{(1)}(\mathbf{v})(\mathbf{x},t)\right\rangle = \rho(\mathbf{x},t)\int \mathrm{d}\mathbf{v} P(\mathbf{v};\mathbf{x},t)\mathbf{f}^{(1)}(\mathbf{v}) \equiv \rho(\mathbf{x},t)\mathbf{f}^{s}(\mathbf{x},t) \tag{6.23}$$

$$\begin{aligned}\left\langle D^{(\mathrm{int})}(\mathbf{x},t)\right\rangle &= -d\rho^2(\mathbf{x},t)\int \mathrm{d}\mathbf{v}\mathrm{d}\mathbf{v}' P(\mathbf{v};\mathbf{x},t)P(\mathbf{v}';\mathbf{x},t)(\mathbf{v}-\mathbf{v}')\cdot\mathbf{f}^{(2)}(\mathbf{v},\mathbf{v}') \\ &\equiv -d\rho^2(\mathbf{x},t)\Delta^d(\mathbf{x},t)\end{aligned} \tag{6.24}$$

$$\left\langle D^{(\mathrm{self})}(\mathbf{x},t)\right\rangle = \rho(\mathbf{x},t)\int \mathrm{d}\mathbf{v} P(\mathbf{v};\mathbf{x},t)\mathbf{v}\cdot\mathbf{f}^{(1)}(\mathbf{v}) \equiv d\rho(\mathbf{x},t)\Delta_0^s(\mathbf{x},t) \tag{6.25}$$

$$\left\langle D^{(\mathrm{noise})}(\mathbf{x},t)\right\rangle = \rho(\mathbf{x},t)\int \mathrm{d}\mathbf{v} P(\mathbf{v};\mathbf{x},t)B(\mathbf{v}) \equiv d\rho(\mathbf{x},t)\Delta^n(\mathbf{x},t) \tag{6.26}$$

and - for the following - it is also useful to define

$$\Delta^s(\mathbf{x},t) \equiv \int \mathrm{d}\mathbf{v} P(\mathbf{v};\mathbf{x},t)\left[\mathbf{v}-\mathbf{u}(\mathbf{x},t)\right]\cdot\mathbf{f}^{(1)}(\mathbf{v})/d. \tag{6.27}$$

With the above assumptions and definitions, through a direct local averaging of Eqs. (6.5), (6.8) and (6.10) and in the large volume limit one gets the following hydrodynamic equations:

$$\partial_t \rho = -\nabla \cdot \mathbf{j}, \tag{6.28a}$$

$$\rho \partial_t \mathbf{u} = -\nabla \cdot \mathsf{J} + \mathbf{u}(\nabla \cdot \mathbf{j}) + \rho \mathbf{f}^s, \tag{6.28b}$$

$$\rho \partial_t T = \left(T - \frac{u^2}{d}\right) \nabla \cdot \mathbf{j} + \frac{2}{d} \mathbf{u} \nabla : \mathsf{J} - \frac{2}{d} \nabla \cdot \mathbf{J} - 2\rho^2 \Delta^d + 2\rho(\Delta^s + \Delta^n). \tag{6.28c}$$

Eqs. (6.28) are the most general hydrodynamic equations which can be derived for our system. Since we retained only the first order gradients from analytical expansion of averaged fields in (6.18), Eqs. (6.28) are equivalent to the "Euler" hydrodynamic equations (3.32). At this stage, their meaning is formal: we do not know the actual expressions of currents and source terms. These can be computed only once the specific forms of projection function $g(\sigma v_l)$, interaction $\mathbf{f}^{(2)}$, self-propulsion $\mathbf{f}^{(1)}$ and diffusion tensor B are given. Furthermore, we will see that the one-particle distribution must be specified to close the hydrodynamic equations at this order.

It is remarkable that, without any assumption on velocity distribution, the momentum current associated with interactions vanishes in Eq. (6.22b) at the leading order because of the interplay between Molecular Chaos ansatz and momentum conservation in continuum limit: indeed, if correlations are neglected, the exchange of momentum is symmetrical between two particle with the same one-particle distribution function at the leading order because of the smoothness ansatz (6.18). Thus, its expression is of the first order in spatial gradients and therefore subleading with respect to hopping terms. A clear derivation of this fact is given in Appendix B.2. The physical consequence of this result is the absence of viscosity in hydrodynamic equations at the leading order.

We now derive hydrodynamic equations for some specific microscopic rules. For the "natural active velocity" prescription, we have

$$\begin{aligned} G_l^{(0)}(\mathbf{x},t) &= \int \mathrm{d}\mathbf{v} P(\mathbf{v};\mathbf{x},t) v_l = u_l, \\ G_{kl}^{(1)}(\mathbf{x},t) &= \int \mathrm{d}\mathbf{v} P(\mathbf{v};\mathbf{x},t) v_l v_k = \langle v_l v_k \rangle, \\ G_l^{(2)}(\mathbf{x},t) &= \int \mathrm{d}\mathbf{v} P(\mathbf{v};\mathbf{x},t) v_l \frac{1}{2} v^2 = \frac{1}{2} \sum_{k=1}^{d} \left\langle v_l v_k^2 \right\rangle . \end{aligned} \tag{6.29}$$

The above quantities can be further simplified by defining a "stress" tensor

$$Q_{kl}(\mathbf{x},t) \equiv G_{kl}^{(1)}(\mathbf{x},t) - u_k(\mathbf{x},t) \mathbf{G}_l^{(0)}(\mathbf{x},t) = \int \mathrm{d}\mathbf{v} P(\mathbf{v};\mathbf{x},t) h(v_l) \left[v_k - u_k(\mathbf{x},t)\right] \tag{6.30}$$

and a "heat" vector

$$R_l(\mathbf{x},t) \equiv \int \mathrm{d}\mathbf{v} P(\mathbf{v};\mathbf{x},t) h(v_l) \left[\frac{1}{d} |\mathbf{v} - \mathbf{u}(\mathbf{x},t)|^2 - T(\mathbf{x},t)\right]. \tag{6.31}$$

Within the "natural active velocity" prescription, we have

$$\begin{aligned} G^{(1)}_{kl}(\mathbf{x},t) &= T(\mathbf{x},t)\delta_{kl} + u_k(\mathbf{x},t)u_l(\mathbf{x},t), \\ G^{(2)}_{l}(\mathbf{x},t) &= \langle v_l^3\rangle(\mathbf{x},t) + (d-1)u_l(\mathbf{x},t)T(\mathbf{x},t) + u_l(\mathbf{x},t)u^2(\mathbf{x},t) - u_l^3(\mathbf{x},t), \\ Q_{kl}(\mathbf{x},t) &= T(\mathbf{x},t)\delta_{kl}, \\ R_l(\mathbf{x},t) &= \frac{1}{d}\left[\langle v_l^3\rangle(\mathbf{x},t) - 3u_l(\mathbf{x},t)T(\mathbf{x},t) - u_l^3(\mathbf{x},t)\right], \end{aligned} \tag{6.32}$$

provided that the Cartesian components of the active velocity are statistically independent and that temperature is isotropic, i.e.

$$P(\mathbf{v};\mathbf{x},t) = \prod_{k=1}^{d} P_k(v_k;\mathbf{x},t) \quad , \quad \langle (v_k - u_k)^2\rangle = T \quad \forall k. \tag{6.33}$$

With the additional assumption that central odd velocity moments are zero, we get

$$\langle (v_l - u_l)^3\rangle = 0 \quad \Rightarrow \quad \langle v^3\rangle = 3Tu_l + u_l^3 \tag{6.34}$$

and, as a consequence, $G^{(2)}_l$ and R_l are simplified into

$$G^{(2)}_l(\mathbf{x},t) = \frac{1}{2}u_l(\mathbf{x},t)\left[(d+2)T(\mathbf{x},t) + u^2(\mathbf{x},t)\right] \quad , \quad R_l(\mathbf{x},t) = 0. \tag{6.35}$$

In conclusion, in the continuous limit, the balance Eqs. (6.5), (6.7) and (6.10) with the average currents and noise terms for the case of "natural active velocity" read

$$\partial_t \rho = -\nabla\cdot\left[\rho\,(1-\rho)\,\mathbf{u}\right], \tag{6.36a}$$

$$\rho\partial_t \mathbf{u} = -\left\{\nabla\left[\rho\,(1-\rho)\,T\right] + \rho\,(1-\rho)\,(\mathbf{u}\cdot\nabla)\,\mathbf{u}\right\} + \rho\mathbf{f}^s, \tag{6.36b}$$

$$\rho\partial_t T = -\rho\,(1-\rho)\left[\frac{2}{d}T\,\nabla\cdot\mathbf{u} + (\mathbf{u}\cdot\nabla)\,T\right] - 2\rho^2\Delta^d + 2\rho\,(\Delta^s + \Delta^n). \tag{6.36c}$$

These equations are completely analogous to Euler equations (3.32), except for the terms $\rho(1-\rho)$ appearing in the currents: their presence clarify the meaning of our "active velocity" $\mathbf{v}_i$, which as explained above is not equivalent to the actual infinitesimal displacement of the particle. The excluded volume can be seen as a modification of particle mobility, which is vanishing in the dense case $\rho \to 1$. On the contrary, in the dilute limit $\rho \to 0$ this is not a relevant difference, but it can be appreciated at relatively moderate densities.

We now specify the interaction, self-propulsion and noise terms: the former is taken as

$$\mathbf{f}^{(2)}(\mathbf{v},\mathbf{v}') = \omega_d(\mathbf{v}-\mathbf{v}'). \tag{6.37}$$

This choice deserves some justification: indeed, it shows a sort of "elastic" behavior between velocities of nearest-neighbor particles. Actually, this choice of interaction yield two main properties

1. it mimics the behavior of Kuramoto and Vicsek aligning interactions, with a stable fixed point for $\mathbf{v} = \mathbf{v}'$;

2. it is a source of dissipation because, as we will see, it yields $\Delta^d > 0$.

The interaction in (6.37) is a deterministic force and the result of a compromise between Vicsek model and granular collisions. It must be stressed that the interactions are acting *continuously* instead than being *instantaneous* as for granular hard spheres: this is an important difference with respect to our previous granular model. Also, the characteristic frequency ω_d cannot be directly associated to the restitution coefficient α, and there is no elastic limit for this kind of interaction. However, the comparison between granular and active hydrodynamic equations allows a mapping of inelastic collisions into Vicsek-like force (6.37). Moreover, a further version of the active model may easily include granular collisions as an instantaneous process, with the same procedure described in Sec. 4.2.1 and 6.1.3.

Self-propulsion is taken as

$$\mathbf{f}^{(1)}(\mathbf{v}) = \omega_s \mathbf{v}\left(1 - \frac{v^2}{v_s^2}\right) \tag{6.38}$$

which has the same form of *Rayleigh-Helmoltz* viscosity introduced in Sec. 2.2.3. The effect of self-propulsion is to push the particles towards the stable fixed point $v = v_s$; on the contrary, the fixed point $v = 0$ is unstable. The self-propulsion doesn't change the direction or orientation of the velocity, but rather acts only on its magnitude. The analytical solution of motion equation $\dot{\mathbf{v}} = \mathbf{f}^{(1)}(\mathbf{v})$ is given in Appendix B.1.

Finally, we choose an isotropic and constant diffusion tensor $\mathsf{B}(\mathbf{v})$, namely

$$B_{kl}(\mathbf{v}) = \sqrt{2D}\delta_{kl} \tag{6.39}$$

defining the *diffusivity* D. For all these choice of microscopic features, the average source terms read

$$f_k^s(\mathbf{x},t) = \omega_s u_k(\mathbf{x},t)\left[1 - \frac{1}{v_s^2}\left((d+2)T(\mathbf{x},t) + u^2(\mathbf{x},t)\right)\right], \tag{6.40a}$$

$$\Delta^d(\mathbf{x},t) = 2d\,\omega_d T(\mathbf{x},t), \tag{6.40b}$$

$$\Delta^s(\mathbf{x},t) = \omega_s T(\mathbf{x},t)\left[1 - \frac{d+2}{v_s^2}\left(T(\mathbf{x},t) + \frac{1}{d}u^2(\mathbf{x},t)\right)\right], \tag{6.40c}$$

$$\Delta^n(\mathbf{x},t) = D, \tag{6.40d}$$

where the first and third equations, stemming from self-propulsion force in (6.38), have been derived under the *Local Equilibrium assumption*, namely

$$P(\mathbf{v};\mathbf{x},t) = [2\pi T(\mathbf{x},t)]^{-d/2}\exp\left[-|\mathbf{v}-\mathbf{u}(\mathbf{x},t)|^2/2T(\mathbf{x},t)\right] \tag{6.41}$$

because of the presence of $\langle v^4\rangle$ terms in the averages.

Substituting the above expressions into Eqs. (6.36) we get the average hydrodynamic equations with the above specified prescriptions and the Local Equilibrium

assumption, which read

$$\partial_t \rho = -\nabla \cdot [\rho (1-\rho) \mathbf{u}], \tag{6.42a}$$

$$\rho \partial_t \mathbf{u} = -\{\nabla [\rho (1-\rho) T] + \rho (1-\rho) (\mathbf{u} \cdot \nabla) \mathbf{u}\} + \rho \omega_s \mathbf{u} \left[1 - \frac{1}{v_s^2} \left((d+2)T + u^2\right)\right], \tag{6.42b}$$

$$\rho \partial_t T = -\rho (1-\rho) \left[\frac{2}{d} T \nabla \cdot \mathbf{u} + (\mathbf{u} \cdot \nabla) T\right] - 4 d \omega_d \rho^2 T + 2 \rho \omega_s T \left[1 - \frac{d+2}{v_s^2} \left(T + \frac{1}{d} u^2\right)\right] + 2 \rho D. \tag{6.42c}$$

6.2.1 Homogeneous fixed points

We look at the fixed points of hydrodynamic equations (6.36). Our case of study is the homogeneous case, in analogy with the HCS described in the granular model. Homogeneity greatly simplify hydrodynamic equations, which now read

$$\begin{cases} \dot{\rho} = 0 \\ \dot{\mathbf{u}} = \mathbf{f}^s \\ \dot{T} = -2\rho \Delta^d + 2 (\Delta^s + \Delta^n) \end{cases} \tag{6.43}$$

Thus, the homogeneous density is constant and equivalent to the packing fraction $\rho \equiv \phi$. The stationary velocity and temperature must satisfy the condition of vanishing self-propulsion and balancing energy source terms. For the specific choice of Eqs. (6.40), one has

$$\begin{cases} \dot{u} = \omega_s u \left\{1 - \frac{1}{v_s^2} \left[(d+2)T + u^2\right]\right\} \\ \dot{T} = -4 d \, \phi \omega_d T + 2 \omega_s T \left[1 - \frac{d+2}{v_s^2} \left(T + \frac{1}{d} u^2\right)\right] + 2D \end{cases}, \tag{6.44}$$

where $u = |\mathbf{u}|$ is the speed field. Now, we move to adimensional variables, defining

$$\begin{aligned} \tilde{t} &= \omega_s t \\ \tilde{x} &= (\omega_s / v_s) x \\ \tilde{\mathbf{u}} &= \mathbf{u} / v_s \\ \tilde{T} &= t / v_s^2 \\ \gamma &= \omega_d / \omega_s \\ \Gamma &= D / (\omega_s v_s^2) \end{aligned} \tag{6.45}$$

which will be used in the rest of the chapter, and the tilde will be omitted for the sake of simplicity. The physical parameters of our system can now be defined:

1. the *packing fraction* or density ϕ

2. the relative dissipation γ, i.e. the ratio of dissipation and self-propulsion characteristic frequencies

3. the relative noise Γ, measuring the amplitude of noise with respect to self-propulsion strength

Under the assumptions stated until now, the behavior of the system is completely determined by these parameters together with the boundary conditions (which we always take as periodic).

Homogeneous dimensionless equations have the same form of Eqs. (6.44), because only constant coefficients have been redefined. We observe that there are three possible fixed points

1. A *disordered* fixed point (u_0, T_0), where particles are moving with zero mean velocity but positive temperature, so cooling is avoided. This is similar to a gas of granular particles in presence of a bulk driving, without collective motion. The fixed points read

$$u = 0 \quad , \quad T = T_0 = \frac{1 - 2d\phi\gamma + \sqrt{(1 - 2d\phi\gamma)^2 + 4(d+2)\Gamma}}{2(d+2)} \tag{6.46}$$

   The presence of noise is determinant: indeed, for $\Gamma = 0$, the temperature is positive only until $\gamma < 1/(2d\phi)$. For higher values of dissipation, the stationary solution reads $T = 0$ and self-propulsion cannot prevent the system from cooling. On the contrary, when $\Gamma > 0$ the disordered fixed point is always present.

2. Two *ordered* fixed points $(u_\pm, T_\pm)$, with $u_\pm > 0$. They exist if

$$\Gamma < \frac{(1 + 2d^2\phi\gamma)^2}{2d(d+2)}. \tag{6.47}$$

   and are given by

$$\begin{aligned} u_\pm^2 &= \frac{1}{2}\left(1 - 2d^2\phi\gamma \mp \sqrt{(1 + 2d^2\phi\gamma)^2 - 2d(d+2)\Gamma}\right) \\ T_\pm &= \frac{1 + 2d^2\phi\gamma \pm \sqrt{(1 + 2d^2\phi\gamma)^2 - 2d(d+2)\Gamma}}{2(d+2)} \end{aligned} \tag{6.48}$$

   The first point (u_-, T_-) exists only if $\gamma < 1/(2d^2\phi) \ \vee \ \Gamma < 4d/(d+2)\phi\gamma$. The second point (u_+, T_+) exists only if $\gamma < 1/(2d^2\phi) \ \wedge \ \Gamma > 4d/(d+2)\phi\gamma$.

The existence of fixed points with $u > 0$ suggests the presence of a stationary *swarming* state, where a macroscopic collective motion arises spontaneously breaking the rotational symmetry because in every trajectory the units move together in a random direction. This is actually observed in simulations. However, it must be underlined that homogeneous equations (6.44) have been derived under the Local Equilibrium assumption with a Gaussian distribution, which may have nothing to do with the distribution of the swarming state. On the other hand, the Local Equilibrium assumption is expected to be physically consistent in the disordered state, so we focus on its stability.

6.2.2 Stability analysis of the disordered state

We introduce small, spatially dependent fluctuations around the fully disordered fixed point as

$$\begin{aligned}\delta\rho &= \rho(\mathbf{x},t) - \phi \\ \delta\mathbf{u} &= \mathbf{u}(\mathbf{x},t) \\ \delta T &= T(\mathbf{x},t) - T_0\end{aligned} \tag{6.49}$$

Linearized hydrodynamic equations now read

$$\partial_t \delta\rho = -\phi\,(1-\phi)\,\nabla\cdot\delta\mathbf{u} \tag{6.50a}$$

$$\partial_t \delta\mathbf{u} = -\frac{1-2\phi}{\phi} T_0 \nabla\delta\rho + C(\gamma,\Gamma)\delta\mathbf{u} - (1-\phi)\nabla\delta T \tag{6.50b}$$

$$\partial_t \delta T = -4d\gamma T_0 \delta\rho - \frac{2}{d}(1-\phi)T_0\nabla\cdot\delta\mathbf{u} - 2r(\gamma,\Gamma)\delta T \tag{6.50c}$$

with

$$\begin{aligned} r(\gamma,\Gamma) &= \sqrt{(1-2d\phi\gamma)^2 + 4(d+2)\Gamma} \\ C(\gamma,\Gamma) &= \frac{1}{2}\left(1 + 2d\phi\gamma - r(\gamma,\Gamma)\right). \end{aligned} \tag{6.51}$$

After converting to Fourier space, decomposing $\hat{\mathbf{u}}_\mathbf{k}$ in a parallel (to $\mathbf{k}$) and $d-1$ transverse components $(\hat{u}^{\parallel}_\mathbf{k}, \hat{\mathbf{u}}^{\perp}_\mathbf{k})$, and defining $\hat{\mathbf{\Psi}}_\mathbf{k} = (\hat{\rho}_\mathbf{k}, \hat{u}^{\parallel}_\mathbf{k}, \hat{\mathbf{u}}^{\perp}_\mathbf{k}, \hat{T}_\mathbf{k})$, the time-evolution of the modes linearized near that fixed point reads

$$\partial_t \hat{\mathbf{\Psi}}_\mathbf{k} = \mathsf{L}(\mathbf{k})\hat{\mathbf{\Psi}}_\mathbf{k}, \tag{6.52}$$

with $\mathsf{L}(\mathbf{k})$ equal to

$$\begin{pmatrix} 0 & -\phi(1-\phi)2\pi ik & 0 & 0 \\ -\frac{1-2\phi}{\phi}T_0 2\pi ik & C(\gamma,\Gamma) & 0 & -(1-\phi)2\pi ik \\ 0 & 0 & C(\gamma,\Gamma) & 0 \\ -4d\gamma T_0 & -\frac{2}{d}(1-\phi)T_0 2\pi ik & 0 & -2r(\gamma,\Gamma) \end{pmatrix}. \tag{6.53}$$

The first outcome is that the shear mode - which is reminiscent of swarming phases - separates from other modes and it is stable only when $C(\gamma,\Gamma) < 0$, i.e.

$$\Gamma > \frac{2d}{d+2}\phi\,\gamma. \tag{6.54}$$

Shear modes are stabilized by large enough noise Γ, with the threshold decreasing linearly with the relative dissipation rate γ. At zero dissipation the shear mode is stable for any non-zero noise amplitude. Conversely, at zero noise amplitude, the shear mode is *always* unstable. Noticeably, in the absence of a k-dependent

competing mechanism for stability (such as shear viscosity), stability of the shear mode is lost synchronously at any k. In Sec. 6.4 it will be numerically shown how shear instability is a strong signal of the appearance of a swarming state.

Numerical analysis of the eigenvalues of $\mathsf{L}(\mathbf{k})$ reveals that at a given γ, at least in the range $0 < \gamma < 1/(2\phi)$, the eigenvalue associated with shear is the first to change sign when Γ is reduced, i.e. shear instability is the leading one. Being such a result the outcome of linear stability analysis, it does not imply that the bifurcation leads the system to a macroscopic shear-like state: we can only claim that the fully disordered state is replaced by a different state which - at the beginning - looks ordered in the velocity field.

6.3 Fluctuating hydrodynamics

The last analytical result on the active model is the derivation of fluctuating currents. Hydrodynamic equations (6.28) can be seen as fluctuating hydrodynamics equations; the microscopic currents $\mathbf{j}$, J and $\mathbf{J}$ depend both upon the "fast" variables $\boldsymbol{\xi}_p$, $\boldsymbol{\zeta}_p$ and the "slow" variables $n_{\mathbf{i},p}$, $\mathbf{v}_{\mathbf{i},p}$. Therefore, analogously with Sec. 4.4.1, at finite L the non-averaged currents can be written as the sum of their averages over the fast variables plus remainders. In particular we can write

$$j_l(\mathbf{x},t) = \overline{j_l}(\mathbf{x},t) + \sigma_l(\mathbf{x},t), \tag{6.55a}$$
$$\mathsf{J}_{kl}(\mathbf{x},t) = \overline{\mathsf{J}_{kl}}(\mathbf{x},t) + \varsigma_{kl}(\mathbf{x},t), \tag{6.55b}$$
$$J_l(\mathbf{x},t) = \overline{J_l}(\mathbf{x},t) + \Sigma_l(\mathbf{x},t). \tag{6.55c}$$

for density, momentum and energy respectively. The terms σ_l, ς_{kl} and Σ_l are current noises with zero average. Similarly to the granular case, the correlations and Gaussianity of the noises can be directly computed from microscopic evolution.

The current's noise correlations in Eqs. (6.55) can be deduced from microscopic dynamics, in a the same way as the one used in Sec. 4.4.2 for the granular model. We here focus on the fluctuations of density current, since the derivation of the others follows the same procedure. First of all, one has in discrete space and time variables

$$\langle \sigma_{\mathbf{i},p,l}\sigma_{\mathbf{i}',p',l'}\rangle \sim \langle j_{\mathbf{i},p,l}j_{\mathbf{i}',p',l'}\rangle \tag{6.56}$$

With the definition in (6.6) and the "natural active velocity" prescription, only the diagonal terms are non vanishing and expanding fluctuations in Δt and Δx one obtains

$$\langle j_{\mathbf{i},p,l}j_{\mathbf{i}',p',l'}\rangle = \delta_{\mathbf{i},\mathbf{i}'}\delta_{p,p'}\delta_{l,l'}\,\rho_{\mathbf{i},p}(1-\rho_{\mathbf{i},p})\,\langle|v_l|\rangle_{\mathbf{i},p}\,\frac{\Delta t}{\Delta x} \tag{6.57}$$

hence the current's noise is white in space, time and components; its derivation can be found in Appendix B.3. This expression is meaningful if $\Delta t \ll \Delta x$, introducing a constraint in hydrodynamic scaling.

From Eq. 6.19a, the hydrodynamic limit of the currents reads

$$j_l(\mathbf{x},t) = \frac{\Delta x}{\Delta t} j_{\mathbf{i},p,l} \tag{6.58}$$

and delta functions in continuum limit become

$$\delta_{\mathbf{i},\mathbf{i}'} = \delta(\mathbf{x}-\mathbf{x}')(\Delta x)^d \qquad , \qquad \delta_{p,p'} = \delta(t-t')\Delta t, \tag{6.59}$$

therefore eq. (6.57) reads

$$\langle j_l(\mathbf{x},t) j_{l'}(\mathbf{x}',t)\rangle = \delta(\mathbf{x}-\mathbf{x}')\delta(t-t')\delta_{l,l'}\,\rho(\mathbf{x},t)[1-\rho(\mathbf{x},t)]\,\langle|v_l|\rangle\,(\mathbf{x},t)(\Delta x)^{d+1}. \tag{6.60}$$

With the Gaussian velocity assumption, one finally finds

$$\langle \sigma_l(\mathbf{x},t)\sigma_{l'}(\mathbf{x}',t')\rangle \sim \delta(\mathbf{x}-\mathbf{x}')\delta(t-t')\delta_{l,l'}\rho(\mathbf{x},t)[1-\rho(\mathbf{x},t)]\sqrt{\frac{2}{\pi}T(\mathbf{x},t)}(\Delta x)^{d+1}. \tag{6.61}$$

This result can be generalized to momentum and energy currents given by hopping particles; indeed, computing the current noise correlation $\eta_l^{(\chi)}$ for the generic transported quantity $\chi(n,v)$, with analogous steps one has

$$\left\langle \eta_l^{(\chi)}(\mathbf{x},t)\eta_l^{(\chi)}(\mathbf{x}',t')\right\rangle \sim \delta(\mathbf{x}-\mathbf{x}')\delta(t-t')\delta_{l,l'}\,\left\langle n(1-n)\chi^2(n,v)\,|v_l|\right\rangle(\mathbf{x},t)\,(\Delta x)^{d+1}, \tag{6.62}$$

always considering the leading term in Δt and Δx expansion. Interaction terms in eqs. (6.9), (6.11) are subleading and therefore do not appear at this level. The explicit expressions for momentum and energy are straightforward and read

$$\langle \varsigma_l(\mathbf{x},t)\varsigma_{l'}(\mathbf{x}',t')\rangle \sim \delta(\mathbf{x}-\mathbf{x}')\delta(t-t')\delta_{l,l'}\rho(\mathbf{x},t)[1-\rho(\mathbf{x},t)]\,\langle|v_l|v_k v_{k'}\rangle\,(\Delta x)^{d+1}, \tag{6.63}$$

$$\langle \Sigma_l(\mathbf{x},t)\Sigma_{l'}(\mathbf{x}',t')\rangle \sim \delta(\mathbf{x}-\mathbf{x}')\delta(t-t')\delta_{l,l'}\rho(\mathbf{x},t)[1-\rho(\mathbf{x},t)]\left\langle|v_l|\left(\frac{v^2}{2}\right)^2\right\rangle(\Delta x)^{d+1}. \tag{6.64}$$

Having shown that fluctuating currents are white and having found their amplitudes, we can show they are Gaussian. Again, the procedure adopted is equivalent to the one used in Sec. 4.4.3. Considering the rescaled current $\hat{\jmath}_l = \hat{\jmath}_l^{\mathrm{av}} + \hat{\sigma}_l = (\Delta x)^{(d-1)/2} j_l$, from previous results we have that

$$\langle \hat{\sigma}_l(\mathbf{x},t)\rangle = 0, \tag{6.65a}$$

$$\langle \hat{\sigma}_l(\mathbf{x},t)\hat{\sigma}_{l'}(\mathbf{x}',t')\rangle \sim \delta(\mathbf{x},\mathbf{x}')\delta(t-t')\delta_{l,l'}\mathcal{A}_l^{(2)}(\mathbf{x},t) \tag{6.65b}$$

where $\mathcal{A}_l^{(2)}(\mathbf{x},t)$ is the rescaled amplitude of the second cumulant, which is finite when rescaling the current. For the generic cumulant of order n, we get

$$\begin{aligned}\langle \hat{\sigma}_{l_1}(\mathbf{x}_1,t_1)\cdots\hat{\sigma}_{l_n}(\mathbf{x}_n,t_n)\rangle \sim \prod_{i=1}^{n-1}\left[\delta(\mathbf{x}_i-\mathbf{x}_{i+1})\delta(t_i-t_{i+1})\delta_{l_i,l_{i+1}}\right] \\ \times\,\mathcal{A}_{l_1}^{(n)}(\mathbf{x}_1,t_1)\,(\Delta x)^{(d+1)(\frac{n}{2}-1)}\end{aligned} \tag{6.66}$$

which is non vanishing in the hydrodynamic limit only when $n=2$, because amplitudes $\mathcal{A}_l^{(n)}$ are all finite. Rescaled noise $\hat{\sigma}_l$ is Gaussian in the large size limit and therefore the original noise σ_l is Gaussian too.

6.4 Numerical results

Simulations of the system have shown the existence of two macroscopically ordered states:

1. a *swarming* state, where particles align their velocities and walk across the lattice as a global swarm;
2. a *clustering* state, where a macroscopic fraction of the particles group and form a large, standing aggregate when they all point towards the center of the cluster.

A swarming and a clustering order parameters are defined and their evolution is studied and compared with linear stability analysis of Sec. 6.2.2. A preliminary study on the finite-size behavior suggests that the disorder-swarming transition may be discontinuous in the infinite size limit. Finally, the amplitude of density fluctuating current is computed and compared with theoretical predictions.

6.4.1 General simulation strategy

The simulation strategy for our active model is similar to the one used for the granular model. We reproduced M stochastic trajectories of a system of N particles on a $2d$ periodic square lattice each one defined at a discrete position $\mathbf{r}_i(t) \in \Lambda$ and carrying a continuous $2d$ velocity $\mathbf{v}_i(t)$. For each trajectory, the system starts with a uniform distribution in space and a random extraction of velocities normally distributed with $\langle v_l \rangle = 0$ and $\langle v_l^2 \rangle = T_0$, being T_0 the stationary temperature of the disordered state defined in Eq. (6.46). At each time step Δt, a random uniform number $\chi \in [0, 1]$ is drawn and its value indicates the particle eventually hopping, according to the "natural active velocity" prescription in (6.3): the normalization of the probability yields a constraint on the time interval, which we took $\Delta t \leq (10NL)^{-1}$ to guarantee that the total probability of a hop is $P_h \leq 1$, where P_h is defined as

$$P_h = \sum_{i=1}^{N} \sum_{\substack{l=1,2 \\ \sigma=\pm 1}} (1 - n_{\mathbf{r}_i(t)+\sigma\mathbf{e}_l}) g(\sigma v_{i,l}) \frac{\Delta t}{\Delta x} \tag{6.67}$$

The condition $P_h < 1$ has been verified throughout the simulations: it is reasonable to think that the self-propulsion force is lowering high-velocities tails. Simulations have been carried out for several values of γ and Γ and densities ϕ of 1%, 5% and 10%, since we are interested in the dilute limit. The lattice size has been taken $L = 100$ ($V = 10^4$ sites), except the case of finite-size effects where the size is changed keeping the density constant.

6.4.2 Swarming instability

Fig. 6.2 displays the arising of swarming states in the model. These can be identified through the usual swarming order parameter $r(t)$ identified to be

$$r(t) = \left| \frac{1}{N} \sum_{j=1}^{N} e^{i\theta_j(t)} \right|, \tag{6.68}$$

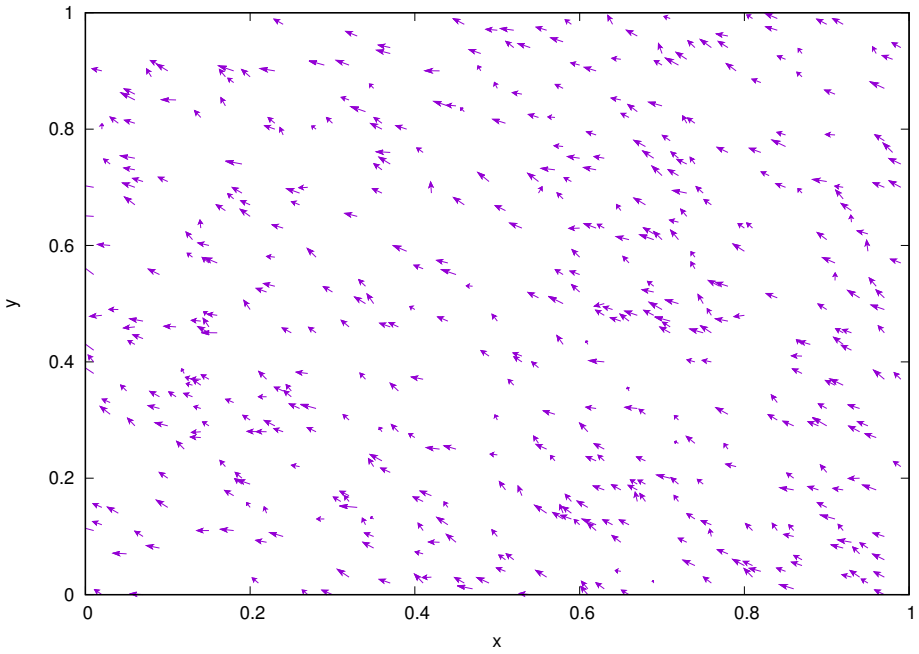

Figure 6.2. A snapshot of the system configuration in the homogeneous swarming regime. Here $\phi = 0.05$, $\gamma = 9$, $\Gamma = 0.135$, and the order parameters result to be $r = 0.994$ (strong swarming) and $C = 0.057$ (negligible clustering).

where θ_j is the direction of velocity of the j-th particle, so that $r(t) \approx 0$ in the fully disordered state and ≈ 1 in the case of all particles' velocities aligned along the same direction.

Monitoring $r(t)$ up to times $t_{\max}$ larger than the inverse of the minimum of the eigenvalues of $\mathsf{L}(\mathbf{k})$ gives a reasonable idea of the fate of this initial condition and allows us to compare the system's phase diagram with the predictions of linear stability analysis. In Fig. 6.3 we show the swarming order parameter r, averaged over the time interval $[t_{\max}/2, t_{\max}]$ so that the system has settled in the stationary regime, for three values of the density ϕ, together with the line predicted in Eq. (6.54). Comparison is fair at all values of ϕ, especially for $\phi = 0.05$. We argue that this value matches our analysis because it is the best compromise between the dilute and the large size limits at fixed volume V: on the contrary, for $\phi = 0.01$ there are $N = 100$ particles in the lattice, and for such a small value the fluctuations seem relevant; nevertheless, for $\phi = 0.1$ we have $N = 1000$ particles, so the fluctuations decrease but at the same time we move away from the dilute limit.

6.4.3 Clustering instability

Clustering is another ordered phase observed in our simulation. Contrarily from swarming, clustering is nonhomogeneous: typically, active units form a single, giant aggregate somewhere in the lattice while the rest of them swarm around, occasionally falling on the cluster or kicking away some particles at its borders. The typical clustered state in shown in Fig. 6.4.

In simulations, we can count the number $N_l(t)$ of pairs of first neighbors at time

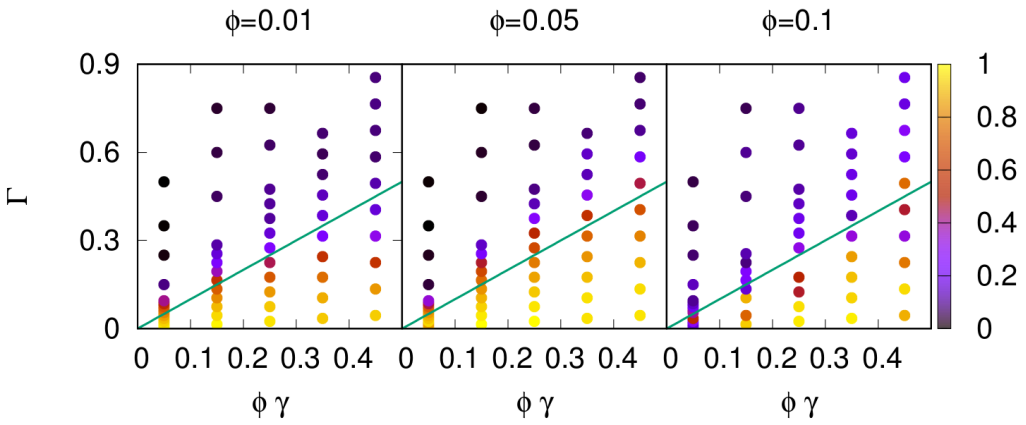

Figure 6.3. Swarming phase parameter r (which goes from 0 in the disordered phase to 1 in the full swarming phase, see color legend on the right) as a function of relative noise amplitude Γ and rescaled relative dissipation rate $\phi\gamma$ at three different average densities ϕ. The solid lines indicate the theoretical transition, Eq. (6.54).

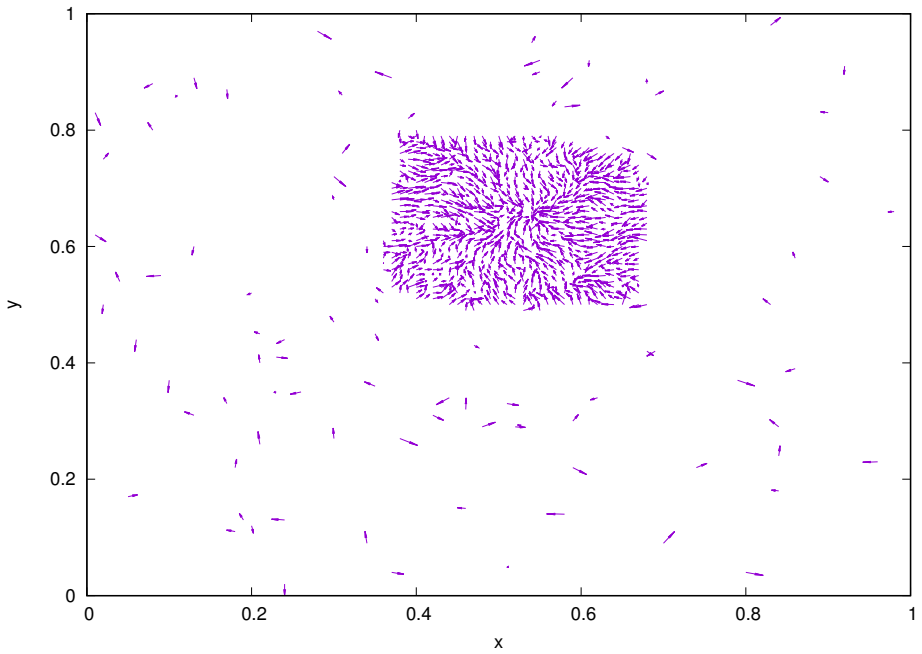

Figure 6.4. A snapshot of the system configuration in the coexistence regime "cluster+gas". Here $\phi = 0.1$, $\gamma = 1.5$, $\Gamma = 4.5$, and the order parameters result to be $r = 0.027$ (negligible swarming) and $C = 0.874$ (macroscopic clustering).

t, a number that goes from $N_l \approx 2\phi N$ in the unclustered case, up to $N_l \approx 2N$ in the fully clustered case, so that

$$C(t) = \frac{N_l(t)}{2N} \in [\phi, 1] \tag{6.69}$$

is a good estimate of the clustering degree in the system. Of course, this parameter

is significant only in dilute cases, with $\phi \ll 1$. We study the clustering together with the swarming and find a phase diagram in the $(\gamma - \Gamma)$ plane similarly as before, see Fig. 6.5.

It is clear that in the dilute cases, roughly speaking $\phi < 10\%$, there is no clustering in both disordered and swarming phases (i.e. above and below the solid line, see also Fig. 6.3).

On the contrary, at larger packing fraction $\phi \geq 10\%$ we observe the appearance of clustering as a stable phase *above* the critical noise amplitude for swarming. Looking at real configurations in the simulations - see Fig. 6.4 - we can attempt an interpretation: it seems that when swarming is possible (e.g. below the transition line), many particles in the dilute phase coordinate and erode efficiently the clusters. This is a sort of of "viscous heating" mechanism.

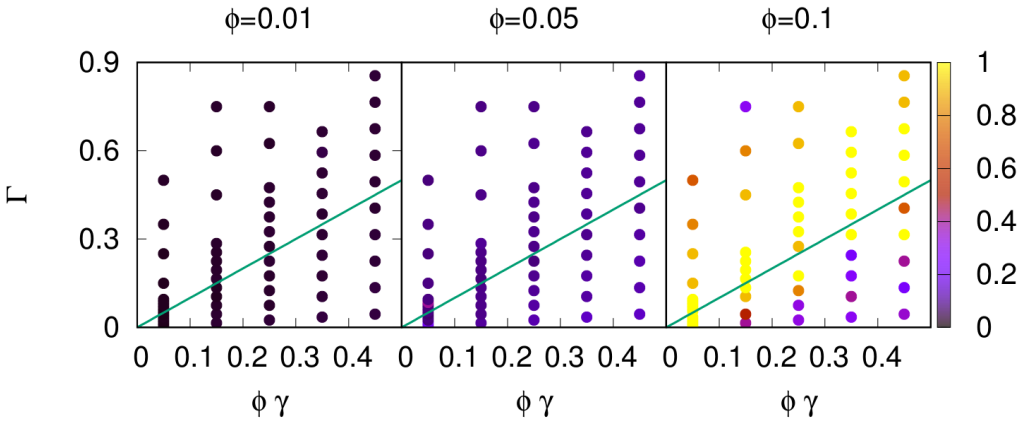

Figure 6.5. Clustering phase parameter C (see color legend on the right) as a function of relative noise amplitude Γ and rescaled relative dissipation rate $\phi\gamma$ at three different average densities ϕ. The solid lines indicate the swarming theoretical transition, Eq. (6.54).

6.4.4 Finite-size effects near the transition

We performed a preliminary study of the effect of lattice volume V in order to assess the quality of the observed gas-swarming transition in the dilute case. We have chosen a dilute value of ϕ and an average value of γ and measured the swarming parameter $\langle r \rangle$ when moving from high noise $\Gamma > \Gamma_c(\gamma, \phi)$ to low noise $\Gamma > \Gamma_c(\gamma, \phi)$, where $\Gamma_c(\gamma, \phi) = \frac{2d}{d+2}\gamma\phi$ (see Eq. (6.54)), repeating this protocol for increasing value of V. If the transition is discontinuous in the continuum limit, we expect that the separation between the swarming phase (high $\langle r \rangle$) and the disordered phase (low $\langle r \rangle$) increases with V. The result of the study is shown in Fig. 6.6. It indicates that the gap $r_+ - r_-$ between the value of r just above and just below the transition tends to increase with V. Based upon this result, we conjecture that the observed transition is discontinuous.

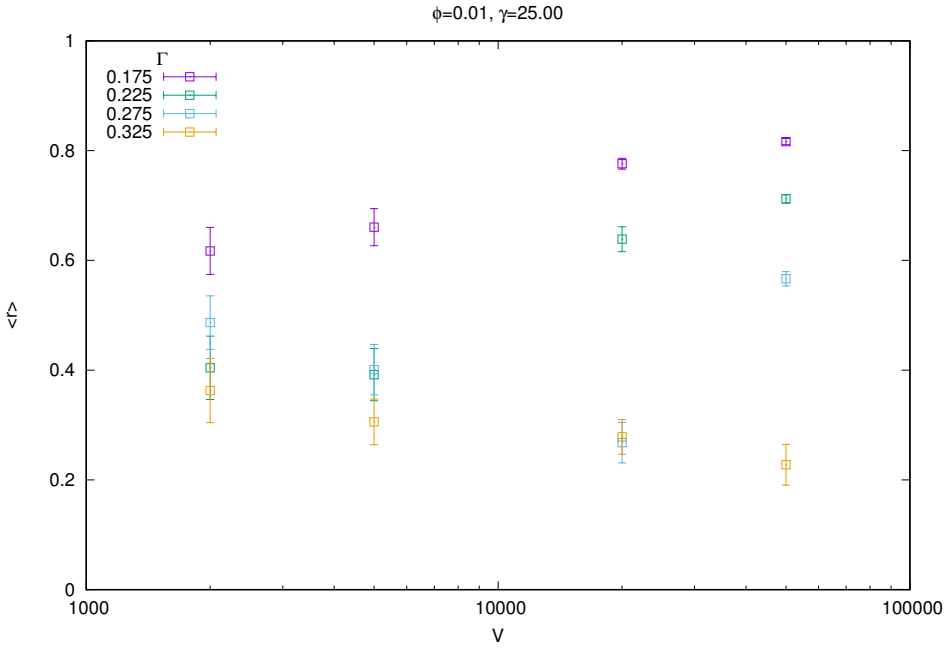

Figure 6.6. Average value of the swarming parameter r, which goes from 0 in the disordered phase to 1 in the full swarming phase, as a function of the lattice volume V at a constant value of ϕ (dilute case) and γ, for four values of the relative noise amplitude Γ: two values are below the instability swarming threshold, two are above.

6.4.5 Fluctuating currents

Numerical simulations have been also implemented in order to verify the prediction about current noises, defined in Eq. (6.55). In the case of Gaussian local velocity distribution, the noise correlation for the hopping current reads

$$\langle \sigma_l(\mathbf{x},t)\sigma_{l'}(\mathbf{x}',t')\rangle = \delta(\mathbf{x}-\mathbf{x}')\delta(t-t')\delta_{l,l'}\phi(1-\phi)\sqrt{\frac{2}{\pi}T(t)}\,(\Delta x)^{d+1}\,. \tag{6.70}$$

In the simulation we measure the microscopic current $j_{i,p,l} = 0, \pm 1$, representing the number of particles hopping - in the p-th time step - from site i to its neighbors in the l-th direction. In the homogeneous fully disordered state, Eq. (6.70) is equivalent, assuming ergodicity, to

$$\sum_{i,i'}^{1,V}\sum_{p,p'}^{1,t_{max}/\Delta t} j_{i,p,l}j_{i',p',l'} \simeq L^3\phi(1-\phi)\sqrt{\frac{2}{\pi}T_0}\;\; t_{max}. \tag{6.71}$$

The verification of this relation is shown in Fig. 6.7: we see that for $\phi < 10\%$ the simulation tends to the theoretical value as $L \to \infty$. This trend is broken when $\phi > 10\%$, as expected in view of the used assumptions (Molecular Chaos and local Gaussian equilibrium) which are reasonable only in the dilute limit.

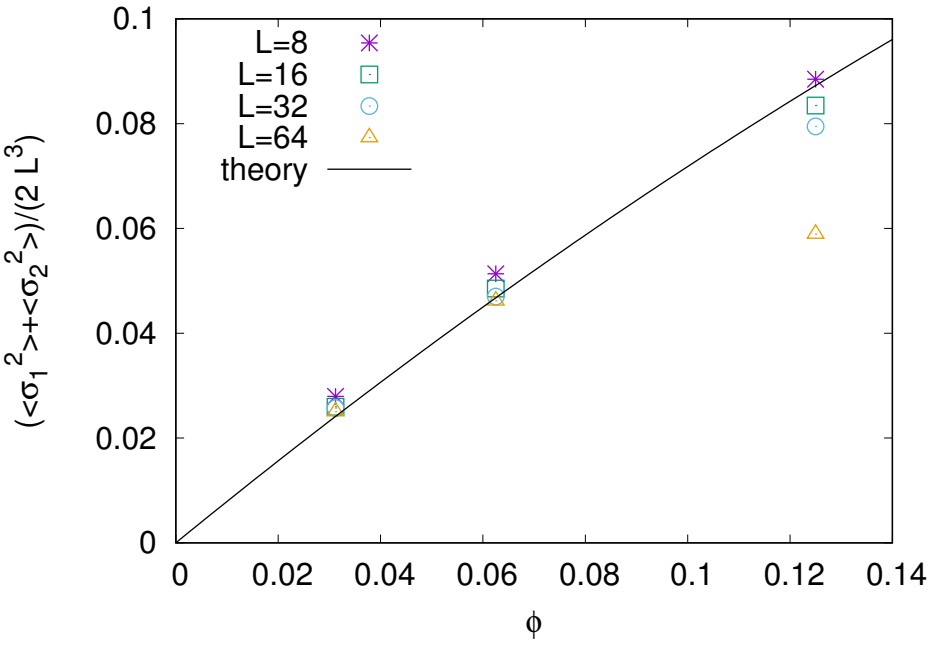

Figure 6.7. Amplitude of fluctuations of the hopping current (symbols), and its theoretical prediction Eq. (6.70)-(6.71) (solid line), as function of ϕ for various sizes L. Here $\phi\gamma = 0.25$, $\Gamma = 4$ and the system is prepared at the steady temperature $T_0 = 1$.

Conclusions

In this thesis, we first of all reviewed the main properties of granular and active matter, underlining remarkable similarities between their physical behavior. The properties of their individual and collective motion have been analyzed in the framework of nonequilibrium statistical mechanics. Experiments and simulations suggested us a specularity between granular and active particles, especially because of the continuous energy exchanges driving the systems out of equilibrium and leading to the observed collective motion. Hydrodynamics has been introduced to describe the macroscopic behavior of fluid systems. Indeed, when many active or granular units are present, they can be seen as a flowing material under some assumptions. A derivation of hydrodynamics for conservative systems has been introduced and later extended to the granular case, while the recent developments on hydrodynamic descriptions of active matter have been reviewed. Finally, we introduced lattice models as a powerful tool to analyze theoretically the behavior of nonequilibrium systems. My thesis' work has been focused on the analysis of granular and active matter through the formulation of two lattice models.

The first model we introduced is a lattice model of granular particles on a linear chain. A hydrodynamic description of the system has been derived: although some realism has been sacrificed in the formulation of the model, the latter has reproduced the average hydrodynamic equations derived from kinetic theory of sheared granular gases. The characteristic granular states like the Homogeneous Cooling State, the Uniform Shear Flow and the Couette Flow have been derived and hydrodynamic equations have been solved for each case, even in the transient or non-homogeneous state. The Homogeneous Cooling instability was recovered, obtaining exact expression for the critical value of dissipation and system size. We derived the fluctuating hydrodynamic currents and computed their noise properties at the leading order from microscopic dynamics, without the need of an equilibrium approximation: the latter has been used only in some cases of need to formulate the noise correlations in terms of hydrodynamic fields.

Interestingly, the interplay between momentum conservation and energy dissipation has shown several unforeseen properties: for finite systems, the global cooling contributes to the development of long-range spatial velocity correlations, which at the same time affect the temperature evolution. Velocity correlations between colliding particles are generally disregarded because of the Molecular Chaos ansatz. In our model, we can avoid this ansatz and obtain a closed set of equations for temperature and correlations from microscopic dynamics: both of them decay in time at the same rate, and the rescaled correlation profile tends to a steady value

independent from initial conditions. Furthermore, the mesoscopic dissipation coefficient has been redefined through a multiple scales analysis. The fluctuations of rescaled total energy have shown a divergent behavior in time, an unexpected feature in our model: again, a microscopic derivation through average balance equations allowed the computation of the multi-particle velocity moments and has shown a multiscaling behavior driving the fluctuations away from a stationary value. So, the model enables direct computations of fluctuating quantities under a few controlled assumptions, by means of a perturbative approach which may be easily extended to next orders, depending on the required accuracy.

The encouraging results on the granular lattice model inspired us in the formulation of a lattice model of active granular particles; the model was enhanced allowing hopping (and therefore compressibility) and moving to a general $d > 1$ case. Again, the model provided a clear and general derivation of hydrodynamic equations in the dilute limit from microscopic rules of the model. For a specific choice of microscopic ingredients, hydrodynamic equations can be derived in the Local Equilibrium Approximation yielding the existence of homogeneous disordered and ordered states. The former has been proved to be unstable depending on the strength of noise, dissipation and self-propulsion: we derived a phase diagram, showing the competition between noise (fostering disorder) and dissipation (fostering order). When the disordered system is unstable, ordered phases like swarming or clustering arise. Two essential points must be underlined: first, hydrodynamic equations have shown that viscosity and heat transport are not required for the existence of a disorder-swarming transition. Second, when moving to the unstable region all the modes become simultaneously unstable: this is in contrast with HCS instability, which was actually caused by the first mode (longest wavelength) amplification and driven by viscosity, which is absent in our model of active matter. Furthermore, fluctuating currents have been computed also in the active case, and the theoretical results have shown a fair agreement with simulations.

	Dissipation	*Injection*	*Noise*	*Disordered state*	*Instability*
Granular model	Inelasticity	Formal rescaling	absent	Homogeneous Cooling State	Shear instability $\nu > \nu_c$
Active model	Aligning forces	Self-propulsion	White noise	Homogeneous Disordered State	Swarming $\gamma > \gamma_c(\Gamma)$

Table 6.1. A comparative recap of granular and active models

Our main result is the development of a class of lattice models and a procedure to reproduce the average hydrodynamic equations of granular and active systems and derive their fluctuating hydrodynamics from microscopic behavior. In addition, the Molecular Chaos ansatz is not always needed because it is sometimes possible to compute the correlations in the system, as it has be shown for granular Maxwell Molecules: analytical results successfully explain the new phenomena observed in simulations. The procedure introduced may be applied to several other

cases.

The results obtained in the two models can be compared: indeed we have found that strong analogies between granular and active model are present. In Tab. 6.1, the main features are presented both considering microscopic ingredients defining the models - dissipation, injection and noise terms - and concerning the hydrodynamic states most analyzed, namely the Homogeneous Cooling State and the homogeneous disordered state. Those are the most suitable for a direct comparison, which can be enhanced in further studies.

The models have shown to be adaptive, i.e. the rules determining their evolution can be easily changed separately. Further perspectives of the granular model include the generalization to $d > 1$, a dilute case with hopping particles and the introduction of hard-spheres collisions. Also, adapting the model to the framework of Macroscopic Fluctuation Theory would be an intriguing challenge, since this has never been done for models with momentum conservation such as the one described here.

The active model can represent a basis for several possible developments: the first one is that the *ordered* phase still needs to be studied analytically. A next step may then be the hydrodynamic analysis of ordered phases such as swarming or clustering. It is probable that the Local Equilibrium Approximation will not be a good assumption any more for these states, so the development of a theory beyond Local Equilibrium and Molecular Chaos may be attempted, following the results derived for the granular model. Thereafter, the generality of the active system allows to introduce several choices for collisions, self-propulsion and all the physical parameters. A comparative study may clarify the role of microscopic parameters in macroscopic behavior, both in theoretical analysis and empirical observations. Further investigations may include the introduction of "Navier-Stokes" terms such as viscosity and heat conductivity.

The models presented can be seen as part of a wider framework, nonequilibrium statistical physics, and further studies may deal with several theoretical problems such as entropy production or fluctuation-dissipation relations. The theoretical achievements could be compared with experimental evidences, pointing out new issues and research directions. The possibility of deriving new and more general results from the theoretical analysis here developed is still to be explored.

Appendices

A

Analytical results for the granular model

A.1 Microscopic derivation of balance equations

Microscopic balance equations in Sec. 4.2.1 can be directly derived computing the gain and loss terms of local velocity $v_{l,p}$ as a stochastic processes in discrete time, writing a pseudo-Langevin equation. For our granular model, velocity $v_{l,p}$ evolves as

$$v_{l,p+1} = (1 - \delta_{y_p,l} - \delta_{y_p,l-1})v_{l,p} + \delta_{y_p,l}\left[v_{l,p} - \frac{1+\alpha}{2}\left(v_{l,p} - v_{l+1,p}\right)\right] + \delta_{y_p,l-1}\left[v_{l,p} + \frac{1+\alpha}{2}\left(v_{l-1,p} - v_{l,p}\right)\right], \quad \text{(A.1)}$$

where $\delta_{y_p,l}$ is selecting the colliding particle at the p-th time step. We can also write

$$\begin{aligned} v_{l,p+1} &= v_{l,p} - \delta_{y_p,l}\frac{1+\alpha}{2}\left(v_{l,p} - v_{l+1,p}\right) + \delta_{y_p,l-1}\frac{1+\alpha}{2}\left(v_{l-1,p} - v_{l,p}\right) \\ &= v_{l,p} - j_{l,p} + j_{l-1,p}, \end{aligned} \quad \text{(A.2)}$$

introducing the momentum current $j_{l,p}$, which for our system reads

$$j_{l,p} = \frac{1+\alpha}{2}\delta_{y_p,l}\left(v_{l,p} - v_{l+1,p}\right). \quad \text{(A.3)}$$

For the evolution of the kinetic energy, we square eq. (A.2) and we obtain

$$v_{l,p+1}^2 = v_{l,p}^2 + \delta_{y_p,l}\left[\left(\frac{1+\alpha}{2}\right)^2\left(v_{l,p} - v_{l+1,p}\right)^2 - (1+\alpha)v_{l,p}\left(v_{l,p} - v_{l+1,p}\right)\right] + \delta_{y_p,l-1}\left[\left(\frac{1+\alpha}{2}\right)^2\left(v_{l-1,p} - v_{l,p}\right)^2 + (1+\alpha)v_{l,p}\left(v_{l-1,p} - v_{l,p}\right)\right], \quad \text{(A.4)}$$

which can be written as

$$v_{l,p+1}^2 = v_{l,p}^2 + \frac{\alpha^2-1}{4}\left[\delta_{y_p,l}\left(v_{l,p}-v_{l+1,p}\right)^2 + \delta_{y_p,l-1}\left(v_{l-1,p}-v_{l,p}\right)^2\right] - (v_{l,p}+v_{l+1,p})j_{l,p} + (v_{l-1,p}+v_{l,p})j_{l-1,p}. \quad \text{(A.5)}$$

We now compute the averages. For the velocity we have that

$$u_{l,p+1} - u_{l,p} = -\langle j_{l,p} - j_{l-1,p}\rangle, \quad \text{(A.6)}$$

with

$$u_{l,p} = \langle v_{l,p}\rangle. \quad \text{(A.7)}$$

Reminding that $\langle \delta_{y_p,l}\rangle = 1/L$ in the MM case, we can compute the mean current

$$\begin{aligned}\langle j_{l,p}\rangle &= \langle \frac{1+\alpha}{2}\delta_{y_p,l}\left(v_{l,p}-v_{l+1,p}\right)\rangle \\ &= \frac{1+\alpha}{2L}\langle v_{l,p}-v_{l+1,p}\rangle \\ &= \frac{1+\alpha}{2L}(u_{l,p}-u_{l+1,p}). \end{aligned} \quad \text{(A.8)}$$

Then, the time evolution equation for the mean velocity is

$$u_{l,p+1} - u_{l,p} = \frac{1+\alpha}{2L}(u_{l+1,p}+u_{l-1,p}-2u_{l,p}). \quad \text{(A.9)}$$

For the mean quadratic velocity, from eq. (A.5) we have that

$$\left\langle v_{l,p+1}^2\right\rangle - \left\langle v_{l,p}^2\right\rangle = \frac{\alpha^2-1}{4L}\langle (v_{l,p}-v_{l+1,p})^2 + (v_{l-1,p}-v_{l,p})^2\rangle - \frac{1+\alpha}{2L}\langle (v_{l,p}+v_{l+1,p})\left(v_{l,p}-v_{l+1,p}\right) - (v_{l-1,p}+v_{l,p})\left(v_{l-1,p}-v_{l,p}\right)\rangle. \quad \text{(A.10)}$$

Developing the terms on the rhs, we find

$$\left\langle v_{l,p+1}^2\right\rangle - \left\langle v_{l,p}^2\right\rangle = \frac{\alpha^2-1}{4L}\left[\left\langle v_{l+1,p}^2\right\rangle + 2\left\langle v_{l,p}^2\right\rangle + \left\langle v_{l-1,p}^2\right\rangle - 2\langle v_{l,p}v_{l+1,p} + v_{l-1,p}v_{l,p}\rangle\right] - \frac{1+\alpha}{2L}\left[2\left\langle v_{l,p}^2\right\rangle - \left\langle v_{l+1,p}^2\right\rangle - \left\langle v_{l-1,p}^2\right\rangle\right] \quad \text{(A.11)}$$

In order to close the rhs of the last equation, we factorize the 2-points correlations $\langle v_{l,p}v_{l\pm1,p}\rangle = u_{l,p}u_{l\pm1,p}$: this assumption correspond to the Molecular Chaos ansatz assumed in Sec. 4.2.1. Now, in the rhs of eq. (A.5) we have

$$\left\langle v_{l,p+1}^2\right\rangle - \left\langle v_{l,p}^2\right\rangle = -\frac{1-\alpha^2}{L}\left[\left\langle v_{l,p}^2\right\rangle - \frac{1}{2}u_{l,p}(u_{l+1,p}+u_{l-1,p})\right] + \left(\frac{1+\alpha}{2}\right)^2\frac{1}{L}\left(\left\langle v_{l+1,p}^2\right\rangle + \left\langle v_{l-1,p}^2\right\rangle - 2\left\langle v_{l,p}^2\right\rangle\right). \quad \text{(A.12)}$$

Eqs. (A.9) and (A.12) are the balance equations for our lattice system, with discrete sites l at discrete times p. Introducing the hydrodynamic scaling of Eq. (4.25)

$$x = \frac{l}{L}, \qquad \Delta x = \frac{1}{L}, \qquad \Delta t = \frac{1}{L^3}, \tag{A.13}$$

and by assuming that $u_{l,p}$ and $T_{l,p}$ are both smooth functions $x = l/L$, we can develop the following terms

$$u_{l\pm1,p} = u_{l,p} \pm \frac{\partial u}{\partial x}\frac{1}{L} + \frac{1}{2}\frac{\partial^2 u}{\partial x^2}\frac{1}{L^2} + O(L^{-3}) \tag{A.14}$$

$$\langle v^2_{l\pm1,p}\rangle = \left\langle v^2_{l,p}\right\rangle \pm \frac{\partial\langle v^2\rangle}{\partial x}\frac{1}{L} + \frac{1}{2}\frac{\partial^2\langle v^2\rangle}{\partial x^2}\frac{1}{L^2} + O(L^{-3}). \tag{A.15}$$

and with a similar development in $\Delta t = 1/L^3$ we have the evolution equations for the fields $u(x,t)$ and $\langle v^2\rangle(x,t)$

$$\frac{1}{L^3}\frac{\partial u}{\partial t} = \frac{1+\alpha}{2}\frac{1}{L^3}\frac{\partial^2 u}{\partial x^2} + O(L^{-4}) \tag{A.16a}$$

$$\begin{aligned}\frac{1}{L^3}\frac{\partial\langle v^2\rangle}{\partial t} =& -\frac{1-\alpha^2}{L}(\langle v^2\rangle - u^2) + \left(\frac{1+\alpha}{2}\right)^2\frac{1}{L^3}\frac{\partial^2\langle v^2\rangle}{\partial x^2} \\ &+ \frac{1-\alpha^2}{4}\frac{1}{L^3}2u\frac{\partial^2 u}{\partial x^2} + O(L^{-4})\end{aligned} \tag{A.16b}$$

We here introduce the macroscopic inelasticity coefficient ν, that in this case reads

$$\nu = L^2(1-\alpha^2) > 0, \tag{A.17}$$

and if we want ν to be finite we need $1-\alpha = O(L^{-2})$. So, multiplying by L^3 and neglecting $O(L^{-1})$ terms, we have

$$\frac{\partial u}{\partial t} = \frac{1+\alpha}{2}\frac{\partial^2 u}{\partial x^2} \tag{A.18a}$$

$$\begin{aligned}\frac{\partial\langle v^2\rangle}{\partial t} =& -\nu(\langle v^2\rangle - u^2) + \left(\frac{1+\alpha}{2}\right)^2\frac{\partial^2\langle v^2\rangle}{\partial x^2} \\ &+ \frac{1-\alpha^2}{4}2u\frac{\partial^2 u}{\partial x^2}.\end{aligned} \tag{A.18b}$$

Now, we find evolution equations for $u(x,t)$ and $T(x,t)$ by replacing $\langle v^2\rangle(x,t) = T(x,t) + u^2(x,t)$ in eq. (A.18b); the derivatives read

$$\frac{\partial\langle v^2\rangle}{\partial t} = \frac{\partial T}{\partial t} + 2u\frac{\partial u}{\partial t} = \frac{\partial T}{\partial t} + \frac{1+\alpha}{2}2u\frac{\partial^2 u}{\partial x^2} \tag{A.19a}$$

$$\frac{\partial^2\langle v^2\rangle}{\partial x^2} = \frac{\partial}{\partial x}\left(\frac{\partial T}{\partial x} + 2u\frac{\partial u}{\partial x}\right) = \frac{\partial^2 T}{\partial x^2} + 2\left(\frac{\partial u}{\partial x}\right)^2 + 2u\frac{\partial^2 u}{\partial x^2} \tag{A.19b}$$

and substititung them into eq. (A.18b), the $2u\,\partial^2 u/\partial x^2$ terms vanish and we have

$$\frac{\partial u}{\partial t} = \frac{1+\alpha}{2}\frac{\partial^2 u}{\partial x^2} \tag{A.20a}$$

$$\frac{\partial T}{\partial t} = -\nu T + \left(\frac{1+\alpha}{2}\right)^2 \left[\frac{\partial^2 T}{\partial x^2} + 2\left(\frac{\partial u}{\partial x}\right)^2\right], \tag{A.20b}$$

which are the evolution equations for u and T continuous in our model. Since the limit $L \to \infty$ yields $(1+\alpha)/2 \to 1$, we finally have

$$\frac{\partial u}{\partial t} = \frac{\partial^2 u}{\partial x^2} \tag{A.21a}$$

$$\frac{\partial T}{\partial t} = -\nu T + \frac{\partial^2 T}{\partial x^2} + 2\left(\frac{\partial u}{\partial x}\right)^2. \tag{A.21b}$$

We found then that the velocity field $u(x,t)$ follows a diffusion equation, while the temperature evolution equation (A.21b) shows the presence of sink, diffusion processes and viscous heating, represented respectively by the first, second and third term in Eq. (A.21b). The obtained results are equivalent to the ones discussed in Sec. 4.2.1: I presented an alternative derivation of hydrodynamic equations, without the need of a Boltzmann Equation, which has been our first derivation of hydrodynamic equations in this work.

A.2 Balance equations for moments with $n \geq 3$

Starting from the microscopic evolution equation (A.2), we can get the dynamic equations for any moment of the velocity with few considerations.

First of all, let's look at the δ-functions in Eq. (A.2); since we need to compute averages over trajectories, it is useful to see that for MM one has

$$\left\langle \delta^n_{y_p,l} \right\rangle = \left\langle \delta_{y_p,l} \right\rangle = \frac{1}{L}, \qquad \left\langle \delta^n_{y_p,l}\delta^m_{y_p,l'} \right\rangle = 0 \qquad \forall\, m,n > 1\ (l \neq l') \tag{A.22}$$

So, we can write

$$\begin{aligned} v^n_{l,p+1} - v^n_{l,p} &= \sum_{k=1}^{n} \binom{n}{k} v_{lp}^{n-k} \left(j_{l-1,p} - j_{l,p}\right)^k \\ &= \sum_{k=1}^{n} \binom{n}{k} v_{lp}^{n-k} \sum_{h=0}^{k} \binom{k}{h} \left(\frac{1+\alpha}{2}\right)^k \times \\ &\quad \times \delta^{k-h}_{y_p,l-1}\delta^h_{y_p,l} \left(v_{l-1,p} - v_{l,p}\right)^{k-h} \left(v_{l+1,p} - v_{l,p}\right)^h . \end{aligned} \tag{A.23}$$

When we average the two sides over the trajectories, we can exploit the properties in eq. (A.22): the only terms remaining in the sum over h are for $h = 0, k$. Then, defining $\zeta = (1+\alpha)/2$

$$\left\langle v^n_{l,p+1} \right\rangle - \left\langle v^n_{l,p} \right\rangle = \frac{1}{L}\sum_{k=1}^{n} \binom{n}{k} \zeta^k \left\langle v_{lp}^{n-k} \left[\left(v_{l-1,p} - v_{l,p}\right)^k + \left(v_{l+1,p} - v_{l,p}\right)^k\right] \right\rangle . \tag{A.24}$$

After some algebra, the term into square brackets reads

$$(v_{l-1,p} - v_{l,p})^k + (v_{l+1,p} - v_{l,p})^k = \sum_{j=0}^{k} \binom{k}{j} (-1)^{k-j} v_{l,p}^{k-j} \left(v_{l-1,p}^j + v_{l+1,p}^j \right), \quad \text{(A.25)}$$

then

$$\left\langle v_{l,p+1}^n \right\rangle - \left\langle v_{l,p}^n \right\rangle = \frac{1}{L} \sum_{k=1}^{n} \binom{n}{k} \zeta^k \sum_{j=0}^{k} \binom{k}{j} (-1)^{k-j} \left\langle v_{l,p}^{n-j} \left(v_{l-1,p}^j + v_{l+1,p}^j \right) \right\rangle. \quad \text{(A.26)}$$

We can now use the *Local Equilibrium approximation* to split the average into two parts: namely, the LEA is equivalent to

$$\begin{aligned} \langle v_{l,p}^m v_{l+1,p}^n \rangle_{\mathrm{LE}} &= \frac{1}{2\pi\sqrt{T_{l,p}T_{l+1,p}}} \int_{-\infty}^{+\infty} dv_l \int_{-\infty}^{+\infty} dv_{l+1}\, v_l^m\, v_{l+1}^n \\ &\quad \times \exp\{-\frac{(v_l - u_{l,p})^2}{2T_{l,p}}\} \exp\{-\frac{(v_{l+1} - u_{l+1,p})^2}{2T_{l+1,p}}\} \\ &= \left\langle v_{l,p}^m \right\rangle_{\mathrm{LE}} \left\langle v_{l+1,p}^n \right\rangle_{\mathrm{LE}}, \end{aligned} \quad \text{(A.27)}$$

which includes not only Molecular Chaos but also the Gaussianity of the velocity distribution. This assumption allows us to compute all the moments independently. Furthermore, the expansion in eq. (A.15) can be generalized and then

$$\left\langle v_{l,p+1}^n \right\rangle - \left\langle v_{l,p}^n \right\rangle = \frac{1}{L} \sum_{k=1}^{n} \sum_{j=0}^{k} \binom{n}{k} \binom{k}{j} \zeta^k (-1)^{k-j} \left\langle v_{l,p}^{n-j} \right\rangle \left[2 \left\langle v_{l,p}^j \right\rangle + \frac{1}{L^2} \partial_x^2 \left\langle v_{l,p}^j \right\rangle \right]. \quad \text{(A.28)}$$

We now move to the $L \to \infty$ limit: to lighten the notation, we introduce the momentum fields $u_n(x,t)$ defined as

$$u_n(x,t) = \lim_{L\to\infty} \left\langle v_{l,p}^n \right\rangle, \quad \text{(A.29)}$$

so that, with the continuum limit defined in eq. (A.13), eq. (A.28) yields

$$\partial_t u_n(x,t) = \sum_{k=1}^{n} \sum_{j=0}^{k} \binom{n}{k} \binom{k}{j} \zeta^k (-1)^{k-j} u_{n-j}(x,t) \left[2L^2 u_j(x,t) + \partial_x^2 u_j(x,t) \right], \quad \text{(A.30)}$$

where the L^2 factor doesn't baffle us because the sum of the ζ^k will give the leading and also the subleading terms, knowing that $1 - \zeta = O(L^{-2})$. It is then possible to derive all the required moments, and to compute the central moments. For $n = 1, 2$, we recover the results of the previous paragraph; for $n \geq 3$, we have all the new dynamic equations we were looking for. For instance,

$$\partial_t u_3(x,t) = -\frac{3}{2}\nu \left[u_3(x,t) - u_1(x,t)u_2(x,t) \right] + \partial_x^2 u_3(x,t) \quad \text{(A.31a)}$$

$$\partial_t u_4(x,t) = -2\nu \left[u_4(x,t) - u_1(x,t)u_3(x,t) \right] + \partial_x^2 u_4(x,t) \quad \text{(A.31b)}$$

. . . and so on.

The last equations are the first step of an infinite hierarchy. Interestingly, they are closed at each order: the equation for u_3 contains only $n \leq 3$ fields, the equation for u_4 only $n \leq 4$, etc. etc. So, starting from the equation for $u_1 \equiv u(x,t)$ one can solve the equations at any order for given boundary conditions. Eqs. (A.31) give us the evolution equations for central moments $\mu_n = \langle (v-u)^n \rangle$, which have been written in (4.36b).

A.3 Sum rule

Here, we rigorously derive, in the continuum limit and up to $O(L^{-1})$, the sum rule (5.10) that stems from momentum conservation.

Our starting point is (5.5), which is equivalent to

$$T(t) + 2\sum_{k=1}^{\frac{L-1}{2}} D_k(t)\Delta x = 0, \quad \Delta x = L^{-1}. \tag{A.32}$$

Now, we go to the continuum limit by making use of (5.7). To be precise, we denote here $x = (k-1)/L$ by x_k. Then,

$$\int_{x_k}^{x_{k+1}} dx\, D(x,t) = L^{-1} D(x_k,t) + \frac{L^{-2}}{2}\partial_x D(x,t)|_{x_k} + O(L^{-3}). \tag{A.33}$$

Hence,

$$\begin{aligned}\sum_{k=1}^{\frac{L-1}{2}} \underbrace{D(x_k,t)}_{D_k(t)}\Delta x &= \int_0^{\frac{1}{2}-\frac{1}{2L}} dx\, D(x,t) - \frac{L^{-1}}{2}\int_0^{\frac{1}{2}-\frac{1}{2L}} dx\, \partial_x D(x,t) + O(L^{-2}) \\ &= \int_0^{\frac{1}{2}-\frac{1}{2L}} dx\, D(x,t) - \frac{L^{-1}}{2}\left[D\left(\frac{1}{2}-\frac{1}{2L},t\right) - D(0,t)\right] + O(L^{-2}).\end{aligned} \tag{A.34}$$

The expression above can be further simplified to

$$\sum_{k=1}^{\frac{L-1}{2}} D_k(t)\Delta x = \int_0^{\frac{1}{2}} dx\, D(x,t) + \frac{L^{-1}}{2}\left[\psi(t) - 2\chi(t)\right] + O(L^{-2}), \tag{A.35}$$

where we have made use of the definitions of ψ and χ in (5.9). If we insert (A.35) into (A.32), we obtain (5.10) of the main text.

A.4 Energy fluctuations

We here look at the normalized energy fluctuations for the granular model with Maxwell molecules. Our aim is a theoretical derivation of the quantity

$$\Sigma^2(t) \equiv \frac{\langle E^2(t)\rangle - \langle E(t)\rangle^2}{\langle E(t)\rangle^2} \tag{A.36}$$

where $E(t) = \lim_{L\gg 1} E_p = \lim_{L\gg 1} \sum_{l=1}^{L} v_{lp}^2$.

From now on all our calculations will be done in the homogeneous state, i.e. where the system is invariant for space translation and inversion; hence, all the one-point fields become spatially flat fields, all the two-point fields become one-point fields, and so on.

If we assume local equilibrium, we have $\langle E(t)\rangle = LT(t)$ and $\langle E^2(t)\rangle = 3LT^2(t)$. So, local equilibrium prediction is $L\Sigma^2(t) = 2$. However, numerical results diverge from this value as time increases in trajectories. The numerical behavior of $L\Sigma^2(t)$ is shown in Fig. 5.4. This behavior cannot be explained with a local equilibrium assumption. We need to compute a result without using it, so let's go back to Eq. (A.36): we can see that

$$\begin{aligned}\left\langle E^2(t)\right\rangle &= \left\langle \sum_{l,l'}^{1,L} v_{lp}^2 v_{l'p}^2 \right\rangle = \sum_{l=1}^{L} \left\langle v_{lp}^4 \right\rangle + \sum_{l=1}^{L} \sum_{l'\neq l}^{1,L} \left\langle v_{lp}^2 v_{l'p}^2 \right\rangle \\ &= L\left[q_p + \sum_{k=1}^{L-1} \left(C_{kp}^{22} + T_p^2 \right) \right] \end{aligned} \tag{A.37}$$

with the following definitions (the last will appear later)

$$\left\langle v_{lp}^4 \right\rangle \equiv q_p, \tag{A.38a}$$

$$\left\langle v_{lp}^2 v_{l\pm k,p}^2 \right\rangle \equiv C_{kp}^{22} + T_p^2, \tag{A.38b}$$

$$\left\langle v_{lp}^3 v_{l\pm k,p} \right\rangle \equiv C_{kp}^{31}, \tag{A.38c}$$

$$\left\langle v_{l\mp m,p} v_{lp}^2 v_{l\pm n,p} \right\rangle \equiv C_{mnp}^{121}. \tag{A.38d}$$

Hence, in the continuum limit we have

$$\begin{aligned}\Sigma^2(t) &= \frac{1}{L^2T^2(t)} \left[Lq(t) + L(L-1)T^2(t) + L^2 \int_0^1 \mathrm{d}x\, C^{22}(x,t) - L^2T^2(t) \right] \\ &= \frac{1}{L} \frac{q(t) - T^2(t) + L\int_0^1 \mathrm{d}x\, C^{22}(x,t)}{T^2(t)} \end{aligned} \tag{A.39}$$

From Sec. 5.1, we already know $T(t)$ up to the L^{-1} order; we need to compute $q(t)$ and $C^{22}(x,t)$ out of a local equilibrium approximation.

In Eq. (A.38) there are all the quartic fields that we will consider in these notes; they are all evolving in time with a Langevin equation that depends on the microscopic dynamics, as usual. For instance, reminding the velocity current definition

$$j_{lp} = \zeta \delta_{y_p,l} \left(v_{lp} - v_{l+1,p} \right) \quad \text{with } \zeta = \frac{1+\alpha}{2} \tag{A.40}$$

for q_p we have

$$\begin{aligned}
q_{p+1} &= \left\langle v_{l,p+1}^4 \right\rangle = \left\langle (v_{lp} - j_{lp} + j_{l-1,p})^4 \right\rangle = \\
&= \left\langle v_{lp}^4 \right\rangle - 4 \left\langle v_{lp}^3 \left(j_{lp} - j_{l-1,p}\right) \right\rangle + 6 \left\langle v_{lp}^2 \left(j_{lp}^2 + j_{l-1,p}^2\right) \right\rangle \\
&\qquad - 4 \left\langle v_{lp} \left(j_{lp}^3 - j_{l-1,p}^3\right) \right\rangle + \left\langle j_{lp}^4 + j_{l-1,p}^4 \right\rangle = \\
&= q_p + \frac{1}{L} \Big\{ - 4\zeta \left\langle v_{lp}^3 \left(v_{lp} - v_{l+1,p} - v_{l-1,p} + v_{lp}\right) \right\rangle \\
&\qquad + 6\zeta^2 \left\langle v_{lp}^2 \left[\left(v_{lp} - v_{l+1,p}\right)^2 + \left(v_{l-1,p}^2 - v_{lp}\right)^2 \right] \right\rangle \\
&\qquad - 4\zeta^3 \left\langle v_{lp} \left[\left(v_{lp} - v_{l+1,p}\right)^3 - \left(v_{l-1,p}^2 - v_{lp}\right)^3 \right] \right\rangle \\
&\qquad + \zeta^4 \left\langle \left(v_{lp} - v_{l+1,p}\right)^4 + \left(v_{l-1,p}^2 - v_{lp}\right)^4 \right\rangle \Big\} = \\
&= \ldots = \\
&= q_p - \frac{4\zeta\left(1-\zeta\right)}{L} \left\{ \left[2 - \zeta\left(1-\zeta\right)\right] \left(q_p - C_{1p}^{31}\right) + 3\zeta\left(1-\zeta\right) \left(C_{1p}^{31} - C_{1p}^{22}\right) \right\},
\end{aligned} \tag{A.41}$$

where we exploited the delta properties in the partial averages of the velocity current, which for Maxwell molecules read (from Eq. (A.40))

$$\left\langle f(\mathbf{v}_p) j_{lp} \right\rangle = \frac{\zeta}{L} \left\langle f(\mathbf{v}_p) \left(v_{lp} - v_{l+1,p}\right) \right\rangle \tag{A.42a}$$

$$\left\langle f(\mathbf{v}_p) j_{lp} j_{l'p} \right\rangle = \frac{\zeta^2}{L} \delta_{l,l'} \left\langle f(\mathbf{v}_p) \left(v_{lp} - v_{l+1,p}\right)^2 \right\rangle \tag{A.42b}$$

$$\ldots$$

$$\left\langle f(\mathbf{v}_p) \left(\prod_{i=1}^{n} j_{l_i,p} \right) \right\rangle = \frac{\zeta^n}{L} \left(\prod_{i=2}^{n} \delta_{l_1,l_i} \right) \left\langle f(\mathbf{v}_p) \left(v_{l_1,p} - v_{l_1+1,p}\right)^n \right\rangle. \tag{A.42c}$$

Eq. (A.41) is very similar to Eqs (5.4) in Sec. 5.1. Indeed, for the temperature we had

$$T_{p+1} = T_p - \frac{4\zeta\left(1-\zeta\right)}{L} \left(T_p - C_{1p}\right) \tag{A.43}$$

where from its definition in Eq. (A.40) we have that $4\zeta\left(1-\zeta\right) = 1 - \alpha^2 = \nu L^{-2}$.

We write Eq. (A.41) with its explicit dependence on L as

$$q_{p+1} - q_p = -\frac{2\nu}{L^3} \left[\left(1 - \frac{\nu}{8L^2}\right) \left(q_p - C_{1p}^{31}\right) + \frac{3\nu}{8L^2} \left(C_{1p}^{31} - C_{1p}^{22}\right) \right], \tag{A.44}$$

hence, neglecting $\mathcal{O}(L^{-2})$ terms in the rhs, for $L \gg 1$ we have the continuous equation

$$\dot{q}(t) = -2\nu \left[q(t) - \Gamma^{31}(t) \right] \tag{A.45}$$

using the same continuum limit of Sec. 5.1, i.e. $\Gamma^{31}(t) = \lim_{x\to 0} C^{31}(x,t)$ and $\Gamma^{22}(t) = \lim_{x\to 0} C^{22}(x,t)$.

Since we don't have any information about the magnitude of C^{31} and C^{22}, we perform a cluster expansion; in our homogenous case with $\langle v_{lp} \rangle = 0$, we have

$$\begin{aligned} \left\langle v_{lp}^3 v_{l\pm k,p} \right\rangle &= 3 \left\langle v_{lp}^2 \right\rangle \langle v_{lp} v_{l\pm k,p} \rangle + g_{kp}^{31} \\ &= 3T_p C_{kp} + g_{kp}^{31}, \end{aligned} \tag{A.46}$$

$$\begin{aligned} \left\langle v_{lp}^2 v_{l\pm k,p}^2 \right\rangle &= \left\langle v_{lp}^2 \right\rangle \left\langle v_{l\pm k,p}^2 \right\rangle + 2 \langle v_{lp} v_{l\pm k,p} \rangle^2 + g_{kp}^{22} \\ &= T_p^2 + 2C_{kp}^2 + g_{kp}^{22}, \end{aligned} \tag{A.47}$$

where g^{31} and g^{22} are the purely correlated terms. Then, continuous fields are

$$C^{31}(x,t) = 3T(t)C(x,t) + g^{31}(x,t), \tag{A.48}$$

$$C^{22}(x,t) = 2C^2(x,t) + g^{22}(x,t). \tag{A.49}$$

The leading terms in the rhs of Eqs. (A.46,A.47) are respectively $3TC = \mathcal{O}(T_0^2/L)$ and T^2. Then, we assume[1] that purely correlated terms are subleading with respect to previous ones, then $g^{31}(x,t) = \mathcal{O}(T_0^2/L^2)$ and $g^{22}(x,t) = \mathcal{O}(T_0^2/L)$. So, we have that both C^{31} and C^{22} are at most $\mathcal{O}(T_0^2/L)$. Then, Γ^{31} in Eq. (A.45) is a L^{-1} correction and introducing the same expansion of Sec. 5.1[2]

$$q(t) = q_0(t) + \frac{1}{L} q_1(t) + \frac{1}{L^2} q_2(t) + \dots, \tag{A.50a}$$

$$LC^{31}(x,t) \equiv D^{31}(x,t) = D_0^{31}(x,t) + \frac{1}{L} D_1^{31}(x,t) + \dots, \tag{A.50b}$$

$$LC^{22}(x,t) \equiv D^{22}(x,t) = D_0^{22}(x,t) + \frac{1}{L} D_1^{22}(x,t) + \dots, \tag{A.50c}$$

we can solve Eq. (A.45) at the zeroth order that is

$$\begin{cases} \dot{q_0} = -2\nu q_0 \\ q_0(t=0) = 3T_0^2(t=0) \end{cases} \quad \Rightarrow \quad q_0(t) = 3T_0^2(t=0)e^{-2\nu t}. \tag{A.51}$$

This solution is the local equilibrium solution that is exact when $L = \infty$. We see that the quartic velocity field is cooling as $T_0^2(t)$, so we introduce the usual rescaled fields

$$\tilde{q}(t) \equiv q(t)/T_0^2(t) = q(t)e^{2\nu t}/T_0^2(t=0), \tag{A.52}$$

and analogously we define $\tilde{D^{31}}$ and $\tilde{D^{22}}$. The tilde represent the Haff's law scaling taking into account the dimension of the field, so $\tilde{T}(t)$ and $\tilde{D}(x,t)$ are still scaled with $T_0(t=0)e^{-\nu t}$.
Hence, we have the following equations for $\tilde{q_0}$ and $\tilde{q_1}$

$$\frac{\mathrm{d}}{\mathrm{d}t}\tilde{q_0} = 0, \tag{A.53}$$

$$\frac{\mathrm{d}}{\mathrm{d}t}\tilde{q_1} = 2\nu\psi^{31}(t). \tag{A.54}$$

[1] **Ansatz n.1**

[2] where we use the rescaled fields D^{31} and D^{22}, which shouldn't necessarily vanish in the continuum limit, and we define $\psi^{31} = L\Gamma^{31}$, $\psi^{22} = L\Gamma^{22}$

So we have $\tilde{q_0} = 3$, and the first order correction for $q(t)$ may be computed once we know $D^{31}(x,t)$.
We then move to the study of the time evolution of D^{31} and D^{22}: first, we introduce the following exact initial conditions for our model

$$T(t=0) = T_0(t=0)\left(1-\frac{1}{L}\right), \tag{A.55a}$$

$$D(x,t=0) = -T_0(t=0), \tag{A.55b}$$

$$q(t=0) = 3T_0^2(t=0)\left(1-\frac{1}{L}\right)^2, \tag{A.55c}$$

$$D^{31}(x,t=0) = -3T_0^2(t=0)\left(1-\frac{1}{L}\right), \tag{A.55d}$$

$$D^{22}(x,t=0) = \frac{2}{L}T_0^2(t=0). \tag{A.55e}$$

which derivation can be found in Sec. A.4.1. Second, we derive evolution equations for D^{31} and D^{22} with the same technique used for D field; then, we write the difference in time for C^{31}_{1p}, C^{31}_{kp}, C^{22}_{1p}, C^{22}_{kp} (with $k \geq 2$); we neglect the equation for $k = L/2$ because the symmetry of the system yields a reflecting boundary at all orders at $x = 1/2$ (however I studied it in calculations, you can check this result if you wish).
After some painful algebra one gets

$$\begin{aligned}
C^{31}_{1,p+1} &= \left\langle (v_{lp} - j_{lp} + j_{l-1,p})^3 (v_{l+1,p} - j_{l+1,p} + j_{lp}) \right\rangle = \\
&= \ldots = \\
&= C^{31}_{1p} + \frac{1}{L}\Big\{ -7\zeta(1-\zeta)\left[1 - \frac{8}{7}\zeta(1-\zeta)\right] C^{31}_{1p} + \\
&\quad + \left(\zeta^3 + \zeta\right)\left(C^{31}_{2p} - C^{31}_{1p}\right) + \\
&\quad + \zeta(1-\zeta)\left[1 - 2\zeta(1-\zeta)\right]\left(q_p + 3T_p^2 + 3C^{22}_{1p}\right) + \\
&\quad + 3\zeta(1-\zeta)\left[(1-\zeta)C^{121}_{1,1,p} + \zeta C^{121}_{-2,1,p}\right]\Big\}
\end{aligned} \tag{A.56}$$

$$\begin{aligned}
C^{31}_{k,p+1} &= \left\langle (v_{lp} - j_{lp} + j_{l-1,p})^3 (v_{l+k,p} - j_{l+k,p} + j_{l+k-1,p}) \right\rangle = \\
&= \ldots = \\
&= C^{31}_{kp} + \frac{1}{L}\Big\{ -6\zeta(1-\zeta) C^{31}_{kp} + \\
&\quad + \left(\zeta^3 + \zeta\right)\left(C^{31}_{k+1,p} + C^{31}_{k-1,p} - 2C^{31}_{kp}\right) + \\
&\quad + 3\zeta(1-\zeta)\Big[(1-\zeta)\left(C^{121}_{-1,k,p} + C^{121}_{1,k,p}\right) + \\
&\quad + \zeta\left(C^{121}_{1,k-1,p} + C^{121}_{-1,k+1,p}\right)\Big]\Big\}
\end{aligned} \tag{A.57}$$

$$
\begin{aligned}
C^{22}_{1,p+1} &= \left\langle \left(v_{lp} - j_{lp} + j_{l-1,p}\right)^2 \left(v_{l+1,p} - j_{l+1,p} + j_{lp}\right)^2 \right\rangle - T^2_{p+1} = \\
&= \ldots = \\
&= C^{22}_{1p} + \frac{1}{L}\Big\{ -8\zeta\left(1-\zeta\right)\left[1 - \frac{3}{4}\zeta\left(1-\zeta\right)\right] C^{22}_{1p} + \\
&\qquad + 2\zeta^2\left(C^{22}_{2p} - C^{22}_{1p}\right) - 8\zeta\left(1-\zeta\right) T_p C_{1p} + \\
&\qquad + 4\zeta\left(1-\zeta\right)\left[1 - 2\zeta\left(1-\zeta\right)\right] C^{31}_{1p} + \\
&\qquad + 2\left[\zeta\left(1-\zeta\right)\right]^2\left(q_p + 3T^2_p\right) + 4\zeta\left(1-\zeta\right) C^{121}_{-2,1,p} + \\
&\qquad - 16\frac{\left[\zeta\left(1-\zeta\right)\right]^2}{L}\left(T_p - C_{1p}\right)^2 \Big\}
\end{aligned}
\tag{A.58}
$$

$$
\begin{aligned}
C^{22}_{k,p+1} &= \left\langle \left(v_{lp} - j_{lp} + j_{l-1,p}\right)^2 \left(v_{l+k,p} - j_{l+k,p} + j_{l+k-1,p}\right)^2 \right\rangle - T^2_{p+1} = \\
&= \ldots = \\
&= C^{22}_{kp} + \frac{1}{L}\Big\{ -8\zeta\left(1-\zeta\right)\left(C^{22}_{kp} + T_p C_{1p}\right) \\
&\qquad + 2\zeta^2\left(C^{22}_{k+1,p} + C^{22}_{k-1,p} - 2C^{22}_{kp}\right) + \\
&\qquad + 4\zeta\left(1-\zeta\right)\left(C^{121}_{-k,k-1,p} + C^{121}_{-(k+1),k,p}\right) + \\
&\qquad - 16\frac{\left[\zeta\left(1-\zeta\right)\right]^2}{L}\left(T_p - C_{1p}\right)^2 \Big\}
\end{aligned}
\tag{A.59}
$$

where the $\cdots$ indicate long, painful but straightforward algebra.

These equations rule the time evolution of C^{31} and C^{22}; before going to the continuum limit, we notice that they all contain the 3-point correlation function $C^{121}_{i,j,p} = \left\langle v_{l\mp i,p} v^2_{lp} v_{l\pm j,p} \right\rangle$ defined in Eq. (A.38d). We *don't* want to derive ad hydrodynamic equation for this field too; so, we use a cluster expansion to approximate it, and we find

$$
\begin{aligned}
C^{121}_{ijp} &= \left\langle v^2_{lp} \right\rangle \left\langle v_{l\mp i,p} v_{l\pm j,p} \right\rangle + 2\left\langle v_{lp} v_{l\mp i,p} \right\rangle \left\langle v_{lp} v_{l\pm j,p} \right\rangle + g^{121}_{i,j,p} \\
&= T_p C_{i+j,p} + 2C_{ip} C_{jp} + g^{121}_{i,j,p}
\end{aligned}
\tag{A.60}
$$

so we see that the leading term is $T_p C_{1p} = \mathcal{O}(L^{-1})$. To get a closed set of equations, we neglect $g^{121}_{i,j,p}$ [3] and we write

$$
C^{121}_{1,1,p} \simeq T_p C_{2p} + 2C^2_{1p} \tag{A.61a}
$$

$$
C^{121}_{-2,1,p} \simeq T_p C_{1p} + 2C_{1p} C_{2p} \tag{A.61b}
$$

$$
C^{121}_{-1,k,p} \simeq T_p C_{k-1,p} + 2C_{1p} C_{kp} \tag{A.61c}
$$

$$
\ldots
$$

[3] **Ansatz n.2**

... and so on.
With this second ansatz and the quasielastic limit $4\zeta\,(1-\zeta) = \nu L^{-2}$, through the usual hydrodynamic scaling for space and time

$$\Delta x = \frac{1}{L}\,, \quad x = \frac{k-1}{L} \tag{A.62a}$$

$$\Delta t = \frac{1}{L^3}\,, \quad t = \frac{p}{L^3} \tag{A.62b}$$

we get the continuous evolution equations for both fields:

$$\begin{aligned}\frac{1}{L^4}\partial_t\psi^{31}(t) = \frac{1}{L^4}\Bigg\{&-\frac{7\nu}{4}\left(1-\frac{2\nu}{7L^2}\right)\psi^{31}(t)+\\ &+2L\left(1-\frac{\nu}{2L^2}+\mathcal{O}(L^{-4})\right)\left(\partial_x D^{31}|_{x=0}+\frac{1}{2L}\partial_x^2 D^{31}|_{x=0}+\mathcal{O}(L^{-2})\right)\\ &+\frac{\nu}{4}\left(1-\frac{\nu}{2L^2}\right)\left[L\left(q(t)+3T^2(t)\right)+3\psi^{22}(t)\right]+\\ &+\frac{3\nu}{4}\Bigg[\frac{\nu}{4L^2}\left(T(t)\left(\psi(t)+L^{-1}\partial_x D|_{x=0}+\mathcal{O}(L^{-2})\right)+2L^{-1}\psi^2(t)\right)+\\ &\quad+\left(1-\frac{\nu}{4L^2}\right)\left(T(t)\psi(t)+2L^{-1}\psi(t)\left(\psi(x,t)+L^{-1}\partial_x D|_{x=0}+\mathcal{O}(L^{-2})\right)\right)\Bigg]\Bigg\}\end{aligned} \tag{A.63}$$

$$\begin{aligned}\frac{1}{L^4}\partial_t D^{31}(x,t) = \frac{1}{L^4}\Bigg\{&-\frac{3\nu}{2}D^{31}(x,t)+\\ &+2\left(1-\frac{\nu}{2L^2}+\mathcal{O}(L^{-4})\right)\left(\partial_x^2 D^{31}\right)+\\ &+\frac{3\nu}{4}\Bigg[\frac{\nu}{4L^2}\left(2T(t)D(x,t)+\mathcal{O}(L^{-2})\right)+\\ &\quad+\left(1-\frac{\nu}{2L^2}\right)\left(2T(t)D(x,t)+4L^{-1}\psi(t)D(x,t)+\mathcal{O}(L^{-2})\right)\Bigg]\Bigg\}\end{aligned} \tag{A.64}$$

$$\begin{aligned}\frac{1}{L^4}\partial_t\psi^{22}(t) = \frac{1}{L^4}\Bigg\{&-2\nu\left(1-\frac{3\nu}{16L^2}\right)\psi^{22}(t)-\nu T(t)\psi(t)+\\ &+2L\left(1-\frac{\nu}{2L^2}+\mathcal{O}(L^{-4})\right)\partial_x D^{22}|_{x=0}+\nu\left(1-\frac{\nu}{2L^2}\right)\psi^{31}(t)+\\ &+\frac{2\nu}{L}\psi(t)\left(\psi(t)+L^{-1}\partial_x D|_{x=0}+\mathcal{O}(L^{-2})\right)+\\ &+\frac{\nu^2}{8L}\left(q(t)+3T^2(t)\right)-\frac{\nu^2}{L^2}\left(T(t)-\frac{1}{L}\psi(t)\right)^2\Bigg\}\end{aligned} \tag{A.65}$$

$$\begin{aligned}\frac{1}{L^4}\partial_t D^{22}(x,t) = \frac{1}{L^4}\Bigg\{&-2\nu D^{22}(x,t)+\frac{4\nu}{L}D^2(x,t)+\mathcal{O}(L^{-2})+\\ &+2\left(1-\frac{\nu}{2L^2}+\mathcal{O}(L^{-4})\right)\left(\partial_x^2 D^{22}+\mathcal{O}(L^{-2})\right)+\\ &-\frac{\nu^2}{L^2}\left(T(t)-\frac{1}{L}\psi(t)\right)^2\Bigg\}\end{aligned} \tag{A.66}$$

Eqs. (A.63)-(A.66) are the coupled evolution equations for the 4th order correlations: they can be solved separately at each order, together with the perturbative solution of $q(t)$ from Eq. (A.45). we then write the first order with the help of the expansion defined in Eq. (A.50), in terms of rescaled fields as defined in Eq. (A.52). So, we get

$$\begin{cases} \partial_t \tilde{D}_0^{31}(x,t) = 2\partial_x^2 \tilde{D}_0^{31}(x,t) + \dfrac{\nu}{2}\left[\tilde{D}_0^{31}(x,t) + 3\tilde{D}_0(x,t)\right] \\ \partial_x \tilde{D}_0^{31}(x,t)|_{x=0} = -\dfrac{3}{4}\nu \\ \partial_x \tilde{D}_0^{31}(x,t)|_{x=1/2} = 0 \\ \tilde{D}_0^{31}(x,t=0) = -3 \end{cases} \tag{A.67}$$

where we used the result $\tilde{T}_0 = 1$, and for long times we have the solution

$$\tilde{D}_0^{31}(x) = 3\tilde{D}_0(x) \tag{A.68}$$

which confirm that at the first order the clustering approximation is good.
For $\tilde{D}_0^{22}(x,t)$ we have

$$\begin{cases} \partial_t \tilde{D}_0^{22}(x,t) = 2\partial_x^2 \tilde{D}_0^{22}(x,t) \\ \partial_x \tilde{D}_0^{22}(x,t)|_{x=0} = 0 \\ \partial_x \tilde{D}_0^{22}(x,t)|_{x=1/2} = 0 \\ \tilde{D}_0^{22}(x,t=0) = 0 \end{cases} \tag{A.69}$$

that immediately lead to the flat solution

$$\tilde{D}_0^{22}(x,t) \equiv 0 \tag{A.70}$$

So, we can compute the correction to the cooling of $q(t)$ and solve Eq. (A.53): for long times we have

$$\tilde{q}_1(t) = \tilde{q}_1(t_s) + 6\tilde{\psi}_\infty \nu (t - t_s) \tag{A.71}$$

where t_s is the time at which we have $\partial_t \tilde{D}(x,t)|_{t \geq t_s} = 0$.
The results of Eqs. (A.68,A.70,A.71) can be plugged into Eq. (A.39), yielding

$$\begin{aligned} L\sigma^2(t) &= \frac{\tilde{q}(t) + \int_0^1 \mathrm{d}x \tilde{D}^{22}(x,t)}{\tilde{T}^2(t)} - 1 = \\ &= \frac{\tilde{q}_0 + \int_0^1 \mathrm{d}x \tilde{D}_0^{22} + L^{-1}\left(\tilde{q}_1 + \int_0^1 \mathrm{d}x \tilde{D}_1^{22}\right) + \cdots}{\tilde{T}_0 + 2L^{-1}\tilde{T}_0\tilde{T}_1 + \cdots} - 1 = \\ &= 2 + \frac{1}{L}\left[\tilde{q}_1(t_s) + 6\tilde{\psi}_\infty \nu (t - t_s) + \int_0^1 \mathrm{d}x \tilde{D}_1^{22} - 6\left(\tilde{T}_1(t_s) + \tilde{\psi}_\infty \nu (t - t_s)\right)\right] + \mathcal{O}(L^{-2}) \end{aligned} \tag{A.72}$$

Eq. (A.72) shows that local equilibrium result is valid only at first order in L^{-1}; corrections are found, but linearly increasing contributions vanish. So, the time

dependence shown in Fig. 5.4 must come from $D_1^{22}(x,t)$; going to this order (now the leading order for D^{22}), from Eqs. (A.65,A.66) we have that

$$\begin{cases} \partial_t \tilde{D_1^{22}} = 2\partial_x^2 \tilde{D_1^{22}}(x,t) + 4\nu \tilde{D_0}^2(x,t) \\ \partial_x \tilde{D_1^{22}}|_{x=0} = -\nu\tilde{\psi_0}(t) \\ \partial_x \tilde{D_1^{22}}|_{x=1/2} = 0 \\ \tilde{D_1^{22}}(x,t=0) = 2 \end{cases} \tag{A.73}$$

We don't know how to solve this system; however, all we need to know to compute the fluctuations is $\int_0^1 \mathrm{d}x D_1^{22}(x,t) = \tilde{d_1}(t)$. So, integrating over x the first equation in Eq. (A.73), we have

$$\begin{aligned} \frac{\mathrm{d}}{\mathrm{d}t}\tilde{d_1}(t) &= 2\left[\partial_x \tilde{D_1^{22}}|_{x=1^-} - \partial_x \tilde{D_1^{22}}|_{x=0^+}\right] + 4\nu \int_0^1 \mathrm{d}x \tilde{D_0}^2(x,t) = \\ &= 4\nu\left[\tilde{\psi_0}(t) + \int_0^1 \mathrm{d}x \tilde{D_0}^2(x,t)\right] \end{aligned} \tag{A.74}$$

when for long times we have

$$\tilde{D_0}(x,t) \underset{t\gg 1}{\to} \tilde{D}_\infty(x) = -\frac{1}{2}\sqrt{\frac{\nu}{2}}\frac{\cos\left(\frac{1}{2}\sqrt{\frac{\nu}{2}}(1-2x)\right)}{\sin\left(\frac{1}{2}\sqrt{\frac{\nu}{2}}\right)} \tag{A.75}$$

$$\tilde{\psi_0}(t) \underset{t\gg 1}{\to} \tilde{\psi}_\infty = -\frac{1}{2}\sqrt{\frac{\nu}{2}}\cot\left(\frac{1}{2}\sqrt{\frac{\nu}{2}}\right) \tag{A.76}$$

hence the long times solution of Eq. (A.74) reads

$$\tilde{d_1}(t) = \tilde{d_1}(t_s) + 4\left[-\frac{1}{2}\sqrt{\frac{\nu}{2}}\cot\left(\frac{1}{2}\sqrt{\frac{\nu}{2}}\right) + \frac{\nu}{16\sin^2\left(\frac{1}{2}\sqrt{\frac{\nu}{2}}\right)}\left(1+\frac{\sin\sqrt{\nu/2}}{\sqrt{\nu/2}}\right)\right]\nu(t-t_s) \tag{A.77}$$

$$= \tilde{d_1}(t_s) + m_\Sigma(\nu)\nu(t-t_s) \tag{A.78}$$

for which fluctuations can be written as

$$L\Sigma^2(t) = 2 + \frac{1}{L}\left(\tilde{q_1}(t_s) - 6\tilde{T_1}(t_s) + \tilde{d_1}(t_s) + m_\Sigma(\nu)\nu(t-t_s)\right) + \mathcal{O}(L^{-2}) \tag{A.79}$$

We have derived an analytical prediction for the slope of $L\Sigma^2(t)$ for long times; the constant term depends on the transient evolution and cannot be computed at this stage. The final result is the slope of energy fluctuations

$$m(\nu) = \frac{\sqrt{\nu/2}}{\sin\left(\frac{1}{2}\sqrt{\frac{\nu}{2}}\right)}\left[\frac{\frac{1}{2}\sqrt{\frac{\nu}{2}}}{\sin\left(\frac{1}{2}\sqrt{\frac{\nu}{2}}\right)} - \cos\left(\frac{1}{2}\sqrt{\frac{\nu}{2}}\right)\right]\nu \tag{A.80}$$

leading to the result in (5.36).

The result has been derived through a linear perturbative expansion; however, a multiple-scales approach has been developed as well. The calculations are very complicated and don't lead to a improved agreement with simulation, so we don't report them here.

A.4.1 Initial conditions in the center of mass frame

To get the initial conditions in Eqs. (A.55), we have to consider the correct velocity distribution to perform the averages.

At $t = 0$, we draw L velocities w_l with zero average and T_0 variance, hence their pdf is

$$P(\mathbf{w}) = \prod_{l=1}^{L} p(w_l)$$

with $p(w_l) = \exp\left(-w_l^2/2T_0\right)/\sqrt{2\pi T_0}$.
We move to the center of mass inertial frame, so we make a change of variables with the new ones

$$v_i = w_i - \frac{1}{L}\sum_{l=1}^{L} w_l$$

Then we can compute the averages: to compute the initial variance, for example, we have

$$\begin{aligned}
\left\langle v_i^2 \right\rangle &= \int \mathrm{d}w_i\, p(w_i) \left(w_i - \frac{1}{L}\sum_{l=1}^{L} w_l \right)^2 \\
&= \int \mathrm{d}w_i\, p(w_i) \left(w_i^2 - \frac{2}{L} w_i \sum_{l=1}^{L} w_l + \frac{1}{L^2}\sum_{l,l'}^{1,L} w_l w_{l'} \right) \\
&= \left\langle w_i^2 \right\rangle - \frac{2}{L}\sum_{l=1}^{L} \langle w_i w_l \rangle + \frac{1}{L^2}\left(\sum_{l=1}^{L} \left\langle w_l^2 \right\rangle + \sum_{l\neq l'}^{1,L} \langle w_l w_{l'} \rangle \right) \\
&= T_0 - \frac{2}{L}\sum_{l=1}^{L} T_0 \delta_{il} + \frac{1}{L^2}\sum_{l=1}^{L} T_0 \\
&= T_0 \left(1 - \frac{1}{L} \right)
\end{aligned}$$

To compute the initial correlation function, we exploit the property that velocities are i.i.d., i.e. correlations are flat and all site pairs are equivalent; so, when $i \neq j$

$$\begin{aligned}
\langle v_i v_j \rangle &= \int \mathrm{d}w_i\, p(w_i) \left(w_i - \frac{1}{L}\sum_{l=1}^{L} w_l \right) \left(w_j - \frac{1}{L}\sum_{l'=1}^{L} w_{l'} \right) \\
&= \langle w_i w_j \rangle - \frac{1}{L}\sum_{l=1}^{L} \langle (w_i + w_j)\, w_l \rangle + \frac{1}{L^2}\sum_{l,l'}^{1,L} \langle w_l w_{l'} \rangle \\
&= -\frac{1}{L}\sum_{l=1}^{L} T_0 \left(\delta_{il} + \delta_{jl} \right) + \frac{1}{L^2}\sum_{l=1}^{L} T_0 \\
&= -\frac{T_0}{L}
\end{aligned}$$

Similarly all the initial fields can be computed with the right correction in powers of L^{-1}.

B

Analytical results for the active model

B.1 Self-propulsion with nonlinear friction

The Rayleigh-Helmoltz friction (2.19b) used as a self-propulsion force in (6.38) is a first-order differential equation equivalent to the Cauchy problem

$$\begin{aligned} y'(x) &= y(x)(1-y^2(x)) \\ y(0) &= y_0 \end{aligned} \tag{B.1}$$

in adimensional variables, namely $y = v/v_s$ and $x = \omega_s t$. The equation can be integrated by separating its variables, and the solution reads

$$y(x) = \frac{y_0 e^x}{\sqrt{e^{2x} + e^C}} \tag{B.2}$$

when $|y_0| < 1$ and C is an integration constant. A similar solution showing exponential approach to the fixed point $y = 1$ can be found for $|y_0| > 1$. Note that the solutions are symmetrical when changing $y_0 \to -y_0$, then $y(x) \to -y(x)$. In Fig. B.1 the solutions for three different initial values $y_0 = -0.2, 0.5, 4$: it is worth remarking the absence of oscillations when approaching the fixed point $y = 1$ and the fast relaxation when $|y_0| > 1$ compared to the slow one for $|y_0| < 1$.

B.2 Absence of viscosity at first-order

The momentum current given by momentum transport in pairwise interaction is given by Eq. (6.9) and reads

$$J^{(int)}_{\mathbf{i},kl} \equiv n_{\mathbf{i}} n_{\mathbf{i}+\mathbf{e}_l} f^{(2)}_k(\mathbf{v}_{\mathbf{i}}, \mathbf{v}_{\mathbf{i}+\mathbf{e}_l}) \Delta t \tag{B.3}$$

Its averaged value can be computed as

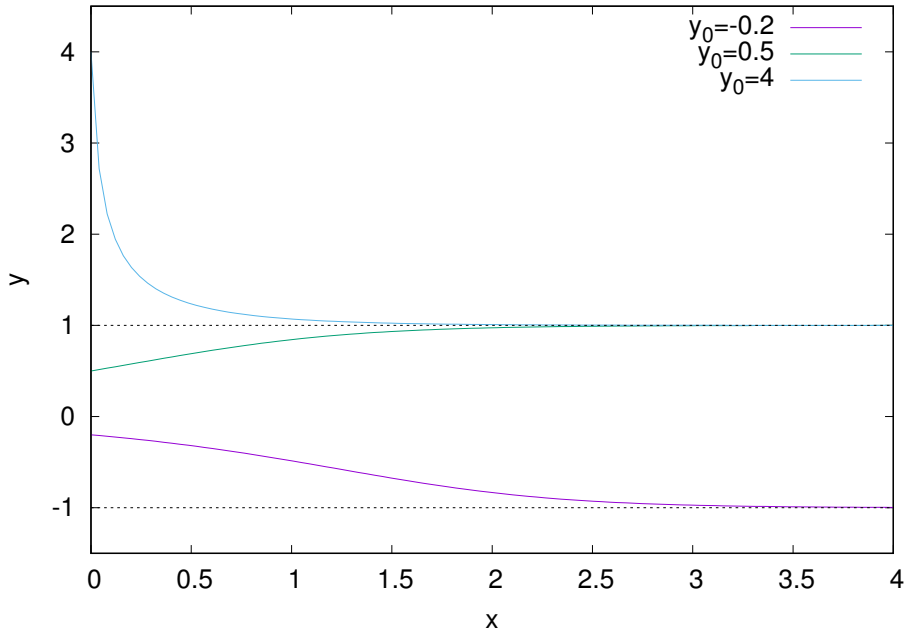

Figure B.1. Solution of the differential equation in (B.1) for three different values of initial conditions, see legend.

$$\left\langle J^{(int)}_{\mathbf{i},kl} \right\rangle = \rho_{\mathbf{i}}(1-\rho_{\mathbf{i}+\mathbf{e}_l}) \int \mathrm{d}\mathbf{v}\,\mathrm{d}\mathbf{v}'\, P_{\mathbf{i}}(\mathbf{v},t)\, P_{\mathbf{i}+\mathbf{e}_l}(\mathbf{v}',t)\, f^{(2)}_k(\mathbf{v},\mathbf{v}')\,\Delta t \tag{B.4}$$

where we have used the Molecular Chaos assumption stated in (6.16) and the factorization in (6.17). Now we move to the continuum limit through the smoothness ansatz in (6.18), which is equivalent to

$$P_{\mathbf{i}+\mathbf{e}_l}(\mathbf{v},t) = P(\mathbf{v};\mathbf{x},t) \pm \frac{1}{L}\left.\frac{\partial P}{\partial x_l}\right|_{(\mathbf{x},t)} + O(1/L^2). \tag{B.5}$$

This expansion can be introduced in Eq. (B.4), leading to

$$\begin{aligned}\left\langle J^{(int)}_{kl} \right\rangle(\mathbf{x},t) &= \rho[1-\rho+O(1/L)] \\ &\times \int \mathrm{d}\mathbf{v}\,\mathrm{d}\mathbf{v}'\, P(\mathbf{v};\mathbf{x},t) \left[P(\mathbf{v};\mathbf{x},t) \pm \frac{1}{L}\frac{\partial P}{\partial x_l} + O(1/L^2)\right] f^{(2)}_k(\mathbf{v},\mathbf{v}')\Delta t\end{aligned} \tag{B.6}$$

but the first term in the parenthesis vanishes because of momentum conservation in (6.1), $\mathbf{f}^{(2)}(\mathbf{v},\mathbf{v}') = -\mathbf{f}^{(2)}(\mathbf{v}',\mathbf{v})$. So, one has $\left\langle J^{(int)}_{kl} \right\rangle(\mathbf{x},t) = O(\Delta t/L)$ and $J^{(int)}_{kl}$ does not enter in the average momentum evolution equation (6.20b) at the first order $O(\Delta t)$.

B.3 Fluctuating currents of active matter

The noise correlations of the density current can be derived substituting microscopic (fluctuating) density current from Eq. (6.6) into Eq. (6.56), yielding

$$\langle j_{\mathbf{i},p,l} j_{\mathbf{i}',p,l'} \rangle = \left\langle (\delta_{\boldsymbol{\xi}_p,\mathbf{i}}\delta_{\boldsymbol{\zeta}_p,\mathbf{e}_l} - \delta_{\boldsymbol{\xi}_p,\mathbf{i}+\mathbf{e}_l}\delta_{\boldsymbol{\zeta}_p,-\mathbf{e}_l})(\delta_{\boldsymbol{\xi}_p,\mathbf{i}'}\delta_{\boldsymbol{\zeta}_p,\mathbf{e}'_l} - \delta_{\boldsymbol{\xi}_p,\mathbf{i}'+\mathbf{e}'_l}\delta_{\boldsymbol{\zeta}_p,-\mathbf{e}'_l}) \right\rangle \tag{B.7}$$

taking the current at equal time $p = p'$ because fast variables $\boldsymbol{\xi}_p$ and $\boldsymbol{\zeta}_p$ are independent at different times, so the correlations must vanish.

The only non vanishing terms are the product between the first and ones in the two parenthesis, because they respectively account for particles hopping in the positive or negative directions. One easily sees that

$$\begin{aligned} \left\langle \delta_{\boldsymbol{\xi}_p,\mathbf{i}}\delta_{\boldsymbol{\zeta}_p,\mathbf{e}_l}\delta_{\boldsymbol{\xi}_p,\mathbf{i}'}\delta_{\boldsymbol{\zeta}_p,\mathbf{e}'_l} \right\rangle &= \delta_{\mathbf{i},\mathbf{i}'}\delta_{l,l'} \left\langle \delta_{\boldsymbol{\xi}_p,\mathbf{i}}\delta_{\boldsymbol{\zeta}_p,\mathbf{e}_l} \right\rangle \\ &= \delta_{\mathbf{i},\mathbf{i}'}\delta_{l,l'} \left\langle n_{\mathbf{i}}(1-n_{\mathbf{i}+\mathbf{e}_l})\Theta(v_{\mathbf{i},l}|v_{\mathbf{i},l}|\right\rangle \frac{\Delta t}{\Delta x} \end{aligned} \tag{B.8}$$

and analogously

$$\left\langle \delta_{\boldsymbol{\xi}_p,\mathbf{i}+\mathbf{e}_l}\delta_{\boldsymbol{\zeta}_p,-\mathbf{e}_l}\delta_{\boldsymbol{\xi}_p,\mathbf{i}'+\mathbf{e}_l}\delta_{\boldsymbol{\zeta}_p,-\mathbf{e}'_l} \right\rangle = \delta_{\mathbf{i},\mathbf{i}'}\delta_{l,l'} \left\langle n_{\mathbf{i}+\mathbf{e}_l}(1-n_{\mathbf{i}})\Theta(-v_{\mathbf{i}+\mathbf{e}_l,l}|v_{\mathbf{i}+\mathbf{e}_l,l}|\right\rangle \frac{\Delta t}{\Delta x}. \tag{B.9}$$

Separating the (independent) density and velocity contribution and using Molecular Chaos one has

$$\begin{aligned} \langle j_{\mathbf{i},p,l} j_{\mathbf{i}',p,l'} \rangle = \delta_{\mathbf{i},\mathbf{i}'}\delta_{p,p'}\delta_{l,l'}[&\rho_{\mathbf{i}}(1-\rho_{\mathbf{i}+\mathbf{e}_l}) \left\langle \Theta(v_{\mathbf{i},l})|v_{\mathbf{i},l}| \right\rangle \\ &+ \rho_{\mathbf{i}+\mathbf{e}_l}(1-\rho_{\mathbf{i}}) \left\langle \Theta(-v_{\mathbf{i}+\mathbf{e}_l,l})|v_{\mathbf{i}+\mathbf{e}_l,l}| \right\rangle]. \end{aligned} \tag{B.10}$$

Smoothness assumption on the probability distribution in (B.5) yields

$$\langle \Theta(-v_{\mathbf{i}+\mathbf{e}_l,l})|v_{\mathbf{i}+\mathbf{e}_l,l}| \rangle = \langle \Theta(-v_{\mathbf{i},l})|v_{\mathbf{i},l}| \rangle + O(1/L) \tag{B.11}$$

so the two terms in the rhs of Eq. (B.10) sum up and at the first order give

$$\langle j_{\mathbf{i},p,l} j_{\mathbf{i}',p,l'} \rangle \sim \delta_{\mathbf{i},\mathbf{i}'}\delta_{p,p'}\delta_{l,l'}\rho_{\mathbf{i}}(1-\rho_{\mathbf{i}}) \langle |v_{\mathbf{i},l}| \rangle \frac{\Delta t}{\Delta x} \tag{B.12}$$

because $[\Theta(x) + \Theta(-x)]|x| = |x|$. The procedure shown is completely general and holds as well for momentum and energy currents: one simply has to compute the correlations through Eq. (B.7) substituting the current of the transported quantity $\chi(\mathbf{v})$, namely

$$J^{(\chi)}_{\mathbf{i},l} \equiv= \delta_{\boldsymbol{\xi}_p,\mathbf{i}}\delta_{\boldsymbol{\zeta}_p,\mathbf{e}_l}\chi(\mathbf{v}_{\mathbf{i}}) - \delta_{\boldsymbol{\xi}_p,\mathbf{i}+\mathbf{e}_l}\delta_{\boldsymbol{\zeta}_p,-\mathbf{e}_l}\chi(\mathbf{v}_{\mathbf{i}+\mathbf{e}_l}) \tag{B.13}$$

C Videos

This appendix contains a collection of links to video showing experiments and simulations on granular matter, active matter and hydrodynamics, cited in Part II, which can be useful to clarify the meaning of the discussed phenomenology.

C.1 Granular matter

- Granular jamming through a hopper: https://youtu.be/lWSJwZhqoQw, by J. Tang and R.P. Behringer, Duke Physics.
- A demonstration of possible applications of granular jamming: https://youtu.be/ZKOI_lVDPpw by Cornell Creative Machines Lab.
- Convection and segregation can be seen through an experimental realization of the Brazil-nut effect, see https://youtu.be/PGDP5DomhWc by Chung, Liaw and Ju.
- Pattern formation is shown at https://youtu.be/s0XYrW1X0ig (experiment and simulations) and https://youtu.be/CpZaRn0Bez0 (simulations), respectively made by Howard Duan at Toronto university and by Simons Foundation.
- A granular simulation showing clustering during cooling of a granular gas is shown at https://youtu.be/0byE8mrDjRE, made by Stefan Luding at Twente University ; another clustering simulation can be found at https://youtu.be/ap_PcMC2cdE, made by the MPIDS-DCF group.
- Experimental visualization and qualitative explaination of granular jets: https://youtu.be/Nt4jzVUEJjo, by Sixty Symbols with Roger Bowley.

- An experiment on a shaken granular showing several granular phases and Leidenfrost effect: https://youtu.be/ueCtAlHXxCU, by Bagnoli and Guarino at Florence University
- A granular rotor used to build a ratchet is shown at https://youtu.be/aHrdY4BC71k, made by the GranularChaos group in Rome.

C.2 Active matter

- Synchronization of metronomes (Kuramoto): https://youtu.be/Aaxw4zbULMs, by Harvard Natural Science Lectures Demonstrations.
- Swarming bacteria: https://youtu.be/q27Jn3h4kpE by Matthew Copeland, University of Wisconsin.
- Bird flocks in Rome: https://youtu.be/8V6qUUWa4zk (Science Channel).
- Simulations showing active matter phase separation: https://youtu.be/JtY2rtwP9v0, ratchet effect: https://youtu.be/oOtKNO-AEbY and shepherding: https://youtu.be/aIcaAuqP_KY. Made by Danielle McDermott at Wabash University.

C.3 Hydrodynamic instabilities

Here the main hydrodynamic instabilities connected with the

- The Rayleigh-Taylor instability: https://youtu.be/yabqo7VFTYs, by Jens Niemeyer at Göttingen University
- The Kelvin-Helmoltz instability is experimentally presented at https://youtu.be/UbAfvcaYr00 and numerically shown at https://youtu.be/mZ19gLn6Fx4. Videos respectively made by the DAMTP, University of Cambridge, and by Jens Niemeyer.
- The Plateau-Rayleigh instability: https://youtu.be/UYRGEINpO50, by the BYUSplashLab, Ira A. Fulton College.
- The Saffman-Taylor instability: https://youtu.be/FqC7VGTGh4U, by Fluid Dynamics students at Dalhousie University, lecturer David Barclay.

Papers

[1] Alessandro Manacorda, Andrea Puglisi, and Alessandro Sarracino. Coulomb friction driving brownian motors. *Communications in Theoretical Physics*, 62(4):505, 2014.

[2] Antonio Lasanta, Alessandro Manacorda, Antonio Prados, and Andrea Puglisi. Fluctuating hydrodynamics and mesoscopic effects of spatial correlations in dissipative systems with conserved momentum. *New J. Phys.*, 17:083039, 2015.

[3] Alessandro Manacorda, Carlos A Plata, Antonio Lasanta, Andrea Puglisi, and Antonio Prados. Lattice models for granular-like velocity fields: Hydrodynamic description. *J. Stat. Phys.*, 164(4):810–841, 2016.

[4] Carlos A Plata, Alessandro Manacorda, Antonio Lasanta, Andrea Puglisi, and Antonio Prados. Lattice models for granular-like velocity fields: finite-size effects. *J. Stat. Mech. (Theor. Exp.)*, 2016(9):093203, 2016.

[5] Alessandro Manacorda and Andrea Puglisi. A lattice model to derive the fluctuating hydrodynamics of granular active particles. submitted.

Bibliography

[1] J. A. Acebrón, L. L. Bonilla, C. J. Pérez Vicente, F. Ritort, and R. Spigler. The Kuramoto model: A simple paradigm for synchronization phenomena. *Rev. Mod. Phys.*, 77:137–185, Apr 2005.

[2] S. Alexander, J. Bernasconi, W. R. Schneider, and R. Orbach. Excitation dynamics in random one-dimensional systems. *Rev. Mod. Phys.*, 53:175–198, Apr 1981.

[3] I. S. Aranson and L. S. Tsimring. Patterns and collective behavior in granular media: Theoretical concepts. *Rev. Mod. Phys.*, 78:641–692, Jun 2006.

[4] A. Baldassarri, F. Dalton, A. Petri, S. Zapperi, G. Pontuale, and L. Pietronero. Brownian forces in sheared granular matter. *Phys. Rev. Lett.*, 96:118002, Mar 2006.

[5] A. Baldassarri, U. Marini Bettolo Marconi, and A. Puglisi. Cooling of a lattice granular fluid as an ordering process. *Phys. Rev. E*, 65:051301, May 2002.

[6] A. Baldassarri, U. Marini Bettolo Marconi, and A. Puglisi. Influence of correlations on the velocity statistics of scalar granular gases. *EPL (Europhysics Letters)*, 58(1):14, 2002.

[7] A. Baldassarri, A. Puglisi, and U. Marini Bettolo Marconi. Kinetic models of inelastic gases. *Mathematical Models and Methods in Applied Sciences*, 12(07):965–983, 2002.

[8] M. Ballerini, N. Cabibbo, R. Candelier, A. Cavagna, E. Cisbani, I. Giardina, V. Lecomte, A. Orlandi, G. Parisi, A. Procaccini, et al. Interaction ruling animal collective behavior depends on topological rather than metric distance: Evidence from a field study. *Proc. Natl. Acad. Sci.*, 105(4):1232–1237, 2008.

[9] A. Baskaran and M. C. Marchetti. Hydrodynamics of self-propelled hard rods. *Phys. Rev. E*, 77:011920, Jan 2008.

[10] A. Baskaran and M. C. Marchetti. Statistical mechanics and hydrodynamics of bacterial suspensions. *Proc. Natl. Acad. Sci.*, 106(37):15567–15572, 2009.

[11] C. Becco, N. Vandewalle, J. Delcourt, and P. Poncin. Experimental evidences of a structural and dynamical transition in fish school. *Physica A: Statistical Mechanics and its Applications*, 367:487 – 493, 2006.

[12] C. Bechinger, R. Di Leonardo, H. Löwen, C. Reichhardt, G. Volpe, and G. Volpe. Active particles in complex and crowded environments. *Rev. Mod. Phys.*, 88:045006, Nov 2016.

[13] E. Ben-Naim and P. L. Krapivsky. Maxwell model of traffic flows. *Phys. Rev. E*, 59:88–97, Jan 1999.

[14] E. Ben-Naim and P. L. Krapivsky. Multiscaling in inelastic collisions. *Phys. Rev. E*, 61:R5–R8, Jan 2000.

[15] C. M. Bender and S. A. Orszag. *Advanced Mathematical Methods for Scientists and Engineers*. Springer, 1999.

[16] E. Bertin. *Statistical Physics of Complex Systems*. Springer, 2016.

[17] E. Bertin. Theoretical approaches to the steady-state statistical physics of interacting dissipative units. *J. Phys. A: Math. Theor.*, 50(8):083001, 2017.

[18] E. Bertin, M. Droz, and G. Grégoire. Boltzmann and hydrodynamic description for self-propelled particles. *Phys. Rev. E*, 74:022101, Aug 2006.

[19] E. Bertin, M. Droz, and G. Grégoire. Hydrodynamic equations for self-propelled particles: microscopic derivation and stability analysis. *J. Phys. A: Math. Theor.*, 42(44):445001, 2009.

[20] L. Bertini, A. De Sole, D. Gabrielli, G. Jona-Lasinio, and C. Landim. Macroscopic fluctuation theory for stationary non-equilibrium states. *J. Stat. Phys.*, 107(3):635–675, 2002.

[21] L. Bertini, A. De Sole, D. Gabrielli, G. Jona-Lasinio, and C. Landim. Macroscopic fluctuation theory. *Rev. Mod. Phys.*, 87:593–636, Jun 2015.

[22] W. Beverloo, H. Leniger, and J. van de Velde. The flow of granular solids through orifices. *Chemical Engineering Science*, 15(3):260 – 269, 1961.

[23] W. Bialek, A. Cavagna, I. Giardina, T. Mora, E. Silvestri, M. Viale, and A. M. Walczak. Statistical mechanics for natural flocks of birds. *Proc. Natl. Acad. Sci.*, 109(13):4786–4791, 2012.

[24] M. Bixon and R. Zwanzig. Boltzmann-Langevin equation and hydrodynamic fluctuations. *Phys. Rev.*, 187:267–272, Nov 1969.

[25] D. Blackwell and R. D. Mauldin. Ulam's redistribution of energy problem: Collision transformations. *Letters in Mathematical Physics*, 10(2):149–153, Jun 1985.

[26] D. L. Blair and A. Kudrolli. Velocity correlations in dense granular gases. *Phys. Rev. E*, 64:050301, Oct 2001.

[27] A. Bortz, M. Kalos, and J. Lebowitz. A new algorithm for Monte Carlo simulation of Ising spin systems. *Journal of Computational Physics*, 17(1):10 – 18, 1975.

[28] J. J. Brey, A. Domínguez, M. I. García de Soria, and P. Maynar. Mesoscopic theory of critical fluctuations in isolated granular gases. *Phys. Rev. Lett.*, 96:158002, Apr 2006.

[29] J. J. Brey, J. W. Dufty, C. S. Kim, and A. Santos. Hydrodynamics for granular flow at low density. *Phys. Rev. E*, 58:4638–4653, Oct 1998.

[30] J. J. Brey, P. Maynar, and M. I. García de Soria. Fluctuating hydrodynamics for dilute granular gases. *Phys. Rev. E*, 79:051305, May 2009.

[31] J. J. Brey and A. Prados. Memory effects in vibrated granular systems. *Journal of Physics: Condensed Matter*, 14(7):1489, 2002.

[32] J. J. Brey, M. J. Ruiz-Montero, and D. Cubero. Homogeneous cooling state of a low-density granular flow. *Phys. Rev. E*, 54:3664–3671, Oct 1996.

[33] J. J. Brey, M. J. Ruiz-Montero, and F. Moreno. Steady-state representation of the homogeneous cooling state of a granular gas. *Phys. Rev. E*, 69:051303, May 2004.

[34] N. Brilliantov and T. Pöschel, editors. *Kinetic Theory of Granular Gases*. Oxford University Press, 2004.

[35] N. V. Brilliantov, F. Spahn, J.-M. Hertzsch, and T. Pöschel. Model for collisions in granular gases. *Phys. Rev. E*, 53:5382–5392, May 1996.

[36] R. Brown and J. Richards. *Principles of Powder Mechanics*. Pergamon Press, 1970.

[37] J. Buhl, D. J. T. Sumpter, I. D. Couzin, J. J. Hale, E. Despland, E. R. Miller, and S. J. Simpson. From disorder to order in marching locusts. *Science*, 312(5778):1402–1406, 2006.

[38] I. Buttinoni, J. Bialké, F. Kümmel, H. Löwen, C. Bechinger, and T. Speck. Dynamical clustering and phase separation in suspensions of self-propelled colloidal particles. *Phys. Rev. Lett.*, 110:238301, Jun 2013.

[39] M. Cates, J. Wittmer, J.-P. Bouchaud, and P. Claudin. Jamming, force chains, and fragile matter. *Phys. Rev. Lett.*, 81(9):1841, 1998.

[40] M. E. Cates and J. Tailleur. When are active Brownian particles and run-and-tumble particles equivalent? consequences for motility-induced phase separation. *EPL (Europhysics Letters)*, 101(2):20010, 2013.

[41] M. E. Cates and J. Tailleur. Motility-induced phase separation. *Annu. Rev. Condens. Matt. Phys.*, 6(1):219–244, 2015.

[42] A. Cavagna, A. Cimarelli, I. Giardina, G. Parisi, R. Santagati, F. Stefanini, and M. Viale. Scale-free correlations in starling flocks. *Proc. Natl. Acad. Sci.*, 107(26):11865–11870, 2010.

[43] A. Cavagna and I. Giardina. Bird flocks as condensed matter. *Annu. Rev. Condens. Matt. Phys.*, 5(1):183–207, 2014.

[44] M. Cencini, F. Cecconi, and A. Vulpiani. *Chaos: from simple models to complex systems*. World Scientific, 2010.

[45] C. Cercignani, R. Illner, and M. Pulvirenti. *The mathematical theory of dilute gases*. Springer Science & Business Media, 2013.

[46] S. Chapman and T. G. Cowling. *The Mathematical Theory of Non-Uniform Gases. 3rd edition*. Cambridge University Press, 1990.

[47] H. Chaté, F. Ginelli, G. Grégoire, F. Peruani, and F. Raynaud. Modeling collective motion: variations on the Vicsek model. *The European Physical Journal B*, 64(3):451–456, 2008.

[48] A. Chepizhko and V. Kulinskii. On the relation between Vicsek and Kuramoto models of spontaneous synchronization. *Physica A: Statistical Mechanics and its Applications*, 389(23):5347 – 5352, 2010.

[49] L. H. Cisneros, R. Cortez, C. Dombrowski, R. E. Goldstein, and J. O. Kessler. Fluid dynamics of self-propelled microorganisms, from individuals to concentrated populations. *Experiments in Fluids*, 43(5):737–753, 2007.

[50] G. Costantini, U. Marini Bettolo Marconi, and A. Puglisi. Granular Brownian ratchet model. *Phys. Rev. E*, 75:061124, Jun 2007.

[51] G. Costantini, U. Marini Bettolo Marconi, and A. Puglisi. Velocity fluctuations in a one-dimensional inelastic Maxwell model. *Journal of Statistical Mechanics: Theory and Experiment*, 2007(08):P08031, 2007.

[52] G. Costantini and A. Puglisi. Fluctuating hydrodynamics in a vertically vibrated granular fluid with gravity. *Phys. Rev. E*, 84:031307, Sep 2011.

[53] G. Costantini, A. Puglisi, and U. Marini Bettolo Marconi. Models of granular ratchets. *J. Stat. Mech. (Theor. Exp.)*, 2009(07):P07004, 2009.

[54] Z. Csahók and T. Vicsek. Lattice-gas model for collective biological motion. *Phys. Rev. E*, 52:5297–5303, Nov 1995.

[55] A. Czirók, E. Ben-Jacob, I. Cohen, and T. Vicsek. Formation of complex bacterial colonies via self-generated vortices. *Phys. Rev. E*, 54:1791–1801, Aug 1996.

[56] A. Czirók, H. E. Stanley, and T. Vicsek. Spontaneously ordered motion of self-propelled particles. *J. Phys. A: Math. Gen.*, 30(5):1375, 1997.

[57] A. Czirók and T. Vicsek. Collective behavior of interacting self-propelled particles. *Physica A: Statistical Mechanics and its Applications*, 281(1–4):17 – 29, 2000.

[58] O. Dauchot, G. Marty, and G. Biroli. Dynamical heterogeneity close to the jamming transition in a sheared granular material. *Phys. Rev. Lett.*, 95:265701, Dec 2005.

[59] P. G. de Gennes. Granular matter: a tentative view. *Rev. Mod. Phys.*, 71:S374–S382, Mar 1999.

[60] M. I. G. de Soria, P. Maynar, S. Mischler, C. Mouhot, T. Rey, and E. Trizac. Towards an H-theorem for granular gases. *J. Stat. Mech. (Theor. Exp.)*, 2015(11):P11009, 2015.

[61] B. Derrida. Velocity and diffusion constant of a periodic one-dimensional hopping model. *J. Stat. Phys.*, 31(3):433–450, 1983.

[62] B. Derrida. Non-equilibrium steady states: fluctuations and large deviations of the density and of the current. *J. Stat. Mech. (Theor. Exp.)*, 2007(07):P07023, 2007.

[63] B. Derrida and Y. Pomeau. Classical diffusion on a random chain. *Phys. Rev. Lett.*, 48:627–630, Mar 1982.

[64] J. Deseigne, O. Dauchot, and H. Chaté. Collective motion of vibrated polar disks. *Phys. Rev. Lett.*, 105:098001, Aug 2010.

[65] P. G. Drazin and W. H. Reid. *Hydrodynamic stability*. Cambridge University press, 2004.

[66] J. Elgeti, R. G. Winkler, and G. Gompper. Physics of microswimmers—single particle motion and collective behavior: a review. *Reports on Progress in Physics*, 78(5):056601, 2015.

[67] M. Ernst. Nonlinear model-Boltzmann equations and exact solutions. *Physics Reports*, 78(1):1 – 171, 1981.

[68] M. Ernst, J. Dorfman, W. Hoegy, and J. V. Leeuwen. Hard-sphere dynamics and binary-collision operators. *Physica*, 45(1):127 – 146, 1969.

[69] M. H. Ernst, E. Trizac, and A. Barrat. The rich behavior of the Boltzmann equation for dissipative gases. *EPL (Europhysics Letters)*, 76(1):56, 2006.

[70] P. Eshuis, K. van der Weele, D. Lohse, and D. van der Meer. Experimental realization of a rotational ratchet in a granular gas. *Phys. Rev. Lett.*, 104:248001, Jun 2010.

[71] P. Eshuis, K. van der Weele, D. van der Meer, and D. Lohse. Granular Leidenfrost effect: Experiment and theory of floating particle clusters. *Phys. Rev. Lett.*, 95:258001, Dec 2005.

[72] E. Falcon, S. Fauve, and C. Laroche. Cluster formation, pressure and density measurements in a granular medium fluidized by vibrations. *The European Physical Journal B - Condensed Matter and Complex Systems*, 9(2):183–186, 1999.

[73] E. Falcon, R. Wunenburger, P. Évesque, S. Fauve, C. Chabot, Y. Garrabos, and D. Beysens. Cluster formation in a granular medium fluidized by vibrations in low gravity. *Phys. Rev. Lett.*, 83:440–443, Jul 1999.

[74] T. F. F. Farage, P. Krinninger, and J. M. Brader. Effective interactions in active Brownian suspensions. *Phys. Rev. E*, 91:042310, Apr 2015.

[75] J. J. Faria, J. R. Dyer, C. R. Tosh, and J. Krause. Leadership and social information use in human crowds. *Animal Behaviour*, 79(4):895 – 901, 2010.

[76] J. H. Ferziger and H. G. Kaper. *Mathematical theory of transport processes in gases*. North Holland, 1972.

[77] Y. Fily and M. C. Marchetti. Athermal phase separation of self-propelled particles with no alignment. *Phys. Rev. Lett.*, 108:235702, Jun 2012.

[78] E. Fodor, C. Nardini, M. E. Cates, J. Tailleur, P. Visco, and F. van Wijland. How far from equilibrium is active matter? *Phys. Rev. Lett.*, 117:038103, Jul 2016.

[79] G. Gallavotti and E. G. D. Cohen. Dynamical ensembles in nonequilibrium statistical mechanics. *Phys. Rev. Lett.*, 74:2694–2697, Apr 1995.

[80] C. Gardiner. *Stochastic Methods. A Handbook for the Natural and Social Sciences. 4th Edition*. Springer, 2009.

[81] V. Garzó. Transport coefficients for an inelastic gas around uniform shear flow: Linear stability analysis. *Phys. Rev. E*, 73:021304, Feb 2006.

[82] F. Ginelli and H. Chaté. Relevance of metric-free interactions in flocking phenomena. 105:168103, Oct 2010.

[83] I. Goldhirsch and G. Zanetti. Clustering instability in dissipative gases. *Phys. Rev. Lett.*, 70:1619–1622, Mar 1993.

[84] A. Goldshtein and M. Shapiro. Mechanics of collisional motion of granular materials. part 1. general hydrodynamic equations. *Journal of Fluid Mechanics*, 282:75–114, 1995.

[85] G. Gradenigo, A. Sarracino, D. Villamaina, and A. Puglisi. Fluctuating hydrodynamics and correlation lengths in a driven granular fluid. *J. Stat. Mech. (Theor. Exp.)*, 2011(08):P08017, 2011.

[86] G. Gradenigo, A. Sarracino, D. Villamaina, and A. Puglisi. Non-equilibrium length in granular fluids: From experiment to fluctuating hydrodynamics. *EPL (Europhysics Letters)*, 96(1):14004, 2011.

[87] D. Grossman, I. S. Aranson, and E. B. Jacob. Emergence of agent swarm migration and vortex formation through inelastic collisions. *New J. Phys.*, 10(2):023036, 2008.

[88] P. K. Haff. Grain flow as a fluid-mechanical phenomenon. *Journal of Fluid Mechanics*, 134:401–430, 1983.

[89] B. Hancock and A. Baskaran. Statistical mechanics and hydrodynamics of self-propelled hard spheres. *J. Stat. Mech. (Theor. Exp.)*, 2017(3):033205, 2017.

[90] D. Helbing, I. Farkas, and T. Vicsek. Simulating dynamical features of escape panic. *Nature*, 407(6803):487–490, 2000.

[91] D. Helbing, J. Keltsch, and P. Molnar. Modelling the evolution of human trail systems. *Nature*, 388(6637):47–50, 1997.

[92] D. Hoare, I. Couzin, J.-G. Godin, and J. Krause. Context-dependent group size choice in fish. *Animal Behaviour*, 67(1):155 – 164, 2004.

[93] D. Howell, R. P. Behringer, and C. Veje. Stress fluctuations in a 2d granular Couette experiment: A continuous transition. *Phys. Rev. Lett.*, 82:5241–5244, Jun 1999.

[94] K. Huang. *Statistical Mechanics. 2nd Edition*. John Wiley & Sons, 1987.

[95] D. A. Huerta and J. C. Ruiz-Suárez. Vibration-induced granular segregation: A phenomenon driven by three mechanisms. *Phys. Rev. Lett.*, 92:114301, Mar 2004.

[96] P. I. Hurtado, A. Lasanta, and A. Prados. Typical and rare fluctuations in nonlinear driven diffusive systems with dissipation. *Phys. Rev. E*, 88:022110, Aug 2013.

[97] T. Ihle. Kinetic theory of flocking: Derivation of hydrodynamic equations. *Phys. Rev. E*, 83:030901, Mar 2011.

[98] H. M. Jaeger, S. R. Nagel, and R. P. Behringer. Granular solids, liquids, and gases. *Rev. Mod. Phys.*, 68:1259–1273, Oct 1996.

[99] Jan-Martin Hertzsch, Frank Spahn, and Nikolai V. Brilliantov. On low-velocity collisions of viscoelastic particles. *J. Phys. II France*, 5(11):1725–1738, 1995.

[100] H. Janssen. Versuche über getreidedruck in silozellen. *Zeitschr. d. Vereines deutscher Ingenieure*, 39(35):1045–1049, 1895.

[101] C. Jarzynski. Nonequilibrium equality for free energy differences. *Phys. Rev. Lett.*, 78:2690–2693, Apr 1997.

[102] C. Josserand, A. V. Tkachenko, D. M. Mueth, and H. M. Jaeger. Memory effects in granular materials. *Phys. Rev. Lett.*, 85:3632–3635, Oct 2000.

[103] N. G. V. Kampen. *Stochastic Processes in Physics and Chemistry*. North-Holland, 1992.

[104] Y. Katz, K. Tunstrøm, C. C. Ioannou, C. Huepe, and I. D. Couzin. Inferring the structure and dynamics of interactions in schooling fish. *Proc. Natl. Acad. Sci.*, 108(46):18720–18725, 2011.

[105] E. F. Keller and L. A. Segel. Model for chemotaxis. *Journal of Theoretical Biology*, 30(2):225 – 234, 1971.

[106] R. Khosropour, J. Zirinsky, H. K. Pak, and R. P. Behringer. Convection and size segregation in a Couette flow of granular material. *Phys. Rev. E*, 56:4467–4473, Oct 1997.

[107] K. Kim and H. K. Pak. Coarsening dynamics of striped patterns in thin granular layers under vertical vibration. *Phys. Rev. Lett.*, 88:204303, May 2002.

[108] C. Kipnis, C. Marchioro, and E. Presutti. Heat flow in an exactly solvable model. *J. Stat. Phys.*, 27(1):65–74, 1982.

[109] N. Koumakis, C. Maggi, and R. Di Leonardo. Directed transport of active particles over asymmetric energy barriers. *Soft Matter*, 10:5695–5701, 2014.

[110] W. T. Kranz, M. Sperl, and A. Zippelius. Glass transition for driven granular fluids. *Phys. Rev. Lett.*, 104:225701, Jun 2010.

[111] J. Krim, P. Yu, and R. P. Behringer. Stick–slip and the transition to steady sliding in a 2d granular medium and a fixed particle lattice. *Pure and Applied Geophysics*, 168(12):2259–2275, 2011.

[112] R. Kubo, M. Toda, and N. Hashitsume. *Statistical physics II: nonequilibrium statistical mechanics*. Springer Science & Business Media, 2012.

[113] A. Kudrolli and J. Henry. Non-Gaussian velocity distributions in excited granular matter in the absence of clustering. *Phys. Rev. E*, 62:R1489–R1492, Aug 2000.

[114] A. Kudrolli, G. Lumay, D. Volfson, and L. S. Tsimring. Swarming and swirling in self-propelled polar granular rods. *Phys. Rev. Lett.*, 100:058001, Feb 2008.

[115] A. Kudrolli, M. Wolpert, and J. P. Gollub. Cluster formation due to collisions in granular material. *Phys. Rev. Lett.*, 78:1383–1386, Feb 1997.

[116] N. Kumar, H. Soni, S. Ramaswamy, and A. Sood. Flocking at a distance in active granular matter. *Nature Communications*, 5, 2014.

[117] Y. Kuramoto. *Self-entrainment of a population of coupled non-linear oscillators*, pages 420–422. Springer, 1975.

[118] Y. Kuramoto. *Chemical oscillations, waves, and turbulence*. Springer, 1984.

[119] L. Landau and E. Lifshitz. *Fluid Mechanics. Course of Theoretical Physics, volume 6*. Pergamon Press, 1987.

[120] A. Lasanta. *Algunas propiedades de los estados estacionarios de sistemas disipativos sencillos*. PhD thesis, Universidad de Granada, 2014.

[121] A. Lasanta, P. I. Hurtado, and A. Prados. Statistics of the dissipated energy in driven diffusive systems. *The European Physical Journal E*, 39(3):35, 2016.

[122] A. Lasanta, A. Manacorda, A. Prados, and A. Puglisi. Fluctuating hydrodynamics and mesoscopic effects of spatial correlations in dissipative systems with conserved momentum. *New J. Phys.*, 17:083039, 2015.

[123] J. L. Lebowitz and H. Spohn. A Gallavotti–Cohen-type symmetry in the large deviation functional for stochastic dynamics. *J. Stat. Phys.*, 95(1):333–365, 1999.

[124] A. W. Lees and S. F. Edwards. The computer study of transport processes under extreme conditions. *Journal of Physics C: Solid State Physics*, 5(15):1921, 1972.

[125] A. J. Liu and S. R. Nagel. Nonlinear dynamics: Jamming is not just cool any more. *Nature*, 396(6706):21–22, 1998.

[126] C.-h. Liu and S. R. Nagel. Sound in sand. *Phys. Rev. Lett.*, 68(15):2301, 1992.

[127] C.-h. Liu and S. R. Nagel. Sound in a granular material: disorder and nonlinearity. *Phys. Rev. B*, 48(21):15646, 1993.

[128] W. Losert, D. Cooper, J. Delour, A. Kudrolli, and J. Gollub. Velocity statistics in excited granular media. *Chaos: An Interdisciplinary Journal of Nonlinear Science*, 9(3):682–690, 1999.

[129] S. Luding, E. Clément, A. Blumen, J. Rajchenbach, and J. Duran. Studies of columns of beads under external vibrations. *Phys. Rev. E*, 49:1634–1646, Feb 1994.

[130] C. Maggi, U. Marini Bettolo Marconi, N. Gnan, and R. Di Leonardo. Multidimensional stationary probability distribution for interacting active particles. *Scientific Reports*, 5:10742, 2015.

[131] T. S. Majmudar and R. P. Behringer. Contact force measurements and stress-induced anisotropy in granular materials. *Nature*, 435(7045):1079–1082, 2005.

[132] T. S. Majmudar, M. Sperl, S. Luding, and R. P. Behringer. Jamming transition in granular systems. *Phys. Rev. Lett.*, 98:058001, Jan 2007.

[133] A. Manacorda, C. A. Plata, A. Lasanta, A. Puglisi, and A. Prados. Lattice models for granular-like velocity fields: Hydrodynamic description. *J. Stat. Phys.*, 164(4):810–841, Aug 2016.

[134] A. Manacorda and A. Puglisi. A lattice model to derive the fluctuating hydrodynamics of granular active particles. Submitted.

[135] M. C. Marchetti, J. F. Joanny, S. Ramaswamy, T. B. Liverpool, J. Prost, M. Rao, and R. A. Simha. Hydrodynamics of soft active matter. *Rev. Mod. Phys.*, 85:1143–1189, Jul 2013.

[136] U. Marini Bettolo Marconi and C. Maggi. Towards a statistical mechanical theory of active fluids. *Soft Matter*, 11:8768–8781, 2015.

[137] U. Marini Bettolo Marconi, A. Puglisi, and C. Maggi. Heat, temperature and clausius inequality in a model for active Brownian particles. *Scientific Reports*, 7, 2017.

[138] U. Marini Bettolo Marconi, A. Puglisi, L. Rondoni, and A. Vulpiani. Fluctuation–dissipation: Response theory in statistical physics. *Phys. Rep.*, 461(4–6):111 – 195, 2008.

[139] U. Marini Bettolo Marconi, A. Puglisi, and A. Vulpiani. About an H-theorem for systems with non-conservative interactions. *J. Stat. Mech. (Theor. Exp.)*, 2013(08):P08003, 2013.

[140] J. Marro and R. Dickman. *Nonequilibrium phase transitions in lattice models*. Cambridge University Press, 2005.

[141] S. McNamara and W. R. Young. Inelastic collapse and clumping in a one-dimensional granular medium. *Physics of Fluids A: Fluid Dynamics*, 4(3):496–504, 1992.

[142] S. McNamara and W. R. Young. Inelastic collapse in two dimensions. *Phys. Rev. E*, 50:R28–R31, Jul 1994.

[143] S. McNamara and W. R. Young. Dynamics of a freely evolving, two-dimensional granular medium. *Phys. Rev. E*, 53:5089–5100, May 1996.

[144] F. Melo, P. Umbanhowar, and H. L. Swinney. Transition to parametric wave patterns in a vertically oscillated granular layer. *Phys. Rev. Lett.*, 72:172–175, Jan 1994.

[145] F. Melo, P. B. Umbanhowar, and H. L. Swinney. Hexagons, kinks, and disorder in oscillated granular layers. *Phys. Rev. Lett.*, 75:3838–3841, Nov 1995.

[146] M. E. Möbius, B. E. Lauderdale, S. R. Nagel, and H. M. Jaeger. Brazil-nut effect: Size separation of granular particles. *Nature*, 414(6861):270–270, 2001.

[147] T. Mora, A. M. Walczak, L. Del Castello, F. Ginelli, S. Melillo, L. Parisi, M. Viale, A. Cavagna, and I. Giardina. Local equilibrium in bird flocks. *Nature Physics*, 12(12):1153–1157, 2016.

[148] D. M. Mueth, H. M. Jaeger, and S. R. Nagel. Force distribution in a granular medium. *Phys. Rev. E*, 57(3):3164, 1998.

[149] V. Narayan, N. Menon, and S. Ramaswamy. Nonequilibrium steady states in a vibrated-rod monolayer: tetratic, nematic, and smectic correlations. *J. Stat. Mech. (Theor. Exp.)*, 2006(01):P01005, 2006.

[150] J. S. Olafsen and J. S. Urbach. Clustering, order, and collapse in a driven granular monolayer. *Phys. Rev. Lett.*, 81:4369–4372, Nov 1998.

[151] J. S. Olafsen and J. S. Urbach. Velocity distributions and density fluctuations in a granular gas. *Phys. Rev. E*, 60:R2468–R2471, Sep 1999.

[152] M. Paoluzzi, C. Maggi, U. Marini Bettolo Marconi, and N. Gnan. Critical phenomena in active matter. *Phys. Rev. E*, 94:052602, Nov 2016.

[153] A. Peshkov, E. Bertin, F. Ginelli, and H. Chaté. Boltzmann-Ginzburg-Landau approach for continuous descriptions of generic Vicsek-like models. *The European Physical Journal Special Topics*, 223(7):1315–1344, 2014.

[154] C. A. Plata. Ph.d. thesis. To be defended.

[155] C. A. Plata, A. Manacorda, A. Lasanta, A. Puglisi, and A. Prados. Lattice models for granular-like velocity fields: finite-size effects. *J. Stat. Mech. (Theor. Exp.)*, 2016(9):093203, 2016.

[156] C. A. Plata and A. Prados. Global stability and H theorem in lattice models with nonconservative interactions. *Phys. Rev. E*, 95:052121, May 2017.

[157] G. Pontuale, A. Gnoli, F. V. Reyes, and A. Puglisi. Thermal convection in granular gases with dissipative lateral walls. *Phys. Rev. Lett.*, 117:098006, Aug 2016.

[158] T. Pöschel and N. V. Brilliantov. *Granular gas dynamics*. Springer Verlag, 2003.

[159] T. Pöschel and S. Luding, editors. *Granular Gases*. Springer Verlag, 2001.

[160] A. Prados, J. J. Brey, and B. Sánchez-Rey. A dynamical Monte Carlo algorithm for master equations with time-dependent transition rates. *J. Stat. Phys.*, 89(3):709–734, 1997.

[161] A. Prados, A. Lasanta, and P. I. Hurtado. Large fluctuations in driven dissipative media. *Phys. Rev. Lett.*, 107:140601, Sep 2011.

[162] A. Prados, A. Lasanta, and P. I. Hurtado. Nonlinear driven diffusive systems with dissipation: Fluctuating hydrodynamics. *Phys. Rev. E*, 86:031134, Sep 2012.

[163] A. Prados and E. Trizac. Kovacs-like memory effect in driven granular gases. *Phys. Rev. Lett.*, 112:198001, May 2014.

[164] A. Puglisi. *Transport and fluctuations in granular fluids*. Springer, 2014.

[165] A. Puglisi, A. Gnoli, G. Gradenigo, A. Sarracino, and D. Villamaina. Structure factors in granular experiments with homogeneous fluidization. *J. Chem. Phys.*, 136(1):014704, 2012.

[166] A. Puglisi, V. Loreto, U. Marini Bettolo Marconi, A. Petri, and A. Vulpiani. Clustering and non-Gaussian behavior in granular matter. *Phys. Rev. Lett.*, 81:3848–3851, Nov 1998.

[167] A. Puglisi, V. Loreto, U. Marini Bettolo Marconi, and A. Vulpiani. Kinetic approach to granular gases. *Phys. Rev. E*, 59:5582–5595, May 1999.

[168] S. Ramaswamy. The mechanics and statistics of active matter. *Annu. Rev. Condens. Matt. Phys.*, 1(1):323–345, 2010.

[169] G. S. Redner, M. F. Hagan, and A. Baskaran. Structure and dynamics of a phase-separating active colloidal fluid. *Phys. Rev. Lett.*, 110:055701, Jan 2013.

[170] P. Romanczuk, M. Bär, W. Ebeling, B. Lindner, and L. Schimansky-Geier. Active Brownian particles. *The European Physical Journal Special Topics*, 202(1):1–162, 2012.

[171] M. J. Schnitzer. Theory of continuum random walks and application to chemotaxis. *Phys. Rev. E*, 48:2553–2568, Oct 1993.

[172] U. Seifert. Stochastic thermodynamics, fluctuation theorems and molecular machines. *Reports on Progress in Physics*, 75(12):126001, 2012.

[173] L. E. Silbert, D. Ertaş, G. S. Grest, T. C. Halsey, and D. Levine. Analogies between granular jamming and the liquid-glass transition. *Phys. Rev. E*, 65:051307, May 2002.

[174] A. P. Solon, M. E. Cates, and J. Tailleur. Active Brownian particles and run-and-tumble particles: A comparative study. *The European Physical Journal Special Topics*, 224(7):1231–1262, Jul 2015.

[175] A. P. Solon and J. Tailleur. Revisiting the flocking transition using active spins. *Phys. Rev. Lett.*, 111:078101, Aug 2013.

[176] S. H. Strogatz. From Kuramoto to Crawford: exploring the onset of synchronization in populations of coupled oscillators. *Physica D: Nonlinear Phenomena*, 143(1):1 – 20, 2000.

[177] K. Sugawara, M. Sano, T. Mizuguchi, and Y. Hayakawa. Collective motion of multi-robot system based on simple dynamics. In *Human Robot Interaction*. INTECH Open Access Publisher, 2007.

[178] J. Tailleur and M. E. Cates. Statistical mechanics of interacting run-and-tumble bacteria. *Phys. Rev. Lett.*, 100:218103, May 2008.

[179] J. Tang and R. Behringer. How granular materials jam in a hopper. *Chaos-Woodbury*, 21(4):041107, 2011.

[180] J. Tang, S. Sagdiphour, and R. P. Behringer. Jamming and flow in 2d hoppers. *AIP Conference Proceedings*, 1145(1):515–518, 2009.

[181] A. G. Thompson, J. Tailleur, M. E. Cates, and R. A. Blythe. Lattice models of nonequilibrium bacterial dynamics. *J. Stat. Mech. (Theor. Exp.)*, 2011(02):P02029, 2011.

[182] S. T. Thoroddsen and A. Q. Shen. Granular jets. *Physics of Fluids*, 13(1):4–6, 2001.

[183] K. To, P.-Y. Lai, and H. K. Pak. Jamming of granular flow in a two-dimensional hopper. *Phys. Rev. Lett.*, 86:71–74, Jan 2001.

[184] J. Toner and Y. Tu. Long-range order in a two-dimensional dynamical XY model: How birds fly together. *Phys. Rev. Lett.*, 75:4326–4329, Dec 1995.

[185] J. Toner and Y. Tu. Flocks, herds, and schools: A quantitative theory of flocking. *Phys. Rev. E*, 58:4828–4858, Oct 1998.

[186] J. Toner, Y. Tu, and S. Ramaswamy. Hydrodynamics and phases of flocks. *Adv. Phys.*, 318(1):170 – 244, 2005. Special Issue.

[187] P. B. Umbanhowar, F. Melo, and H. L. Swinney. Localized excitations in a vertically vibrated granular layer. *Nature*, 382(6594):793–796, Aug 29 1996.

[188] T. van Noije and M. Ernst. Velocity distributions in homogeneous granular fluids: the free and the heated case. *Granular Matter*, 1(2):57–64, 1998.

[189] T. P. C. van Noije, M. H. Ernst, R. Brito, and J. A. G. Orza. Mesoscopic theory of granular fluids. *Phys. Rev. Lett.*, 79:411–414, Jul 1997.

[190] T. P. C. van Noije, M. H. Ernst, E. Trizac, and I. Pagonabarraga. Randomly driven granular fluids: Large-scale structure. *Phys. Rev. E*, 59:4326–4341, Apr 1999.

[191] T. Vicsek, A. Czirók, E. Ben-Jacob, I. Cohen, and O. Shochet. Novel type of phase transition in a system of self-driven particles. *Phys. Rev. Lett.*, 75:1226–1229, Aug 1995.

[192] T. Vicsek and A. Zafeiris. Collective motion. *Phys. Rep.*, 517(3–4):71 – 140, 2012.

[193] A. Vulpiani, F. Cecconi, M. Cencini, A. Puglisi, and D. Vergni. Large deviations in physics. Springer, 2014.

[194] S. Warr, J. M. Huntley, and G. T. H. Jacques. Fluidization of a two-dimensional granular system: Experimental study and scaling behavior. *Phys. Rev. E*, 52:5583–5595, Nov 1995.

[195] C. A. Weber, T. Hanke, J. Deseigne, S. Léonard, O. Dauchot, E. Frey, and H. Chaté. Long-range ordering of vibrated polar disks. *Phys. Rev. Lett.*, 110:208001, May 2013.

[196] R. D. Wildman, J. M. Huntley, and J.-P. Hansen. Self-diffusion of grains in a two-dimensional vibrofluidized bed. *Phys. Rev. E*, 60:7066–7075, Dec 1999.

[197] Y. Wu, A. D. Kaiser, Y. Jiang, and M. S. Alber. Periodic reversal of direction allows myxobacteria to swarm. *Proc. Natl. Acad. Sci.*, 106(4):1222–1227, 2009.

Credits for pictures

Here I report the sources of pictures used in this thesis, except the ones not listed which have been made by the author.

- Fig. 1.1 is made by the author, including pictures taken from Pexels and Raumrot photo archives. Saturn image was taken in visible light by Cassini spacecraft on May 21, 2016, and is available at NASA image gallery.
- Fig. 1.2 comes from the article of Majmudar and Behringer [132].
- Fig. 1.3 can be found at Junyao Tang's webpage at Duke University, `http://www.phy.duke.edu/~jt41/research.html#granular`. The authors also provide a clarifying video of the experience at `https://www.youtube.com/watch?v=lWSJwZhqoQw`.
- Figs. 1.4 come from the article of To, Lai and Pak [183].
- Fig. 1.5a comes from the article of Melo, Umbahnowar and Swinney [145].
- Fig. 1.5b has been made by paul Umbahnowar and reprinted by Aranson and Tsimring [3].
- Fig. 1.6b has been taken and rearranged from the article of Falcon *et al.* [73].
- Fig. 1.7 comes from the article of Olafsen and Urbach [150].
- Figs. 1.10 come both from articles of McNamara and Young, respectively [141] (left) and [143] (right).
- Fig. 2.1 is taken from the review of Vicsek and Zafeiris [192].
- Fig. 2.2 is taken from the article of Buttinoni *et al.* [38]
- Fig. 2.3 comes from the article of Cisneros *et al.* [49]
- Fig. 2.4a comes from the article of Cavagna *et al.* [43], while Fig. 2.4b is taken by the review of Vicsek and Zafeiris [192] who adapted it from Ballerini *et al.* [8]
- Fig. 2.5 is taken from Narayan *et al.* [149]
- Figs. 2.6 come from the article of Blair *et al.* [26]
- Fig. 2.7 is taken from the review of Elgeti, Winkel and Gompper [66]

- Figs. 2.8 are taken from the article of Strogatz [176]
- Figs. 2.9 and 2.10 come from the original article of Vicsek *et al.* [191]
- Fig. 2.11 comes from the review of Romanczuk *et al.* [170]
- Fig. 2.12 has been taken from the review of Bechinger *et al.* [12]
- Fig. 2.13 comes from the article of Grossman, Aranson and Ben Jacob [87]
- Fig. 3.1 is taken from the book of Brilliantov and Pöschel [34]
- Fig. 3.2 comes from the article of Derrida [62]

[..] vel, quod brevius dici potest,
vulgarem locutionem asserimus
quam sine omni regola
nutricem imitantes accipimus.

Ringraziamenti

Nella mia tesi di laurea non feci nessun ringraziamento, quindi qui mi prenderò qualche riga in più per farli.

Il primo ringraziamento è per Andrea Puglisi, mio relatore e maestro di fisica che mi ha accompagnato costantemente nel mio percorso di crescita come ricercatore e, inseparabilmente, come persona. In questi anni ho potuto apprezzare la sua disponibilità e pazienza (anche di fronte alle mie tante stranezze) combinata con le varie angolazioni teoriche, numeriche e sperimentali che riesce a combinare nella sua ricerca, e che mi hanno affascinato dall'inizio. Spero che questa tesi riesca a corrispondere almeno in parte alle aspettative che ci siamo fatti insieme ormai quattro anni fa, che possa tornare utile nel futuro ed essere il primo di tanti lavori insieme.

Conseguentemente ringrazio chi ha condiviso con me i passaggi più importanti del lavoro scientifico: in primo luogo Antonio Lasanta, la cui presenza è stata fonte di discussioni e confronti sempre utili nel corso di tutto il suo soggiorno a Roma, insieme al suo spirito vivace ed espansivo. Ringrazio il professor Antonio Prados, che in questi anni mi ha ispirato e formato con la sua meticolosità e tenacia da fisico teorico, e che ha seguito con attenzione costante il mio lavoro di tesi. Ringrazio Carlos A. Plata, che ho avuto il piacere di incontrare a Siviglia e di avere come collaboratore, conoscendo uno studente brillante che mi ha stimolato molto a dare il meglio di me e a intrecciare le nostre conoscenze per ottenere dei risultati comuni. Il suo valore scientifico mi è stato prezioso, insieme alla sua accoglienza a Siviglia, che mi ha permesso di scoprire una città stupenda con i divertenti e stravaganti giovani fisici che la abitano. A Carlos, Mário, Laura, Carlos, Miguel e tutta la banda, grazie!

In questi anni di tesi, il gruppo TNT è stato il mio punto di riferimento scientifico. Ringrazio in particolare Luca Cerino, per le discussioni sempre stimolanti e il sostegno psicologico, scientifico e tecnico che mi ha dato in vari passaggi mentre svolgevamo le nostre tesi; ringrazio Angelo Vulpiani per la disponibilità, i consigli e l'ascolto che mi ha prestato ogni qualvolta ci fosse bisogno, sia nelle questioni di fisica che nelle prospettive future; e ringrazio Alessandro Sarracino, fondamentale per capire tanti argomenti di fisica al di là del mio raggio d'azione e un interlocutore sempre stimolante e curioso. Insieme a lui ringrazio Umberto Marini Bettolo Marconi per averci dato i primi riscontri sulla ricerca in materia attiva quando era ancora in uno stato poco più che embrionale. Ringrazio Giorgio Pontuale, Alberto Petri, Andrea Baldassarri, Mario Alberto Annunziata, Fabio Cecconi e Massimo Cencini per l'accoglienza in questi anni, con una dedica particolare ad Andrea Gnoli, di cui ammiro sempre la gentilezza ed eleganza.

Tanto di questa tesi è passato dalla stanza 413, che ho potuto condividere con tanti fisici alle prese con il dottorato tra il 2013 e il 2017. In particolare ringrazio Fabrizio Antenucci, per il piacere della sua conscenza tanto nel confronto scientifico quanto nel dialogo umano, e Daniele Conti per il confronto e il sostegno che mi ha offerto, augurandogli in bocca al lupo per la sua tesi e sperando che prima o poi riuscirà a mettermi un cross giusto.

Ringrazio anche i vicini di stanza Massimiliano Viale e Stefania Melillo, che soprattutto negli ultimi mesi hanno rappresentato un grande sostegno morale mentre mi vedevano affogare nella scrittura della tesi. La loro solidarietà, curiosità ed empatia sono state preziose, come dimostra Massimiliano anche attraverso la fantasia e l'altruismo con cui gioca a calcetto.

Questa tesi conclude una fase importante della mia vita da studente nel Dipartimento di Fisica, dopo essermi iscritto dieci anni fa al corso di laurea triennale ed aver messo piede per la prima volta nell'Edificio Marconi. Ho avuto fin dall'inizio dei compagni straordinari. Tra di loro, voglio ringraziare prima di tutto Marco Sciannamea, avendo il piacere di discutere questa tesi di dottorato subito dopo la sua tesi di laurea. È stato bello studiare in questi mesi e vedere come gli sforzi dell'uno aiutavano l'altro, lavorando insieme da vecchi amici, al termine di percorsi anche travagliati ma sempre uniti. Oltre all'amicizia e l'affetto che ci lega, scrivere questa tesi sarebbe stato molto più difficile e pesante senza di lui.

In ultima analisi tutti i contenuti qui esposti non sarebbero presenti senza Marco o tutti i fisici con cui abbiamo studiato insieme da quando affrontavamo i corsi di geometria e meccanica al primo anno. Ringrazio Alessandro Calandri, che mi ispira da sempre con la sua solarità, curiosità e generosità accompagnate alla sua sensibilità ideale. Ringrazio Riccardo Junior Buonocore per essere un compagno di studi formidabile e non solo. Ringrazio Eleonora Frau, con cui ho condiviso il principio del nostro percorso e che è stata un sostegno e una ragione di felicità meravigliosi mentre intraprendevamo questa avventura. Voglio ringraziare tantissimo Ferdinando Randisi per essere un amico insostituibile oltre che un fisico brillante, per la sua genialità e creatività che ammiro ma ho un certo timore di incoraggiare troppo. Ringrazio Ferdinando anche per la sua giraffa.

Ringrazio Daniele per essere un mio amico e punto fermo da sempre, per le discussioni infinite in macchina sotto casa e i pensieri e i sentimenti intrecciati con cui torniamo, per condividere il mistero di essere molto simili e molto diversi e volersi molto bene.

Ringrazio Michele Angelo per essere la persona che è. Per la sua generosità e il suo ascolto, per la forza della sua affettività ed emotività, per la moralità che profonde nelle relazioni e per la scelta di intrecciare nuovamente le nostre strade, che mi rende felice.

Ringrazio Beatrice (Bicio) per essere un'amica fantastica, per i momenti di gioia o tristezza condivisi, perché c'è, per le serate di "svago" insieme, per aver sempre sostenuto le mie iniziative, o per averle corrette, per sopportarmi, per la fiducia che mi ha sempre trasmesso.

Ringrazio Gaia per essere un mio punto di riferimento da una vita, amica e vicina anche a distanza di tempo o di spazio, per tutto quello che mi ha insegnato e per tutto quello che avremo da scoprire ancora.

Ringrazio Francesca Romana (Fra) per illuminare ogni giorno in cui è presente

con la sua risata, la sua ironia, la sua semplicità, la sua forza, la sua dolcezza.

Ringrazio Carlotta per essere stata una nuova luce che mi ha ispirato con la sua vivacità, la sua vicinanza e riflessività.

Ringrazio Ludovica per quasi vent'anni di amicizia ininterrotta, cresciuti sapendo di trovarla sempre al mio fianco in modo affettuoso, positivo ed intelligente.

Ringrazio Kalipso per la fiducia che mi trasmette, per la sua socialità coinvolgente e per tutto quello che abbiamo condiviso in tanti anni e condivideremo ancora.

Ringrazio Nico per tutto l'affetto e il sostegno, per i sorrisi condivisi e regalati che porto con me.

Ringrazio la Corrente Umanista Socialista (CUS) tutta, per aver contribuito a rendermi chi sono e per i sogni che ispira in tante persone. Ringrazio Federica D'Alessio per la sua presenza fondamentale e indispensabile, per essere un punto di riferimento sincero e leale, trasparente e tenace, per l'affetto che mi trasmette anche nei momenti in cui non sembra, e per ricordarmi che ci sta che non tutti siano appassionati di fisica. Ringrazio Maria Giordano, che in questi ultimi anni è stata una maestra di dialogo e di riflessioni teoretiche, per la sua capacità di valorizzare il pensiero di tutti, compreso il mio, e per la sua curiosità instancabile. Ringrazio Dario Renzi, per la sua opera generale e in particolare per farmi pensare quanto l'amore per la fisica e l'amore per l'umanità possano andare a braccetto. Ringrazio Manu Voto, amica, compagna, coinquilina, dottoressa, imbianchina e sportello psicologico, per la felicità che ho ogni volta nel sentirla e per la positività che mette nell'affrontare ogni avversità. Ringrazio Francesca Raineri (Paca) per la strada condivisa e la guida morale che ha rappresentato e che tuttora rappresenta, ivi compresi dubbi, distanze e contraddizioni. Ringrazio Micol Drago per tutto quello che abbiamo imparato e scoperto insieme, considerando le tante scelte differenti che possono arricchire i nostri percorsi. Ringrazio Marcin Trycz per la sua proverbiale generosità e disponibilità d'animo, e per essere sempre stato un esempio per me.

Ringrazio Francesco Totti, per aver incarnato i miei sogni insieme a quelli di milioni di persone, creatore di nuove geometrie e dinamiche spazio-temporali mentre accendeva nei nostri cuori la gioia e le lacrime per tutto quello che ci ha regalato e che continuerà a farci sognare.

Ringrazio Nerina Marcon per aver acceso in me la passione per la matematica e le scienze fin da piccolo, per avermi dato gli strumenti per farlo e, soprattutto, per avermi sempre messo alle corde.

Ringrazio Emanuela Salciccia per avermi sempre coinvolto e saputo darmi la fiducia e l'ambizione di perseguire i miei sogni di adolescente innamorato della matematica e della fisica, continuando a farlo oggi di fronte alle nuove sfide che ci aspettano.

Ringrazio i miei genitori, che mi hanno permesso di arrivare fin qui con il loro sostegno continuo e quotidiano, con la loro benevolenza, l'amore e la serenità che mi hanno sempre trasmesso, dandomi la possibilità di vivere le mie scelte, anche quelle magari un po' incomprese. Ringrazio mia sorella per essere da sempre la mia sorella grande, e per i tanti momenti in cui mi ha fatto crescere, ascoltandomi e responsabilizzandomi.

Infine desidero ringraziare i miei nonni per tutto l'amore che mi hanno dato, con le loro storie e le loro personalità agli antipodi, per essere stati i compagni grandi della mia infanzia e adolescenza fino ad oggi. Ringrazio Valeria per essere stata un grande esempio di dolcezza e la gentilezza, e Giuliano per avermi insegnato che un uomo con tante qualità e autorevolezza può anche essere tenero. Ringrazio Carlo per la fiducia e la passione ideale e scientifica che mi ha sempre trasmesso, sperando di aver in parte ricambiato la dedica che mi fece dieci anni fa, e ringrazio Silvia per essere la nonna più straordinaria del mondo, per la sua forza, determinazione e affetto concretamente vissuto con cui ci ha cresciuti e che ho sempre ammirato di lei. Tutti insieme rappresentano il mio background culturale e sono stati all'origine di tante mie vocazioni e passioni. Questa tesi è dedicata a loro.